SPE

Society of Petroleum Engineers of AIME

SPE 8322

POST IN-SITU URANIUM LEACHING SITE RESTORATION — NUMERICAL ANALYSIS

by Robert S. Schechter, Univ. of Texas at Austin; and
Paul M. Bommer, Bommer Engineering, Members SPE-AIME

This paper was presented at the 54th Annual Fall Technical Conference and Exhibition of the Society of Petroleum Engineers of AIME, held in Las Vegas, Nevada, September 23-26, 1979. The material is subject to correction by the author. Permission to copy is restricted to an abstract of not more than 300 words. Write 6200 N. Central Expy., Dallas, Texas 75206

ABSTRACT

This paper presents the development of and results from a computer model of post in situ uranium leaching site restoration. This model uses a stream-line-concentration balance approach and is useful with a wide range of reservoirs. It can be used with any type of well system, in a bounded or unbounded, layered, and/or anistropic reservoir.

From a well pattern and reservoir point of view the effects of areal sweep, layering, and anisotropy are shown. Also the effects of the reservoir's cation exchange capacity and affinity for the leaching cation are demonstrated. These variables along with the effects of varying types of clean up solutions are related to restoration schemes and cautions are outlined for not just restoration but leaching as well.

INTRODUCTION

Leaching solutions commonly used for in situ uranium extraction generally include an oxidant such as dissolved oxygen or hydrogen peroxide to oxidize uranium from its relatively insoluble U^{+4} valence state to the more soluble U^{+6} form. To enhance the solubility of the oxidized uranium, carbonates are often included in the lixiviant formulation.[1] These form stable, highly soluble uranyl dicarbonate or uranyl tricarbonate ions[1] which can be recovered in surface ion exchange facilities. At present most solution mining employs ammonium carbonate/bicarbonates as the carbonate source. These solutions have been found to be effective in South Texas sandstones. Ammonium carbonates have been preferred to sodium carbonates because many of the formations experience severe permeability reduction when contacted with sodium ions. Potassium carbonates are more expensive than ammonium carbonates.

References and illustrations at end of paper

These leaching operations are conducted in aquifers. The injection and production rates are adjusted to minimize lixiviant excape from the immediate vicinity of the mineralized zone. After the mineral values have been produced, the mined zone must be restored. Restoration is generally defined by the terms of a mining permit issued by a responsible governmental agency and approved by the mining company[2]. Because of the technology of in situ uranium mining is in the developmental stages, standardized rules for restoration have not yet been developed. The practice to date has been to require that groundwater samples drawn from the aquifer in the mined area have a composition similar to that which existed prior to mining. For example, if ammonium carbonate is one component of the lixiviant, then the levels of ammonium allowed to remain in the groundwater are related to those initially present. Since these initial levels are often quite small, restoration may require that a large portion of the ammonia be recovered from the aquifer. The difficulty of accomplishing this goal and the best procedure to use will depend on a number of factors, including the reservoir dimensions and its characteristics, the type of cation used in the lixiviant, the well pattern and the type and concentration of the eluting solution. The particular problem addressed in this paper is the removal of the lixiviant cation; however, there may be, and in general are, other criteria which must be satisfied. Vanadium, arsenic and manganese must all be reduced to tolerable concentration. Dissolved solids and radioactivity must both be reduced to near baseline levels.

Lixiviant cation restoration is considered here because this is believed to be one of the more complex tasks, especially if the residual concentrations are set at very small values. The removal process considered involves ion exchange since commonly occurring minerals, especially clays, exhibit a considerable cation exchange capacity[3].

This paper describes a computer model which is believed to include the effects of many of the important factors such as the size and shape of the mineralized zone, reservoir characteristics such as

the cation exchange capacity, and directional permeabilities, the type of lixiviant cation and the nature of the eluting fluid used to displace the sorbed lixiviant cation.

THE FLOW MODEL

In this model the flow is assumed to be single phase and two-dimensional so that the fluid velocity at a point can be calculated using the well known source and sink equations (see Appendix A). The source and sink equations have been written in anisotype form such that they are a function of the location and volume rates of production and injection wells and the directional permeabilities (k_x and k_y) of the reservoir. Given the fluid velocities, streamlines can be traced. A typical isotropic example is shown in Figure 1.

Once streamlines have been defined, the pressure drop along them can be calculated. In the approach used here, the streamlines are divided into equal pressure increments or nodes which will be used later in developing a finite difference analog of the concentration balance. The fluid velocity at each node is recorded for future use in the finite difference equations.

It should be noted that the streamline model can be modified to approximately account for variations in reservoir thickness provided they can be assumed to change linearly between wells[4]. The calculation requires that the formation thickness be known at each point along a streamline. These values of thickness are entered using a grid system over the area of the pod, as shown in Figure 2. This information is used to adjust the fluid velocities at each node. In the subsequent concentration calculations the modified velocities will be used. In this way, thickness variations are considered.

Most uranium pods are small in area compared to the aquifers in which they occur, and these are effectively unbounded systems as represented by Figure 1. In some cases bounded systems are encountered. Bounding may occur for natural reasons such as faults or permeability pinch outs or bounding may be artificially imposed by mechanisms such as groundwater injection in guard wells drilled around the outside of the pod. If bounding is desired the model uses a method of image wells developed by Lin[5] to simulate the bounding which can be achieved by the proper injection rates through a given system of guard wells. This process can be used to form a boundary in the model regardless of whether or not the boundary on the pod is created by natural or artificial means. An example of an isotropic bounded pod is shown in Figure 3.

CONCENTRATION BALANCE

Once the flow system has been defined, bounding completed if required, and each streamline divided into nodes at which velocities are stored, the next step is to calculate the concentrations of both cations and the anion at each node point. The calculations reported here assume that two cations are present and at each point the sum of their concentrations must equal the anion concentration to preserve electroneutrality. Thus

$$C_1 + C_2 = C_A \tag{1}$$

Also the fluid is assumed to be in local equilibrium with the minerals. Assuming that this equilibrium can be represented by the law of mass action neglecting activity coefficient corrections (see Griffith[5] for an excellent discussion), we write

$$\frac{Q_1}{Q_2} = K\frac{C_1}{C_2} \tag{2}$$

where Q_1 is the amount sorbed per unit mass of mineral. Cation 1 will represent the one which is to be displaced and for K>1, it will exhibit a stronger affinity for the surface than does cation 2. It is furthermore assumed that the sorption process is one of cation exchange so that

$$Q_2 = Q_v - Q_1 \tag{3}$$

where Q_v is the cation exchange capacity.

At any point in the reservoir, the amount of cation i per unit pore volume is

$$L_i = \frac{1-\phi}{\phi}\rho_R Q_i + C_i \tag{4}$$

where $Q_A = 0$, that is, anion adsorption is neglected.

The component balance can be written as

$$\alpha(\phi,\Psi)\frac{\partial C_i}{\partial \phi} + \beta(\phi,\Psi)\frac{\partial^2 C_i}{\partial \phi^2} = \phi\frac{\partial L_i}{\partial t} \tag{5}$$

neglecting dispersion along lines of constant potential (perpendicular to flow, transverse dispersion) as shown in Appendix B and by Bommer and Schechter[7]. The quantities α and β depend on the velocities along the streamlines which are known, but are independent of concentration. ϕ is the potential function which for horizontal single phase systems is the pressure.

To solve Equation (5), it is most convenient to solve first for the anion concentration as a function of time and position. Since anion sorption is neglected, this involves the integration of a linear partial differential equation with variable coefficients. A numerical approach has been adopted. A finite difference analog involving an implicit fourth order central difference has been employed. Three point forms have been used near the boundaries when necessary to preserve the pentadiagonal matrix system. Because of this certain computational errors are introduced and these are especially troublesome at fronts where concentrations tend to change rapidly. Numerical experiments have shown that these errors are manageable. Further discussion of the numerical techniques is given in Appendix B and a complete report of the studies relating to stability of the numerical techniques are reported elsewhere[6].

Once the anion concentration is established, the concentration of one of the cations can be eliminated using the conditions of electroneutrality, Equations (1) and (3). Equation (5) then can be reduced to a form containing one unknown, a cation concentration.

This equation is not, however, linear in the concentration and an iterative procedure is required. Further discussion is provided in Appendix B.

DISCUSSION OF RESULTS

The most important contribution of this work is believed to be the development of a versatile computer program, able to accomodate, for example, a variety of initial conditions, well patterns, reservoir characteristics and fluid injection strategies, which simulates the elution of a sorbed cation. However, some general observations can be made by comparing the results of different computer runs even though the reservoir studied is a hypothetical one. These conclusions are presented in this section.

The case studied is defined by the parameters listed in Table 1. The aquifer is assumed to have a thickness of 30 feet throughout the 2.75 acre mineralized zone. For most calculations the initial lixiviant cation concentration is assumed to be 1.04×10^{-3} equivalents/liter. It is recognized that this number is at least several times that concentration now used in South Texas mining operations; however, the effect of the lixiviant concentration will be considered and shown to be unimportant. The cation exchange capacity given in Table 1 is equivalent to 5 meq/100 grams of ore. This is a small value. Many South Texas ores have been studied[9] and only those having very small concentrations of clays or zeolites exhibit such small cation exchange capacities. Many deposits have cation exchange capacities ranging two to five times this value. The influence of the cation exchange capacities is also investigated.

The elution fluid concentration is equivalent to 61,000 ppm sodium chloride solution. There may be some disagreement regarding the use of an eluent which has a considerable higher dissolved solids content than does the natural groundwater since once the lixiviant cation (as, for example, ammonium) has been displaced, a second stage process will be required to displace the high concentration brines from the pore spaces. We shall, however, see that considerable advantage may be gained eluting with high concentration brines, and this may offset the disadvantage of a second stage. This aspect will be discussed in greater detail.

Restoration of the mined zone should be a factor in the selection of a well pattern since the same wells are used for both restoration and production. Unfortunately, optimum recovery of the mineral values is often the overriding consideration governing the development of a field. This may be a poor strategy. Focusing on the removal of sorbed cation as one important aspect of the restoration problem, the rate of recovery can be studied as a function of the well pattern, all other factors being held constant. Several well patterns have been selected for study to illustrate the point. They are the unbounded inverted five spot (Figure 1), the unbounded line drive (Figure 4), the unbounded circle pattern (Figure 5) and the unbounded expanded inverted five spot (Figure 6). The fraction of the leaching cation initially present in the mined zone denoted by the rectangular region which is recovered is shown in Figure 7 as a function of pore volumes injected. The conditions of the study common to all computer runs are given in Table 1.

From Figure 7 it can be seen that the inverted five spot and the line drive recover the smallest proportion of the leach cation in a given time. Since the flow is one phase and the reservoir is homogeneous, eventually all of the lixiviant cation will be recovered regardless of the pattern. This result shows, however, that some patterns result in a more efficient areal sweep than others. The rules seem to be that streamlines should be of uniform length and should penetrate the entire formation if possible. For example, the circle pattern appears to recover less than the inverted five spot due mainly to the longer streamlines associated with the circle pattern which result in a longer fluid transit time.

The results shown in Figure 7 indicate that if extremely small levels of the lixiviant cation must be achieved, then very long restoration times will be required, thereby requiring considerable fluid volume. For example, we have continued the computer simulation of the inverted five spot for injection times extending to one year. A part of these results are shown in Figure 8. Notice that the percentage recovery of the lixiviant cation is slowly increasing. Indeed after one year, about 5 pore volumes have been injected and produced and only 90% of the cation initially present has been recovered. Furthermore, those lixiviant cations still remaining in the reservoir were found to be near the boundaries of the region or to have been displaced outside of the region. Of course these cations will all eventually be produced.
The concentration of the lixiviant cation in the produced fluids is 5.46×10^{1} equivalents/m^3 (930 ppm expressed as NH_3) at the end of one year. This is a value which may still be excessive when compared to permitted values. Our conclusion from this part of the study is that ultralow concentrations of the lixiviant cation in the produced fluids will be expensive to achieve because excessively large quantities of eluent will be required. This point is emphasized, perhaps over emphasized, because it is important to stress that the cost of restoration may not be negligible.

The lixiviant cation concentration used in the calculations described above and given in Table 1 is probably larger than those used in most basic leaching solutions. This prompts us to inquire as to whether or not the long times required to recover the lixiviant cation is not a function of the somewhat large values of the lixiviant concentration. To understand the results to follow, one must recognize that the total cation sorbed is independent of the lixiviant concentration. This is based on a very reasonable assumption that the leaching process was conducted for a sufficient time to ensure that all of the cation exchange sites contain lixiviant cations. Thus the cation ion exchange capacity determines the sorption. As the lixiviant concentration is varied, the initial amount of cation in reservoir changes, because of that portion contained in the pores. Figure 9 shows the cation recovery as

a function of the pore volumes injected for the case when the lixiviant cation concentration is reduced from 1.04×10^3 to 1.04×10^1 equivalents/m^3. This latter concentration is much smaller than would normally be employed. Even if the lixiviant concentration is greatly reduced, the results shown in Figure 9 indicate that the recovery is not made easier. Actually comparing the results shown in Figures 8 and 9, one is tempted to conclude that it is more difficult to recover the lixiviant cation if the initial concentration is reduced. This is, however, not the case. As shown in Figure 9, the cation concentration in the produced fluids is initially small, but as the anion concentration increases (the injected concentration is maintained high), the concentration of the lixiviant cation also increases. After about 1.0 pore volumes, the concentrations for the two different cases do not differ greatly. This implies that the remaining sorbed cation which was the same for both cases are being removed at about the same rate. We conclude that the difficulty of recovering lixiviant cation does not depend critically on the lixiviant concentration.

The concentration of the eluting fluid is larger than that found in naturally occuring groundwaters in shallow aquifers. The concentration corresponds to about 61,000 ppm NaCl. Generally the concentration of dissolved solids should be reduced to levels consistent with the initial state of the groundwater. This means that it may be necessary to flush the system with groundwater, perhaps by producing from a central well. It may seem desireable to avoid this second stage by using a less concentrated eluting fluid. The difficulty with this approach is that the displacement of the sorbed cation is speeded by using higher concentrations of cation in the eluting solution. The effect of reducing the ionic strength of the eluting solution is shown in Figure 10. The curve labeled 1.04×10^3 equivalents/m^3 (58,000 ppm NaCl) corresponds to that given in Figure 7. As the concentration of the eluting fluid is reduced, the displacement is seen to be progressively less effective. In fact the dependence on ionic strength is much more profound than is indicated by Figure 10. For the case studied only 25% of the lixiviant cation is sorbed on the surface, the remainder is initially contained within the pores and is easily displaced even by solutions which do not remove sorbed cations. Thus 75% of the lixiviant cation can be removed without reducing the surface concentration. This can be seen in Figure 10 because the concentration used is important only after the breakthrough of the injected fluid.

Curves showing the disposition of the sorbed leaching cation are not included here, but an examination of them further emphasizes the advantages of using concentrated elution solutions. The decision as to the desireability of using a two stage process depends on a number of factors including, for example, the availability of highly saline waters. In the final analysis, the decision will be based on economic considerations.

The amount and types of clays largely determine the difficulty in displacing the lixiviant cation. For the purposes of ion exchange calculations the minerals can be characterized by their ion exchange capacity and their relative affinity for the competing cations. This affinity is characterized by the thermodynamic constant K appearing in Equation (2). To illustrate the importance of these parameters several runs have been made using the inverted five spot pattern (Figure 1). Figure 11 shows the recovery of the lixiviant cation when the cation exchange capacity is increased by an order of magnitude. As expected, larger volumes of fluid are required.

It is also instructive to alter the value of K. For $K > 1$, the displaced cation exhibits the greatest affinity for the surface. (See Equation 2) Figure 12 shows the displacement to be more efficient if the affinity for the displacing cation is greatest. In this case the displacing front is self-sharpening and dispersion reduced. The desireability of utilizing cations in the eluting solution which have a high affinity for the surface has been discussed by Hill et al[3].

As mentioned earlier, reservoir characteristics play a very important role in leaching and restoration. Several types of reservoir hetergeneities can be considered by this model. Reservoirs consisting of noncommunicating strata can be accomodated. In leaching and restoration the flow is single phase and the viscosities are not changed substantially as the lixiviant concentration changes during the leaching process. Under such conditions communication between strata is small[10]. To illustrate the effect of layering the reservoir defined in Table 1 is assumed divided into three layers of equal thickness having permeabilities of 25, 20 and 15 Darcies, respectively. The porosities of these layers are assumed to be 30%, 25% and 20%. It can be seen from Figure 13 that after four months the layered system is not as well restored. The low permeability layer does not accept as much fluid as the other two and longer injection times will be required to complete the task.

The second type of heterogeneity that can be considered by this model is anisotropy. For anisotropic systems the x direction and the y direction permeabilities must be known. Pods having permeability contrasts other than unity ($k_x = k_y$) show streamline patterns that are elongated and distorted when compared to isotropic systems. As an example of this, the inverted five spot pattern of Figure 1 has been modeled again with a permeability contrast of 20 (k_x = 1D, k_y = .05D). The streamline pattern for the anisotropic pod is shown in Figure 14. The restoration results, after four months of restoration, for the isotropic and anisotropic systems are shown in Figure 15. This figure shows that the anisotropic system has recovered about 12% less of the leaching cation than the isotropic pod. This is due to the disruption and elongation of the streamline pattern by the permeability difference.

CONCLUSIONS

Several points have emerged as a result of this study which should be emphasized. The most important one is that restoration costs may be

significant and should be considered in all stages of the development and operation of an in situ process. More specific conclusions are

(1) Well pattern is important. Clean-up is best obtained with wells which span the entire contaminated zone and arranged so that the streamlines are of roughly the same length.

(2) The ease with which the lixiviant cation can be removed from the formation does not depend strongly on the lixiviant concentration, however, increasing the cation exchange capacity or decreasing the relative affinity of the displacing cation for the mineral surfaces does increase the volumes of eluting fluid required.

(3) To rapidly displace the sorbed lixiviant cation, the use of a high ionic strength eluting solution is essential. This may require a two stage process to meet the requirements for restoration.

(4) Reservoir heterogeneities complicate the restoration problem and in general result in the need to use larger volumes to displace the sorbed lixiviant cation. Layering and directional permeabilities have been studied here.

NOMENCLATURE

C_i = concentration of component i
D_o = molecular diffusion coefficient
F = formation resistance factor
h = formation thickness
K_L = axial dispersion coefficient
K = equilibrium constant
k = permeability
L_i = total (including sorbed) equivalents of component i per unit of pore volume
P = average formation particle diameter
q = injection (+) or production (-) rate
Q_i = equivalents of component i sorbed per unit mass of mineral
Q_v = cation exchange capacity expressed in equivalents per unit mass of mineral
RI = two percent of the average distance between production and injection wells
t = time
u = $u_x^2 + u_y^2$
u_x = x component of flux
u_y = y component of flux
v = fluid velocity

Subscripts

A = anion
L = longitudinal
i = cation number

Greek

α = complex function of velocity defined by Equation (B.4)
β = function of velocity defined by Equation (B.5)
μ = fluid viscosity
Φ = potential
ϕ = porosity
ρ = density
σ = formation inhomogeneity factor

REFERENCES

1. Garrels, R. M. and Christ, C. L.; Solutions, Minerals and Equilibria, p. 253, Freeman, Cooper and Co., San Francisco (1965).

2. Whittington, D. and Taylor, W. R.; "Regulations and Restoration of In Situ Uranium Mining in Texas," in South Texas Uranium Seminar, Society of Mining Engineers of American Institute of Mining, Metallurgical and Petroleum Engineers, Inc. (1979).

3. Hill, A. D., Walsh, M. P., Breland, W. M., Silberberg, I. H., Humenick, M. J. and Schechter, R. S.; "Restoration of Uranium In Situ Leaching Sites," Society of Petroleum Engineers' Preprint 7534, presented at the 53rd Annual Technical Meeting, Houston, Texas (October, 1978).

4. Wessels, J. W.; Application of the Streamline Reservoir Model to Reservoirs Having Variations in Formation Thickness, Master's Thesis, The University of Texas at Austin, Austin, Texas (May, 1973).

5. Lin, J. K.; An Image Well Method for Bounding Arbitrary Reservoir Shapes in the Streamline Model, Doctoral Dissertation, The University of Texas at Austin, Austin, Texas (December, 1972).

6. Griffith, T. D.; "Application of the Ion Exchange Process to Reservoir Preflushes," Society of Petroleum Engineers Preprint 7587, presented at the 53rd Annual Technical Meeting, Houston, Texas (October, 1978).

7. Bommer, P. M. and Schechter, R. S.; "Mathematical Modeling of In Situ Uranium Leaching," Society of Petroleum Engineers Preprint 7533 presented at the 53rd Annual Technical Meeting, Houston, Texas (October, 1978).

8. Bommer, P. M.; A Streamline-Concentration Balance Model for In Situ Uranium Leaching and Site Restoration, Doctoral Dissertation, The University of Texas at Austin, Austin, Texas (August, 1978).

9. Garwacka, K., Johnson, D., Walsh, M., Breland, M., Humenick, M. and Schechter, R.; Investigation of the Fate of Ammonia from In Situ Uranium Solution Mines, Technical Report EHE 79-01, The University of Texas at Austin, Austin, Texas (February, 1979).

10. Collins, R. E.; Flow of Fluids through Porous Materials, p. 197, The Petroleum Publishing Co., Tulsa, Oklahoma (1976).

11. Perkins, T. K. and Johnston, O. C.; "A Review of Diffusion and Dispersion in Porous Media," Society of Petroleum Engineers Journal, p. 70 (March, 1963).

12. Muskat, M.; The Flow of Homogeneous Fluids Through Porous Media, p. 225, J.W. Edwards, Inc., Ann Arbor. 1946.

APPENDIX A: ANISOTROPIC STREAMLINE GENERATION

It is well known that the following potential is a solution of the Laplace equation with line sources and sinks .

$$\phi(\bar{x},\bar{y}) = \phi_m - \frac{\mu}{4\pi\bar{h}} \sum_{i=1}^{n} q_i \ln\{(\bar{x}-\bar{x}_i)^2 + (\bar{y}-\bar{y}_i)^2\} \quad (A.1)$$

where

$$\bar{x} = \frac{x}{k_x} , \bar{y} = \frac{y}{k_y} , \bar{q}_i = \frac{q_i}{k_x k_y k_z}$$

and

$$\bar{h} = h/ k_z$$

The components of velocity are, therefore,

$$v_x(x,y) = \frac{k_x/k_y}{2\pi\phi h} \sum_{i=1}^{n} q_i \frac{(x-x_i)}{(x-x_i)^2 + \frac{k_x}{k_y}(y-y_i)^2} \quad (A.2)$$

and

$$v_y(x,y) = \frac{k_x/k_y}{2\pi\phi h} \sum_{i=1}^{n} q_i \frac{(y-y_i)}{(x-x_i)^2 + \frac{k_x}{k_y}(y-y_i)^2} \quad (A.3)$$

Define RI as two percent of the average distance between wells and assume that the velocity is constant over this small distance. Sum the vectorial components of velocity to obtain the total velocity

$$v(x,y) = (v_x^2 + v_y^2)^{1/2} \quad (A.4)$$

The time required for a fluid particle to move the distance RI is

$$\Delta t = RI/v(x,y) \quad (A.5)$$

The new location of the fluid particle along a streamline can be calculated by

$$X_{i+1} = X_i + v_x(x,y)\ \Delta t \quad (A.6)$$

$$Y_{i+1} = Y_i + v_y(x,y)\ \Delta t \quad (A.7)$$

This procedure is repeated for each streamline of each production well. Thus, the streamlines are traced between production and injection wells.

APPENDIX B: CONCENTRATION BALANCE

A concentration balance, which includes dispersion that varies in the axial as compared to the radial direction and adsorption can be written as

$$(1-\phi)\rho_R \frac{\partial Q_i}{\partial t} + \phi\frac{\partial C_i}{\partial t} + u_x\frac{\partial C_i}{\partial x} + u_y\frac{\partial C_i}{\partial y} = \frac{\partial}{\partial x}(K_{xx}\frac{\partial C_i}{\partial x}) +$$

$$+ \frac{\partial}{\partial y}(K_{yx}\frac{\partial C_i}{\partial x}) + \frac{\partial}{\partial x}(K_{xy}\frac{\partial C_i}{\partial y}) + \frac{\partial}{\partial y}(K_{yy}\frac{\partial C_i}{\partial y}) \quad (B.1)$$

Define

$$L_i = \{\frac{1-\phi}{\phi}\rho_R Q_i + C_i\} \quad (B.2)$$

and transform Equation (B.3) from rectangular coordinates to stream function and potential coordinates. If dispersion in the transverse direction is neglected, and if K_L is taken to be constant, it can be shown that

$$\alpha\frac{\partial C_i}{\partial\phi} + \beta\frac{\partial^2 C_i}{\partial\phi^2} = \phi\frac{\partial L_i}{\partial t}$$

$$\text{for } i = 1,\ 2 \text{ and } A \quad (B.3)$$

where

$$\alpha(\phi,\Psi) = u^2\eta + u_x\{\frac{\partial}{\partial\phi}(\frac{\mu^2\eta u_x K_L}{k_x}) + \frac{\partial}{\partial\Psi}(\mu\eta u_y K_L)\}$$

$$+ u_y\{\frac{\partial}{\partial\phi}(\frac{\mu^2\eta u_y K_L}{k_y}) - \frac{\partial}{\partial\Psi}(\mu\eta u_x K_L)\} \quad (B.4)$$

and

$$\beta = (\mu\eta u)^2 K_L \quad (B.5)$$

The quantity η is defined as

$$\eta = \frac{1}{u^2}(\frac{u_x^2}{k_x} + \frac{u_y^2}{k_y}) \quad (B.6)$$

K_L is the axial dispersion coefficient. In the numerical calculations reported here, Equation (B.7) which was used by Perkins and Johnston[11] has been used.

$$K_L = \frac{D_o}{F\phi} + 0.5\alpha P\frac{U}{\phi} \quad (B.7)$$

To solve Equation (B.3) the finite difference analog shown by Equation (B.8) is used at interior points.

$$\alpha_n \frac{C_{n+2,i} - 8C_{n+1,i} + 8C_{n-1,i} - C_{n-2,i}}{12\Delta\phi} + \beta_n \frac{C_{n+2,i} - 16C_{n+1,i} + 30C_{n,i} - 16C_{n-1,i} + C_{n-2,i}}{12\Delta\phi^2} = \phi \frac{L_{n,i} - L_{n,i-1}}{\Delta t} \quad (B.8)$$

This is a five point representation and it is applied at all interior points; however, at the boundaries a three point form is used. This procedure which preserves the pentadiagonal structure is detailed elsewhere[8]. In all of the expressions n represents a given node and i a given time. The same equation applies to each of the cations as well as to the anion. At the first node, $C_{1,i}$, is given as the composition of the injected fluids. At the second node, a three point form is used. At all interior nodes until the next to last node (n-1) is reached the five point forms, Equation (B.9), are used. At the next to last node, the three point form is again used. At the last node, n, which is at the face of the wellbore, a three point form requiring the concentration at a fictitious n+1 node is used. The fictitious concentration is determined so that

$$\left(\frac{\partial C}{\partial \phi}\right)_{n+1} = 0 \quad (B.9)$$

Now an expression for each node has been written and since the equations are implicit in time, they must be solved simultaneously. If the equations were linear, this procedure would be straightforward since the matrix of the coefficients is pentadiagonal. However, for adsorbed cations L is nonlinear. In solving Equation (B.8) for a cation an iterative procedure is used. $L_{n,i}$ is represented using a Taylor series expansion

$$L_{n,i} = L^*_{n,i} + \frac{dL^*_{n,i}}{dC^*_{n,i}} (C_{n,i} - C^*_{n,i}) \quad (B.10)$$

$L^*_{n,i}$ is calculated using an estimated concentration $C^*_{n,i}$. The linear relationship, Equation (B.10), is substituted into Equation (B.4) and the concentrations $C_{n,i}$ found by inverting the pentadiagonal matrix. This concentration is used to obtain a better estimate of the derivative $\frac{dL^*_{n,i}}{dC^*_{n,i}}$ and the process repeated until $C^*_{n,i}$ equals $C_{n,i}$. It was found that this procedure converged well[8].

Table 1

PARAMETERS USED FOR BASE CASE STUDY

Properties of the Reservoir	
Porosity	0.30
Thickness	9.14m (30 feet)
Area	11,130m^2 (2.75 acre)
Cation Exchange Capacity	5 X 10^{-2} equivalents/kg (5 meq/100 gram)
Density of Solid	2,500 kg/m^3 (2.5 g/cm^3)
Pore Volume	3.05 X 10^{-1} m^3 (192,00 bbls)
Properties of the Lixiviant	
Cation Concentration	1.041 X 10^3 equivalents/m^3 (1.041 X 10^{-3} equivalents/cm^3)
Process Characteristics	
Thermodynamic Constant	2.0
Elution Fluid Concentration	1.041 X 10^3 equivalents/m^3 (100,000 ppm NaCl Solution)
Injection Rate (assumed equally divided among all injection wells)	436 m^3/day (2740 bbls/day)
Production Rate (assumed equally divided among all production wells)	436 m^3/day (2740 bbls/day)

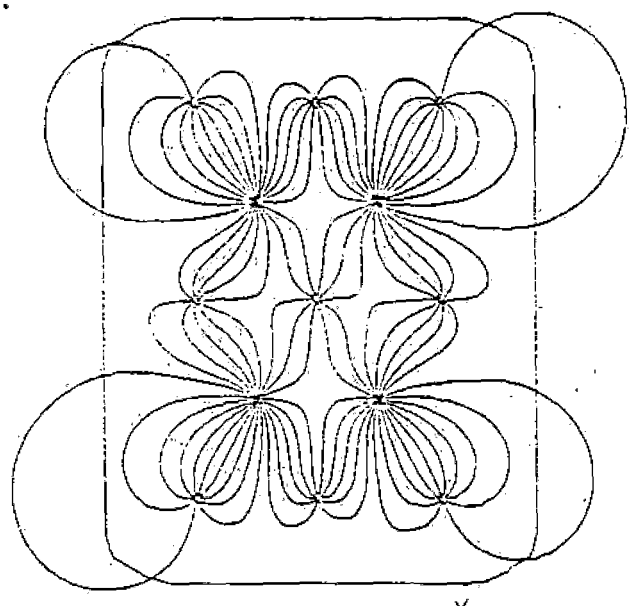

Fig. 1 - Streamline pattern for inverted five spot in an unbounded aquifer. The retangle represents the mineralized zone.

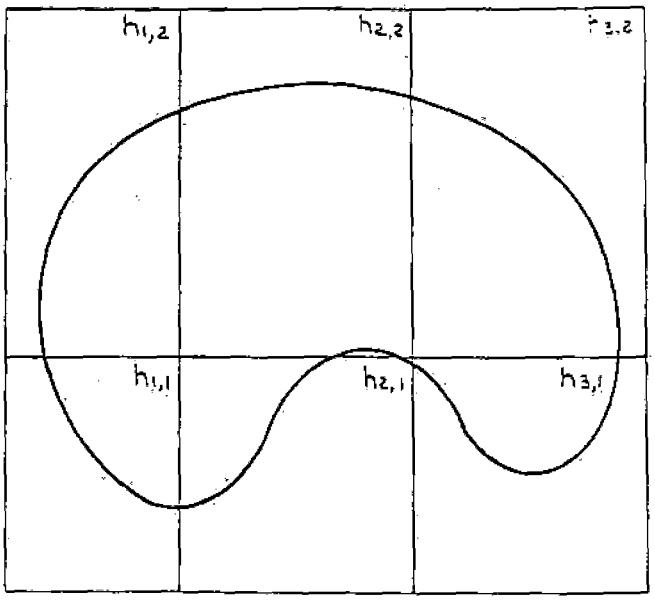

Fig. 2 - Example reservoir thickness-concentration grid. Values specified at the nodes are averages for upper right hand quadrant.

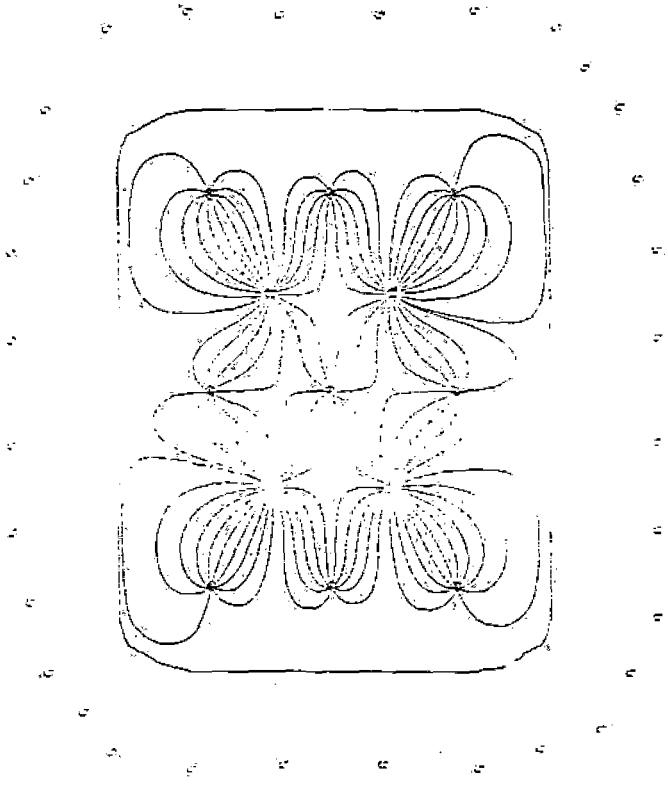

Fig. 3 - Bounded inverted five spot pattern.

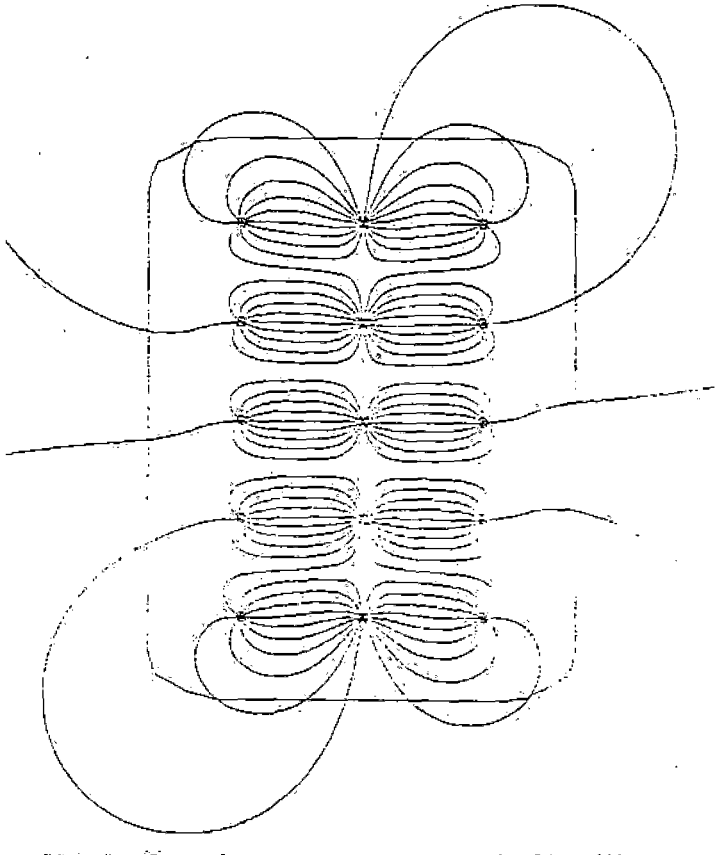

Fig. 4 - Streamline pattern for unbounded line drive

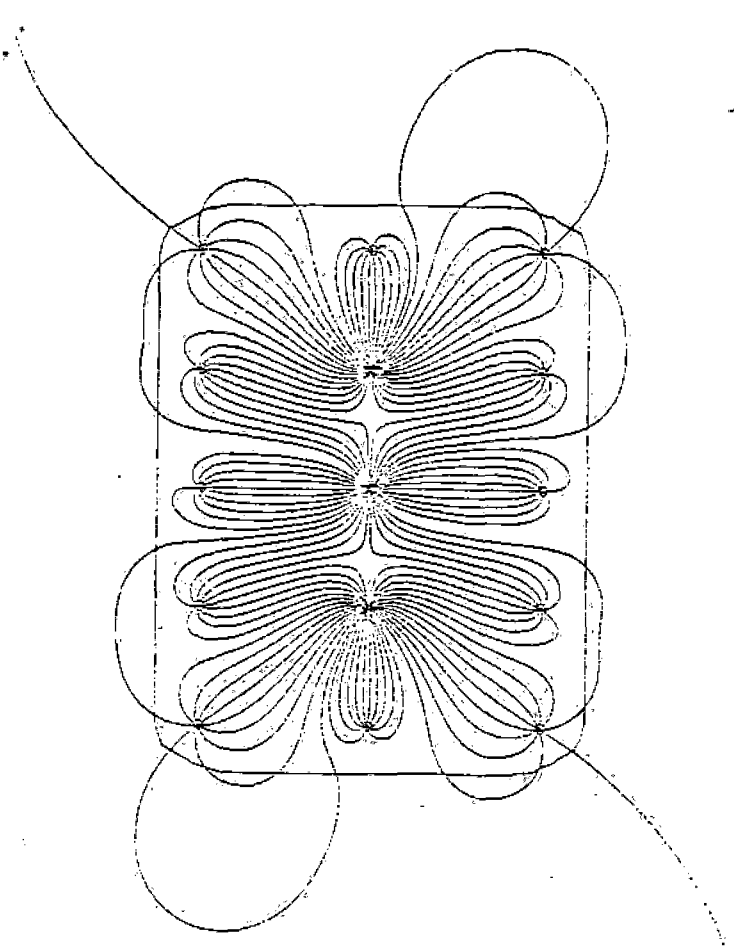

Fig. 5 - Unbounded circle pattern.

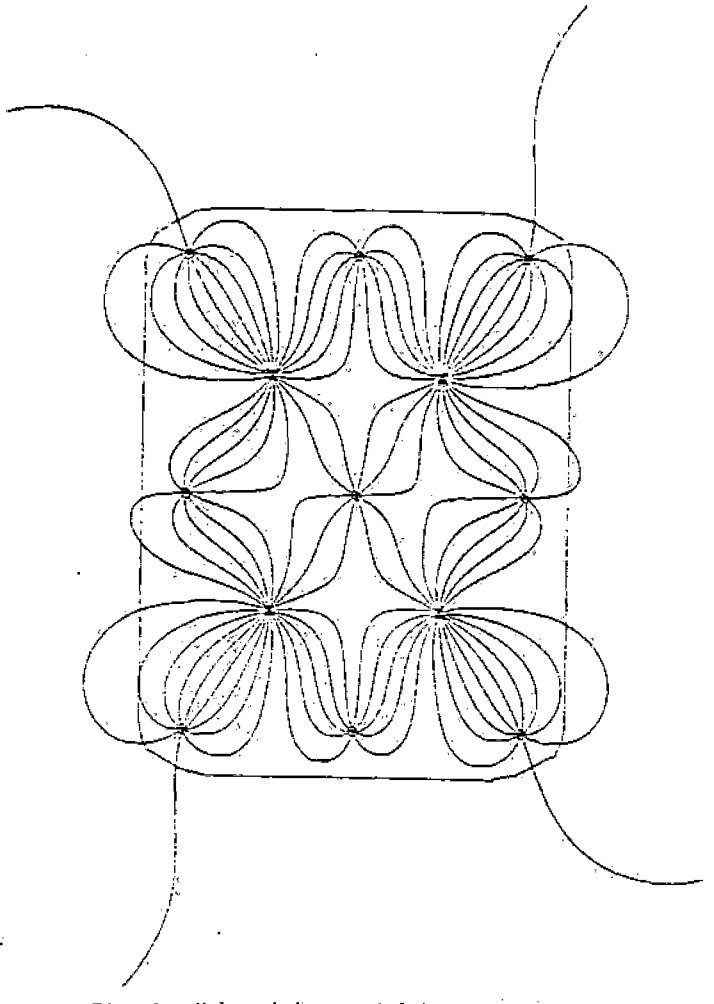

Fig. 6 - Unbounded expanded inverted five spot pattern.

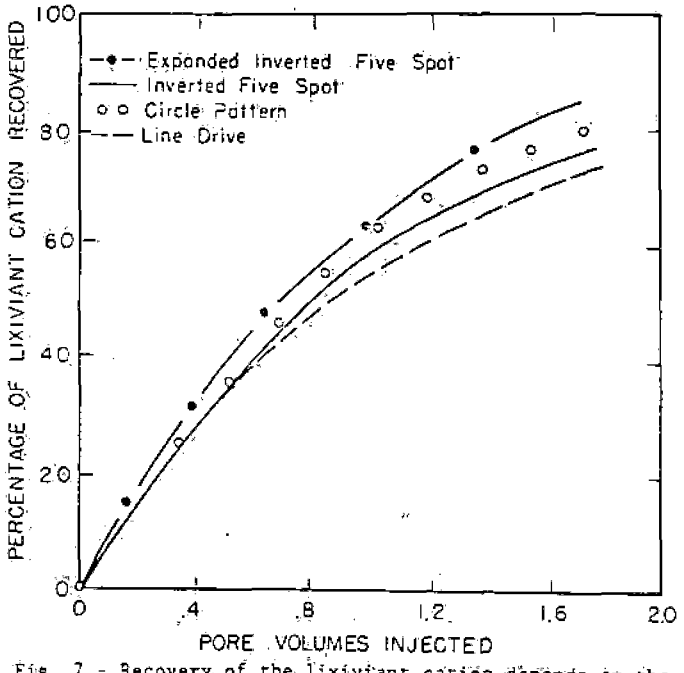

Fig. 7 - Recovery of the lixiviant cation depends on the well pattern.

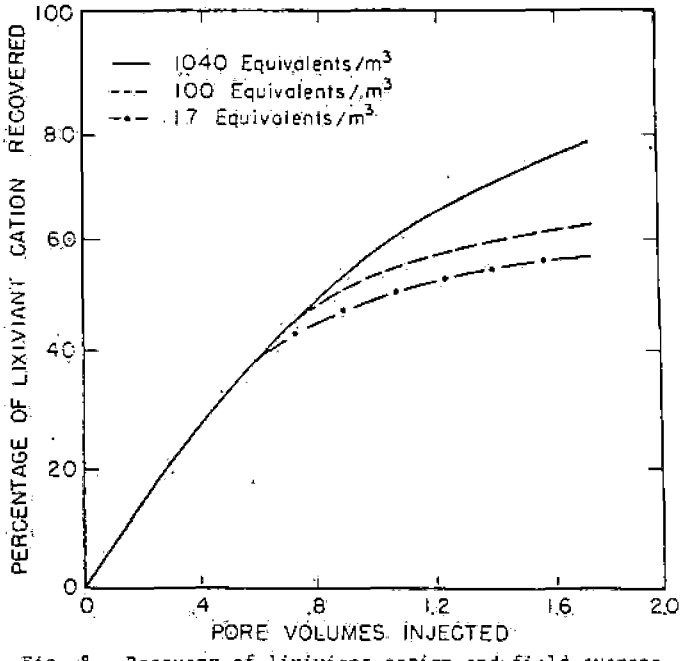

Fig. 8 - Recovery of lixiviant cation and field average concentration in produced fluids for the case of an initially high lixiviant cation concentration.

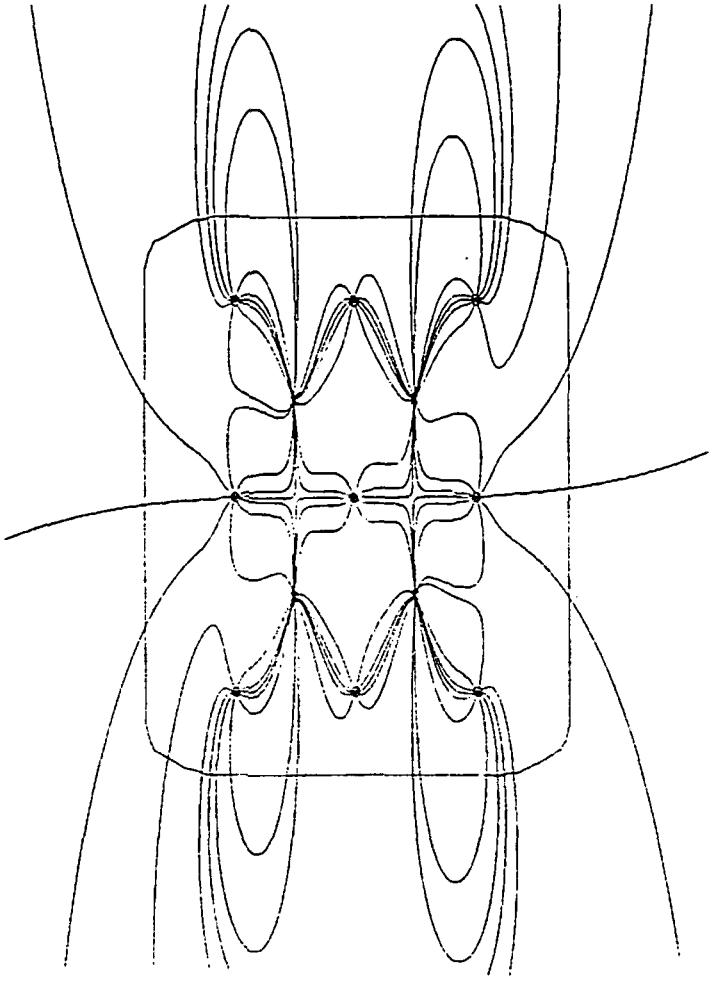

Fig. 14 - Streamline pattern for inverted five spot in an anisoirropic formation.

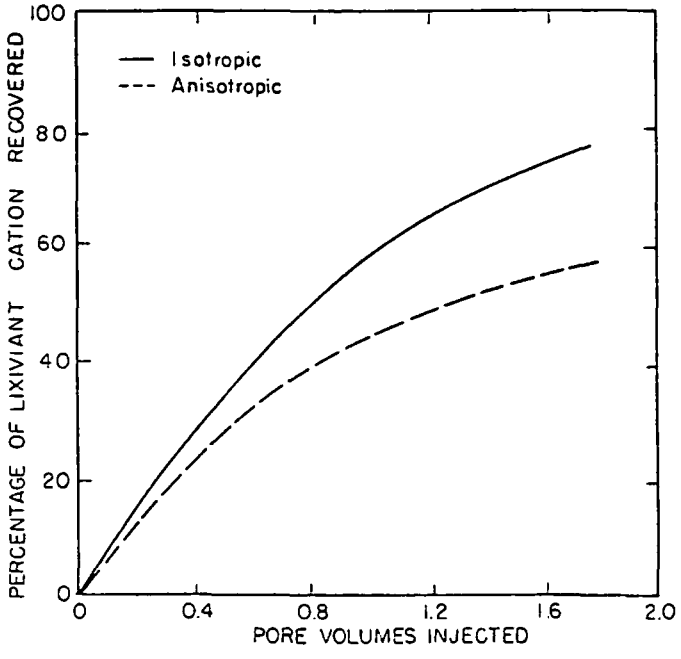

Fig. 15 - The recovery rate for the anisotropic system.

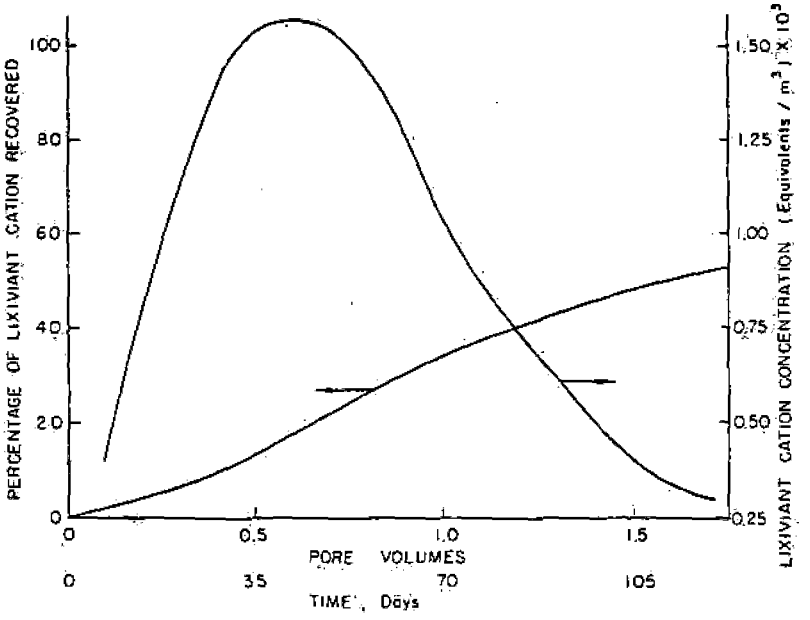

Fig. 9 - Recovery of lixiviant cation and field average concentration in produced fluids for the case of an initially low lixiviant cation concentration.

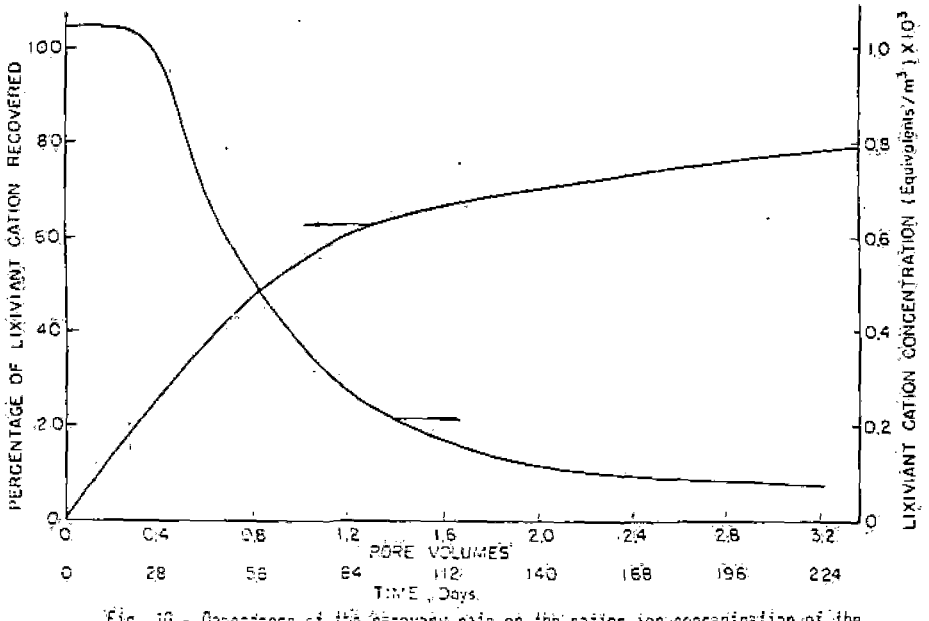

Fig. 10 - Dependence of the recovery rate on the cation ion concentration of the eluting fluid.

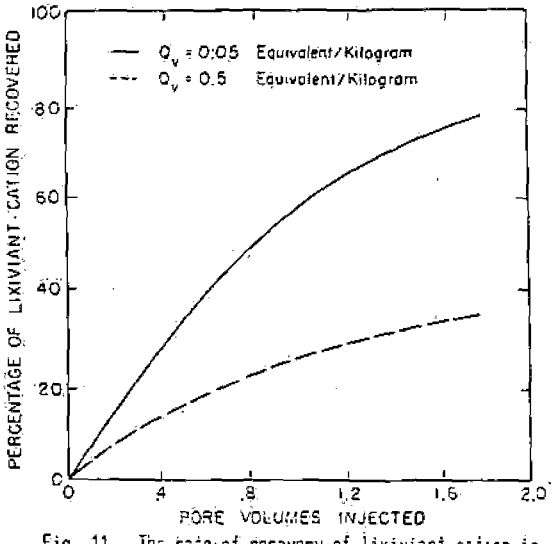

Fig. 11 - The rate of recovery of lixiviant cation is strongly dependent on the cation exchange capacity of the formation materials.

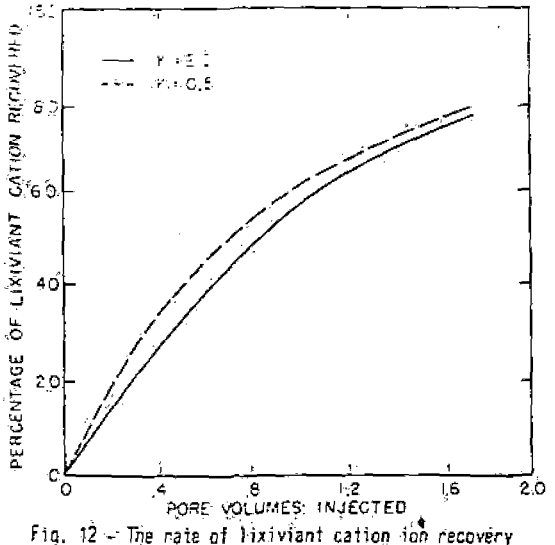

Fig. 12 - The rate of lixiviant cation ion recovery shown as a function of the relative affinity of the eluting cation for the adsorption sites.

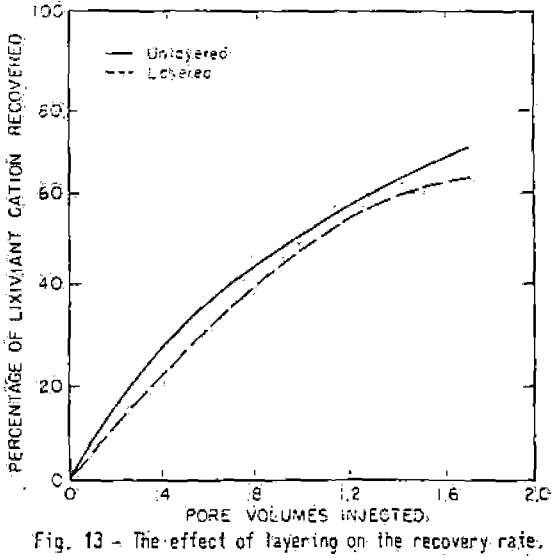

Fig. 13 - The effect of layering on the recovery rate.

UDC 542.943.5+546.815

Precipitation of lead as the dioxide by ozone in an acidic medium

A F Chudnov (Kuzbass Polytechnic Institute - Department of General and Inorganic Chemistry)

Earlier it was reported that divalent lead is precipitated by ozone from aqueous solutions of the hydroxide in the form of the dioxide at pH 6-8 and in the form of the monoxide at pH>9 [1]. Under normal conditions divalent lead is not precipitated and is not oxidised by ozone in neutral and acidic media. (An exception is lead iodide). On the other hand, it would be useful to realise an analogous process for solutions with pH< 6, since the need often arises to precipitate Pb^{2+} ions in neutral and acidic solutions in hydrometallurgy, for example, for purification of effluents, etc.

We have established that the oxidation of divalent lead by ozone with its simultaneous precipitation as the dioxide can be realised in a weakly acidic medium in the presence of manganese compounds as catalyst. As model we used 0.01M aqueous solutions of lead acetate and lead nitrate, which were acidified by addition of the acid with the like anion (acetic and nitric acids respectively) with variation of the pH in the range of 1-6. The catalyst was manganese acetate or nitrate (2-5% on the weight of the lead salt).

In a series of experiments to determine the possibility of separating a mixture of cations the precipitation of lead by ozone was realised in the presence of cadmium and zinc nitrates. All the reagents were of analytical grade. The ozonisation conditions were as follows: duration 4h, temperature 20°C, volume of solution 300 ml. It was established that intense precipitation of lead (together with manganese) in the form of the dioxides takes place in neutral and moderately acidic medium (up to pH ~ 3). In a more acidic medium the oxidation rate of divalent lead is greatly reduced, and manganese dioxide mostly separates in the precipitate. In an acidic medium part of the manganese is oxidised to water-soluble permanganate, and the solution acquires the characteristic violet colour. The precipitates were filtered off, dried to constant weight, and weighed. The averaged results from the ozonisation of synthetic mixtures of lead acetate in the presence of manganese, zinc, and cadmium ions at various pH values are given in the table. (Theoretically the weight of the oxide precipitate was 0.398 g.).

Composition of initial mixture	pH of solution	Experimental weight of oxide precipitate, g
0.602 g $Pb(CH_3COO)_2 \cdot 3H_2O$ + 0.06 g $Mn(CH_3COO)_2 \cdot 4H_2O$ + 1.31 g $Zn(CH_3COO)_2$	6	0.415
	4	0.412
	2	0.254
	1	0.194
The same mixture, but 1.3 g of $Cd(NO_3)_2$ was added instead of $Zn(CH_3COO)_2$	6	0.403
	4	0.400
	2	0.236
	1	0.200

The results of the experiments show that at pH 6-3 divalent lead is precipitated by ozone together with manganese almost entirely in the form of compact heavy precipitates of the dioxides. The zinc and cadmium ions remain in the solution. Thus, the table illustrates the possibility of separating zinc and cadmium ions from lead by precipitation of the latter in the form of the dioxide with ozone as precipitating agent. Divalent manganese is readily oxidised by ozone in neutral and weakly acidic media and is precipitated as the dioxide [2]. This effect is used in practice for the removal of Mn^{2+} from drinking waters by ozonisation [3].

The catalytic action of manganese (II) additions can be explained in the following way. Ozone oxidises manganese (II) to manganese (IV) and then to manganese (VII). The latter oxidise divalent lead to tetravalent, being reduced back to manganese (II). The reduced divalent manganese is again oxidised by ozone and oxidises the lead, and the process is repeated. The proposed mechanism is confirmed by the oxidation of manganese (II) by ozone [2]) and by the oxidation of divalent lead by potassium permanganate solution in a moderately acidic medium. Thus, ozonisation of moderately acidic solutions of lead (II) salts in the presence of catalytic amounts of manganese (II) leads to rapid and quantitative oxidisation of the divalent lead to tetravalent and precipitation of the latter as the dioxide. The precipitate is separated from the solution by usual methods (filtration or centrifuging).

Conclusion

It was established that it is possible to precipitate divalent lead as the dioxide by means of ozone in neutral and moderately acidic medium in the presence of catalytic amounts of manganese (II) salts. Lead and manganese ions can be separated from zinc and cadmium by precipitation as the dioxides with ozone in a moderately acidic medium.

References

1) A F Chudnov and G V Kokhno: Izv. Vuz Tsvetnaya Metallurgiya 1975, (4).
2) I Marcy and F Matches: Chem. Technik 1967, 19, (7), 430.
3) V F Kozhinov and I V Kozhiniv: Ozone treatment of water. Stroiizdat, Moscow 1974.

Thus, the sulphide melts of iron and nickel, which were qualified as complex ionic-electronic polyfunctional conductors with a preponderance of the metallic contribution to the conductivity, can be reduced to a state where the ionic component of the conductivity becomes determining.

To confirm this conclusion experiments were set up on the electrolysis of melts with the following compositions, mole %: 35 FeS + 65 Na_2S; 3.5 Ni_3S_2 and 96.5 Na_2S. The electrolysis of the melts in both systems was realised at temperatures 500-600°C below the melting points of iron and nickel.

During the electrolysis of the FeS-Na_2S melts iron was released at the cathode. The current efficiency (η %) at 970°C amounted to 29% (cathodic current density d_c = 1.5 A/cm², voltage at the cell terminals 6-9 V). The current efficiency was reduced by a reduction in the cell voltage and also by departure of the current density from 1.5 A/cm².

The results from investigation of the dependence of the yield of the metal on temperature in nickel-sodium mattes at 900-1070°C showed that with other conditions equal (current density, voltage, electrolysis time) increase in temperature as a rule led to a decrease in the current efficiency.

Increase in the cathodic current density from 0.5 to 2.5 A/cm² was accompanied first by a smooth (from 14.0 to 11.6%) and, beginning with d_c = 1.5 A/cm², by a sharp decrease in the current yield of nickel to 2.0%.

The decrease in the yields with increase in temperature and current density must be attributed to the appearance of depolarisation effects, i.e., dissolution of the metal in the melt and reaction of the electrolysis products to form the initial compound.

Thus, the possibility of suppressing the electronic component of conduction in melts of liquid ionic-electronic (polyfunctional) conductors with clearly defined metallic type of conduction was demonstrated. By the introduction of heteropolar addition these melts can be reduced to the ion-conducting state and can be decomposed electrochemically into metal and sulphur. The results are significant for the electrochemical technology of the treatment of polymetallic sulphide ores which contain metals of the iron family.

References

1) A A Velikanov: Proceedings of All-Union Interuniversity Scientific Conference on the theory of processes in nonferrous metallurgy. Izd. Kaz. Politekhn. Inst., Alma-Ata 1971, p.318.
2) A A Velikanov et alia: Elektrokhimiya 1971, 7, (2), 203.
3) A A Velikanov: Author's Abstract of Doctoral Thesis. Kiev 1971.

UDC 542.943.5-546.815-

Precipitation of lead from aqueous solutions by ozone

A F Chudnov and G V Kokhno (Kuzbassk Polytechnical Institute - Dept. of General and Inorganic Chemistry)

A widespread method for the removal of lead iron (Pb^{2+}) from solutions is its precipitation in the form of poorly soluble compounds. The principle of the method is based on the reaction of divalent lead with sodium or potassium carbonates, sulphates, or sulphides. The most complete precipitation as applied to effluents is obtained with sodium carbonate as precipitant[1]):

$$Pb(NO_3)_2 + Na_2CO_3 \longrightarrow PbCO_3\downarrow + 2NaNO_3$$

The increased salt content is one of the disadvantages of the classical method of precipitation with the above-mentioned precipitatnts, particularly in hydrometallurgical processes during the separation of mixtures of cations.

We studied the reaction of ozone with Pb^{2+} in order to determine the optimum conditions for precipitation of the latter in aqueous solutions. Unlike known precipitants, ozone does not introduce extraneous impurities into the reaction medium and can be used for purification of lead-containing effluents, the separation of Pb^{2+} in the form of oxides from a mixture of cations in the solution, and for the production of lead monoxide and dioxide. Ozone oxidises lead hydroxide to the dioxide and lead sulphide to the sulphate[2]).

The work was carried out on an ordinary laboratory set-up. Ozonised air containing 6-10 mg of ozone per litre was bubbled through a porous glass partition into a solution of the lead salt. Aqueous solutions of divalent lead salts (acetate and nitrate of chemical purity) with concentrations of 0.5-50 g/l were used. The volume of the solutions was 200-500 ml, and the experiments were carried out at room temperature. The ozonised solutions were periodically analysed for Pb^{2+} content by a gravimetric method by reaction with sulphate ion. The figure shows the curves for the removal of Pb^{2+} from the solution during ozonisation.

It was established that the reaction of ozone with Pb^{2+} in aqueous solution depends on the pH of the medium. The reaction does not occur at pH<6. At pH 6-7.5 ozone reacts both with the hydroxide and with the salts of lead to form dark-brown lead dioxide PbO_2, which separates as a precipitate. The reaction evidently takes place according to the following scheme:

$$Pb(NO_3)_2 + H_2O + O_3 \longrightarrow PbO_2\downarrow + 2HNO_3 + O_2$$

The time required for complete precipitation of Pb^{2+} depends on the concentration of the reactants. Under the experimental conditions, for ecample, purification of 200 ml of a solution containing 1.5 g of $Pb(NO_3)_2$ required about 6 h. The ozone concentration was 5 mg/l, and the volume of ozonised air passed was 18 litres.

At pH 8-9 all the salt changes into white lead hydroxide. During ozonisation of such a solution a bright-yellow suspension of lead dioxide PbO is initially formed, and this then becomes orange and finally dark-brown lead dioxide PbO_2. Since the colour of lead oxides depends to some degree on the composition, the orange precipitate clearly has the formula Pb_2O_3 [3]). The formulae of the monoxide and dioxide were established by chemical methods.

In a more alkaline medium (pH 10-12) the lead hydroxide which initially separates when the solution is made alkaline dissolves completely in the excess of alkali to form a plumbite. Ozonisation of such a solution is accompanied by the formation of a bright-yellow precipitate of PbO. It is interesting that in this case there is no change in the degrees of oxidation of the reactants. The possible reaction scheme is as follows:

$$Pb(NO_3)_2 + 2NaOH + O_3 \longrightarrow PbO\downarrow + 2NaNO_3 + H_2O + 1\text{-}5O_2$$

In all three cases the oxides are formed rapidly and quantitatively, and the pH of the solutions is shifted into the acidic region. In a strongly alkaline solution (pH>14), as in an acidic solution, lead oxides are not formed.

The precipitated oxides take the form of finely dispersed homogeneous precipitates, which can be separated by centr

fuging or on a filter. Experiments showed that the most complete removal of Pb^{2+} from aqueous solutions with ozone is obtained by its precipitation in the form of the dioxide at pH 6-8. Here the residual concentration of Pb^{2+} amounts to less than 0.1 mg/l i.e., less than the maximum permissible concentration[4]). The monoxide is partly soluble in an alkaline medium, and it is not therefore advisable to use ozone for the precipitation of lead from effluents in solutions with pH ≥ 10.

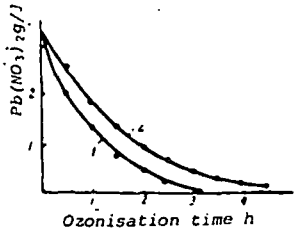

Curves for the precipitation of divalent lead by ozone: 1 - from a solution of lead nitrate in the form of the dioxide, pH 7; 2 - from a solution of sodium plumbite in the form of the monoxide pH 10.7. The plumbite was obtained by addition of sodium hydroxide to a solution of lead nitrate.

Conclusions

1. The possibility of removing divalent lead from aqueous solutions by precipitation with ozone in the form of monoxide and dioxide was demonstrated. The oxides are formed rapidly and quantitatively.
2. The most complete precipitation of Pb^{2+} is obtained in the form of the dioxide at pH 6-8.

References

1) L Hartinger: Metalloberfläche 1973, 27, (5), 157.
2) Encycl. of Industrial Chem. Anal., 1971, 16, 538.
3) Concise Chemical Encyclopaedia, Moscow 1965, 4, p.767.
4) V I Pryanikov (editor): Manual on the protection of labour and safety techniques in the chemical industry. Khimiya 1971, p.268.

UDC 621.357.13+669.73

Anodic behaviour of cadmium and its alloys with zinc in a eutectic melt of potassium and lithium chlorides

A V Volkovich, O G Potapenko, A N Semin, and I F Nichkov (Novomoskovsk Branch, Moscow Chemical-Technological Institute and Urals Polytechnic Institute)

In recent years interest in the problems of electrolytic refining of low-melting heavy non-ferrous metals in molten salts has increased. However, for the organisation of the technological processes it is necessary to undertake a detailed investigation of the kinetics of the electrode reactions. The present work was devoted to an investigation of the anodic dissolution of metallic cadmium and zinc-cadmium alloys in a eutectic mixture of potassium and lithium chlorides.

Cadmium of Kd-O grade and zinc of TsV grade conforming to GOST 3640-65 were used in the experiments. The salt melt was prepared from previously dried salts of chemical purity or analytical grade. The remelted, chlorinated, and vacuum-treated electrolyte was stored in tubes of pyrex glass. The electrolysis cell and the experimental procedure were similar to those described in the literature [1,2]). The anode potentials were recorded at the moment of disconnection of the polarising current by means of a digital electronic voltohmeter of the VK7-10A/1 type.

The results from polarisation potential measurements for binary alloys with various zinc contents at 500°C are shown in fig.1. With increase of the zinc content in the alloy the initial electrode potential is shifted towards the negative side. At current densities higher than 2.10^{-3} A/cm² linear sections, the extent of which increases with increase in the zinc concentration, are observed on the curves for the anodic dissolution of the alloys (curves 2-4). From comparison of the polarisation curves of the alloys and metallic zinc (fig.1, curve 1) it follows that these sections correspond to the ionisation potentials of zinc.

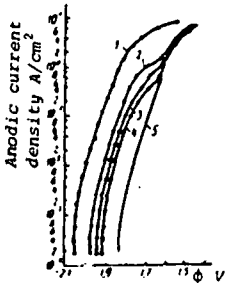

Fig.1 Polarisation curves for the anodic dissolution of Cd-Zn alloys at 500°C in KCl-LiCL melt. ϕ is the potential with reference to a chlorine reference electrode. Zinc content of alloy wt.% Zn: 1 - 100; 2 - 4.6; 3 - 1.1; 4 - 0.5; 5 - 0.0.

Increase of the current density leads to substantial changes in the surface layer of the alloy. The zinc dissolution rate becomes higher than its diffusion rate from the volume of the alloy to the anode/electrolyte boundary, and its limiting dissolution current is reached. Here the anode potential is displaced sharply towards the positive side, reaching values at which dissolution of cadmium occurs. This is seen from comparison of the polarisation curves of the alloys (fig.1 curves 2-4) and metallic cadmium (fig.1 curve 5).

Temperature has different effects on the kinetics of the anodic dissolution of cadmium and its alloys with zinc. For the pure metal the form of the polarisation curves does not change with increase in temperature. Only a regular displacement towards more electropositive potentials is observed. The self-dissolution currents of cadmium are insignificant and amount ot $2.8 \cdot 10^{-4}$, $3.9 \cdot 10^{-4}$, and $4.7 \cdot 10^{-4}$ A/cm² for 500, 600, and 700°C respectively. The presence of fluoride ions in the electrolyte does not have an appreciable effect on the electrode potentials. With a lithium fluoride content of 10 wt.% in the melt the potential of the cadmium becomes only 15-20 mV more negative.

For cadmium-zinc alloys the form of the polarisation curves changes with increase in temperature (fig.2). The limiting diffusion currents for the dissolution of zinc from its alloys with cadmium increase with increase in temperature, and at 700°C they disappear. This can evidently be explained by approach to a temperature close to the boiling point of cadmium (~700°C), when there is a sharp reduction in its viscosity and the conditions for the diffusion of zinc are improved. With increase in the current density to $(3\text{-}3.5) \cdot 10^{-2}$ A/cm² (curve 3) the ionisation potential of pure cadmium is reached (curve 4). Consequently, increase in temperature leads to more rapid attainment of the process of joint dissolution of zinc and cadmium.

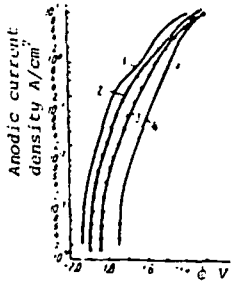

Fig.2 Temperature dependence of the anodic polarisation of Cd + 1.1 wt.% Zn alloy in KCl-LiCl melt at 500 (1), 600 (2) and 700°C (3) and of pure cadmium at 700°C (4).

From the obtained values of the limiting current for the dissolution of zinc (i_{lim}) with a knowledge of the concentration of zinc (C) and its diffusion coefficient in cadmium (D) it is possible to determine the thickness of the diffu-

2317.
6) M F Lantratov and E V Tsarenko: Zh. Fiz. Khim. 1972, 33, 1959.
7) M F Lantratov and A F Alabyshev: Zh. Fiz Khim. 1959, 33, 2429.
8) L S Darken: J. Am. Chem. Soc. 1950, 72, 2909.

UDC 669.2/8:661.482:621.039.32

Behaviour of the ions of some elements during sorption from HF, $NH_4F{\cdot}HF$, and NH_4F solutions with ion-exchange resins

V A Pakholkov and A S Suntsov (Urals Polytechnical Institute. Department of the Metallurgy of Rare Metals)

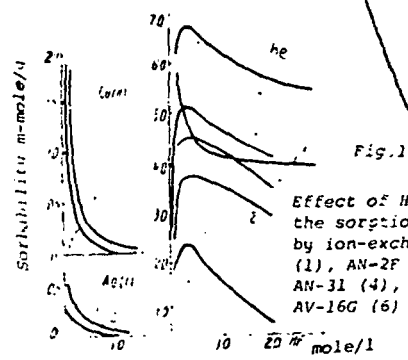

Fig.1 Effect of HF concentration on the sorption of Cu, Ag and Be by ion-exchange resins ÉDE-10P (1), AN-2F (2), AV-17 (3), AN-31 (4), AN-251 (5) and AV-16G (6) in the chloride form.

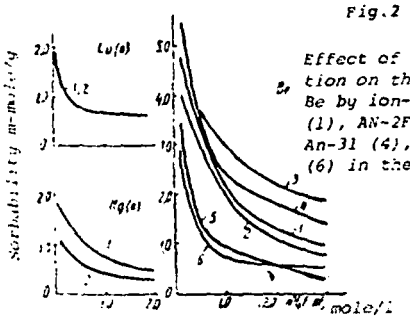

Fig.2 Effect of the $NH_4F{\cdot}HF$ concentration on the sorption of Cu, Hg and Be by ion-exchange resins ÉDE-10P (1), AN-2F (2), AV-16G (3), An-31 (4), An-251 (5) and AV-17x8 (6) in the chloride form.

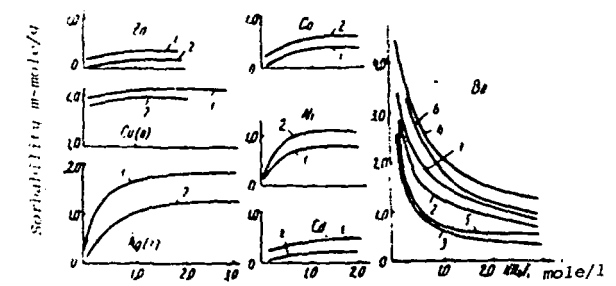

Fig.3 Effect of the NH_4F concentration on the sorption of certain elements by ion-exchange resins ÉDE-10P (1), AN-2F (2), AV-17x8 (3), AN-31 (4), AN-251 (5) and AV-16G (6) in the chloride form.

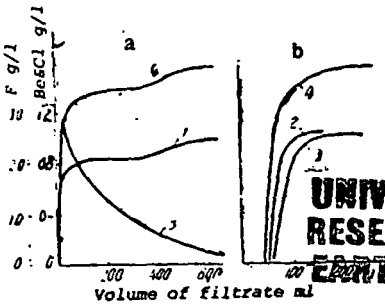

Fig.4 Output curves for the sorption of beryllium (1,2,3) and fluorine (4) by ion-exchange resin AV-17 in the chloride (a), fluoride (2), and carbonate (3)(b) forms and the curve for the displacement of the chloride ions from the resin during sorption (5).

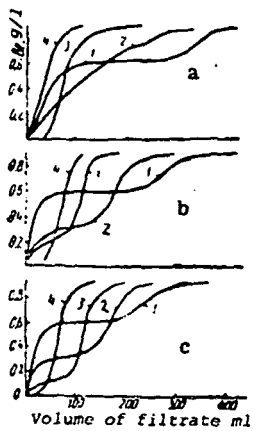

Fig.5 Output curves for the sorption of beryllium from 0.1M BeF_2 solutions with ion-exchange resins AV-17x8 (a), AN-2F (c), ÉDE-10P (b) in the chloride form. NH_4F concentration, m/l: 1 - 0.0, 2 - 0.1, 3 - 0.3, 4 - 1.0

Summary

Experimental data obtained during investigations of the sorption of some elements of groups 1 and 2 of the periodic system and also of cobalt and nickel from solutions of hydrofluoric acid, ammonium fluoride and ammonium bifluoride with various ion-exchange resins are given.

The results show that there is sufficient difference in behaviour in the sorption of beryllium, on the one hand, and the other elements investigated, on the other. This can be used in the production and purification of such important compounds as BeF_2, $(NH_4)_2BeF_4$, and Na_2BeF_4. The isolation, concentration and purification of beryllium in fluorine-containing solutions can be realised not only with strongly basic, but with weakly basic ion-exchange resins. It is necessary, however, to take account of the possibility of and the conditions for the absorption of metal cations through the formation of basic salts and complexes with the resin itself.

Sov. Non-Fe
1975 v.3 N3

UDC 669.712.1

Peculiarities of the leaching of KMA bauxites

A I Lainer (deceased), R G Gol'tseva and I V Nikolaev (Moscow Institute of Steel and Alloys. Department of Light Metals)

The increasing need for alumina has led to the search for new forms of alumina-containing raw materials. As a rule, this is low-grade material (high-silicon and high-iron), and an important task therefore is to develop rational technological schemes for its treatment.

The purpose of the present work was to study the char-

acteristics of the leaching of bauxites from the Belenikhin section of the Belgorod deposit of the Kursk magnetic anomaly (KMA). The KMA bauxite deposits are promising, being characterised by a high content of alumina, considerable reserves, and favourable geological geographical conditions. An average sample of the bauxites from the Belenikhin section had the following chemical composition: (%): 45.25 Al_2O_3, 10.46 SiO_2, 13.23 Fe_2O_3, 0.28 CaO, 0.93 MgO, 1.67 TiO_2, calcination loss 25.12; μ_{Si} = 4.32. The material composition of the bauxites is characterised by the presence of the following minerals: hydrargillite, chlorite, clay minerals and, to a lesser degree, quartz, pyrite, siderite, haematite and iron hydroxides.

Leaching was carried out in an alkaline solution having a concentration of 200g/l Na_2O_c, calculated to produce α_c = 1.5, for various times at 98 and 220°C. The pulp after leaching was submitted to filtration under vacuum. The filtrate together with the washing waters was collected in a measuring flask, and the slime was dried and weighed. The solution and the slime were subjected to chemical analysis, and the slime was in addition subjected to X-ray and thermographic analysis.

As shown by the leaching results, the extraction of aluminium oxide amounted to 70% at 98°C and 75% at 220°C. The red mud (composition %: 26.3 Al_2O_3, 18.6 SiO_2, 35 Fe_2O_3, 3.31 Na_2O, 2.35MgO, 0.15 MnO; μ_{Si} = 1.42), differed greatly from industrial muds in its alkali content. An alkali content below 4% indicated that it contained not more than 15-20% of hydrated sodium aluminosilicate[1]).

Investigation of the phase composition of the bauxites abd muds by X-ray diffraction method showed that undecomposed chlorite remains in the mud as a result of leaching (d/n = 7.06 and 3.46 Å). Thermal analysis of the muds from leaching of the bauxite showed the presence of an endothermic effect at 580°C, due to removal of water from the brucite layer of chlorite. Thus, the alumina not extracted during leaching (~12%) was represented by undecomposed chlorites and, to a slight degree, hydrated sodium aluminosilicate in the red mud. A red mud with such a composition is hardly ever encountered in the production of alumina by the Bayer method.

The group of chlorites combines minerals with extremely variable composition, largely reminiscent of micas. Minerals of this group can be characterised by the general formula $(Mg, Fe)_{6-x-y}(Al, Fe)_{x+2/3y}\{Si_{4-x}Al_xO_{10}\}(OH)_8$, which includes an equal amount of interbedded packages - mica and brucite (x = 0.75-2; y = 0.25-0.75). In both structural layers wide structural substitutions appears, and this gives rise to the existence of a large amount of mineral forms of chlorites: chamosite, daphnite, bavalite, thuringite etc.

Component	wt.%	Molecular amount x1000	Atomic amount of cations	No.of atoms of cations	W_c
SiO_2	15.60	260	260	1.78	7.12
Al_2O_3	26.38	259	518	3.55	10.65
Fe_2O_3	18.32	115	230	1.58	4.74
FeO	27.01	376	376	2.57	5.14
MgO	2.97	73.6	73.6	0.50	1.00
MnO	0.18	2.54	2.54	0.02	0.04
H_2O^+	9.54				
	100.00		1460	10.00	28.69

On the basis of chemical analysis of the chlorite entering into the composition of the bauxite from the Belgorod deposit and representing the red muds from its leaching the crystal-chemical formula of the chlorite was calculated in ten cations by the method of Borneman-Starynkevich[1]). Calculation of the formula of a mineral by this method is possible on the condition that the valence of the cations is equal to the valence of the anions. To calculate the formula of chlorite it is necessary to determine the valence of the anions (O, OH) the sum of which is 18. If the number of divalent oxygen atoms is denoted by X and the number of hydroxide ions by Y, the condition for equality of the valences of the anions and cations in the crystal-chemical formula of the chlorites is as follows:

$$W_c = W_a = 2X + (18 - X)$$

where:

W_c and W_a = the sums of the valences of the cations and the anions.

The number of oxygen atoms is them $X = W_c - 18$, and the number of hydroxide ions is $Y = 18 - X$.

By statistical analysis of the chlorites[3]) it was established that calcium and alkali do not enter into the structure of the chlorites, and they were not therefore taken into account in the calculation[2]). The results from chemical analysis of the chlorite and the conversion to the crystal-chemical formula are given in the table.

It was established that the red muds after the leaching of the Belgorod bauxites are represented by high-iron chlorites. The crystal-chemical formula of the red mud fits well into the structural formula of the trioctahedral chlorites and has the following form:

$$\{(Al_{1.38}Fe^{3+}_{1.58})(Fe^{2+}_{2.57}Mg_{0.50}Mn_{0.02})\}_6(Si_{1.78}Al_{2.22})_4[O_{10.69}(OH)_{7.31}]_{18}$$

The chlorite, present in the bauxite, and the red mud after leaching have similar chemical composition and a common crystal-chemical formula

Most effective for accurate diagnosis of iron-containing chlorites is thermal analysis of the sample in an inert atmosphere. This rules out the possibility of oxidation of ferrous iron, which makes it possible to assess the isomorphous $Mg\text{-}Fe^{2+}$ substitution. With heating in an atmosphere of nitrogen a strong endothermic effect is clearly recorded on the DTA curve at ~600°C, due to release of the structural water from the "brucite-like" layer, and this gives rise to the instability of the structure and the possibility of its rearrangement. At 800°C there is a weak endothermic effect, corresponding to removal of water from the "mica-like" layer, and this passes immediately into the exothermic effect of a phase transformation, corresponding to the formation of a new olivine structure.

Conclusions

1. The comparatively low extraction of alumina from KMA bauxites (not more than 75%) and the low alkali content of the red mud are due to the presence of iron-containing chlorites, which are not decomposed during the leaching process.
2. The results from chemical analysis and subsequence crystal-chemical calculation and also from X-ray and thermal analysis showed that the chlorite in KMA bauxites is represented by a high-iron form.

References

1) I D Borneman-Starynkevich: Manual on calculation of the formulae of minerals: Nauka, Moscow 1964.

2) E P Val'yashikhina et alia: Collection: The ideas of D S Belyankin in the region of petrography and mineralogy: Nauka, Moscow 1971.

3) K B Kepezhinskas: Statistical analysis of chlorites and their paragenetic types: Nauka, Moscow 1965.

Economic Geology
Vol. 74, 1979, pp. 377-388

The Potash-bearing Members of the Devonian Prairie Evaporite of Southeastern Saskatchewan, South of the Mining Area

NEIL WORSLEY AND ANNE FUZESY

Abstract

In southeastern Saskatchewan the uppermost 200 ft of Prairie Evaporite includes four groups of potash-bearing halite beds, the Esterhazy, White Bear, Belle Plaine, and Patience Lake Members. This sequence thins southward, although local thickening of members occurs where carnallite, not sylvite, is the dominant potash mineral.

Some boreholes penetrate anomalous sequences where beds normally potash bearing are halitic or missing. The distribution of these anomalies suggests tectonically unstable areas less favorable for the deposition of potash salts.

Major areas affected by complete salt solutioning are well defined seismically; localized areas of partial or complete salt solutioning appear fewer than farther north, but this could be a function of limited exploration of horizons below the petroliferous Mississippian.

Introduction

THE thin, deep, Devonian potash beds of southeastern Saskatchewan, not being of economic dimensions comparable to those found elsewhere in the province, tend to be neglected. They do, however, provide a stratigraphic link between the potash beds in Montana and North Dakota and the mining areas of Saskatchewan.

This study supplements Holter's 1969 report on the Prairie Evaporite of Saskatchewan. Holter had some misgivings about his correlations in the southeast where, at the time, well control was poor. Petroleum exploration has since added substantially to the number of deep tests available, although such wells, where drilled on geophysical targets, may reveal anomalies in the Prairie Evaporite rather than its normal development. One of the reasons for the initial slow development of the potash industry in Saskatchewan was the low potash values encountered in exploratory drilling of seismic anomalies which, as subsequently became apparent, are often basement-controlled areas of salt solutioning where the salt beds are partially leached.

Geographical and Geological Setting

The area examined (Fig. 1) lies immediately to the north of eastern Montana and western North Dakota. Southeastern Saskatchewan is more renowned for its Mississippian oil fields than for potash, although it was here, in 1942, that potassium salts were first identified in salt core from a depth of 7,653 feet in Norcanols Radville No. 1 well (Lsd. 16-36-5-19w2). Deep wells in this area that have penetrated the potash-bearing salt beds of the Prairie Evaporite now number close to 100. Many of these wells are concentrated within 50 miles of the international border, reflecting their primary economic objective, hydrocarbons. Over large areas, the Prairie Evaporite, particularly beneath Mississippian oil fields and near the Manitoba border, remains unexplored.

The Prairie Evaporite, pock-marked with solution hollows and downwarped toward the center of the Williston Basin in the south, is the massive remnant of a more widespread, thicker salt precipitated in an inland sea that in Middle Devonian time stretched diagonally across what is now the prairies, from the Peace River country of Alberta almost as far as the Red River. The arid climate led ultimately to extreme desiccation and the repetitive precipitation of potassium and magnesium salts in halite at the southeastern extremity of the basin.

In this part of Saskatchewan the Prairie Evaporite is between 3,000 and 9,000 ft below the surface. The underlying formation is the Winnipegosis and lying unconformably above the salt are the basal red and green mudstones of the Dawson Bay Formation. Total thickness is from 0 to over 500 ft; depositional variations are gradual, but more pronounced changes in thickness result from complete or partial solution, pre-Dawson Bay erosion, or underlying build-ups of Winnipegosis carbonates (Figs. 2 and 3). In the western part of the area the Hummingbird trough, a salt solution feature, separates a peninsula of salt from the main salt body to the east. The trough continues a few miles south into Montana.

Apart from a few localities, layered potash salts are present in the uppermost 200 ft of halite throughout southeastern Saskatchewan.

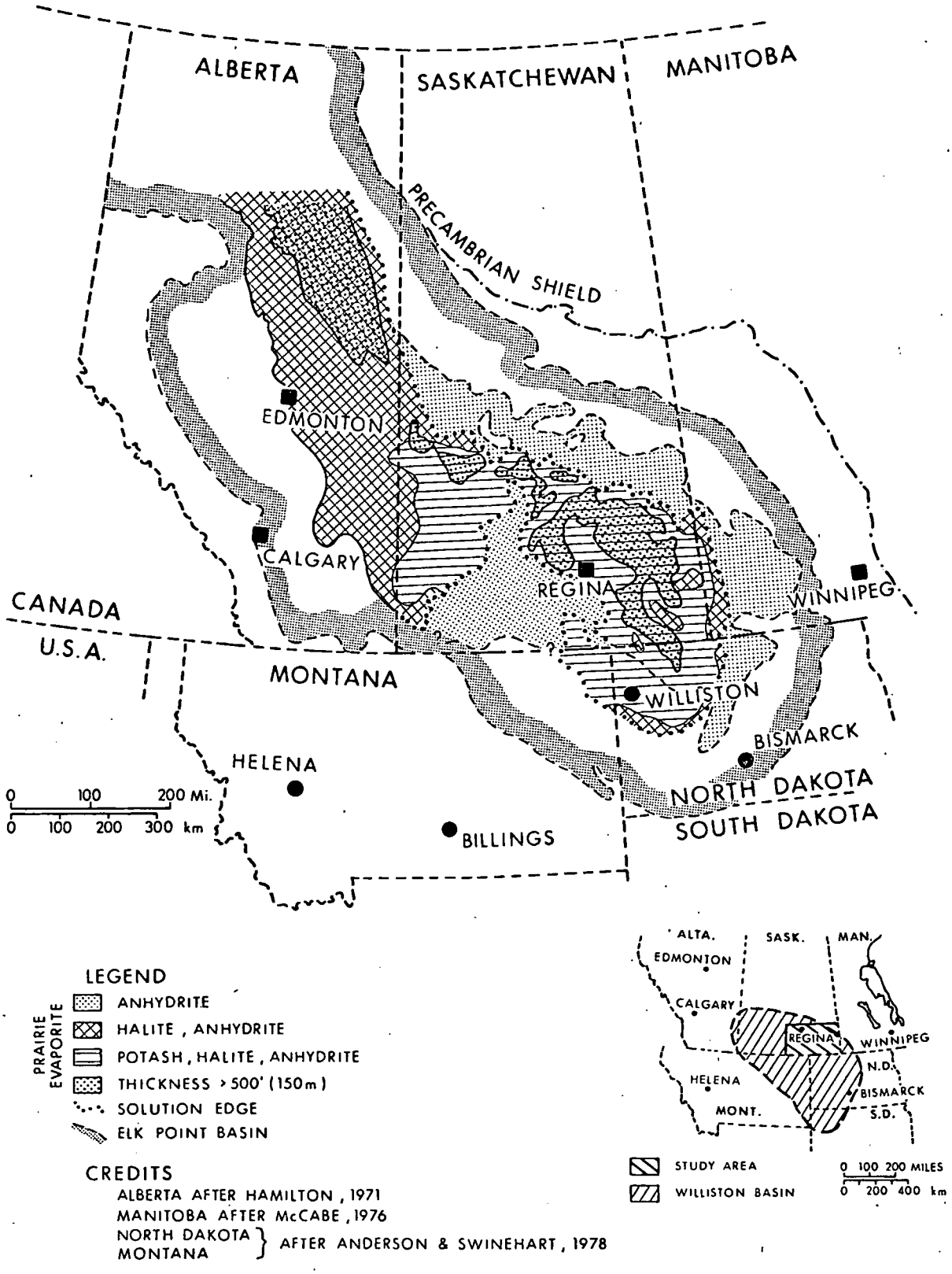

FIG. 1. Regional setting.

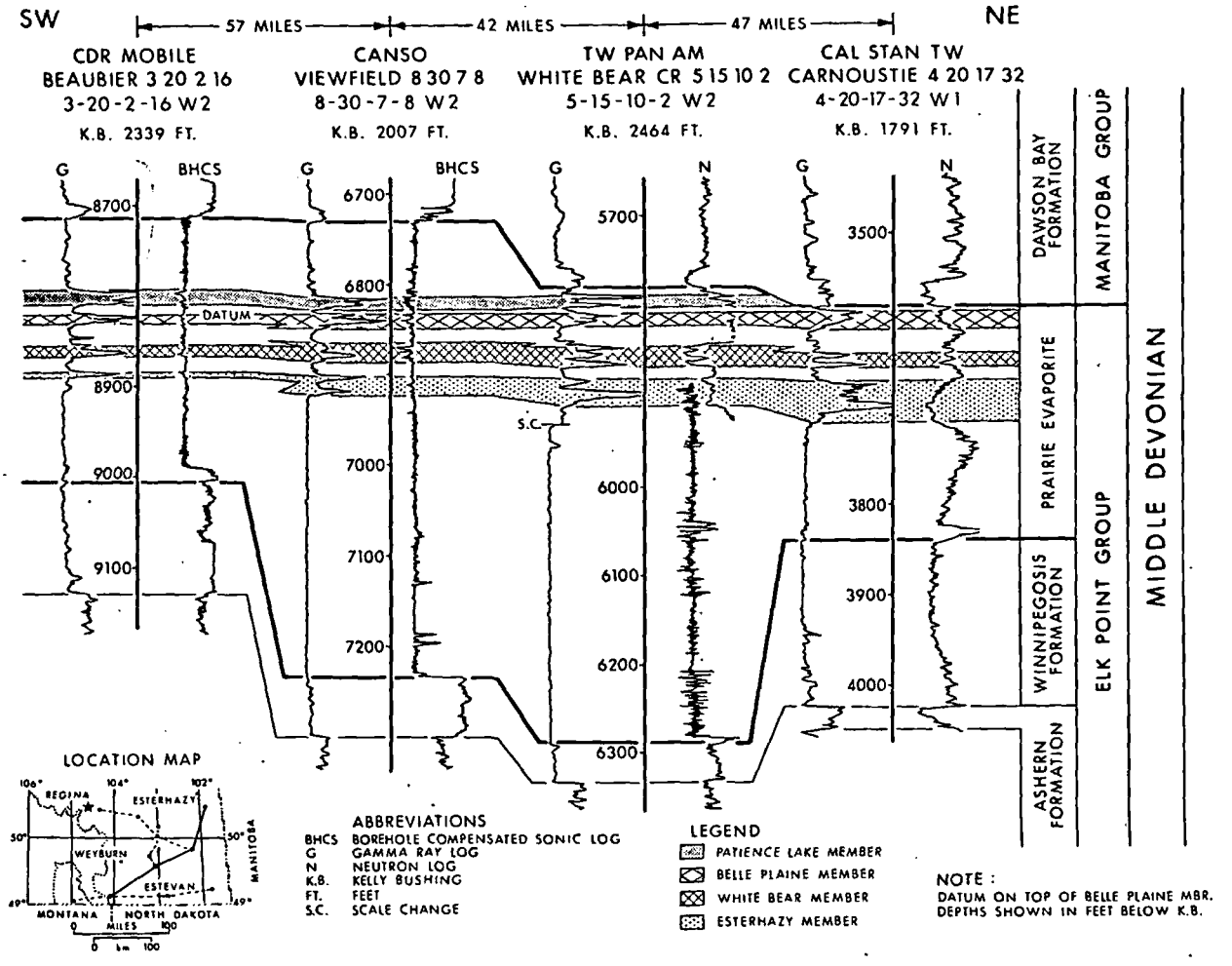

FIG. 2. Southwest to northeast stratigraphic cross section.

Scope of Study

Geophysical well logs of approximately 100 wells were interpreted in order to establish the southern stratigraphic equivalents of four groups of potash-bearing salt beds recognized farther north.

Previous Work

Much has been written about potash in Saskatchewan in the 36 years since its discovery, but most geological studies have concentrated on the area between Saskatoon and Esterhazy.

Goudie (1957) established potash zones, estimated reserves, and indicated the widespread effects of salt solution in the potash area of central Saskatchewan. Holter (1969) expanded this investigation and included the southern part of the province; his report remains the most comprehensive geological account of potash in Saskatchewan. Klingspor (1969) considered the interrelationships of the thicker halites of Alberta with those of Saskatchewan.

Other studies, although not pertaining to either potash or salt, include data relevant to the Prairie Evaporite since dissolution of the salt has a structural effect on overlying formations that is important in the search for hydrocarbons. Wilson et al. (1963), using seismic data, plotted a convoluted salt edge in southeastern Saskatchewan and the neighboring parts of Montana and North Dakota that has since required only minor modifications. The underlying Winnipegosis Formation has been examined by Jones (1965) and Fuzesy (1975). Nichols (1970) in his study of the Birdbear Formation in southeastern Saskatchewan presents an isopach of the Prairie Evaporite; computer-plotted versions of this and the underlying Winnipegosis are also available in Paterson (1973).

Nomenclature

The history of Middle Devonian nomenclature is discussed by Holter (1969, p. 10). He gave the names Esterhazy, Belle Plaine, and Patience Lake Members to three major, widespread, potash zones first recognized by Goudie (1957). The relatively

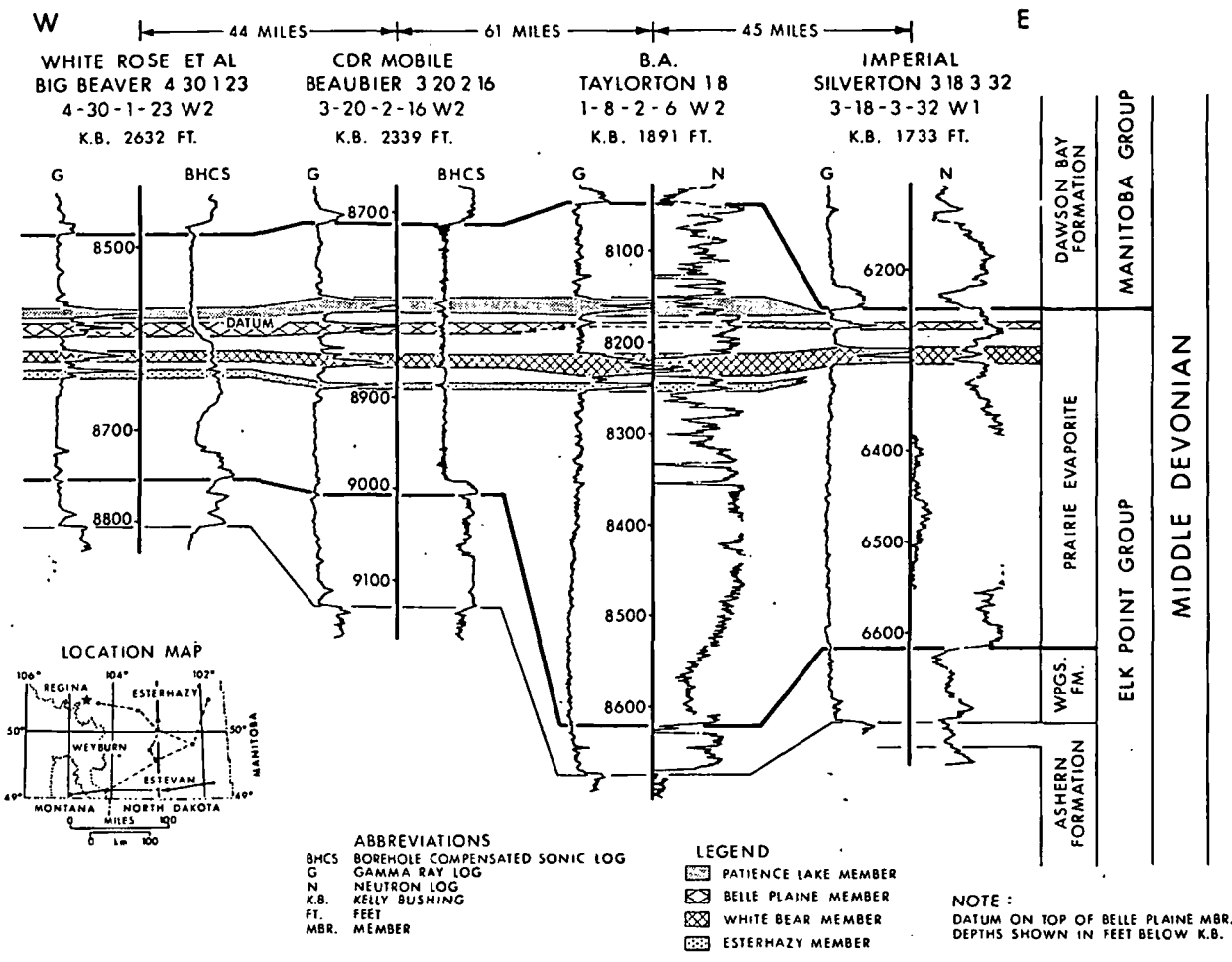

FIG. 3. West to east stratigraphic cross section.

barren halite beds between the potash members were referred to by Holter as interbeds. Thin potash beds midway through the Esterhazy–Belle Plaine interbeds proved to be important stratigraphic marker horizons and were termed the White Bear Marker Beds. In the southeast their development is comparable to that of the three named members (Fig. 4). In view of this similarity these beds are referred to in this paper as the White Bear member. (It is not being formally designated at this time since this paper is based only on a geophysical log study.)

Mineralogy

Salt core, or the suite of logs necessary for quantitative analysis, is rarely available in this area, but the uniformity of potash deposition observed farther north suggests that the mineralogy can be extrapolated southward.

Potash beds in the Prairie Evaporite have a simple mineralogy, consisting predominantly of halite (NaCl) with two potassium chloride minerals: sylvite (KCl) and carnallite ($KCl \cdot MgCl_2 \cdot 6H_2O$). Claylike material becomes increasingly prevalent upward in the succession, particularly in the Saskatoon region. It occurs in interstices between crystals, in partings, as thin seams, or in beds a few feet thick. Commonly referred to in analyses as insolubles, this material has been identified as largely quartz, dolomite, and anhydrite with minor quantities of clay minerals. Quartz and dolomite were dominant in the samples examined by Dunn (pers. commun., 1978), whereas in the sample analyzed by Dean (1971) the insoluble material was mainly anhydrite.

Salt Solution

Salt solution has virtually decimated the Prairie Evaporite in south-central Saskatchewan, an area sometimes referred to as the Swift Current platform, where only the insoluble portion remains. Salt removal of this magnitude has had a pronounced effect on the structure of overlying formations enabling its extent to be estimated from seismic structure contour maps of younger horizons (see Wilson et al., 1963). The salt edge shown in Figure 5 marks the eastern

limit of this salt-free salient and its tributary feature, the Hummingbird trough.

Within the main body of the Prairie Evaporite localized areas of salt solution can also be identified on seismic maps; in those that have been drilled, the soluble fraction of the Prairie Evaporite is missing. For example, in Tidewater Imperial South Kisbey Crown well 16-34-7-6 (Lsd. 16-34-7-6w2) there are 34 ft (Holter, 1969, p. 66) of Prairie Evaporite, largely dolomite and anhydrite. A well near Torquay (Lsd. 2-4-4-11w2) and other wells to the west of the Hummingbird trough reveal other localized salt-free areas (indicated in Fig. 5); some of these are not visible on regional seismic maps. This suggests that, whereas these maps show fewer anomalies within the Prairie Evaporite of southeastern Saskatchewan than farther north, the difference may be illusory.

There may be a relationship between carbonate mounds in the Winnipegosis and loss of salt, as suggested by Gendzwill (1978): for example, two wells drilled near Langbank (Township. 12, Range 2w2) penetrated barely 100 ft of Prairie Evaporite above a thick Winnipegosis section.

Member Distribution and Thickness

Wells selected by Holter as typical of the Esterhazy Member and the White Bear Marker Beds are located in the southeast and have been included in Figure 2 (Lsd. 4-20-17-32w1 and Lsd. 5-15-10-2w2, respectively). The type sections of the Belle Plaine and Patience Lake Members are farther to the northwest, outside the area studied.

The areal extent of the potash-bearing members is shown in Figure 6. In compiling this map the Esterhazy, Belle Plaine, and Patience Lake Members

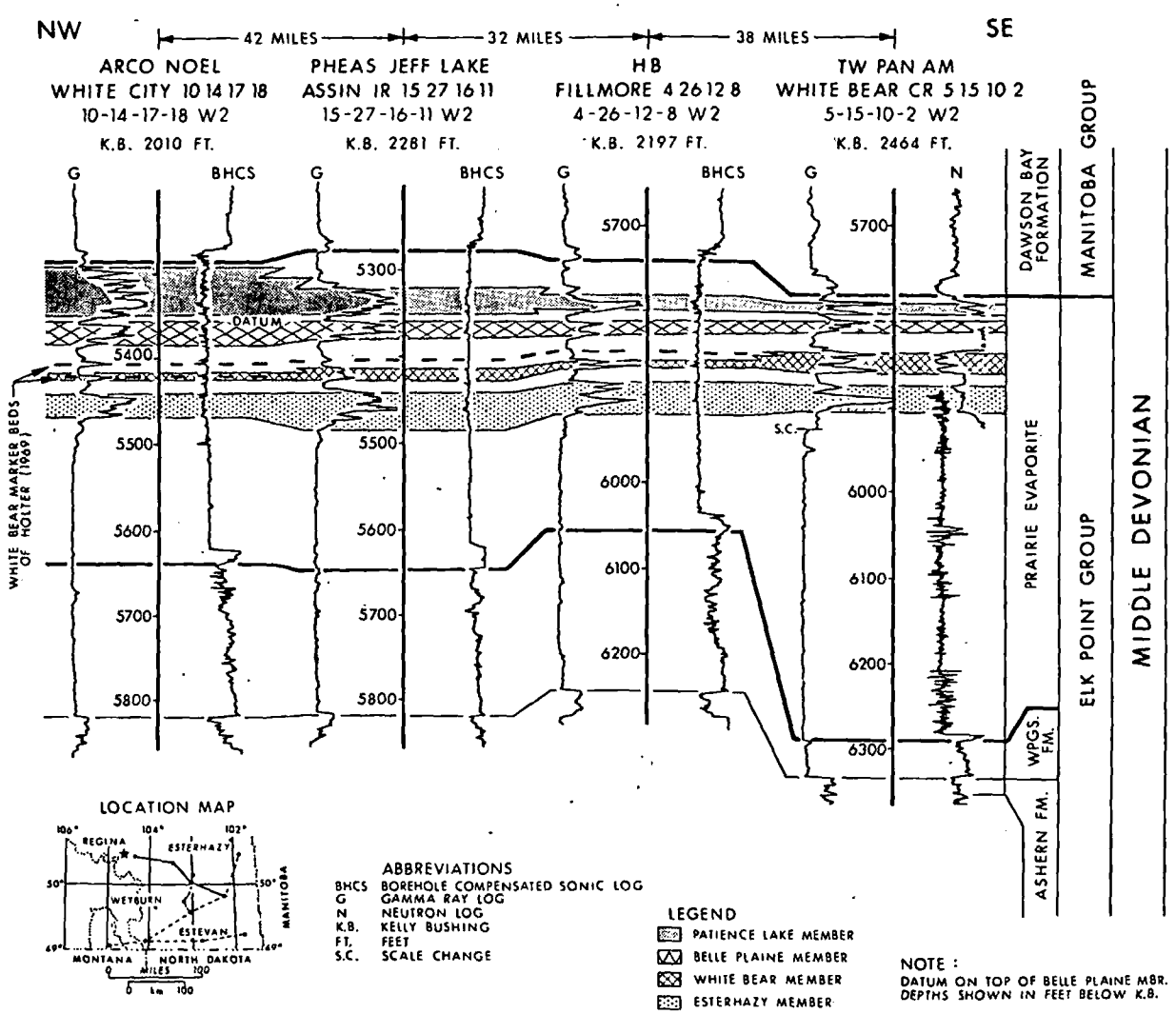

FIG. 4. Relationship of White Bear member (this paper) and White Bear Marker Beds (Holter, 1969).

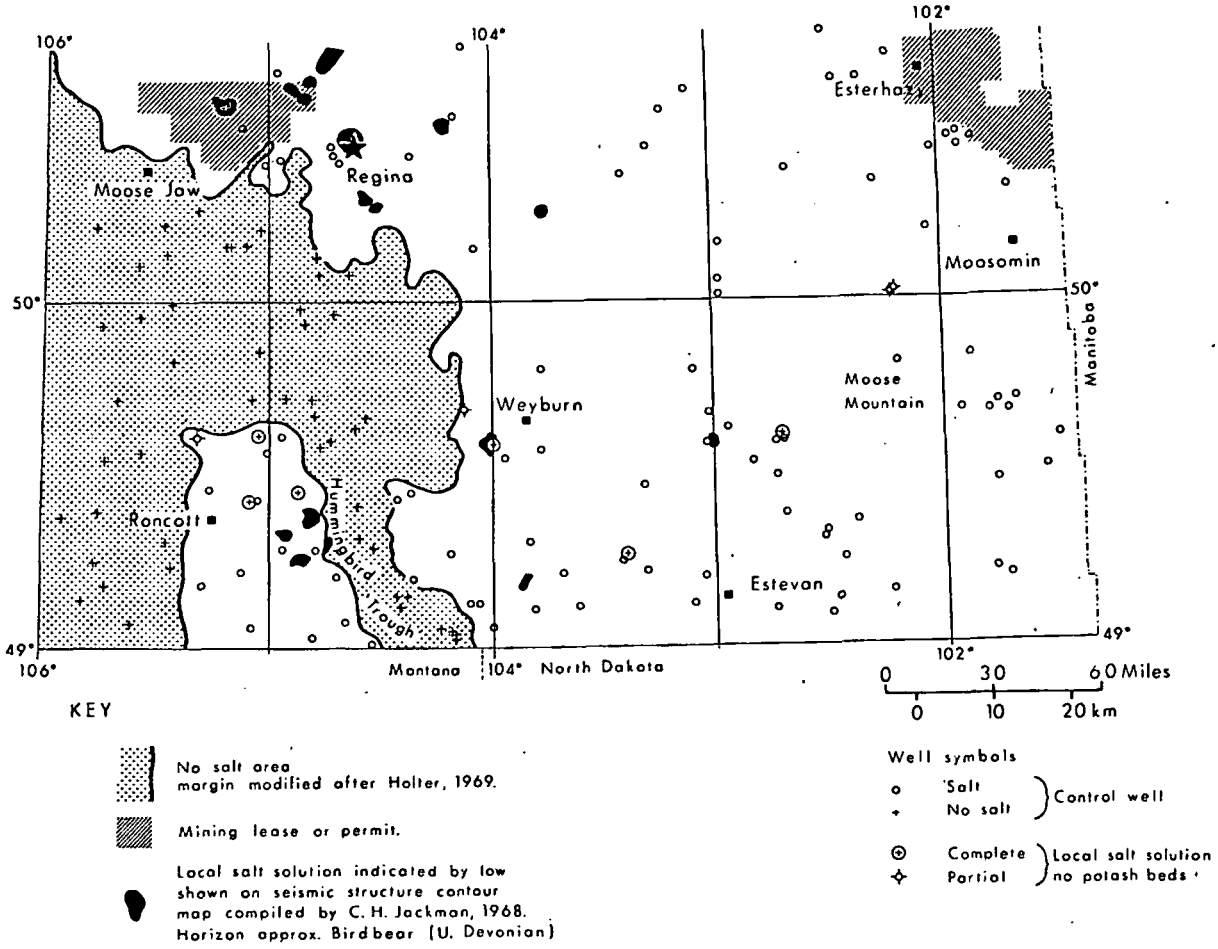

FIG. 5. Areas of complete salt solutioning resulting in loss of potash beds.

were traced laterally until the last, most persistent, component potash bed feathered out. Beyond this point, although it is possible to recognize on a log a laterally equivalent halite section, the member as defined is not mappable. The Esterhazy Member differs slightly from the other two in that it is defined to include a weakly potassic basal section; this has an inflationary, somewhat misleading effect on thickness values but little bearing on distribution since the edge mapped represents the limit of potash-rich halite. In this respect, the White Bear member was mapped using the same criteria, thus delineating the area where this unit is potash bearing.

Comparing the edges in Figure 6, which represent the zero isopach for each member, there is an evident similarity in the distribution of successive members. Changes in areal extent from that mapped by Holter (1969, figs. 12B and 14A to C) arise from new wells and, in a few cases, a reinterpretation of some of the earlier data. It becomes apparent from detailed correlations that individual potash members are more widespread and more consistent in thickness than had previously been thought.

Isopach maps of the individual members are shown in Figures 7 through 10. In areas where carnallite rather than sylvite is present, as deduced by the shift to the left of the neutron log trace, members may be thicker than average. This is especially noticeable in the Moose Mountain area. Some anomalous "thicks" on earlier isopach maps, however, have been created by mistaking two members, brought together by interbed thinning, for a single thickened member. An example of this can be seen in Figure 3 where the logs for the British American Oil Company well Taylorton 1–8 (Lsd. 1-8-2-6w2) show only a few feet of barren halite separating the Esterhazy and the White Bear potash beds. Most of the White Bear in this well was previously included with the Esterhazy Member. Throughout much of southeastern Saskatchewan the White Bear has thickened at the expense of the adjacent interbeds.

In the area reviewed, the Esterhazy and Patience Lake Members may be up to 50 ft thick; the White Bear and Belle Plaine Members are thinner, with a maximum approaching 30 ft. Apart from the White Bear, the members are thickest in an area southeast

of Regina and north of Weyburn, while all four members are well developed in the vicinity of Moose Mountain, the White Bear type area. An equally thick development of the White Bear potash beds is present near the international border, north and east of Estevan.

All the potash members thin gradually to the southwest as is clearly illustrated by the two lower members, the Esterhazy and White Bear, in Figure 2. By correlating clay markers an individual potash bed can be traced laterally into an equivalent halite bed. In the extreme southwest, near Roncott (Fig. 9), the zero edge of the White Bear marks its lateral passage into barren halite. Elsewhere in the west the potash members, although impoverished, appear to extend as far as the salt edge. This observation is somewhat at variance with that of Klingspor (1969, p. 947) who, in discussing whether or not salt formerly extended over the Swift Current platform, reports that "all the potash beds . . . show consistent thinning and phase out into halite before the edge of the salt is reached."

The eastern limits of the members are partly depositional, reflecting a facies change to halite, although beveling by pre-Dawson Bay erosion has affected the Patience Lake Member and, over a lesser area, the Belle Plaine Member. There is also some evidence of earlier erosion and possible channeling following potash deposition. An example of this is shown in Figure 11 where potash-bearing beds above the White Bear are missing in Imperial Kegworth 3-14-14-8, yet the uppermost halite beds are typical of those normally found above the Patience Lake Member, as in Canso Viewfield 8-30-7-8, to the south. The areal extent of this erosion, or its linearity, is conjectural without supporting seismic or well data.

Apart from the anomalous salt-free localities indicated in Figure 5 and discussed previously, there are three separate, wider areas where all or most potash beds are absent. Halite is dominant in an area alongside the international border west of Estevan, where attenuation of the surrounding potash members accompanied by no loss of salt section indicates non-

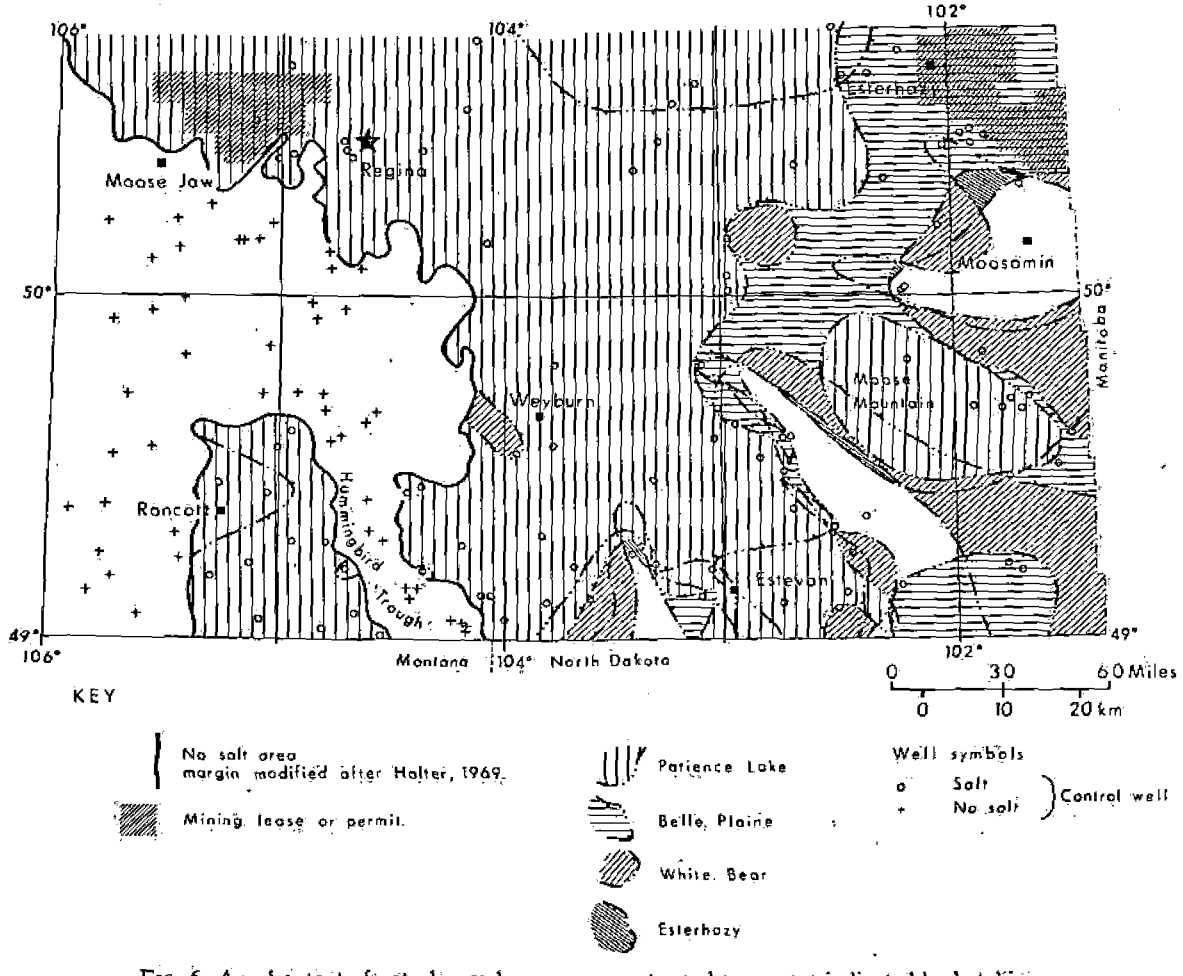

FIG. 6. Areal extent of potash members: uppermost member present indicated by hatching, member limits by dash-dotted lines as shown in legend.

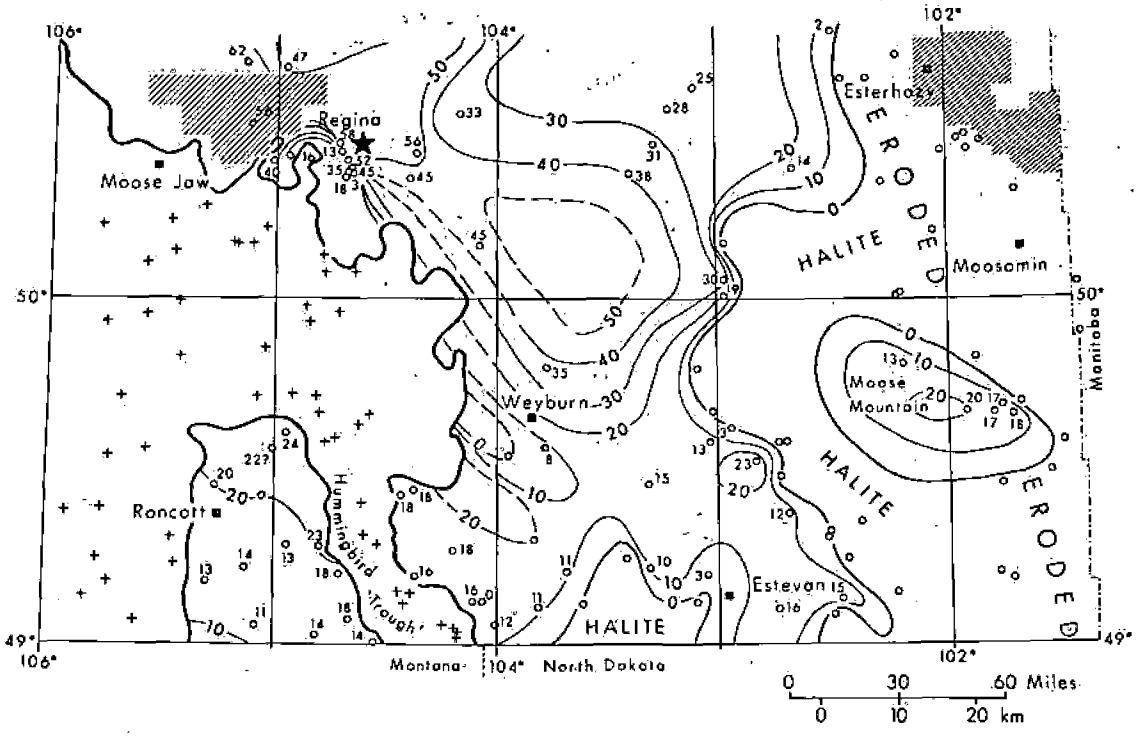

FIG. 7. Isopach map of Patience Lake Member of the Prairie Evaporite; values shown are member thickness in feet, other symbols same as Figure 6.

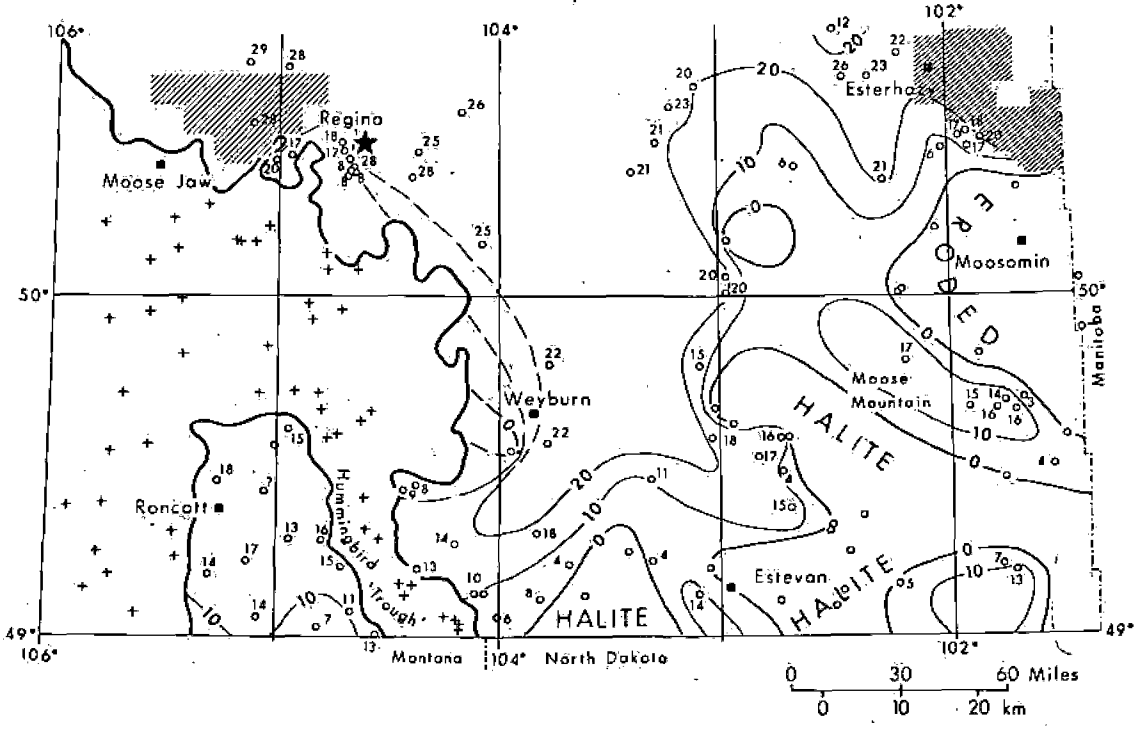

FIG. 8. Isopach map of Belle Plaine Member of the Prairie Evaporite; values shown are member thickness in feet, other symbols same as Figure 6.

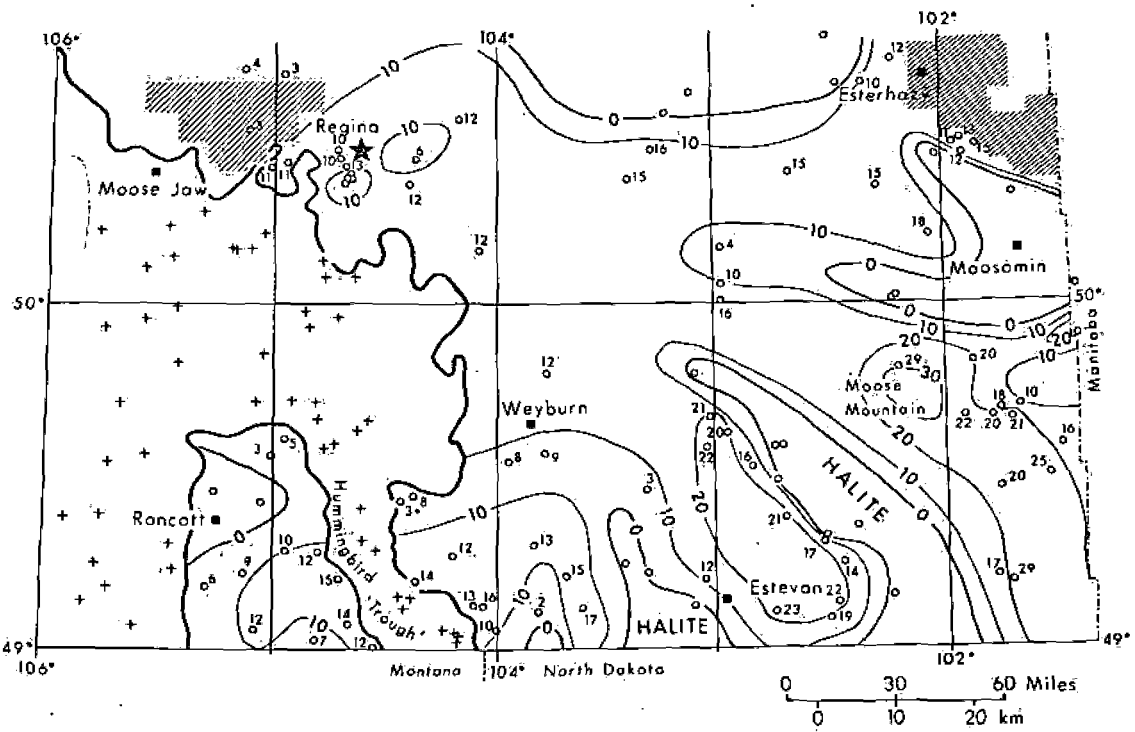

FIG. 9. Isopach map of White Bear member of the Prairie Evaporite; values shown are member thickness in feet, other symbols same as Figure 6.

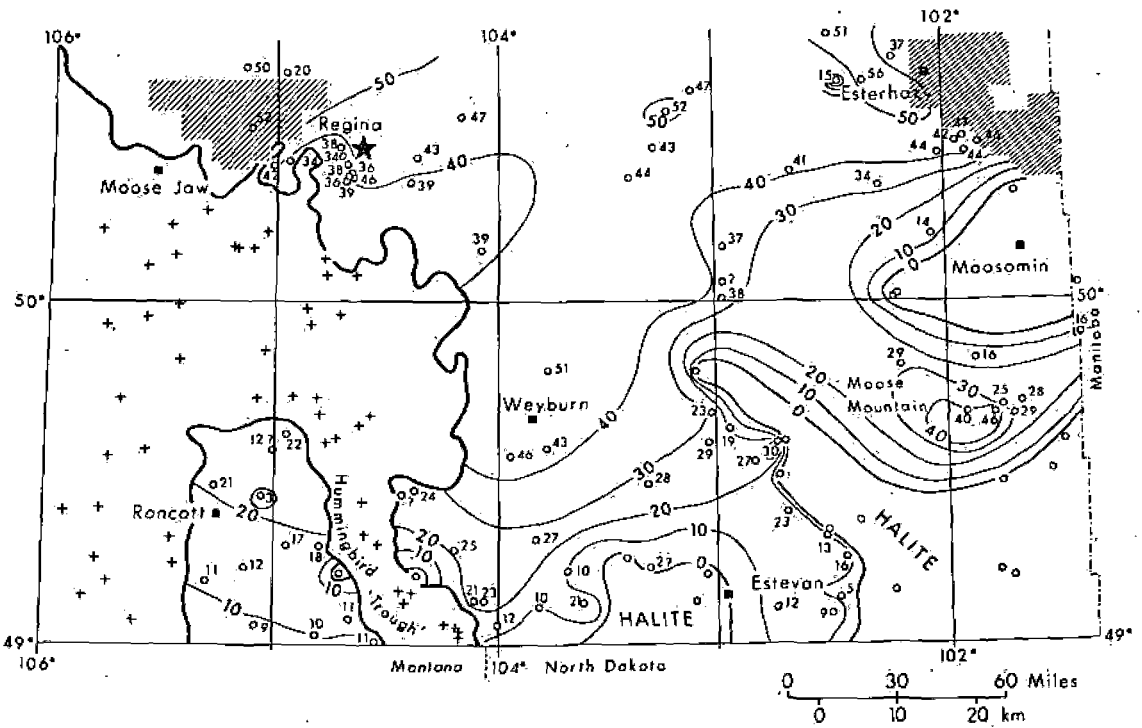

FIG. 10. Isopach map of Esterhazy Member of the Prairie Evaporite; values shown are member thickness in feet, other symbols same as Figure 6.

deposition. A similar situation occurs in an elongate area, extending northwestward from the southeast corner of the province, although in the east there has also been erosion of the upper salt beds (see Imperial Silverton 3-18-3-32 in Fig. 3) and the White Bear and Belle Plaine Members are locally present (Figs. 8 and 9, respectively). The third area is at the Manitoba border around Moosomin, also a combination of nondeposition and erosion of the upper beds.

Isopach maps suggest structural control, although it must be borne in mind that the majority of wells are probably testing geophysical targets, and the results obtained may, therefore, have an unknown bias.

Tectonics

Lines of weakness between basement blocks may have provided the loci for subsequent salt removal. Such controls have been discussed by several authors, e.g., Wilson et al. (1963) and Kent (1974). Linearity and angularity suggestive of control by basement lineaments are best observed in the salt edge southwest of Regina and flanking the Hummingbird trough and in the alignment of salt solution features (both drilled and indicated by seismic data) in the Roncott area (Fig. 12).

The limits of potash members shown in Figure 12 suggest the outlines of potash basins or pans. Their prominent northwesterly and less prominent northeasterly grain, and their tendency to recur in the same place, could be attributed to the influence of basement tectonics, with the tilting and differential vertical movement of basement blocks controlling potash deposition and preservation. These movements, perhaps stimulated by tilting in response to continued

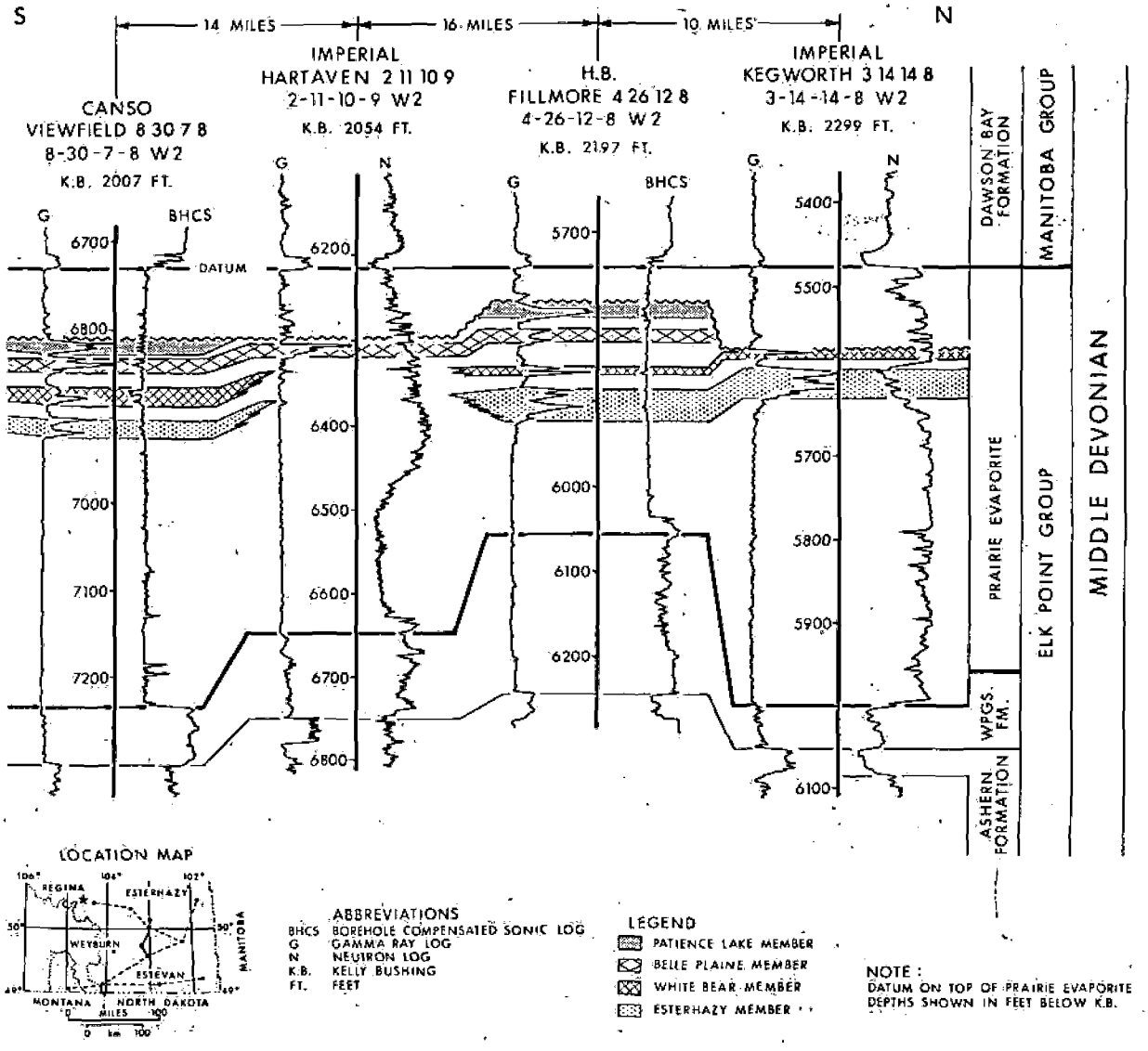

FIG. 11. North-south stratigraphic cross section illustrating the possibility of intraformational erosion within the Prairie Evaporite.

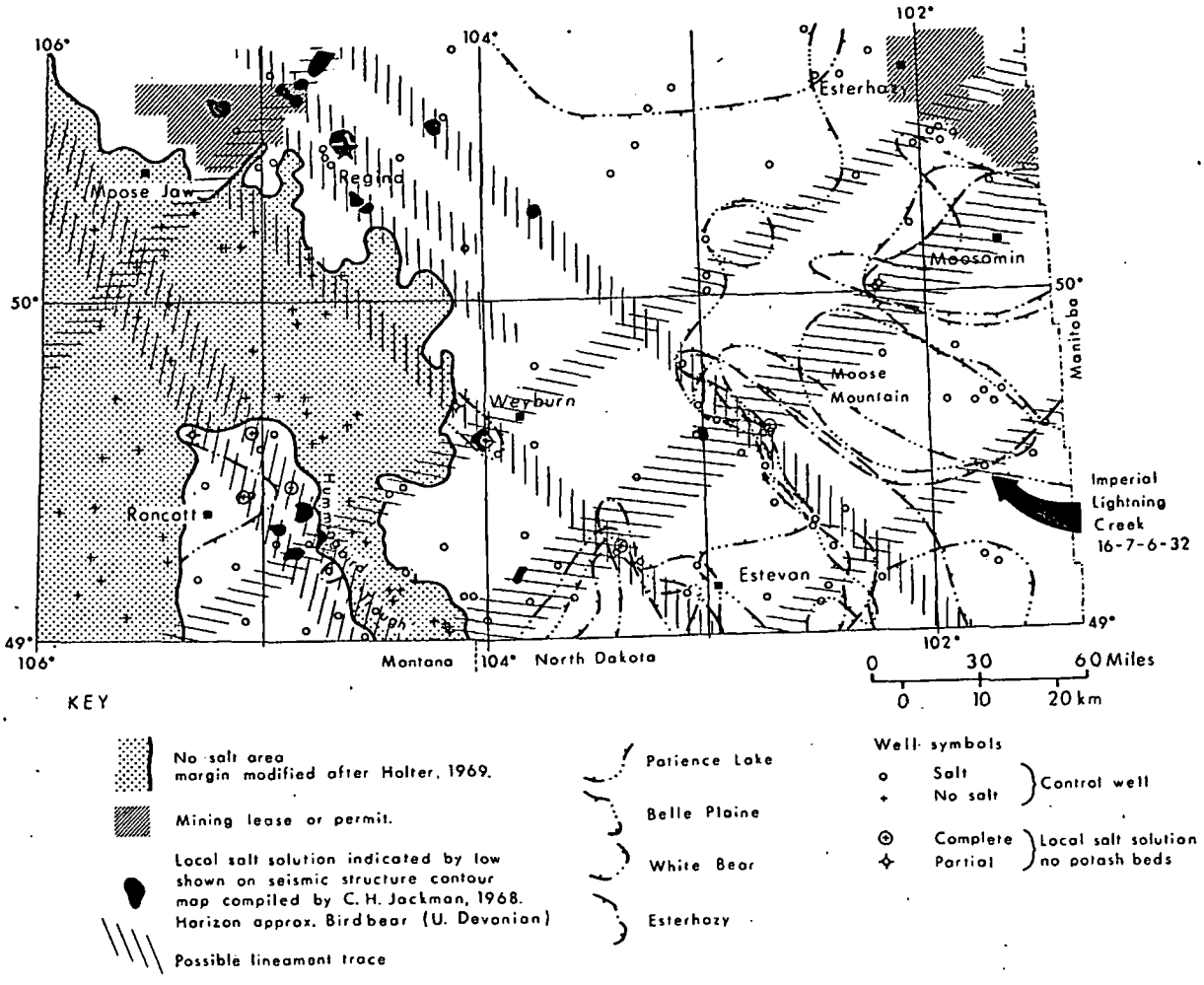

FIG. 12. Controlling lineaments suggested by salt solution features and outlines of potash members.

subsidence of the Williston Basin, created negative areas where bitterns collected and positive areas characterized by nondeposition and erosion. The effects of erosion, including the truncation of some potash members, are most noticeable in the relatively raised areas in the east.

Basement control is evident at the southeastern limit of the Esterhazy Member (Fig. 12), marked by a facies change to halite (Fig. 3). This depositional limit appears to coincide with structural anomalies in Imperial Lightning Creek 16-7-6-32w1, in which the absence of the Ordovician Winnipeg Formation and an unusually thin Cambrian Deadwood Formation were noted by Paterson (1971), and repetition of part of the Ordovician Big Horn Group was described by Kendall (1976).

Economic Potential

Because of the depths involved, recovery of potash minerals from most of the area under consideration would require solution rather than conventional mining methods. The data presently available, sometimes suggesting little potash potential, result from exploratory drilling of structural anomalies for oil and gas. Therefore, other less structurally disturbed areas not tested for hydrocarbons should be evaluated for potash when Saskatchewan's reserves need to be augmented. The largely unexplored area lying to the southeast of Regina and north of Weyburn is promising in this regard. Most of the potash members are apparently well developed in this area and the poor well control may itself be an indication of the absence of significant geophysical anomalies.

Conclusions

In southeastern Saskatchewan the four potash members recognized are more widespread and consistent in thickness than had previously been thought. Their areal extents are similar, curtailed in the west by solution and in the east by nondeposition and erosion. Thickness trends are also similar in all members and parallel to those of the Prairie Evaporite as a whole. Local thick areas occur when members are carnallitic. Evidence of depositional margins

is scant but indicates nondeposition was restricted to three separate areas.

Basement tectonics influenced both potash deposition and its preservation. Tilting or relative uplift has caused truncation of the salt beds in the east, most noticeably beneath the Dawson Bay Formation. Salt dissolution has emphasized lines of weakness created by basement movement.

Drilling based on geophysical targets may introduce an unknown bias into Prairie Evaporite data and thus have a nonquantifiable effect on its interpretation. The presently defined boundaries will be subject to modification; future drilling may show areas of nondeposition to be more restricted and locate more salt solution features.

Acknowledgments

This paper was originally presented in September 1978 at the Williston Basin Symposium hosted by the Montana Geological Society. The guidebook issued at the meeting contains a slightly abbreviated version of the paper presented.

Many thanks are due to D. B. Wolf and J. R. Evans for the timely redrafting of the figures and to D. F. Paterson and C. E. Dunn for suggesting improvements to an earlier manuscript. This paper is published with the permission of the Saskatchewan Department of Mineral Resources.

MINES BRANCH
SASKATCHEWAN DEPARTMENT OF MINERAL RESOURCES
REGINA, SASKATCHEWAN, CANADA S4P 4V4
November 22, December 4, 1978

REFERENCES

Anderson, S. B., and Swinehart, R. P., 1978, Potash salts in Williston Basin, U. S. A.: ECON. GEOL., v. 74, p. 358–376.

Dean, R. S., 1971, Clay mineralogy of a sample of sylvite ore from Duval Corporation mine, Saskatchewan: Canada Dept. Energy, Mines, Resources, Mines Br., Inv. Rept. 71–19, 17 p.

Fuzesy, L. M., 1975, Geology and hydrocarbon potential of the Winnipegosis Formation in southeastern Saskatchewan, *in* Christopher, J. E., and MacDonald, R., eds., Summary of Investigations 1975 by the Saskatchewan Geological Survey: Saskatchewan Dept. Mineral Resources, p. 66–70.

Gendzwill, D. J., 1978, Winnipegosis mounds and Prairie Evaporite Formation of Saskatchewan—seismic study: Am. Assoc. Petroleum Geologists Bull., v. 62, p. 73–86.

Goudie, M. A., 1957, Middle Devonian Prairie Evaporite of Saskatchewan: Saskatchewan Dept. Mineral Resources, unpub. rept., 81 p.

Hamilton, W. N., 1971, Salt in east-central Alberta: Research Council of Alberta, Bull. 29, 53 p.

Holter, M. E., 1969, The Middle Devonian Prairie Evaporite of Saskatchewan: Saskatchewan Dept. Mineral Resources, Rept. 123, 133 p.

Jackman, C. H., 1968, Seismic contour maps SC-series (top Birdbear): Saskatchewan Dept. Mineral Resources.

Jones, L., 1965, The Middle Devonian Winnipegosis Formation of Saskatchewan: Saskatchewan Dept. Mineral Resources, Rept. 98, 101 p.

Kendall, A. C., 1976, The Ordovician carbonate succession (Bighorn Group) of southeastern Saskatchewan: Saskatchewan Dept. Mineral Resources, Rept. 180, 185 p.

Kent, D. M., 1974, The relationship between hydrocarbon accumulations and basement structural elements in the northern Williston Basin, *in* Parslow, G. R., ed., Fuels: a geological appraisal: Geol. Soc. Saskatchewan, Spec. Pub. 2, p. 63–79.

Klingspor, A. M., 1969, Middle Devonian Muskeg evaporites of western Canada: Am. Assoc. Petroleum Geologists Bull., v. 53, p. 927–948.

McCabe, H. R., 1976, Structure contour and isopach map, Devonian-Prairie Evaporite Formation; stratigraphic map series Dpe-1: Manitoba Dept. Mines, Mineral Resources Div.

Nichols, R. A. H., 1970, The petrology and economic geology of the Upper Devonian Birdbear Formation in southeastern Saskatchewan: Saskatchewan Dept. Mineral Resources, Rept. 125, 93 p.

Paterson, D. F., 1971, The stratigraphy of the Winnipeg Formation (Ordovician) of Saskatchewan: Saskatchewan Dept. Mineral Resources, Rept. 140, 57 p.

—— 1973, Computer plotted isopach and structure maps of Devonian formations in Saskatchewan: Saskatchewan Dept. Mineral Resources, Rept. 164.

Wilson, W., Surjik, D. L., and Sawatzky, H. G., 1963, Hydrocarbon potential of the south Regina area, Saskatchewan: Saskatchewan Dept. Mineral Resources, Rept. 76, 17 p.

SUBJ
MNG
PND

PUBLICIZING NEW DEVELOPMENTS IN METALLURGY OF THE RARE METALS

UDC 669.27/.87

E. P. Bochkarev

L. Ya. Krol'

L. E. Bolotnikov

The tasks of non-ferrous metallurgy in the first years of Soviet power were clear. The country could not be industrialized without Soviet copper, lead, zinc, aluminum, tin, nickel, and precious metals. The necessity for developing our own industry was obvious.

The metallurgy of the rare metals orginated in a different way. At that time it was still difficult to answer the question as to what any rare metals were specifically required for or whether it was worth working on them when there was a shortage of resources and specialists. However, only a visionary could have predicted the technical revolution, with its indispensible condition: the development of the rare metals industry.

Of course it was impossible during the first years of industrialization to predict the true future or to imagine the far-reaching changes in technology; however, the Supreme Council for the National Economy recognized the necessity for work on new substances, because that which is new always has within it exceptional and often unexpected possibilities.

This journal was the publication which drew the attention of the engineering community to the new and apparently not very important or well-known metals, as well as dealing with the urgent problems in non-ferrous metallurgy.

As is well known, the term "rare metals" is a provisional one and does not reflect the concentration of the elements in the earth's crust (titanium is 600 times more abundant than copper).

In the 1930s, with minor exceptions, metals which could not yet be extracted and the applications and properties of which were insufficiently known were included among rare metals. Mercury, antimony and bismuth (the minor metals) were also assigned to the rare metals group because the content of these metals in non-ferrous metal ores was very low.

The appearance in the journal of material on particular problems in the technology of the rare elements and in organizing their production reflected both the history of development of research on rare metals and their production and application and the history of changes in the "rare metals" concept itself.

During the first years of industrialization, tungsten and molybdenum were required for the electric lamp industry and for hard alloys. Antifriction alloys and storage cells could not be manufactured and printing presses could not operate without Soviet antimony.

In its early years the journal "Tsvetnye Metally" published papers by G. A. Shakhov and Ya. Ya. Slobodskii entitled "Processes for Producing Antimony and its Oxides from Ores" (1930, No. 10) and "Study of Pyrometallurgical Methods of Processing Lean Antimony Ores" (1932, No. 4). These publications were timely in that they explained a paradoxical phenomenon: the reduction of antimony extraction when the temperature of distillation roasting rose. The authors demonstrated the conditions of non-volatile tetroxide formation when the CO content of the furnace gases was low. The publication was of great practical importance. Equally vital problems in the technology and subsequent effective utilization of antimony in the storage cell industry were considered in a paper by N. A. Izgaryshev and S. A. Pletnev (1931, No. 4).

The journal published a paper by K. A. Bol'shakov (1931, No. 4) describing a simple method for determination of vanadium in iron ores; this made it possible to organize correct ore sorting and so to extend the ore resources of the metal, which was essential for the production of high-speed steels and which has now also been transformed into a vital structural material for the most important branches of technology.

The journal has published material on a wide range of problems connected both with production and with information on the properties of materials based upon rare metals or employing those metals. An example of this is provided by the abstract by A. Lyubimov (1930, No. 3).

During the pre war years the journal "Redkie Metally" appeared alongside "Tsvetnye Metally"; this naturally limited the volume of publications on rare metals topics in "Tsvetnye Metally". However, the publication of this material was renewed immediately after the war.

The difficult war years demonstrated the vital importance of rare metals in defense technology. A paper by P. F. Lomako (1946, No. 2) remarked upon the vital importance of our armor-piercing shells, made from tungsten carbide. He observed that the difficulties of war time did not interfere with increasing the production of molybdenum by four times and of tungsten by more than two times.

New methods were also publicized in the journal, with evidence in support of the necessity for using them and of their effectiveness. Academician N. P. Sazhin was an active supporter of the new methods and technologies. His three review papers which were published by the journal are particularly interesting in this respect.

Referring to a resolution of the Twenty-Third Party Congress, the author speaks of the necessity for developing rare metals production and notes the increasing role of rare metals in the development of modern technology in papers entitled "Accelerated Development of Rare Metals Production: A Vital Factor in Technical Progress" (1966, No. 6), "Development of Chloride Metallurgy for Rare Metals in the USSR" (1967, No. 7), and "Ultra-High-Purity Metallurgy of Non-Ferrous Metals and Technical Progess in Industry" (1965, No. 2).

The papers emphasize that the properties of rare metals have become clear gradually, as the purity of the metals has been increased: "Zirconium and columbium were long regarded as extremely brittle, and only thorough purification to eliminate gaseous impurities (oxygen, nitrogen, and hydrogen) revealed their surprising plasticity."

A number of unique properties are enumerated: the corrosion resistance of titanium, the superconducting properties of columbium, and the semiconductor properties of germanium, silicon, and certain intermetallic compounds. It is emphasized that the metallurgy of ultrapure substances has developed into a new branch of industry.

N. P. Sazhin G. A. Meerson

G. V. Samsonov B. A. Sakharov

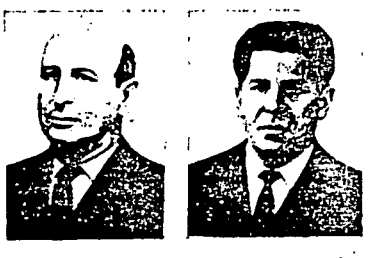

A. N. Zelikman P. S. Anikin

A long list of methods for purification and separation is given: fractional distillation, solvent extraction, ion-exchange methods, recrystallization, electron-beam melting, zone melting, and transport reactions. The author indicates a broad range of possible applications for the ultrapure substances: they have found applicable to the atomic energy industry, the radio and electronics industry, and in power engineering.

When considering the sources of rare earth metals, the author spends some time upon the methods of exposing such material by chlorination. Previous theoretical work by Academicians G. G. Urazov and V. I. Sputsyn, D. N. Chizhikov, Corresponding Member of the Academy of Sciences of the USSR, Professor I. S. Morozov, and O. N. Gvozdevaya and work by a number of institutes has made it possible to organize the industrial use of chlorination to produce titanium tetrachloride and a number of rare earth element chlorides.

The author points out that the development of the new branch of industry, metallurgy of ultrapure substances, has necessitated the development of new monitored methods (tracer atoms, activation analysis, electrophysical method) and convinced the reader of the necessity for further research to increase the purity of the materials and for research in growing defect-free single crystals.

The author points out the advantages of the chloride method, the most important of which are the high degree of ore exposure and the opportunity for comparatively easy separation and purification of individual chlorides by heat and fractional distillation. The possibility of producing oxygen-free metals by the metallothermic method is emphasized. At the same time the author draws attention to the difficulties involved in chloride metallurgy and to the necessity for studying the structure of complex organochloride compounds, the properties of which determine the reasons for failure in chloride purification by fractional distillation due to the formation of azeotropic mixtures.

A. A. Shumeiko and his co-workers (1968, No. 4) published material on the chlorination of zircon concentrate. N. P. Sazhin and I. E. Vil'komirskii (1969, No. 11) examined the problem of chlorination for exposure of beryl and subsequent production of metal by electrolysis. N. V. Galitskii and M. K. Baibekov (1971, No. 5) and some other authors examined the problems of chlorinating titanium raw material in the melt in their papers. In particular a paper by A. B. Bezukladnikov and his co-workers (1967, No. 2) was devoted to some vital problems in the same method for determining the optimum titanium concentration in the melt and to the reason for accumulation of fusible chlorides in the condensation system.

A wide range of problems in developing a production technology for titanium metal has been examined in detail in many papers in the journal. V. A. Garmata, V. S. Ustinov, Yu. G. Olesov, A. N. Petrun'ko, V. V. Rodyakin, and many others have considered the problems in the metallothermic production of titantium, the quality of titanium sponge, the production of titanium powders, and a number of other matters in their papers.

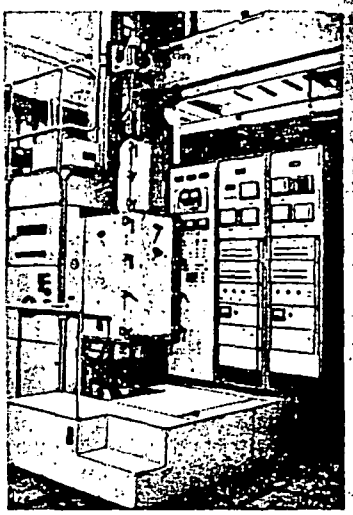

"Redmet" type automated installation for production of single crystals in semiconductor crystals.

However, in selecting material for publication the journal has not permitted a one-sided examination of the problem, but has organized a wide-ranging creative discussion by providing space for various viewpoints. Thus papers on the exposure of raw material containing rare elements, by Ya. G. Goroshchenko and others (1960, No. 12) on the exposure of loparite concentrate by sulfatizing and by G. E. Kaplan and co-workers (1961, No. 6) on the use of sintering with chalk to expose zircon concentrate, have been published.

Papers giving a comparative analysis of various methods of exposure have been extremely interesting. These include papers by O. F. Poletaev (1973, No. 2) and A. G. Muravin (1973, No. 9).

The paper by I. F. Pletaev gave recommendations on the choice of optimum reagents for the exposure of various forms of alumosilicate rare element material. In examining various methods for the production of titanium dioxide for pigments, A. G. Muravin demonstrated the potential of the chlorination method.

The journal has constantly drawn the attention of its readers to the development of hydrometallurgical exposure methods, mainly for tungsten and molybdenum concentrates. For example, the results of research on scheelite concentrate exposure using nitric acid have been described in papers by G. A. Meerson and co-workers (1967, No. 4 and No. 8)

The journal has devoted much attention to the problem of isolating chemical concentrates of extractable elements and to the separation of various elements.

The variety of properties and low concentrations of the elements have given rise to a large number of methods, in most cases borrowed from analytical chemistry.

An interesting publication by I. A. Ul'yanov and A. A. Ivakin (1972, No. 5) deals with the extraction of rhenium from solutions from acid leaching of dusts collected during roasting of molybdenum concentrates, etc.

The journal has actively publicized the hydrometallurgical processes which are now the most advanced; among these are solvent extraction-sorption processes. The use of solvent extraction-sorption methods has been examined in application to the production of molybdenum, tungsten, rare earth elements, gallium, indium, thallium, etc. Papers by M. A. Vinogradov and M. N. Shashkov (1960, No. 8), B. N. Laskorin and A. I. Yuzhin (1961, No. 11), K. Ya. Shapiro (1964, No. 8), I. V. Volk-Karachevskaya and others (1967, No. 8), A. N. Zelikman and V. M. Nerezov (1968, No. 1 and No. 7), and A. N. Zelikman and N. B. Rakova (1972, No. 3) have been devoted to this topic. Apparatus layouts for the solvent-extraction process have also been examined in the journal: a paper by G. V. Korpusov and Yu. A. Tsylov (1965, No. 2) was devoted to these matters.

Pyrometallurgical and combined methods of extraction, separation, and purification of elements and compounds have also been considered in the journal. Publications in this group include a paper by O. K. Jomarov and co-workers (1973, No. 1) devoted to the production of artificial rutile from ilmenite by a promising method combining magnetic separation with pyro- and hydrometallurgical processing, a paper by A. A. Babadzhan and others (1964, No. 6) analyzing the process of germanium and indium distillation in pyrometallurgical processes, and a paper by V. I. Deev and V. I. Smirnov

(1964, No. 3) on ways of improving technology with a view to improving the distillation of rhenium.

A progressive method for element extraction by distillation at reduced pressure was demonstrated in papers by S. M. Mel'nikov and R. A. Isaeva (1967, No. 9) and by A. M. Egorov and M. E. Kazakov (1968, No. 8).

The journal has given quite extensive coverage to the production of elementary substances by chemical or electrochemical reduction. It should be emphasized here that the publications relate to individual elements of the process specifically applicable to rare metals; they are a necessary supplement to the methods described in the technical literature.

A brief account of the most typical of these methods is given below. A paper by O. P. Kolchin and co-workers (1964, No. 7) described a method for producing columbium moldings uniformly alloyed with the necessary addition (tungsten, zirconium, vanadium, etc). A method of producing tantalum-columbium alloy by a powder metallurgy method similar to the previous method was described by O. P. Kolchin and N. P. Chuveleva (1959, No. 2). The metallothermic production of copper-zirconium master alloy by the reduction of potassium fluozirconate with magnesium is described in a paper by A. I. Lainer and others (1965, No. 3).

An original method of selenium reduction from a solution of sodium selenites is described in a paper by A. I. Orlov and others (1963, No. 3).

The urgent problem of producing semiconductor silicon by reduction of the tetrachloride with hydrogen is described in a paper by S. I. Gashenko and co-workers (1970, No. 7). The development of the same topic was described in a paper by B. D. Devyatkin and V. S. Maorossuyanov (1972, No. 8). The reduction of beryllium involves great difficulties. Laboratory experiments in electrolytic reduction of beryllium are dealt with in a paper by I. F. Nichkov and others (1966, No. 1).

Electrolysis conditions which have been carefully worked out to permit the production of high-grade tellurium from sodium telluride solution containing free alkali have been published in a paper by L. A. Soshnikova and M. E. Ezernitskaya (1962, No. 2).

The iodide refining method for refractory rare metals, one of the first to be developed and now widely used, was examined in application to titanium in a paper by A. I. Gribov, M. B. Reifman, and others (1961, No. 5).

The features of the amalgam method of electrolytic refining were demonstrated in a paper by N. I. Ful'man and others (1966, No. 6); with this method the homogeneity of the anode, in combination with electrolytes of various compositions, opens up new opportunities for metal refining.

Ways of solving the major problem of titanium tetrachloride purification were examined in a paper by L. A. Nisel'son and others (1971, No. 11). The authors examined some 250 patents and carried out much experimental work on the removal of vanadium from liquid and vapors with Ti-Cu alloy and Cu powder. The best results were obtained by chemical-thermal purification, making it possible to break down a number of organometallic compounds with subsequent fractional distillation of the product. It is recommended that the final purification scheme should be selected on the basis of the composition of the initial chloride.

The publication of extensive and detailed research on the zone refining of germanium using the tracer atom method by B. A. Sakharov and others (1970, No. 7) revealed the true pattern of the processes which take place during zone refining, taking into account the pick-up of impurities from the container material.

The mathematical problem of the link between the speed of zone travel and the concentration of impurity to be removed is solved in papers by V. N. Vigdorovich and others (1968, No. 7 and 1973, No. 11) using the zone refining of tellurium as an example.

Apparatus and methods for automatically maintaining the zone melting routine are discussed in papers by S. S. Naroichik and others (1971, No. 11) and V. K. Tolpygo (1971, No. 3).

There is an interesting publication by L. I. Klyachko and others (1965, No. 2) on the behavior of a number of impurities in the manufacture of massive tungsten by the powder metallurgy method; the processes of interaction between impurities which accelerate their removal by evaporation are demonstrated (thus the presence of chlorine accelerates the removal of potassium by 2-3 times.

There is an extremely interesting discussion in a paper by A. V. Elyutin and M. I. Ivanova (1970, No. 11) of impurities evaporation during vacuum melting of refractory metals. The presence of two impurities evaporation mechanisms (kinetic and diffusion) is demonstrated; a knowledge of these makes it possible to calculate ingot composition on the basis of the composition of the billet being remelted. The vacuum remelting

of molybdenum containing carbon is discussed in a paper by V. S. Chernov and others (1974, No. 7). The conditions under which its carbides react with oxides are given.

In recent years the journal has been devoting increasing attention to specific problems in semiconductor production technology. The problems of maintaining uniform alloying in single crystals in the process of growth were considered in a series of papers by S. V. Gnilov and A. Ya. Nashel'skii (1973, No. 9 and 12 and 1975, No. 11). Interesting technological problems were touched upon in a paper by D. I. Levinzon (1973, No. 2).

In addition to problems in primary metal production, the journal has given coverage to such vital aspects of the national economy as the processing of waste. The problems of electrolytic refining of titanium waste and processing this waste by the hydrogenation method have been examined in a series of papers by Yu. G. Olesov, V. S. Ustinov, and others (1966, No. 5; 1967, No. 2 and No. 12; 1969, No. 3). The problems of processing germanium waste (both metallic and in the form of compounds) were examined in a paper by I. I. Skakovskii and A. M. Tuzovskii (1968, No. 3).

The vital problem of reducing losses of hard alloys with waste by using initial products of increased purity for their production was considered in a paper by G. N. Levin (1969, No. 5).

Apart from technology, the journal has recently been devoting considerable attention to the automation of production and process control. These problems were examined in papers by I. M. Gol'd and V. S. Leibovich (1974, No. 10; 1975, No. 4) N. V. Degtyarik (1974, No. 8), I. L. Shenderovich (1975, No. 1), and V. V. Stopkevich (1975, No. 4) as they apply to individual processes in semiconductor production. A number of papers were also devoted to problems in rare metals production automation. Thus a paper by L. M. Voloshin and others (1975, No. 5) examined the problems of controlling the process of electron-beam melting for refractory materials, and papers by M. E. Yatko (1973, No. 3) and G. A. Partakov and N. G. Fedorov (1973, No. 7) considered automation of the titanium slag chlorination process.

The journal has regularly allocated space to informative material acquainting readers with the development of the rare metals and semi conductor materials industry abroad. This material includes a series of publications by B. I. Kogan and co-workers (1964, No. 7; 1966, No. 1; 1967, No. 4 and No. 7, etc.) on the use of various rare elements in tehnology, a paper by E. S. Fal'kevich (1968, No. 2) on the production of semiconductor silicon abroad, and many others.

Unfortunately the limited size of the present paper makes it impossible to consider all the problems in the development of rare metals and semiconductor materials technology and industrial production which have been covered in the journal; neither is it possible to mention all the authors.

A great deal of work has been done by the rare metals section of the journal Editorial Board, directed for many years by I. S. Stepanov and in recent years by P. S. Anikin.

The examples given clearly show that during its life the journal "Tsvetnye Metally" has taken an active part in the development of the Soviet rare metals and semiconductor materials industry and has charted its entire splendid course, beginning with the attempts at analytical determination of rare elements in ores fifty years ago to modern scientific and technical developments based upon mathematical simulation and the use of electronic control systems.

UDC 669.2:53.09

Precipitation of nickel from sulphate pulps by metallic iron and elemental sulphur as a subject for automatic control

V A Ivanov, A F Gavrilenko and Yu F Markov (Moscow Institute of Steel and Alloys - Department of Automatic of Nonferrous and Rare Metals Production)

Earlier[1]) it was shown that the control of the precipitation of nickel involves minimisation of the consumption of metallic iron or the pH of the pulp at the outlet from precipitation for a given degree of extraction of the nickel into the sulphide precipitate. Solution of this problem is complicated by the strong effect of the conditions of the preceding technological operations and, particularly, autoclave oxidative leaching. The effect of input influences on the output characteristics of the processes is investigated and the possibility of minimising the pH value is analysed in the present article.

The effect of input influences on the output characteristics was studied by means of a mathematic model, which represented a system of linear regression equations. The experimental data for determining the coefficients of the equations were obtained on a semiindustrial setup. A list of the input influences and the range of their variations are shown in the table. The sample of experimental data amounted to 120 points. The coordinates of each point in the space of the influences were represented by the values of the corresponding variables, which were averaged in the range of 6-8 h of continuous operation under steady conditions. Operating conditions in which the output characteristics of the process (in the indicated range) did not differ from the average values by not more than ±10 rel. % were taken as steady.

The calculations were performed on a Minsk 32 computer by the previously published programme[2]). As a measure of the suitability of the obtained equations for predicting the output characteristics of the process we used the ratio of variances:

$$F_{err} = \frac{S_m^2}{S_{rem}^2}$$

where S_m^2 is the variance in relation to the mean; S_{rem}^2 is the variance calculated in relation to the regression equation.

The dimensionality of the equations was reduced by successive elimination of the variables for which the t criterion was smallest and was continued until the minimum value of S_{rem}^2 was obtained.

The calculations showed that the dependence of the nickel content y_1 in the liquid phase of the pulp at the outlet from precipitation on the input influences has the following form:

$$y_1 = 8.55 - 0.346x_1 - 0.062x_2 - 5.48x_8 \quad (1)$$

where

$R_{rem} = 0.068$, $F_{err} = 2.15$, $F_{cr} = 3.56$ (for $p = 0.01$)

The dependence of the maximum pH value (y_2) at the inlet to precipitation on the input influences is described by the equation:

$$y_2 = 7.41 + 0.161x_1 - 0.09x_2 - 0.093x_3 + 0.015x_6 + 0.062x_7 - 2.31x_8 \quad (2)$$

where

$R_{rem} = 0.0097$, $F_{err} = 6.50$, $F_{cr} = 2.84$ (for $p = 0.01$)

Equations (1) and (2) were used to compare the effects of the individual variables on the output characteristics. The normalised values of the coefficients are given in the table (columns 7 and 8 respectively). Normalisation was realised by means of the equation

$$K = \frac{\Delta y_j / y^*}{\Delta x_i / x_i^*}$$

where: Δx_i and x_i^* = the increments in the i-th input influence and its base value respectively

Δy_j and y_j^* = the same for the j-th output characteristic

As base value we used the mean values of the influences (column 6 in the table). The values calculated in this way are approximate values of the gain factors for the subject in the respective channels.

Comparison of the gain factors shows that the effect of the perturbing influences in the composition of the pulp is significant and in individual channels (x_1, x_4, x_8) is comparable with the effect of the controlling influences (the consumption of metallic iron and elemental sulphur). Since the parameters of the pulp are *not controlled* (the pulp is delivered *directly from the leaching or aggregation autoclaves*), the precipitation process must be regarded as a control subject with a significantly variable input.

The accuracy with which the nickel content at the outlet from the precipitation process can be predicted is low; for equation (1) $F_{err} = 2.15$. It can be increased by using a model of a higher order and including the effect of the interaction of individual variables. However, increase in the order of the equations leads to an increase in the difficulties of their use in operational automated control systems. We therefore investigated the possibility of describing the precipitation process on the basis of complex estimates of the input influences.

As such estimates we used the consumption ratios of the reagent-precipitants, which characterise the ratio of the actual amount of reagent loaded

Characteristics of the input influences and output parameters of the precipitation process

Name of influence, parameter	Notation	Measurement unit	Value			K_{Ni}	K_{pH}
			Minimum	Maximum	Mean		
Consumption:							
Iron powder	x_1	$\frac{kg/h}{m^3\ pulp}$	6	20	13	-0.02	+0.007
Elemental sulphur	x_2	$\frac{kg/h}{m^3\ pulp}$	0	15	8	-0.024	-0.011
Consumption ratio:							
Iron	K	r/u	0.7	3.7	1.7	-0.148	+0.051
Elemental sulphur	K	r/u	0	5.4	2.0	-0.096	-0.046
Content of elemental sulphur in solid of initial pulp	x_3	%	1.0	7.8	2.6	-0.013	-0.001
Content in solution of pulp at inlet to precipitation:							
Ni	x_4	g/l	7.1	13.5	10.0	+0.023	+0.068
Cu	x_5	g/l	0.9	5.6	1.5	+0.171	-0.078
Fe_{tot}	x_6	g/l	3.8	13.1	8.0	+0.02	+0.046
Fe (III)	x_7	g/l	0.5	3.8	2.0	+0.054	+0.025
Density of initial pulp	x_8	g/cm^3	1.2	1.45	1.28	-0.234	-0.19
Content of SO_4^{2-} iron in solution	x_9	g/l	40	70	55	-0.009	-0.013
Content of nickel in solution at outlet from precipitation	y_1	g/l	0.05	3.8	1.2		
pH of the pulp at outlet	y_2	pH value	3.0	5.5	4.4		

to that required theoretically for precipitation according to the reaction

$$MeSO_4 + Fe^0 + S^0 \longrightarrow MeS + FeSO_4 \quad (3)$$

The ratio was determined experimentally by means of the equation

$$K_j = \frac{G_j a_j}{V_p \frac{\gamma_{sd} - \gamma_p}{\gamma_{sd} - \gamma_{sn}} \sum_{i=1}^{n} \varphi_i (C_i^o - C_i)} \quad (4)$$

where: G_j = the consumption of the j-th reagent
a_j = the content of the active component in the reagent
γ_p, γ_{sd}, and γ_{sn} = the densities of the pulp, the solid, and the solution respectively
V_p = the productivity with respect to the pulp
C_i^o = the content of the i-th component in the solution interacting with the reagents at the inlet to the precipitation process
C_i = the same at the outlet
φ_i = coefficients equal to the stoichiometric consumption of the reagents on the precipitation of the respective metal according to reaction (3).

From the expression for calculating the consumption ratio of the reagents it follows that K_j includes estimates of the parameters of the initial and final pulp, the consumption of the pulp and reagent-precipitates, and expresses in implicit form (through the coefficients φ) the contribution from the individual precipitation reactions to the final results.

Treatment of the experimental data used earlier for calculation of the coefficients of Eqs. (1) and (2) led to the following regression equations:

$$y_1 = 3.3 - K_{Fe} - 0.25K_S \quad (5)$$

$$y_2 = 4.3 + 0.266K_{Fe} - 0.172K_S \quad (6)$$

with $S^2_{rem} = 0.047$ and 0.0056; $F_{err} = 5.11$ and 9.51, $F_{cr} = 4.03$ (for $p = 0.01$) respectively. It is clear that the accuracy of the description was considerably increased.

The possibility of using Eqs. (5) and (6) for predicting the output characteristics of the process was checked on a semi-industrial set-up. Setting the y_1 and y_2 values, we calculated K_{Fe} and K_S, and then by means of Eq. (4) for the known composition of the pulp we obtained the consumption of the precipitant reagents. With the technological conditions for the precipitation process specified in such a way the discrepancy between the actual and calculated values of the output parameters was not greater than ±20 rel. % for y_1 and ± 5% for y_2, if the distribution of the pH value was regular throughout the process (fig. 1, curve I). If this condition broke down (curve II) the accuracy with which y_2 was predicted was retained for the maximum pH value reached during precipitation.

For the regime characterised by an extremal curve for the distribution of the pH value the accuracy of the prediction of y_1 was more than ±20 rel.%. The behaviour of the nickel in the solution at the outlet from the precipitation process in this case is described satisfactorily by the following equations for K_S = const):

for $y_1 > 0.2 - 0.3$ g/l $1.5 < pH < 3.5$ and $g_{Fe} > 0$

$$g_{Ni} = kg_{Fe} \quad (7)$$

for $y_1 > 0.2 - 0.3$ g/l $1.5 < pH < 3.5$ and $g_{Fe} = 0$

$$g_{Ni} = 0 \quad (8)$$

for $y_1 < 0.5 \div 1.0$ g/l $pH > 3.5$ and $g_{Fe} = 0$

$$g_{Ni} = K \int_0^{\tau} C_{Ni}^n \, d\tau \quad (9)$$

where: g_{Fe} and g_{Ni} = the weights of loaded metallic iron and precipitated nickel respectively
τ = the time spent by the pulp in the reactors at $pH > 3.5$

The coefficient k in Eq. (7) is numerically equal to $1/K_{Fe}$; the expressions $g_{Fe} > 0$ and $g_{Fe} = 0$ respectively are symbolic representations of the load of iron powder in the i-th reactor.

If the extremal pH value on curve II is less than 4.0-4.2, then $K \equiv 38 \cdot 10^{-3}$, and $n = 0.75$. When $pH_{max} > 4.2$, the coefficients in Eq. (9) can vary within wide limits, right up to a change in the sign of the coefficient K. The physical meaning of this is reverse transfer of nickel into the solution from the precipitate (on account, possibly, of dissolution of the cemented metal)[3]. In this case the accuracy of prediction according to Eq. (5) is significantly reduced (to 30-40 rel. % in the range of $y_1 = 0.05$-0.3 g/l).

With a monotonic distribution curve at $pH < 4.1$-4.2 each of the successively included reactors can be approximated according to Eq. (7) by an amplifying link. The gain factor of the link can vary within the limits of ±20-30 rel. % under the influence of processes whose effect is reflected to a first approximation by Eq. (9).

With an extremal pH distribution curve the reactors following those in which the maximum pH was obtained are satisfactorily approximately by an aperiodic link with a variable gain factor. In this case the structure of the volume varies during precipitation. It is clear that the second case is more difficult for solution of the control problem.

As shown by the investigations, the effect of the consumption of elemental sulphur on the output characteristics of the process is significant up to a K_S value of 5-6. The effectiveness of this parameter then decreases sharply This was explained in the literature[3]), where it is indicated that the sulphi-

disation of nickel requires intimate contact between the particles of iron and elemental sulphur and is realised in thin liquid films separating the phases.

The results from the investigation make it possible to specify the problem of optimisation of the precipitation processes. The following requirements

$$pH \longrightarrow min$$

for $y_1 \leqslant y_1$

must be supplemented by the condition

$$pH_{i+1} > pH$$

and must be fulfilled with restriction of the controlling influence with respect to a consumption of elemental sulphur at the level K_s = 5-6.

As follows from Eq. (5), the fulfillment of the condition (11) is secured by the specification of an absolute value for the consumption ratio of the precipitant reagents. For the fulfillment of condition (12), as shown by the investigations, it is necessary to distribute the loaded metallic iron among the reactors. For instance, if the iron powder is loaded in ratios of 40, 40, and 20% of the total amount in the first, second, and third reactors, the distribution of the pH in the course of precipitation is most often characterised by values grouped about curve I in the figure.

Semi-industrial trials showed that in this case the consumption of iron powder is 20-25 rel. % lower than in the technological regime characterised by the extremal pH distribution curve.

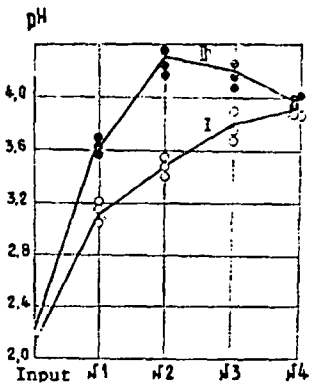

Fig.

Distribution of pH in the reactors with various precipitation conditions. I - Distributed load of metallic iron; 40% of total weight in reactor 1, 40% in reactor 2, 20% in reactor 3. II - Concentrated loading of metallic iron in reactor 1.

ferences

A F Gavrilenko et alia: Scientific works (Gintsvetm Moscow 1976, (41), p. 59-67.

G N Veselaya (Editor): Programmes on mathe mat Minsk-22 computer. Giredmeta, ONTI, Moscow 19

V I Goryachkin et alia: Hydrometallurgy (editor B Nauka, Moscow 1976, p. 48-59.

otometric grading of titanium sponge on a sortex-62

F Tsypin, V A Likhterman, R E Shiryaev, and L P
ning Institute - Department of the Metallurgy of Lig

The photometric grading of titanium sponge accordi ious defects was investigated. The defective spon

Table 1: Results from experiments on the individual grading of defects

Type of defect	Initial material		Graded product			Pr i
	Total number of pieces	Content of defective pieces %	Yield %	Content of defective pieces %	Extraction of pure titanium %	Yield %
...e	200	5.0	68.0	0.7	71.0	32.0
	200	10.0	53.0	3.8	56.7	47.0
...ised	531	38.4	58.0	5.8	88.7	42.0
	368	4.8	86.8	0.6	90.6	13.2
...oride	200	5.0	88.0	1.7	91.0	12.0
	200	10.0	84.0	3.6	90.0	16.0
...-rich	200	5.0	89.5	1.6	92.6	10.5
	200	10.0	84.0	2.4	91.1	16.0
...ent	200	5.0	89.0	0	93.6	11.0
	200	10.0	85.0	0	94.4	15.0

United States Patent [19]

Crnojevich et al.

[11] 4,214,900

[45] Jul. 29, 1980

[54] PRODUCTION OF NONFERROUS METALS WITH LOW SELENIUM CONTENTS

[75] Inventors: Ranko Crnojevich, Gretna; Edward I. Wiewiorowski, New Orleans; Peter H. Yu, Harvey, all of La.

[73] Assignee: Amax Inc., Greenwich, Conn.

[21] Appl. No.: 64,689

[22] Filed: Aug. 8, 1979

[51] Int. Cl.² C22B 23/04

[52] U.S. Cl. 75/109; 75/117; 75/119; 75/121; 423/509; 423/510

[58] Field of Search 75/109, 117, 119, 121; 423/510, 509

[56] References Cited

U.S. PATENT DOCUMENTS

3,914,375	10/1975	Clark et al.	75/121 X
3,933,635	1/1976	Marchant	75/121 X
3,959,097	5/1976	Queneau et al.	75/121 X
4,026,797	5/1977	Nikolec et al.	75/121 X
4,047,939	9/1977	Morrison	75/109 X
4,076,605	2/1978	Bilson	75/117 X

Primary Examiner—G. Ozaki

Attorney, Agent, or Firm—Michael A. Ciomek

[57] ABSTRACT

Selenium is precipitated from solutions or slurries containing nonferrous metals, particularly nickel by contacting the solution or slurries with a semimetallic chromous precipitant of the nonferrous metal, particularly nickel, which has a nonferrous metal to chromium ratio between about 10:1 and about 200:1 and which has a metallic content between about 50% and about 90%. The semimetallic chromous precipitant of the nonferrous metal is prepared by hydrogen reducing a solution of the nonferrous metal or slurries containing chromous salts in amount to provide the aforementioned nickel to chromium ratios.

10 Claims, No Drawings

PRODUCTION OF NONFERROUS METALS WITH LOW SELENIUM CONTENTS

THEORY OF THE INVENTION

The present invention relates to hydrometallurgy, and more particularly to the removal of selenium from nickel-containing solutions.

BACKGROUND OF THE INVENTION

Many alloying uses of metallic nickel require high purity. This is particularly true when metallic nickel is used in forming superalloys. Small amounts of impurities, e.g. tens of parts per or even parts per million, can produce highly detrimental properties. For example, sulfur in amounts greater than 50 parts per million and selenium in evan smaller amounts, i.e., more than about 2 parts per million, can induce hot shortness in superalloys, causing problems during hot working. Metallic nickel can be produced by electrorefining, electrowinning, carbonyl techniques and by precipitation of metallic nickel with a reducing gas from aqueous solutions. The first three of these processes can generally produce a refined nickel product that contains less than 5 ppm selenium. Metallic nickel precipitated from aqueous solutions generally contains about 5 ppm and 40 ppm selenium, and most often between about 10 ppm and about 20 ppm selenium. But even 1 ppm selenium in nickel can be critically detrimental when the nickel is used in the production of special superalloys.

Some selenium is removed by partial volatilization when nickel is produced with intermediate pyrometallurgical treatments. Selenium can also be partially removed by coprecipitation with other hydroxide when iron is precipitated from solutions under oxidizing conditions in a pH range between about 4 and 6. Some selenium can also be removed by cementation with metallic copper at moderate temperatures and with metallic nickel at temperatures above about 200° C. Some selenium can also be removed from nickel solutions with ferric hydroxide produced by hydrolysis at temperatures above 200° C.

These known processes for removing selenium from nickel solutions are very expensive, only partially effective or inapplicable. For example, those processes that require the use of temperatures of 200° C. are frequently commercially unattractive because such reactions require the use of pressurized vessels in a large production stream, can entail the loss of nickel from solution or are effective in removing only selenium that is present in the tetravalent state. These known processes which rely on the coprecipitation of selenium with hydrolyzed ferric hydroxide or other hydroxides are not applicable to the treatment of pure nickel solutions because either these solutions do not contain the coprecipitating compound or are effective in only removing tetravalent selenium. A process for removing both tetravalent and hexavalent selenium from nickel solutions under moderate operating conditions has now been discovered.

BRIEF DESCRIPTION OF THE INVENTION

Broadly stated, the present invention provides a process for precipitating selenium from a solution or a slurry of at least one nonferrous metal selected from the group consisting of cobalt, copper and nickel. The process comprises contacting the solution-slurry with a semimetallic chromous precipitant of the nonferrous metal which has a nonferrous metal to chromium ratio between about 10:1 and about 200:1 and which has a metallic content between about 50% and about 90% to precipitate selenium from the solution or slurry as a selenide of the nonferrous metal. The semimetallic chromous precipitant will be referred to herein as "SRC" standing for "Selenium Removal Compound".

DETAILED DESCRIPTION OF THE INVENTION

Aqueous solutions of at least one nonferrous metal selected from the group consisting of cobalt, copper and nickel can be treated for selenium removal by the process of the present invention. However, the process will be described in conjunction with the treatment of nickel-containing solution in order to facilitate the description thereof. Many nickel containing solutions can be treated by the process in accordance with the present invention. Thus, nickel chloride, nickel sulfate, nickel amine sulfate solutions can be treated to remove selenium by the process in accordance with the present invention. Advantageously as mostly required in the commercial practice, nickel sulfate solutions are treated to precipitate selenium in accordance with the present invention. Nickel solutions that can be treated will generally have nickel concentrations between about 10 gpl and about 120 gpl and between about 2 ppm and 25 ppm, or even 40 ppm, selenium, and most often between about 3 ppm and about 6 ppm selenium. Although the nickel solutions can have a wide range of pH values, it is advantageous to maintain the nickel solution at a pH value between about 0.5 and about 7.0, and advantageously between about 1.5 and about 6.0.

Selenium is removed from nickel solutions or slurry by contacting the solution or slurry with a semimetallic nickel chromous precipitant which has a nickel to chromium ratio between about 10:1 and about 200:1 and which has a metallic content between about 50% and about 90%. The precipitant is prepared by treating nickel-bearing solutions or slurries or combinations thereof containing sufficient amounts of chromous salts dissolved in the aqueous phase to produce the aforementioned nickel to chromium ratios. Thus, the precipitant can be produced from solutions containing nickel sulfate, nickel ammine sulfate $[Ni(NH_3)]SO_4$, where $X=2-6$ or slurries containing nickel hydroxide or basic nickel sulfate, nickel carbonates or basic nickel carbonate. Chromium or chromous compounds that can be employed include chromous sulfate ($CrSO_4$), Cr (II) halogenides, Cr (II) oxides or hydroxides, Cr(II) salts or organic acids and Cr(II) sulfides, etc. The nickel solution or slurry containing the chromous salt is treated with carbon monoxide or hydrogen, advantageously hydrogen, at a temperature between about 50° C. and about 200° C. advantageously between about 80° C. and about 100° C. using a reducing gas overpressure between about 100 pounds per square inch gauge (psig) and about 800 psig, advantageously between about 300 psig and about 600 psig for a time between about 5 minutes and about 45 minutes. Through reduction of the liquor solution or slurry containing a chromous salt the following reaction occurs:

$$MeA + R \rightarrow Me^{\circ} + RA$$

where Me is nickel and chromium, A is either an acid anion or the hydroxyl anion and R is the reducing gas. If A is an acid anion, as the reaction proceeds a required

amount of a neutralizing reagent, generally ammonia, should be supplied to neutralize acid generated by the reaction.

Reduction of the nickel solution or slurry containing the chromous salt produces a finely divided semimetallic nickel chromium precipitant having a very large surface area and a low density but is fast settling. This precipitant is superior to metallic nickel or other metallics not only chemically but also physically because it is very suitable for transporting in a slurry form with common pumping apparatus and can be easily suspended during selenium removal. The semimetallic nickel chromium precipitant is a mixture of metallic nickel and chromium and hydroxides and basic sulfates of these two elements. The degree of metallization of the precipitant is determined by analyzing for the total nickel content and then subtracting the amount of nickel contained in the precipitant from the total weight thereof. The difference between the total weight of the precipitant and the total weight of nickel is basically the weight of the hydroxyl or acid anions associated with the nickel and chromium ions.

The effectiveness of semimetallic nickel chromous precipitant can be further improved by adding small amounts of various reagents to the nickel-containing solution or slurry during the preparation of the precipitant. Reagents that improve the effectiveness of the precipitant include ferric ions, aluminum ions, silver ions, sulfide ions, cyanide ions, alizarin, polyacrylic acids and anthraquinone. These reagents can be added to the nickel slurry in amounts between about 50 ppm and about 200 ppm based on the weight of the nickel in solution or in the slurry. The reagents improve the effectiveness of the precipitant by providing a consistent quality in the precipitant and/or developing a higher surface area for the precipitant.

The semimetallic nickel chromium precipitant can be used directly as made up slurry for selenium removal or can be dewatered (densified) or washed prior to its use. Also before use, the semimetallic nickel chromium precipitant can be dried, providing that drying and storage is done in a reducing atmosphere. Advantageously, the semimetallic nickel chromous precipitant is only dewatered (densified) and used as such.

As noted hereinbefore the semimetallic nickel chromous precipitant can be used for treating most nickel solutions. However, it is particularly advantageous to use the precipitant for purifying nickel solutions produced by a sulfuric acid leaching operation in which the first stage is an atmospheric leach and followed by superatmospheric leaches. Nickel copper matte is atmospherically leached with an acidic sulfate solution containing nickel and substantial amounts of copper to dissolve a substantial part of the nickel contained in the matte while cementing copper from solution and consuming free acid contained in the leaching solution to produce a substantially purified nickel sulfate solution and a residue containing cement copper, hydroxides precipitated during the leaching operation, and unleached material. The residue is subjected to superatmospheric leaching with aeration with an acidic solution containing substantial amounts of free acid to dissolve most of the nickel and copper remaining in the residue. The residue from the first stage pressure leaching operation is then subjected to more severe acid leaching to produce a copper sulfate solution containing any of the undissolved nickel values in the residue from the first stage pressure leaching operation. The pregnant solution from the second stage pressure leaching operation is sent to a tank house where copper is electrowon from the solution and the spent electrolyte is then recycled to the atmospheric leach and the pressure leaching operation.

Selenium is preferentially removed from the nickel solution either during the atmospheric leaching operation or after the atmospheric leaching operation is completed. Although selenium removal can be conducted during the atmospheric leaching, it is advantageous to remove selenium as a separate operation because the oxidizing conditions employed during atmospheric leaching result in a slightly higher consumption of the semimetallic nickel chromous precipitant. But, selenium removal can be carried out in the solutions or slurries following the pressure leach operation.

Selenium removal can be conducted at ambient pressures with mild agitation at temperatures from room temperature to the boiling point of the solution. However, the kinetics of selenium removal are improved by operating at temperatures between about 60° C. and about 90° C. The semimetallic nickel chromium precipitant has a low density; only mild agitation is required to keep the precipitant satisfactorily suspended in the reaction system. The low density of the precipitant minimizes the build-up of the precipitant on the bottom of the reaction vessel or the plugging of lines as is generally experienced with other metallic precipitants. Selenium removal can be completed in as short a time as one hour, advantageously between about one hour and about four hours.

Selenium can be removed from nickel solutions having pH values between about 1 and 8 but is advantageously carried out in nickel solutions that are slightly acidic, i.e., having pH values between about 1.5 and about 6.0. The amount of the semimetallic nickel chromous precipitant added to the nickel solution is mainly dependent upon the amount of selenium contained in the solution and to a far lesser extent on other process variables like temperature, reaction time, oxidizing conditions, pH value, etc. At selenium concentrations between about 1 part per million and about 5 part per million, about 1 gram per liter of metallics in the semimetallic nickel chromium precipitant is required per ppm of selenium to be removed. For nickel solutions containing more than 5 ppm of selenium, the rate of addition of the semimetallic nickel chromium precipitant that must be added to the nickel solution is decreased and about 0.5 gram per liter per ppm selenium is required for the solutions containing more than 10 ppm. selenium. Because the amount of the precipitant required is dependent not only on the amount of selenium in solution but other process variables, it is advantageous to ascertain by tests that level of precipitant additions that will lower the selenium content to the desired levels.

In order to give those skilled in the art a better understanding of the advantages flowing from the present invention, the following illustrative examples are given:

EXAMPLE I

Three semimetallic nickel chromous precipitants were prepared under different conditions and these were compared with known means of removing selenium from nickel-containing solutions. In Test No. 1 the semimetallic nickel chromous precipitant was precipitated from a nickel sulfate solution containing 80 grams per liter nickel and one gram per liter Cr^{2+} ions at 90°

C. for 30 minutes under a hydrogen overpressure of 500 psig. This precipitant contained 75.6% metallics. A second precipitant was prepared by reducing a slurry containing 100 grams per liter nickel as basic nickel sulfate and containing one gram per liter Cr^{2+} ions at 90° C. for 1 hour under a hydrogen overpressure of 500 psig. Precipitants produced under these conditions contained 78.6% metallics. In Test No. 3, the precipitant was prepared by reducing a slurry of basic nickel carbonate having a nickel content equivalent to 80 grams per liter of nickel and containing one gram per liter Cr^{2+} ions for one hour at 90° C. under a hydrogen overpressure of 500 psig. This precipitant contained 62.3% metallics and had a nickel to chromium ratio of approximately 80:1. In Tests 4 through 6 known selenium precitants were prepared as shown in Table I.

A nickel matte was leached at atmospheric pressures with aeration at a temperature of 85° C. for two hours at pH values between about 5 and 6.5 and in each test 2.5 grams per liter of metallics in the precipitant was added during the leach. The initial concentration of selenium in the leach slurry was 3.2 parts per million total selenium and the nickel concentration of the leach liquor was 88 grams per liter. The results of these tests are shown in Table I.

Reference to Table I confirms that the semimetallic nickel chromous precipitant is effective in lowering the selenium content of the nickel solution to below about 1 ppm whereas selenium precipitants commonly used in the art provide final selenium contents of 1.82 ppm or greater. Thus, the semimetallic nickel chromous precipitant of the present invention is at least 44% more effective in removing selenium from solution.

TABLE I

Test No.	Precipitant Preparation	% Metallics In Compound	Terminal Se-Conc.,ppm	Terminal Ni/Se Ratio
1.	SRC-prepared from 80 gpl $NiSO_4$ soln. containing 1 gpl Cr^{++} at 90° C. for 30 minutes under 500 psig H_2.	75.6	0.55	1.6×10^5
2.	SRC-prepared from 100 gpl Ni slurry of 6 $Ni(OH)_2 \cdot NiSO_4$ containing 1 gpl Cr^{++} at 90° C. for 1 hour under 500 psig H_2.	78.6	0.85	1.0×10^5
3.	SRC-prepared from 80 gpl slurry of $Ni(OH)_2 \cdot NiCO_3$ containing 1 gpl Cr^{++} at 90° C. for 15 minutes under 450 psig H_2.	62.3	1.01	0.9×10^5
4.	Metallic nickel prepared from 80 gpl $NiSO_4$ in presence of $Fe^{++} - Al^{+++}$ catalyst at 80° C. for 15 minutes under 500 psig H_2.	95.6	1.82	0.5×10^5
5.	Densified metallic nickel powder produced with a wet reduction with H_2 at 180° C. for 30 minutes.	99.9	3.01	0.3×10^5
6.	Metallic copper powder produced by reduction with SO_2 gas at 180° C.	98.7	3.05	0.3×10^5

EXAMPLE II

This example demonstrates the greater effectiveness of semimetallic nickel chromous percipitants containing lower nickel to chromium ratios. Seven semimetallic nickel chromous precipitants were precipitated from a nickel sulfate solution containing 80 gpl nickel and various amounts of Cr^{2+} ions at 90° C. for 30 minutes under a hydrogen overpressure of 500 psig. These precipitants were then used to precipitate selenium from a nickel sulfate solution containing 85 gpl nickel and 3 ppm total selenium at 90° C. under an unoxidizing condition for two hours with the precipitant being added at a rate of two gpl of the metallics in the precipitant. The results of these tests are shown in Table II.

TABLE II

Cr(II) Addition in SRC Preparation (gpl)	Ni:Cr	Terminal Se-Conc., ppm
0.00	—	2.92
0.05	1600	2.81
0.10	800	2.76
0.50	400	1.85
1.00	80	0.61
2.00	40	0.55
5.00	16	0.56

The results in Table II show that even small amounts of chromium are effective in lowering the selenium content of the nickel solution. However, only those precipitants having a nickel to chromium ratio less than 400:1 provide terminal selenium concentrations in the nickel solution of less than 1 ppm.

EXAMPLE III

This example demonstrates the importance of employing semimetallic nickel chromous precipitates. Four semimetallic nickel chromous precipitants were precipitated from a nickel sulfate solution containing 80 gpl nickel and 1 gpl Cr(II) ion under a hydrogen overpressure of 300 psig for 30 minutes. The reduction temperature was varied between 90° C. and 180° C. to affect the metallic content of the precipitant. The precipitant so produced was used to remove selenium from a nickel sulfate solution containing 60 gpl nickel and 3.7 ppm selenium with aeration at 80° C. for two hours with the precipitant being added to the nickel solution at a rate equivalent to 2 gpl metallics in the precipitant. The results of these tests are shown in Table III.

TABLE III

SRC Prep. Temperature (°C.)	% Metallics In SRC	Terminal Se-Conc. ppm
90	75.6	0.72
120	91.5	0.90
150	98.7	2.4

TABLE III-continued

SRC Prep. Temperature (°C.)	% Metallics In SRC	Terminal Se-Conc. ppm
180	99.2	3.0

Comparison of the results shown in Table III shows that acceptable terminal selenium concentrations can be obtained when the semimetallic nickel chromous precipitant contains about 92% metallics whereas metallics exceeding 95% produce commercially unacceptable terminal selenium concentrations of 2.4 greater.

EXAMPLE IV

This example demonstrates that higher temperatures and longer times of selenium precipitation are more effective in providing a low terminal selenium concentration. A semimetallic nickel chromous precipitant was precipitated from a nickel sulfate solution containing 80 gpl nickel and 1 gpl Cr(II) ion at 90° C. under a hydrogen overpressure of 400 psig for 30 minutes. The precipitant so produced was used to treat a nickel sulfate solution having a total selenium content of 4.5 ppm. During selenium precipitation the nickel sulfate solution was aerated and the precipitant was used at a rate equivalent to 3 gpl metallics in the precipitant. The times, temperatures and the results of these tests are reported in Table IV.

TABLE IV

Time	Temperature (°C.)	Terminal Se-Conc.(ppm)
1	75	1.1
2	75	1.0
3	75	0.9
4	75	0.9
2	20	1.2
2	45	1.0
2	70	1.0
2	95	0.9

The results shown in Table IV confirm that longer precipitation times are effective in producing lower terminal selenium concentrations. However, at a given temperature, times in excess of one hour are only marginally better than those for 1 hour. The results in Table IV also demonstrate that higher temperatures are more effective in providing lower terminal selenium concentrations. Again, the effects of temperature above 45° C. produce only marginally better results. The results in Table IV demonstrate that optimal selenium removal can be achieved by conducting the selenium precipitation operation at temperatures between 50° C. and the boiling point of the solution for a time between about 1 and 2 hours.

EXAMPLE V

This example confirms that copper-bearing electrolytes can be treated by the process in accordance with the present invention to produce electrolytes having low selenium contents.

A semi-metallic nickel chromous precipitant was made from a nickel sulfate solution containing 80 gpl nickel and 1 gpl chromous ion at 90° C. under a hydrogen overpressure of 400 psig. A copper-bearing electrolyte containing between about 40 gpl and about 50 gpl nickel, between about 60 gpl and about 70 gpl copper, between about 2 gpl and about 4 gpl iron and between about 10 ppm and 15 ppm selenium was treated with a precipitant to remove selenium therefrom. Selenium was removed from this solution at ambient pressure at 65° C. for one hour. The results are reported in Table 5.

TABLE V

Solution	Ni-Cr Addition gpl (100% Ni base)	Initial Se ppm	Terminal Se, ppm
I	6.0	9.9	0.52
II	10.0	14.6	0.10

Substantially complete selenium removal was effected by these tests. In copper electrolytes containing selenium both in the hexavalent and quadravalent states in which the major part is present in the hexavalent state (70% to 90%), consumption of the precipitant was reduced to between about 0.6 and about 0.7 gpl precipitant per ppm selenium removed.

Although the present invention has been described in conjunction with preferred embodiments, it is to be understood that modifications and variations may be resorted to without departing from the scope of the invention, as those skilled in the art will readily understand. Such modifications and variations are considered to be within the purview and scope of the invention and appended claims.

We claim:

1. A process for precipitating selenium from solutions of nonferrous metals wich comprises contacting a solution of at least one nonferrous metal selected from the group consisting of cobalt, copper and nickel with a semimetallic chromous precipitant of the nonferrous metal which has a nonferrous metal to chromium ratio between about 10:1 and about 200:1 and which has a metallic content between about 50% and about 90% to precipitate selenium from the solution as a selenide of the nonferrous metal.

2. A process for precipitating selenium from nickel-containing solutions which comprises contacting the nickel solution with a semimetallic nickel chromous precipitant which has a nickel to chromium ratio between about 10:1 and about 200:1 and which has a metallic content between about 50% and about 90% to precipitate selenium from the nickel solutions as nickel selenide.

3. The process as described in claim 2 wherein the nickel-containing solution is at least one solution selected from the group consisting of nickel sulfate and nickel amine sulfate.

4. The process as described in claim 3 wherein the nickel containing solution has a nickel concentrate between about 10 gpl and about 120 gpl.

5. The process as described in claim 4 wherein the nickel solution contains between about 2 ppm and about 40 ppm selenium.

6. The process as described in claim 5 wherein the selenium concentrate is between about 3 ppm and about 6 ppm.

7. The process as described in claims 2 through 6 wherein the semimetallic nickel chromous precipitant is produced by treating a nickel solution or a nickel slurry containing a water-soluble chromium salt in an amount sufficient to provide a nickel to chromium ratio between about 10:1 and about 200:1 with a reducing gas selected from the group consisting of carbon monoxide and hydrogen at a temperature between about 50° C. and about 200° C. using a reducing gas under pressure between about 100 psig and about 800 psig.

8. The process as described in claim 7 wherein the nickel-containing solution or slurry is treated at a temperature between about 80° C. and about 100° C. with a reducing gas under pressure between about 300 psig and about 600 psig.

9. The process as described in claim 8 wherein a nickelcontaining solution is treated to produce a semimetallic nickel chromous precipitant and free acid generated during producing of the precipitant is neutralized with a neutralizing reagent.

10. The process as described in claim 7 wherein the effectiveness of the semimetallic nickel chromous precipitant is improved by adding at least one reagent selected from the group consisting of ferric ions, aluminum ions, silver ions, sulfide ions, cyanide ions, alizarin, polyacrylic acids and anthraquinone in amounts between about 50 ppm and about 200 ppm.

* * * * *

Development work will be conducted at Nine Mile Lake, north of Casper, and at Reno Ranch, approximately 85 mi north of Douglas.

Other participants in the development program are Mono Power Co. and Halliburton Co. The partners have been investigating in-situ leaching technology since 1974 and have successfully demonstrated the commercial feasibility of the technique at the Nine Mile Lake facility since 1976. Following additional investment to establish wells and construct processing facilities, it is anticipated that production from the two sites will reach 500,000 lb of uranium oxide annually in 1981.

For the past several years, RMEC and Marcona Inc. have been engaged in a joint venture to research hydraulic mining of uranium-sandstone through a bore hole. This technique employs a water jet to break and slurry the uranium ore so that it may be pumped to the surface. The test was performed in the Powder River Basin, with encouraging results.

(The Bear Creek operation of Rocky Mountain Energy was described in a paper, "Assessment of New Technology at Bear Creek Uranium Co.," presented at the AMC meeting in Las Vegas in October 1978 by E. A. Lang, a vice president of the company.) □

Producers and newcomers push development plans

WYOMING URANIUM ACTIVITY spans a wide range of companies in various stages of exploration, mine development, and mill planning. Exploration activity, reviewed in greater detail elsewhere in this issue, continues at a fast pace despite governmental red tape. Footage drilled in 1978 is expected to exceed 17 million ft, up from 15.4 million ft in 1977, when it accounted for 37.6% of the US total.

Large petroleum companies lead the drilling activity, followed by smaller petroleum and mining companies and independent operators. In general, drilling depths are increasing and ore grades are falling. However, significant exploration successes are still being recorded.

At the Hauber mine in northeastern Wyoming, Homestake Mining Co., in cooperation with a utility company, is completing the third year of a four-year exploration and development program. The mine, which produced 350 tpd from a 400-ft shaft in 1957, supplied ore to the Edgemont, S. Dak., mill, which is now shut down. TVA recently purchased the mill, but no plans for reactivation have been announced.

Petrotomics mines and mills again

Milling operations have resumed at the 1,500-tpd Petrotomics plant in the Shirley Basin, after a three-year layoff. In early 1975, Getty Oil and Skelly Oil acquired Kerr-McGee Nuclear Corp.'s one-half interest in Petrotomics Co. The mill, with a capacity of 1,500 tpd of uranium ore, had been closed since November 1974, following temporary termination of uranium mining conducted there by KGS-JV, a joint venture of Getty Oil, Skelly Oil, and Kerr-McGee.

Although the Petrotomics mill was idle during 1975, equipment was kept in operating condition, and refurbishing and process improvements were made in anticipation of resuming production in the area in 1977.

The mill is now processing ore from UJV, a joint venture of Getty and Skelly. UJV holds properties in the Shirley Basin estimated to contain 6.9 million tons of in-place reserves having an average grade of 0.19% uranium oxide, or 3.8 lb per ton. Sections 4 and 33 are estimated to contain 4.5 million tons of in-place ore reserves of 0.23% uranium oxide. Construction of a facility for mine equipment maintenance began in 1975, along with removal of overburden.

At present, the Petrotomics mill is also processing ore from the Jenkins project of Utility Fuels Inc., a few miles away.

Getty reached ore in January 1978 in the Section 4 mine. Ore processing began in June. At the rehabilitated mill, a new yellowcake dryer and an improved dust collection system have been installed.

More than 40 million tons of overburden have been removed from the 4-33 mine. Over the estimated 10-yr life of the mine, more than 200 million tons of overburden will be excavated. Stripping is done by two P&H 2300 shovels with 27-cu-yd buckets loading into Unit Rig M120 Lectra Haul trucks.

Mining is done with Cat 2½-cu-yd backhoes loading into 35-ton Euclid trucks. Mine waste is removed by three Marathon LeTourneau Model 1700 front-end loaders with 13-cu-yd buckets, an M-LT Model L80 with a 15-cu-yd bucket, and a Hough Model 580 front-end loader with a massive 25-yd bucket. The MH trucks haul mine waste. Petrotomics will be experimenting in overburden loading and removal with a Unit Rig "Unimatic" bucket wheel loader, which has been beefed up for the job.

Union Carbide adds heap leaching

Union Carbide's Gas Hills operations have responded to stronger uranium demand by stepping up mine production and mill throughput and by installing heap leaching operations. The company's Gas Hills uranium mill has set production records for the last two years.

Capacity of the Gas Hills mill has been expanded to 500,000 tpy of feed. Mill throughput has been increased by speeding up the mill, increasing the sizing on the cyclones, and adding ion exchange capacity. The company expects to produce 1 million lb of uranium oxide this year.

Union Carbide is constructing a large heap leach project that will be 1,200 ft long, 600 ft wide, and 22 ft high.

Major equipment at Union Carbide's open-pit mine

stripping capacity has been increased by 450,000 cu yd per month with a new Marion 191M shovel equipped with a 15-cu-yd bucket, and several new pits have been opened up. The company's scraper fleet stripped the overburden from the Clyde-Bret pit, and mining has begun there. It then moved on to the Sagebrush-Tablestakes site and from there it went to the Sunset property. Stripping is now in progress on the East Gas Hills Cap property.

In addition, an underground mine is being developed to produce ore at the 1,050 level. The main shaft is expected to be completed in late 1978 or early 1979.

A new mine for American Nuclear

American Nuclear Corp., in conjunction with the Tennessee Valley Authority, plans to begin construction of the Cotter Ferguson mine in late 1978. Work will begin upon receipt of the mine permit from the state Department of Environmental Quality. The mine will be located south of the Lucky Mc mine of Pathfinder Mines Corp. The Federal-American Partners mine, in which American Nuclear is a 40% partner, also is nearby.

The Cotter Ferguson mine will be on the Peach claim group, in an established mining district, and mining and reclamation methods will be similar to those being used by other companies in the area.

The project will require a capital investment of $60 million to tap known reserves of 7 million lb of U_3O_8. Stripping will be carried out by a truck-shovel combination, with two 19-cu-yd electric shovels loading into a

firms also have done extensive exploration on top of Beaver Rim and south through the Sweetwater claims.

American is attempting to identify the deep hidden valleys in the Sweetwater area by using seismic techniques. So far, drilling indicates good correlation with the seismic results as deep as 1,100 ft.

Startup at Morton Ranch scheduled for 1980

United Nuclear Corp.'s Morton Ranch mine may be in full production by early 1980, as construction could begin as early as the last quarter of 1978. The mill will take about 15 months to complete. Estimated cost of the mill alone is slightly less than $35 million.

The mine will be located on the Morton Ranch, which is about 18 mi north of Douglas and encompasses about 26,000 acres.

United Nuclear is working on the tailings disposal plan, environmental reports, and radiological assessments. A series of three settling ponds has already been constructed. UNC has been mining some uranium from the first pit for metallurgical testing, and on the northern portion of the property, Teton Drilling Co., a subsidiary of UNC, is doing development drilling to block out orebodies.

In addition to the open-pit mine, United Nuclear is developing an underground mine on the northern edge of the property. The main shaft is 740 ft deep. Track and development work is at the 630-ft level. Drifting is expected to extend about 3,000 ft from the main shaft. The underground mine also is slated to be in full

production by 1980.

United Nuclear and the Tennessee Valley Authority estimate that the properties contain 11.4 million lb of uranium oxide. As half owner, TVA would get 5.7 million lb, or 5% of its identified needs through 1990.

Kerr-McGee mines Bill Smith underground

A new underground mine in the Powder River Basin has returned Kerr-McGee to the ranks of Wyoming uranium producers. The company's Shirley Basin mines were shut down in 1974 after being mined out.

Kerr-McGee's drilling program has included exploration in the Red Desert and Green Mountain districts, which has outlined potentially mineable reserves, and drilling in the Powder River Basin.

The production shaft for the new Bill Smith mine was bottomed out in November 1974, and the main shaft station has been equipped at the 870 level.

The mine will be worked by modified room-and-pillar techniques. The haulage level of the mine is equipped with 36-in.-gauge track. Haulage is carried out by an 8-ton Plymouth locomotive and 110-cu-ft cars.

The 14-ft-dia, concrete-lined shaft is equipped with a Nordberg double-drum hoist and two 110-cu-ft skips in balance.

Kerr-McGee's future uranium development plans, which include several open pit and underground mines, have run into trouble with state agencies. A final decision to settle the disputes should be made in the near future.

Mullen Mining well into four-year project

Mullen Mining Co., operating in the Shirley Basin, relies entirely on large crawler-tractors and a fleet of tractor-scrapers to perform stripping at the four-year Jenkins project. Some 21 million cu yd of overburden will be excavated, at the rate of more than 36,000 cu yd per day.

The scraper hauls tend to be long—3,000 ft to 5,000 ft one way—and the mining company keeps haul surfaces well maintained. The dumps are in previ mined areas of the pit, which makes backhaul fro relatively flat.

Overburden bench areas are often large, with rip and push-loading done on a slight downhill grade speed push-loading by its fleet of 12 Cat 651 and scrapers, Mullen chose a pair of 425-fwhp Fiat-Alli tractors. Their speed and power make it advisabl team each one with two lighter Cat D9s to main push-load balance in the pit.

In the heavy, wet, consolidated sand and clay in upper levels of the pit, the scrapers can take a 45-cu-yd load in 25 sec. Rather than chain-load succeeding scrapers making one long cut down bench, they work the width of the cut in succe passes. This system gives a smoother pit surface, per faster spotting of incoming scrapers, and redu nonproductive tractor time during a long return back to the beginning of the cut.

With production ranging from 35,000 to 50,000 cu per day on two shifts, equipment availability must high.

The Jenkins project being stripped by Mullen managed by Uranium Supply Services Corp. for Ut Fuels Inc., a subsidiary of Houston Industries Inc.

Wyoming Mineral: Solution mine at Irigaray

Wyoming Mineral Corp., wholly owned subsidiar Westinghouse, plans commercial development o Irigaray uranium solution mine in southeastern John County.

The mining method consists of injecting liquid into underground uranium formation, dissolving the ura um, and then pumping it to the surface. The compa which has been mining uranium solution at the rate 100 gpm at the site, plans to increase the rate to 1,000 1,600 gpm. Planned capacity of the leaching proces 500,000 lb of uranium oxide annually—equal to yield from mining about 750,000 tons of average-gra ore. □

State makes it tough to get okays for new projects

STATE AGENCIES AND ENVIRONMENTALISTS are raising a red flag to halt major uranium expansion in Wyoming. The Wyoming Industrial Siting Council, for example, has rejected a proposed compromise and ordered Kerr-McGee Nuclear Corp. instead to file for a permit for a proposed $600 million uranium complex in Converse County.

Minerals Exploration, a subsidiary of Union Oil Co. of California, is under pressure from the Wyoming Environmental Quality Council, which charges that the company has made significant changes in plans since its application for a permit to construct a uranium mine and a 3,000-tpd mill in the Red Desert of southwestern Wyoming. As a result, the council has authorized its staff agency either to dismiss the company's applicat or to accept amendments incorporating the changes

The Wyoming Outdoor Council, an environmental group, has also made its objections known to Miner Exploration and to the state. Minerals Exploration h hoped to be in production by September 1977. But permit application was denied twice by the Wyomi Environmental Quality Council. When the permit finally granted after the plan had been resubmitted, Wyoming Outdoor Council charged that the state age cy had overlooked important issues, such as possib lowering of the water table and improper design for uranium tailings disposal.

A host of other companies are waiting to see how

AMERICAN INSTITUTE OF MINING AND METALLURGICAL ENGINEERS, MINING TECHNOLOGY,

Technical Publication No. 1189

(Class B, Milling and Concentration, No. 101)

Principles of Comminution, I—Size Distribution and Surface Calculations

By R. Schuhmann, Jr.,* Junior Member A.I.M.E.

(New York Meeting, February 1940)

Problems in expressing, interpreting, and using size-distribution data recur in many phases of mineral dressing; therefore it is desirable that size analyses be expressed in such a form, either numerically or graphically, that comparisons can be made readily.

The size distribution of comminuted material is a result of a specific physical operation on the material and therefore should be governed by some definite physical principle, or cause-effect relation. Although this principle has not been discovered, it has been found that the size distribution of comminuted, homogeneous solids may be expressed by relatively simple mathematical equations. Two equations in particular, proposed by Gaudin[1] and by Rosin and Rammler,[2] respectively, have stood out, both having wide demonstrated ranges of application. The form and the method of application of the two appear almost irreconcilably different on the surface, but, as will be shown, they are asymptotic in the fine sizes when expressed in the same units.

This paper gives the results of a further study of the Gaudin and Rosin-Rammler relations, made with the object of developing a form of size-distribution equation that will be more usable and more significant—particularly in comminution studies, both for interpreting the nature of size distribution and for evaluating surface. The work is summarized in the following:

1. An equation relating *cumulative per cent finer* to *particle size* in the fine sizes is derived from Gaudin's original equation. That equation relates *weight per cent retained* on one size and through the next larger size in a geometric series of sizes to *size* (of the retaining screen, for example).

2. Comparisons with Gaudin's equation and with the Rosin-Rammler equation show that the cumulative equation applies to the fine sizes of all size distributions that fit either of these earlier relations, and, furthermore, has some advantages over each.

3. A simple graphical method of surface calculation based on the cumulative-equation plot is evolved and illustrated.

4. Additional confirmation of the cumulative equation was obtained in the more severe test of sizing down to the limit of a sedimentation balance a sample of jaw-crushed quartz. The equation was closely followed over a 200-fold range in size, from approximately 0.4 mm. (35 mesh) down to 0.0023 mm. (2.3 microns), the lower limit of the size analysis made. There is no indication that the equation will not hold further to well below 2.3 microns.

5. Calculations of the surface produced in the jaw-crushing test mentioned above showed that at least 80 per cent of the total new surface was on particles finer than 35 mesh (about $\frac{1}{25}$ of the crusher setting). The minus 35-mesh portion was only

Manuscript received at the office of the Institute Nov. 30, 1939.

* Instructor in Mineral Dressing, Massachusetts Institute of Technology, Cambridge, Mass.

[1] References are at the end of the paper.

Mining Technology, July 1940. Printed in U. S. A.

12 per cent of the total weight of the crushed quartz.

6. The surface calculations for the data from the jaw-crusher test, together with the extrapolations below the measured size range, demonstrate the extreme importance of extending measurements of size distribution and surface into the nearly untouched size range between unit crystal size and about one micron.

Derivation of Cumulative Size-distribution Equation

The starting point of this derivation is Gaudin's equation for comminuted, homogeneous solids:[1]

$$w = Cx^m \qquad [1]$$

in which w is the weight per cent retained on the screen of opening x and passing the next larger screen of opening px in a geometric series of sieves, and C and m are constants.

The *cumulative per cent finer* than x, designated by y, is the sum of the weight per cents retained on all screens finer than x; that is, it is the sum of the series of values of w corresponding to $\frac{x}{p}$, $\frac{x}{p^2}$, $\frac{x}{p^3}$, etc. Thus

$$y = C\left(\frac{x}{p}\right)^m + C\left(\frac{x}{p^2}\right)^m + C\left(\frac{x}{p^3}\right)^m + \text{etc.} \qquad [2]$$

$$= Cx^m(p^{-m} + p^{-2m} + p^{-3m} + \text{etc.}) \qquad [3]$$

If it is assumed that equation 1 holds down to $x = 0$, the series in equations 2 and 3 are infinite geometric series, whose sums are given by simple algebra, and

$$y = Cx^m\left(\frac{p^{-m}}{1 - p^{-m}}\right) \qquad [4]$$

Defining a new constant k in terms of the constants C, m, and p as $\left(\frac{Cp^{-m}}{100(1 - p^{-m})}\right)^{-\frac{1}{m}}$ and substituting in equation 4 gives the *cumulative size-distribution* equation:

$$y = 100\left(\frac{x}{k}\right)^m \qquad [5]$$

The assumption made in the derivation, that equation 1 is valid down to $x = 0$, is probably untrue. If equation 1 is valid only to a lower size limit x_0, then instead of eq. 5 the following is obtained:

$$y = 100\left[\left(\frac{x}{k}\right)^m - \left(\frac{x_0}{k}\right)^m\right] \qquad [5a]$$

Actually, as will be brought out later, eq. 5 in its simplest form has held for all data tested, within the experimental error. This shows that x_0 is negligible compared with x in the present range of size-distribution measurement (down to 1 or 2 microns), and therefore the existence of a definite lower size limit must rest on evidence other than available size-distribution data.

The same constant m appears as an exponent of x both in Gaudin's equation and in the derived cumulative equation. The physical significance of this constant and its importance in interpreting size-distribution data were pointed out and illustrated experimentally by Gaudin in his study of the original equation.[1] In this work the constant m will be called the *distribution modulus*.

One of the disadvantages of Gaudin's original equation is that the constant C has no simple physical interpretation. Actually its value varies with the sieve ratio p, as well as with the material whose size distribution is being expressed. That is, in using the equation, a particular geometric-series sizing system must be adopted and specified. On the other hand, the cumulative equation applies to data relating cumulative per cent and size, obtained by any sizing system. The constant k in the cumulative equation has dimensions of particle size, and hence will be termed the *size modulus*. Thus, the size distribution of a comminuted product

in the fine sizes is specified by giving the two constants of equation 5, the distribution modulus and the size modulus, both of which have definite and easily visualized physical meanings.

Gaudin[1a] and Bond and Maxson,[3a] in applying eq. 1 to extrapolations and surface calculations, have used a mathematical approximation, which has not been so designated heretofore. This approximation is represented in the assumption that the weight of particles in a given size fraction (w between x and px) is evenly distributed over the size range of the fraction (x to px). This assumption is not necessary in dealing with cumulative percentage.

Evaluation of m and k.—Taking common logarithms of both sides of eq. 5,

$$\log y = m(\log x) + 2 - m(\log k) \quad [6]$$

As m and k are constants, it is obvious that a plot of log y (*log cumulative per cent finer*) versus log x (*log size*) gives a straight line of slope m. Also, when $y = 100$ per cent, $x = k$.

This is illustrated in the cumulative curve in Fig. 1, based on data published by Bond and Maxson.[3b] The data for the fine sizes fit a straight line of slope $m = 0.640$. The size modulus k for the fine sizes is 9.0 mm., and is found by extending the line of distribution of fine sizes to find its intersection with the horizontal line corresponding to 100 cumulative per cent finer.

For comparison, the same size analysis is also plotted in Fig. 1 in the manner originally suggested by Gaudin (log weight per cent retained versus log size). This must also fit, in the fine sizes, a straight line of the same slope as the cumulative line, but it is apparent that this method of plotting magnifies screening errors so that accurate location of the line and measurement of the parameters is rather difficult. The difficulty is demonstrated by Bond and Maxson's postulate that this particular analysis should be represented by two straight lines instead of one in the fine sizes. Furthermore, the fact that the cumulative data fit a straight line within the experimental error of the analysis

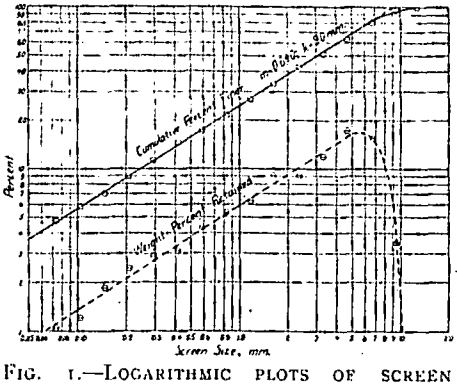

FIG. 1.—LOGARITHMIC PLOTS OF SCREEN ANALYSIS OF GYRATORY CRUSHER PRODUCT.
Data from Bond and Maxson.[3b]

(and therefore fit equation 5) shows that there is no evidence whatever in this size analysis alone for the existence of a lower size limit or of unground colloidal material.

CALCULATION OF SURFACE AREA

The surface area $d\sigma$ of particles ranging in size from x to $x + dx$ in a sample of 100 grams equals the product of the specific surface of these particles, $\frac{S}{x}\left(S = \frac{6}{\text{sp. gr.}}\right.$, for spheres when x is given in centimeters and surface in square centimeters),* and the weight of those particles, dy:

$$d\sigma = \frac{S}{x}dy \quad [7]$$

Differentiating eq. 5,

$$dy = \frac{100\, mx^{m-1}}{k^m} \times dx \quad [8]$$

Substituting eq. 8 in eq. 7, and integrating to find the surface $\sigma_2 - \sigma_1$ between

* Surface on one sphere of diameter x is πx^2. The weight of one sphere is $\frac{\pi x^3}{6} \times$ (sp. gr.). Thus the specific surface, or surface area per unit weight, of spheres of diameter x is $\frac{\pi x^2}{\frac{\pi x^3}{6} \times \text{(sp. gr.)}}$, or $\frac{6}{x \times \text{(sp. gr.)}}$

sizes x_1 and x_2 (assuming S does not vary with size in the range considered),

$$\sigma_2 - \sigma_1 = 100S \times \frac{m}{m-1} \times \frac{x^{m-1}}{k^m}\Big]_{x_1}^{x_2} \quad [9]$$

Thus the surface on particles between two sizes, in the range of validity of the cumulative equation 5, is given by the difference between the values of σ for the two sizes, where

$$\sigma = 100\frac{S}{k^m} \times \frac{m}{m-1} \times x^{m-1} \quad [10a]$$

or,

$$-\sigma = 100\frac{S}{k^m} \times \frac{m}{1-m} \times x^{m-1} \quad [10b]$$

Taking common logarithms of both sides of eq. 10*a*,

$$\log \sigma = (m-1)\log x + \log\left(\frac{m}{m-1}\right) + \log\left(\frac{100S}{k^m}\right) \quad [11a]$$

or of eq. 10*b*, to avoid an equation with the logs of negative numbers when $m < 1$,*

$$\log(-\sigma) = (m-1)\log x + \log\left(\frac{m}{1-m}\right) + \log\left(\frac{100S}{k^m}\right) \quad [11b]$$

From these equations it is apparent that a logarithmic plot of the positive value of σ versus *size* gives a straight line of slope $(m-1)$. Also, when $x = k$,

$$\sigma = 100\frac{S}{k} \times \frac{m}{m-1},$$

or $(-\sigma) = 100\frac{S}{k} \times \frac{m}{1-m}$ (used if $m < 1$). That is, the line passes through the point whose abscissa is $\log k$, and whose ordinate is $\log\left(100\frac{S}{k} \times \frac{m}{m-1}\right)$ when $m > 1$, or $\log\left(100\frac{S}{k} \times \frac{m}{1-m}\right)$ when $m < 1$. (Note: $\frac{S}{k}$ = specific surface corresponding to size k.)

The location of the σ line from a logarithmic plot of size distribution, and the use of the graph for surface estimation are illustrated in Fig. 4 and Table 1, which are taken up in more detail later.

Summary of Graphical Procedure

The graphical process for which the mathematical basis has been given in the preceding pages is as follows:

1. Plot *cumulative per cent finer* against *size* on logarithmic paper (equal intervals along both axes). The succeeding steps are applicable only to the straight-line region established on the graph for the fine sizes.

2. Measure the slope of the line, which is the *distribution modulus* m. Read the *size modulus* k as the abscissa of the point of intersection of the extended distribution line with the horizontal line at 100 cumulative per cent finer (point A in Fig. 4).

3. Calculate the specific surface for particles of size equal to k, the size modulus, assuming that the particles are spheres (in Fig. 4, $k = 4.74$ mm., sp. gr. = 2.65; thus specific surface of particles of size k is $\frac{6}{2.65 \times 0.474}$ or 4.777 sq. cm. per gram).

4. Multiply the figure for specific surface calculated in step 3 by the factor $\frac{100m}{m-1}$, in which m is the distribution modulus measured in step 2. Drop the minus sign obtained when m is less than 1. This product may be designated as σ_k (in Fig. 4, $m = 0.873$; thus

$$\sigma_k = 4.777 \times \frac{100 \times 0.873}{0.127} = 3283 \text{ sq. cm. per 100 grams}).$$

5. Draw a straight line of slope $(m-1)$ through the point whose abscissa is k

* The case for $m = 1$ is not considered, and the graphical method of surface calculation cannot be used when $m = 1$. If this case is encountered, surface is calculated from the following: When $m = 1$, the total surface between two consecutive sizes in a geometric series of sizes is constant over the range of validity of eq. 5.

and whose ordinate is σ_k. Positive values of σ can be read from this line for various values of size (in Fig. 4, a line of slope -0.127 is passed through point B, whose abscissa and ordinatee ar read as 4.74 and 3283, respectively).

6. The surface between two sizes in the range of linearity of the size-distribution plot is the difference between the values of σ for the two sizes.

7. The surface area for sizes above the straight-line region is calculated separately in the customary manner; or the total may be roughly approximated by using the σ line and assuming the upper size limit to be k.

Testing the Cumulative Equation

Reproduction of all data used for testing eq. 5 is not justified, but the method of testing and the principal sources of data require brief consideration.

The testing method consisted simply in plotting the data as log cumulative per cent finer versus log size (or easier, cumulative per cent finer versus size on logarithmic paper), and determining whether the data fitted a straight line in the finer sizes.

The size analyses tried by this method were all on products of crushing or grinding homogeneous or nearly homogeneous minerals or rocks, as the size-distribution principle does not apply unmodified to a mixture of minerals of different physical properties or to a rock with structural heterogeneities, such as a natural grain size, occurring in the size range under consideration.[1]

It should be emphasized that all the data in the literature that have been shown to fit Gaudin's original relation (eq. 1), are mathematically required to fit either eq. 5 or eq. 5*a*. The fact that the data tested all fit the cumulative eq. 5 within experimental error indicates that a lower size limit is well beyond evaluation by the size-distribution technique used. Some of the data extend to 1 or 2 microns, hence the lower size limit must be well below 1 micron.

The size-distribution data tested, all of which, with the few exceptions noted, fit eq. 5 within the probable accuracy of the data, were the following:

Screen analysis of Montana gold ore, gyratory product, Bond and Maxson.[3b] (See Fig. 1.)

Screen and sedimentation-balance analysis of quartz, jaw-crusher product. (See Fig. 4 and later discussion.)

Two typical coal-screen analyses, Geer and Yancey (samples A and B, Table 1).[4] (See Fig. 2.)

Screen analyses of ball-mill ground quartz, Gross (Tables 80, 81, 82 and 83).[5] Exceptions, not fitting the equation, were for grinding tests under the extreme conditions of using "pulps" of 96 and 98 per cent solids.

Screen analyses of flint and dolomite, ball-mill products, Coghill and co-workers (Tables 3 and 4).[6]

Screen analyses of roll-crushed Hollinger quartz and Coniagas conglomerate, Haultain.[7]

Sedimentation-balance analyses of ball-mill ground galena, Schlechten[8] and Diokno.[9] The deviation from eq. 5 found in two of these analyses may have been due to incomplete dispersion before sedimentation.

Comparison with Rosin-Rammler Equation

The Rosin-Rammler equation, in the form used by Bennett[10] and by Geer and Yancey[4] is

$$R = 100e^{-\left(\frac{x}{k'}\right)^{m'}} \qquad [12]$$

in which R is the cumulative per cent coarser than size x, e is the base of natural logarithms, and m' and k' are parameters of essentially the same physical significance as the corresponding parameters m and k in

the cumulative equation. In terms of cumulative per cent finer

$$y = 100 - R = 100\left[1 - e^{-\left(\frac{x}{k'}\right)^{m'}}\right] \quad [13]$$

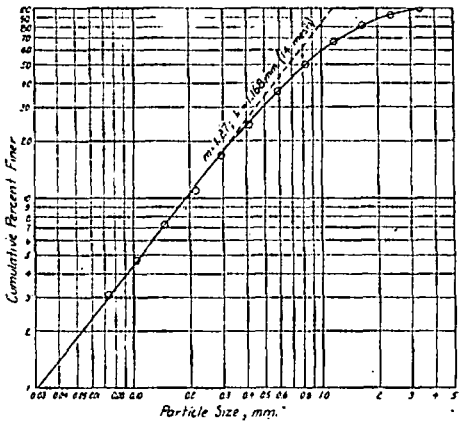

FIG. 2.—SCREEN ANALYSIS OF COAL SAMPLE OBEYING ROSIN-RAMMLER EQUATION.
Data from Geer and Yancey,[4] Table 1, sample A.

The general similarity between these equations and eq. 5 is heightened by expanding the Rosin-Rammler equation. Applying Maclaurin's expansion,[11]

$$1 - e^{-\left(\frac{x}{k'}\right)^{m'}} = \left(\frac{x}{k'}\right)^{m'} - \frac{\left(\frac{x}{k'}\right)^{2m'}}{2!} + \frac{\left(\frac{x}{k'}\right)^{3m'}}{3!} - \cdots \quad [14]$$

which is a converging series when

$$\left(\frac{x}{k'}\right)^{m'} < 1.$$

If all terms except the first term in the right-hand member of eq. 14 are neglected, and the resulting equation is combined with eq. 13, we obtain

$$y = 100\left(\frac{x}{k'}\right)^{m'} \quad [15]$$

which is the same as eq. 5. Actually, later terms of the series in eq. 14 do become negligibly small in comparison with the first term when low values of $\frac{x}{k'}$ are considered. Thus, in the fine sizes, the size-distribution equation derived in this paper agrees with the Rosin-Rammler equation, and the parameters are the same. This is illustrated in Fig. 2, in which a screen analysis following the Rosin-Rammler equation is plotted on the logarithmic basis for testing the applicability of eq. 5. The straight line represents eq. 5, using Geer and Yancey's values

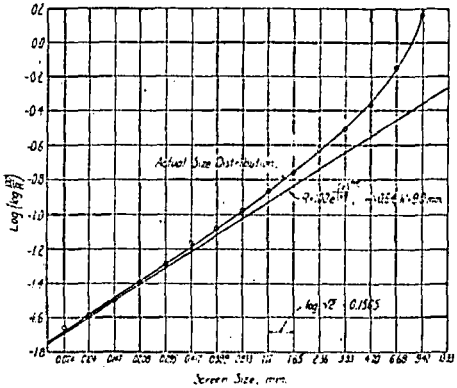

FIG. 3.—ROSIN-RAMMLER PLOT OF SCREEN ANALYSIS OF GYRATORY CRUSHER PRODUCT.
Data from Bond and Maxson.[36]

of the parameters, which they determined by applying the Rosin-Rammler equation.

The graphical method of using the Rosin-Rammler equation consists in plotting $\log\left(\log \frac{100}{R}\right)$ versus log size.[4] The equation gives a straight line. Comparisons of plots obtained by this method with those obtained by plotting log cumulative per cent finer versus log size for the data listed in the preceding section (not including coal) showed: (1) both methods give straight lines in the fine sizes, confirming the mathematics above; and (2) the straight lines generally extended over a wider range with the log cumulative method of plotting. This is illustrated in

Figs. 1 and 3, in which the same analysis is plotted according to the two different systems. The straight line in Fig. 3 is a graph of the Rosin-Rammler equation 12 for $m' = 0.64$ and $k' = 9.0$ mm., values found in Fig. 1 for m and k as described earlier.

Logarithmic-probability Method of Plotting Size Distribution

Another relation, which has been successfully applied to give linear size distribution plots, in certain cases giving straight lines over the range of sizes between 5 and 95 cumulative per cent finer or better, is the logarithmic-probability relation, discussed and illustrated recently by Austin.[13] Austin summarizes the method as follows: " . . . plot particle size on a logarithmic scale and cumulative per cent oversize, or undersize, on a probability scale—that is, a scale whose intervals are based upon values of the probability integral. As graph paper with these coordinates is available, this method is very convenient."

Examination of this method brings out the following significant point: A particulate material whose size distribution is represented by a single straight line over a size range including a large portion by weight (for example, from 10 to 90, or 5 to 95 cumulative per cent) of the material may be described as a material of "symmetrical size distribution." Plotting such a distribution as weight frequency versus log size gives a curve that has the shape of a probability curve (over the range of linearity of the log-probability plot) and is symmetrical about the size corresponding to 50 cumulative per cent. The plot of the screen analysis of this ideal material, as weight per cent retained (on a given size and through the next larger size in a geometric series of sieves) versus log size likewise gives a symmetrical curve of the probability type. In view of the fact that such plots for comminuted products are almost invariably asymmetric or "skewed" to a considerable extent, it is apparent that the logarithmic-probability method of plotting cannot give simple linear plots covering large weight percentages of comminuted products.

Application to Product of Jaw-crushing Test

Experimental.—A 6.7-kg. sample of 1 to 1½-in. quartz was prepared by crushing pure quartz lumps through 1½ in. in a jaw crusher and screening the product on a 26.67-mm. screen. The sized quartz was thoroughly washed free of dust and fines by shaking on a screen under a stream of tap water, and finally was rinsed with distilled water.

The wet quartz sample was then fed to a clean Sturtevant laboratory jaw crusher, set at ⅜ in. The crusher mouth was kept full (choke feeding), and also a good stream of distilled water was used to prevent loss of dust and to wash out the crusher at the end.

The whole of the wet product was then carefully sized according to the following procedure: (1) wet-screen at 8 mesh, dry oversize, and screen dry into fractions above 8 mesh, adding additional minus 8-mesh to remainder; (2) repeat the same procedure at 100 mesh on undersize from 1; (3) wet-screen undersize from step 2 at 400 mesh, and then wet-screen the plus 400-mesh into fractions on 150, 200, 270 and 400 mesh; (4) dry all minus 400-mesh material, mix, sample, disperse in water, and determine its size distribution by the sedimentation-balance method.*

Results of the complete analysis are given in Table 1 and graphically represented in Fig. 4, following the procedure developed earlier in this paper. Fig. 4 shows that the size distribution, plotted as log cumulative per cent finer versus log size, follows a

* A new form of apparatus has been developed at Massachusetts Institute of Technology and checked against other sizing methods. It will be described in a later paper.

straight line over the roughly 200-fold range from 0.4 mm. down to 2 microns. Characteristics of the line are: $m = 0.873$; $k = 4.74$ mm. The characteristics of the three sizing methods (dry screening, wet screening, and sedimentation) show up as small displacements of the line, as might be expected.

of the weight of the sample. However, from the standpoints of surface and of number of size fractions, the straight line includes the major part of the plot.

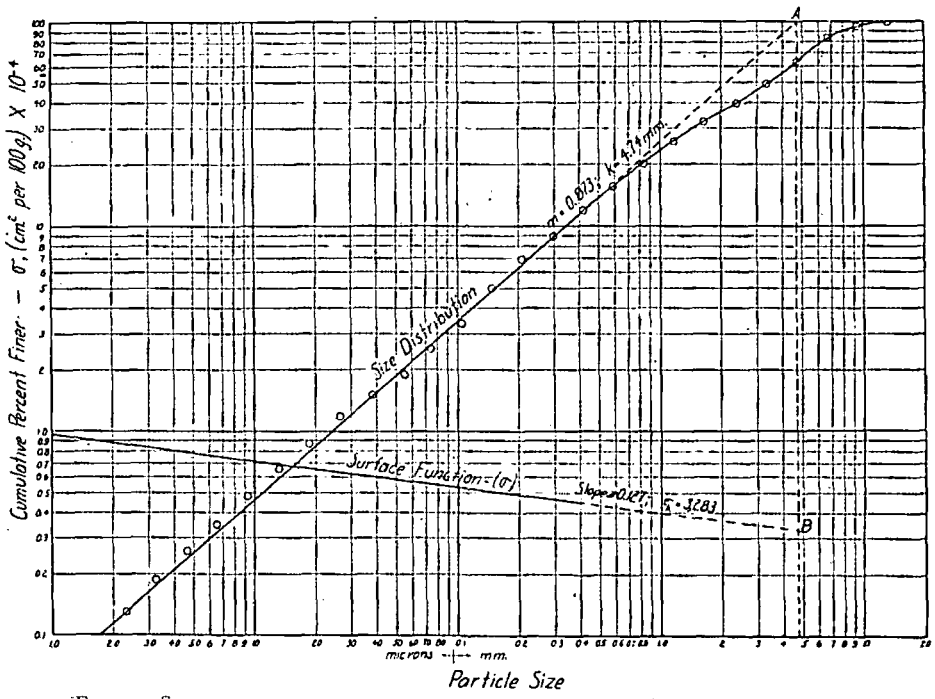

FIG. 4.—SIZE DISTRIBUTION AND SURFACE CALCULATION FOR JAW-CRUSHED QUARTZ.

Theoretical values of the cumulative per cent finer, at sizes 1.0, 0.1, 0.01, and 0.001 micron, were found by extending the straight line (not shown). These extrapolated figures are given in column 4 in Table 1.

The limited experience with this plotting method to date does not justify interpretation of the shape of the curve in the coarse sizes, but it is believed that the plotting method offers good possibilities in studying crushing action, natural grain-size phenomena, etc. From the standpoint of amount of material involved, the straight line covers only about the finest 15 per cent

Surface areas for the sizes in the curved portion of the graph were calculated by the customary method, assuming spheres or cubes, as indicated in columns 2 and 6.

Location of the surface-function (σ) line followed the procedure already outlined, and is indicated in the figure. Values of σ read from this line are given in column 5 of the table, together with extrapolated values for 1.0, 0.1, 0.01, and 0.001 micron, obtained by extending the surface-function line (not shown). Surface areas for the various size groups, found as differences between the σ values, are given in the last column. By comparing the two parts of column 6 for the coarse sizes, it will be noted that in calculating surface for this particular sample no appreciable error is introduced in assuming the whole analysis

TABLE I.—*Size Analysis of Jaw-crushed Quartz and Surface Calculations*
Feed: Pure quartz lumps, through 1½, on 1 inch.
Sturtevant laboratory crusher, setting ⅜ in. (10 mm.).
Product: Size modulus $k = 4.74$ mm. Distribution modulus $m = 0.873$

1 Size		2 Theoretical Specific Surface of Material Retained, Sq. Cm. per Gram[a]	3 Weight Per Cent Retained on	4 Cumulative Weight Per Cent Finer	5 σ from Graph, Sq. Cm. per 100-gram Sample	6 Surface Area, Sq. Cm. per 100-gram Sample	
Mm.	Microns					Col. 2 × Col. 3[a]	From σ Graph
			Tyler screens: dry				
13.33		1.4	0.000	100.000		0.0	
9.423		2.0	1.885	98.115		3.8	
6.680		2.8	14.173	83.942		39.7	
4.699		4.0	20.451	63.491	3,283 for	81.8	
3.327		5.6	14.221	49.270	$k = 4.74$ mm.	79.6	
2.362		8.0	9.561	39.709		76.5	
1.651		11.3	7.545	32.164		85.2	1,157
1.168		15.9	6.147	26.017		97.8	
0.833		22.5	5.833	20.184		131.2	
0.589		31.8	4.477	15.707		142.4	
0.417		45.0	3.718	11.994	4,440	167.0	
			Total surface in plus 0.417-mm. particles			905.0	1,157
0.295			3.011	8.983			
0.208			2.049	6.934			
0.147			1.932	5.002			
			Tyler screens: wet				
							1,560
0.104			1.613	3.389			
0.074			0.848	2.541			
0.053			0.645	1.896			
0.038			0.394	1.502	6,000		
			Total surface in plus 0.038-mm. particles			2,465	
			Sedimentation balance; sizes by Stokes' Law for theoretical quartz spheres				
	26.2		0.331	1.171			
	18.5		0.289	0.882			
	13.1		0.222	0.660			
	9.3		0.175	0.485			
	6.5		0.133	0.352			2,600
	4.6		0.092	0.260			
	3.3		0.073	0.187			
	2.3		0.050	0.131	8,600		
	−2.3		0.131				
1.0 (through 2.3 microns)			Total surface in plus 2.3-micron particles 0.068[b]	0.063[b]	9,600[b]	5,065	1,000[b]
0.1 (through 1.0 microns)			Total surface in plus 1-micron particles 0.055[b]	0.0068[b]	12,800[b]	6,065[b]	3,200[b]
0.01 (through 0.1 micron)			Total surface in plus 0.1-micron particles 0.007[b]	0.001[b]	17,200[b]	9,265[b]	4,400[b]
0.001 (through 0.01 micron)			Total surface in plus 0.01-micron particles 0.00085[b]	0.00015[b]	23,200[b]	13,065[b]	6,000[b]
			Total surface in plus 0.001-micron particles			19,665[b]	

[a] Slide-rule accuracy.
[b] Based on graphical extrapolation.

to be represented by the straight-line relation. Running totals are also given in column 6.

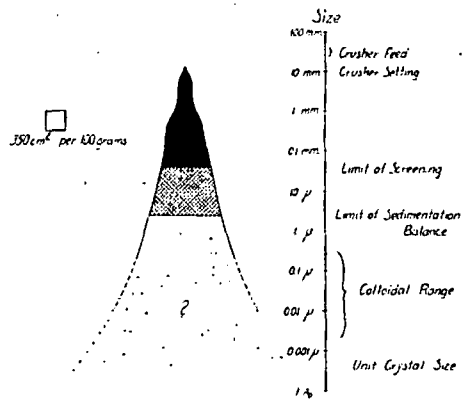

FIG. 5.—SURFACE DISTRIBUTION IN JAW-CRUSHER PRODUCT.

Significance of Surface Calculations.—Before discussion of the calculations, it should be pointed out that there are three questionable, interrelated assumptions in calculating surface from size: (1) that the particles are spheres; (2) that all the surface is on the outside; and (3) that the proportionality constant between specific surface and the reciprocal of size does not vary with size. The first assumption is easily corrected by applying a constant shape factor, and therefore detracts little or nothing from the value of the calculations. On the basis of Gross and Zimmerley's[12] measurements of quartz surface by the dissolution method, it appears that assumptions 2 and 3 are objectionable only in coarser sizes of small specific surface. Therefore, it appears likely that calculation from size distribution is a reliable method for determination of surface in fine sizes.

The schematic diagram in Fig. 5 was constructed to aid in visualizing the results of the surface calculations. Areas on this diagram represent actual surface areas determined in Table 1 and Fig. 4. The portion of the diagram down to 2.3 microns was established experimentally, and the dotted area below is based on the assumption that the size distribution follows the same equation on down to about unit-crystal size.

It is apparent from Fig. 5 that the portion of the jaw-crusher product below 2.3 microns, small as it is (0.13 per cent of the total weight), may conceivably account for most of the surface. From the fact that no deviation from the cumulative size-distribution equation is detected experimentally at 2.3 microns, the extrapolation down to 0.1 or 0.2 micron does not seem at all unreasonable. On the other hand, validity of the equation all the way down to unit-crystal size can well be questioned. There has been a tendency in the past to specify a lower size limit of crushing effect when the portion of the sample involved becomes too small for detection by rough tests, but obviously this is not justified when surface area is as important as it is in comminution.

By the numerical data in column 6, Table 1, it may be seen that of the surface calculated from the part of the size distribution actually measured (down to 2.3 microns), less than 20 per cent is in sizes above 35 mesh; that is, in sizes larger than about $\frac{1}{25}$ of the crusher setting. Over 80 per cent of the product surface thus determined is on particles finer than 35 mesh.

Making the extrapolation to 0.1 micron, which should give at least a first approximation, it appears that about 90 per cent of the total surface above 0.1 micron is on particles finer than 35 mesh.

The further extrapolations, of doubtful validity, to 0.01 and 0.001 micron, suggest that as much as 93 or 95 per cent of the total surface produced in jaw-crushing the quartz through $\frac{3}{8}$ in. may be on particles finer than 35 mesh—also that as much as 80 or 85 per cent of the surface may be below the screen-sizing range.

Just as the first explorations into the subsieve range in the last 20 years have made possible considerable advances in comminution theory, it now seems probable that exploration into the colloidal

range of sizes may reduce still more the formidable array of what we do not know about comminution.

Acknowledgment

The writer wishes to express his appreciation to Prof. A. M. Gaudin for critically reading the manuscript and making helpful suggestions regarding the presentation of this material.

References

1. A. M. Gaudin: An Investigation of Crushing Phenomena. *Trans.* A.I.M.E. (1926) 73, 253–316. (*a*) See equation 4, p. 290.
2. P. Rosin and E. Rammler: Laws Governing the Fineness of Powdered Coal. *Jnl.* Inst. of Fuel, (1933) 7, 29–36.
3. F. C. Bond and W. L. Maxson: Crushing and Grinding Characteristics as Determined from Screen Analyses. *Trans.* A.I.M.E. (1934). 112, 146–160. (*a*) Equations 5, 6 and 9, p. 50–51. (*b*) Table 2, p. 154.
4. M. R. Geer and H. F. Yancey: Expression and Interpretation of the Size Composition of Coal. *Trans.* A.I.M.E. (1938) 130, 250–269.
5. J. Gross: Crushing and Grinding. U. S. Bur. Mines *Bull.* 402 (1938).
6. A. M. Gow, M. Guggenheim, A. B. Campbell and W. H. Coghill: Ball Milling. *Trans.* A.I.M.E. (1934) 112, 24–78.
7. H. E. T. Haultain: A Contribution to the Kick versus Rittinger Dispute. Univ. Toronto *Eng. Research Bull.* (1924) 4, 145–162.
8. A. W. Schlechten: Private Communication.
9. A. W. Diokno: Flotation Rate and Froth Mineralization in Batch Flotation. S. M. Thesis, Mass. Inst. Tech. (1939).
10. J. G. Bennett: Broken Coal. *Coll. Guard.* (1936) 153, 945–948.
11. Handbook of Engineering Fundamentals (O. W. Eshbach Editor), 2, 79. New York, 1936. John Wiley and Sons.
12. J. Gross and S. R. Zimmerley: Crushing and Grinding, II—The Relation of Measured Surface of Crushed Quartz to Sieve Sizes. *Trans.* A.I.M.E. (1930) 87, 27–34.
13. J. B. Austin: Methods of Representing Distribution of Particle Size. *Ind. and Eng. Chem.* (1939) 11, 334–399.

Economic Geology
Vol. 74, 1979, pp. 353-357

Potash and Politics

PAUL A. RITTENHOUSE

Abstract

World demand for potash for agricultural purposes will continue to expand with increasing world demand for food and fiber. World supplies of potash appear more than adequate to meet future increases in demand. However, potash reserves and production facilities are increasingly coming under the control of national governments and in the future the industry outlook will be affected more by political factors than by the economics of the marketplace. As a result, the private enterprise potash producer faces a difficult time competing in a world market dominated by large, politically motivated, government-controlled companies.

Introduction

WHEN the organizers of the potash program for the 1978 annual meeting of the Society of Economic Geologists and the Society of Mining Engineers of the American Institute of Mining Engineers invited me to present a paper on the supply/demand outlook for potash, they did not specify how far into the future they wanted me to look, and it seems to me that the time element is crucial to you who are geologists or miners as well as to me, an economist and forecaster. In your case, you have to look far enough into the future to provide time to explore, discover, evaluate, develop, and bring into production a commerical deposit. My mining associates and friends do not agree on the time required for these accomplishments, but it is probably in the range of eight to fifteen years. They do agree that the time required is continually increasing. My time problem is exactly the opposite of the explorationists and miners: they want more time, I want less. It is relatively easy, and I stress "relatively," to identify and evaluate the importance of the various factors that impact on both the supply of and demand for a commodity such as potash if the time period is today. It becomes more difficult, obviously, the farther one attempts to project into the future and really becomes sticky when one starts talking in terms of years, in which case the old crystal ball becomes mighty cloudy. However, we economists and forecasters are not known for our temerity, so let me get on with the job at hand and take a look at the world potash supply/demand outlook. In my opinion this relationship, during and beyond the time period I will be discussing, will be affected profoundly by the large-scale entry of government entities into potash production, processing, and marketing, hence the title of this paper, "Potash and Politics."

Historical Background

First, it is probably a good idea to get a little historic perspective about potash.

Potassium, phosphorus, and nitrogen make up the three primary nutrients that are required for plant growth and it is as a plant nutrient that potash derives most of its market. About 95 percent of the potash produced in the world is utilized as a fertilizer. The remaining 5 percent is consumed in a large variety of industrial uses including detergents, television tubes, and the production of industrial chemicals. These industrial markets are very small compared to the fertilizer market and the data on them are rather limited. Therefore, most of the demand data which follow refer to the fertilizer market.

Historically, the growth in world demand for all fertilizer has been extraordinary. In the fertilizer year 1976/77, the world consumed over 93 million metric tons of primary plant nutrients. Nearly half was nitrogen and a quarter each, phosphates and potash. The world use of nutrients today is double what it was 10 years ago and more than triple what it was in 1962 (Fig. 1).

The potash component of those consumption data totaled about 23 million metric tons K_2O in 1976/77 and shows a similar historic growth trend (Fig. 2).

Potash is consumed as a fertilizer material in nearly all countries of the world, some 140 by last count. A few areas account for the bulk of the consumption. The USSR, the United States, France, West Germany, and Japan use nearly 60 percent of the world's production. The product is used mainly as KCl (potassium chloride), although potassium sulfate and nitrate are also popular fertilizer product forms.

In contrast to the many consuming countries, potash is produced in only about a dozen countries. Six of them, the USSR, Canada, East and West Germany, the United States, and France, account for over 90 percent of the world's production. Four of these producers, Canada, the USSR, and the two Germanies, also have over 95 percent of known reserves (Table 1).

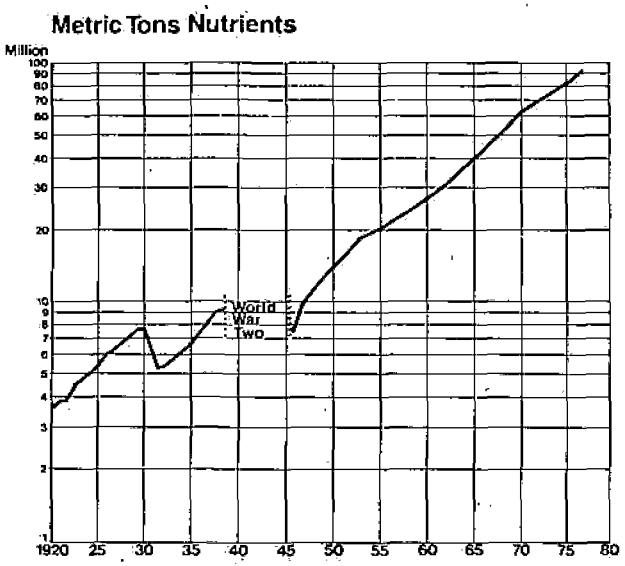

FIG. 1. World fertilizer consumption.

Since there are relatively few producers and many consumers, there is a brisk world trade in potash. In 1976, for instance, nearly 13 million tons of K_2O or 55 percent of the total world's requirements entered world trade. Canada, which supplied 40 percent of the total, is the largest world supplier, while East Germany and the USSR each supply about 20 percent. Figure 3 indicates the major world flows of potash in 1976.

Supply and Demand Outlook

Now let's take a look at the future. We expect that the demand for potash will continue to grow as the world requires more and more fertilizer to produce the food and fiber required by an increasing world population. By 1985 (as shown on Table 2), we expect the world will require about 33 million tons of K_2O per year or nearly 50 percent more than is currently used. This demand figure also includes about 1 million tons for industrial use and a 4 percent factor for losses incurred between the production and consumption point. While the developed areas of the world will continue to account for a major portion of the demand, the lesser developed countries of Latin America, particularly Brazil, and Asia and Africa will expand their requirements most rapidly. Demand in the Eastern Bloc nations also should continue to grow as they attempt to become more self-sufficient in growing their food requirements.

In regard to supply (Table 3), productive capacity including present plants, plants under construction,

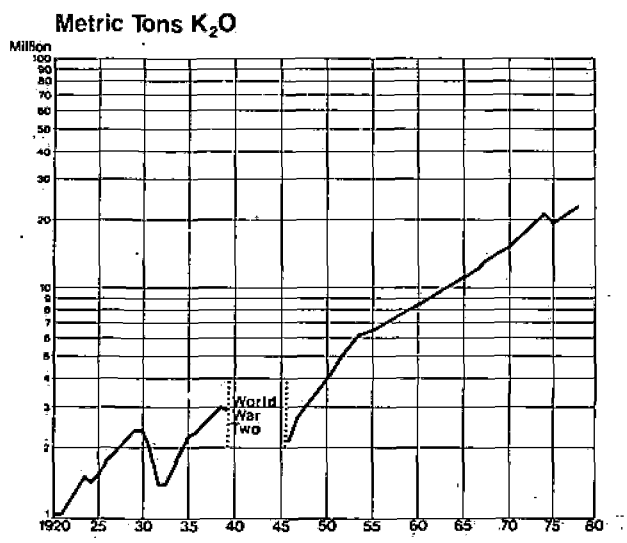

FIG. 2. World potash consumption.

TABLE 1. World Potash 1977

	Metric tons K_2O		
	Production (million)	Consumption (million)	Reserves (billion)
Canada	5.9	0.2	10.0
U. S.	2.2	5.0	0.2
Total No. America	8.1	5.2	10.2
Latin America	—	1.1	—
Western Europe	4.8	4.7	0.3
Africa	—	0.3	—
India	—	0.2	—
Japan	—	0.6	—
Other Asia	1.0	0.7	0.2
Oceania	—	0.2	—
Total Western World	13.9	13.0	10.7
Eastern Europe	3.2	3.9	0.3
USSR	9.0	5.2	2.0
China	—	0.6	—
Total Eastern Bloc	12.2	9.7	2.3
Total World	26.1	22.7	13.0

TABLE 2. World Potash Demand (Million Metric Tons K_2O)

Area	1977	1985	Average annual growth rate
U. S.	5.0	6.8	4 percent
W. Europe	4.7	5.6	2 "
Japan	0.6	0.9	3 "
Oceania	0.2	0.2	—
Developed countries	10.5	13.5	3 "
Latin America	1.3	2.3	8 "
Africa	0.3	0.6	9 "
Asia	0.9	1.9	10 "
Less-developed countries	2.5	4.8	8 "
Eastern Bloc	9.7	14.8	6 "
World	22.7	33.1	5 "

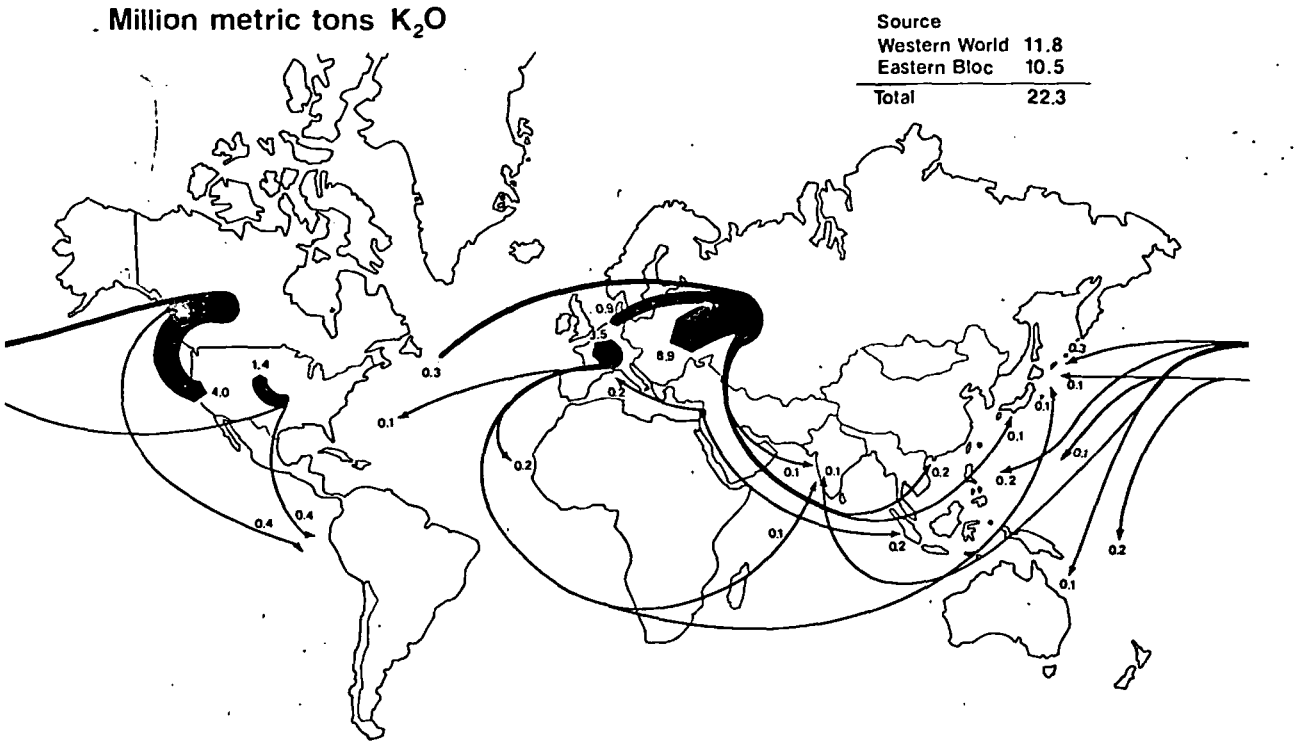

FIG. 3. Major world potash movements in 1976.

and new projects, which appear to have a reasonable chance of being completed by 1985, will exceed 37 million tons K_2O, some 11 million tons above 1977 production and 6.6 million tons above current capacity. Half the increase will result from continued development of the extensive deposits in the Urals area of Russia. In the western world, the Potash Corporation of Saskatchewan has announced expansion of both their Cory and Rocanville mines. Also in Canada, Ideal Basic's PCA Company has recently announced they will move ahead with development of their project in New Brunswick. Overseas, Israel will add some tonnage and it now appears that the Jordan project will be completed by the early 1980s. We also expect that capacity in West Germany may be increased marginally.

I should also mention that there are many other areas of the world where potash deposits are known to exist. At one time or another many have been evaluated, but none appears far enough along to have an impact on the supply/demand picture by 1985.

Now, if we put the supply and demand sides of the equation together, what sort of a picture do we get (Fig. 4)? As you can see, there is considerable excess productive capacity throughout the forecast period and there appears to be little need for anybody to continue to look for and develop new sources of potash. However, I believe this chart does not quite present the real picture. The supply line is "productive capacity" and in most cases represents "nameplate" or theoretical capacity. As we well know, very few plants can operate at capacity over an extended period of time, and, in fact, a sustained operating rate of 90 percent of capacity is considered to be near maximum. In Figure 5 I have added a curve representing 90 percent of installed capacity. As is indicated, the supply/demand balance changes dramatically. Instead of an oversupply situation well into the mid 1980s, the world is nearly in balance by

TABLE 3. World Potash Supply (Million Metric Tons K_2O)

Country	Estimated production 1977	Productive capacity 1985	Percent increase
U. S.	2.2	2.5	14
Canada	5.9	8.5	44
France	1.8	2.0	11
West Germany	2.2	3.0	36
Other Western Europe	0.8	1.6	100
Other	1.0	1.8	80
Total Western World	13.9	19.4	40
German Democratic Republic	3.2	3.8	19
USSR	9.0	14.0	55
Total World	26.1	37.2	43

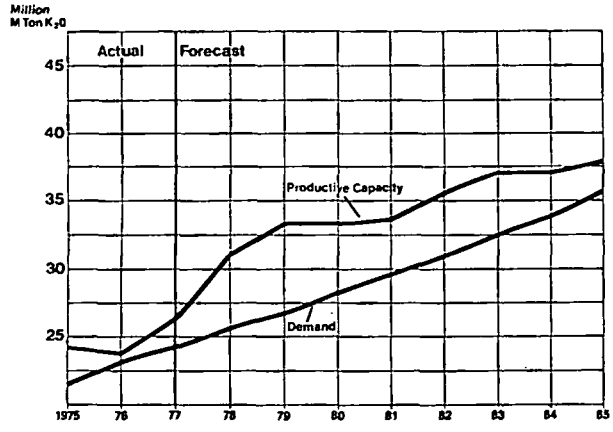

FIG. 4. World potash supply/demand.

1981. That is only three years into the future. I believe the world will require more production capacity in very short order.

But additional capacity is not the only problem facing the potash industry today. We face an even more important problem which has already seriously disrupted the industry and can have a very major impact on the whole future of potash—that problem is the "political problem" facing potash. What do I mean by the political problem? Very simply this: the control of the world potash industry is rapidly shifting from "private hands" into the hands of "political entities" and by 1985 governments will directly control nearly three-quarters of the world's productive capacity.

One might say "O K, that's because of the large production in the USSR." But as Table 4 indicates, even capacity in the western world is increasingly coming under the control of governments.

The next obvious question, then, is "What's so bad about having a major portion of the industry under government control?"

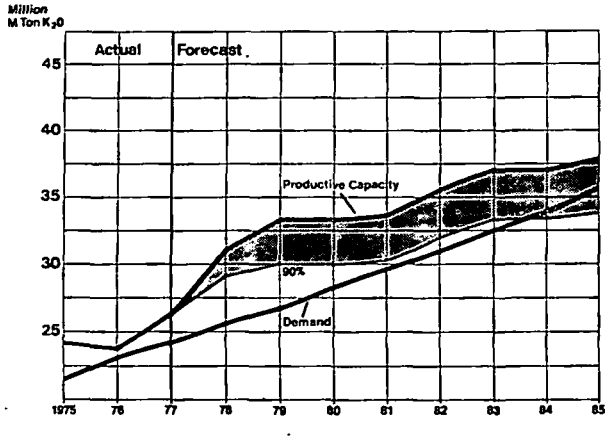

FIG. 5. World potash supply/demand.

TABLE 4. Potash Productive Capacity

	Percent controlled by:			
	World		Western World	
	Private	Govt.	Private	Govt.
1960	52	48	75	25
1970	47	53	74	26
1975	42	58	75	25
1980	32	68	60	40
1985	28	72	54	46

From the viewpoint of the private company which produces potash there are many problems. In the first place, with government as a major industry producer, the economics of the market place cannot operate freely. When there is a change in demand, either up or down, supply will be less responsive to that change. In times of surplus supply a government producer is reluctant to cut production. Lower production may mean lower employment, a politically explosive issue. It may also mean lower government income and affect both the national budget and foreign exchange balances. A developing country, where a mine is a major factor in the total economy, particularly would be affected in such a case.

A good example of what I mean has been occurring in the copper industry. World production has been above demand and the industry has been faced with rapidly falling prices and increasing inventories. How has the industry adjusted to the situation? The private producers have reduced production and in some cases have even closed marginal operations. At the same time, government-controlled producers, mainly in the developing areas of South America and Africa, have increased output in order to maintain employment and the foreign exchange needed to finance their imports. Government producers can even subsidize their copper production, if necessary, a position which a private producer cannot take. It is the private producer who has to bear the burden of lower production and profit or even losses on the down side of the business cycle.

A second problem the private producer faces is that of competing in the market place with the government producer. A government producer carries a great deal more political and economic weight than a private producer and can make government to government barter deals or government to private company deals. As an example, Morocco, a major government phosphate rock producer, made an agreement to supply phosphate to Brazil. The arrangement was with the government and it probably was made possible by the fact that Morocco will take Brazilian automobiles as payment. Morocco also will take sulfur from Poland in payment for ship-

ments of phosphate rock to that country. Algeria has made a similar deal with Finland and will take textiles in return for supplying phosphate rock. Closer to home we can cite the example of Russian potash being traded for phosphoric acid produced by Occidental Petroleum. I think it is quite evident that most private producers are unable to compete equitably if a large segment of the market transactions are barter deals between government producers.

A third problem facing the private producer competing with government producers is that the government not only may be your competitor but also may make the rules by which you must operate. The government sets the taxes and royalties, it can control your levels of production, sales, and even your prices. In fact, in the end the government can take over your whole operation and, as we know, it has in some cases done just that. It's pretty difficult to compete when your competitor can also set the rules.

Now, my purpose here is not to argue whether governments have the right to be involved in mining or any other venture. They *are* involved in mining and many other economic activities and will continue to be. Rather, my purpose is to point out the risks to the private company which operates in a business environment dominated by government production. Consideration should be given to the following factors when looking for and developing commercial mineral orebodies. First, consider the risk involved in holding the deposit after you have spent millions on exploration and development. Second, consider the chances of your project being able to compete on equal terms when your competitor is also the government making the rules under which you must operate. Finally, even if the local government is not a competitive producer, determine if your project's logical markets are dominated by government firms which can utilize their political leverage in order to put a private producer at a competitive disadvantage in the market place.

Now, maybe all of this sounds very pessimistic, but I don't mean to be. On the other hand, one must be realistic and must be careful to consider the political and economic environment within which a potential potash mine must operate. As I pointed out, potash demand is strong, is growing, and will continue to grow. I have also pointed out that the world will need to develop additional potash mines within the next five years, which, by the way, isn't very much time. However, when looking for potash, remember, "potash and politics" don't always go well together.

TEXASGULF, INCORPORATED
MARKETING RESEARCH DEPARTMENT
HIGH RIDGE PARK
STAMFORD, CONNECTICUT 06904
November 10, 1978

Patterns of R&D in the
Non-Ferrous Metals Industries

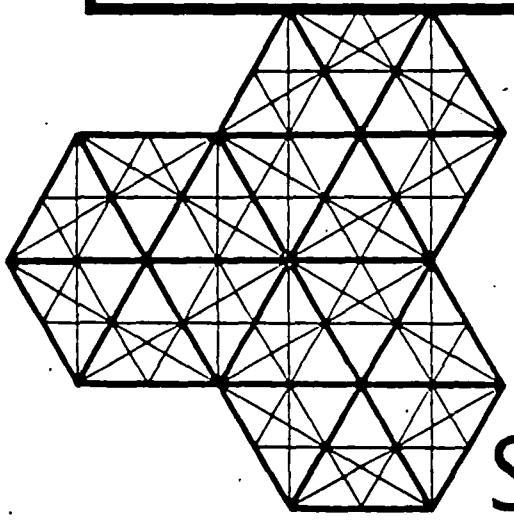

Center for Science and Technology Policy

Graduate School of Public Administration/New York University—A private university in the public service

New York University
A private university in the public service

Graduate School of Public Administration

329 Shimkin Hall
Washington Square
New York, N.Y. 10003
Telephone: (212) 598-2163

Center for Science and Technology Policy
Herbert I. Fusfeld, *Director*

PATTERNS OF R&D IN THE NONFERROUS METALS INDUSTRIES

Submitted by: A.C. Damask
Visiting Professor

Prepared for the

Office of Science and Technology Policy

November 1980

TABLE OF CONTENTS

Objectives

This report is intended (1) to provide some perspective of the magnitude and the scope of R&D in the nonferrous metals and mining industry, and (2) to serve as a basis for identifying potentially constructive areas for government-industry cooperation in view of the needs, the opportunities, and the constraints applicable to that industry.

Background

The continuing concern with our natural resources and their economic importance has given rise to several major materials studies over the past 30 years.[1,2] These have focused largely on questions of supply and demand, both present and future, and have included analyses of the role of science and technology in improving that future.

There are important differences in breadth and substance between this paper and the previous studies mentioned:

1. This particular report is a very brief overview of one principal factor in the health of the metals and mining industry, i.e., research and development. Moreover, it is a necessary first step leading to a particular type of action of a technical nature, not of broad policy changes.

2. Several new pressures of a peculiarly public nature require attention by the metals and mining industry on a scale radically different than in the years prior to 1970. These include environmental controls, safety procedures, and energy conservation.

3. These pressures have mandated actions within the industry which consume a significant fraction of available capital, and lower effective productivity so as to reduce the industry's capacity for capital formation.

4. All of these factors may have resulted in weakening the ability of the industry to generate and absorb technological change necessary to sustain healthy growth, particularly in competition with higher-grade, lower-cost foreign procedures.

Given this environment within which the industry must operate today, the material presented in this report focuses on adequacy and feasibility. First, how adequate is the R&D effort of the private sector, supported by particular government programs, to meet the long-term objectives of the metals and mining industry? Second, in what areas is it feasible to strengthen the current efforts by a substantive cooperative program between government and industry?

This report does not answer these questions directly. It provides data and perspective on which joint government-industry actions can be based to determine those answers.

The public concern with natural resources will continue and intensify because of our need to reduce costs and insure supplies. It is reasonable to expect expanded federal efforts in materials R&D to arise from this concern. Experience with other areas of federal involvement in civilian sector R&D over the past 10 years shows that such efforts can only be effective

when based on intelligent inputs and constructive participation of the private sector. Only then can there be agreement on programs which can be applicable in operating procedures, and avoid efforts that are unneeded and/or uneconomic. This is the justification and necessity for private sector cooperation in the conduct of this particular study.

While the concern is with the broad area of metals and mining, this study has been limited to a relatively few common metals of economic importance in order to permit a reasonable perspective in the short time devoted to the program. These metals are: aluminum, copper, lead and zinc.

Introduction

This report is a survey of available data concerning the R&D effort in the nonferrous metals industries in the United States and how that compares with some other industries. The source of the funds will be examined and, to the extent possible, the division of these funds among the various stages, from exploration to primary processing will be indicated. In addition, new data from a New York University survey are included. From these data areas in which cooperative government-industry research programs could assist in strengthening the economic health of the nonferrous metals industries while improving the strategic position of the United States will be indicated.

For the purposes of this study, four metals were selected: aluminum, copper, lead and zinc.

The U.S. domestic production of these metals is shown in Fig. 1 and the sources of the metals are given. In the case of aluminum there are few economical domestic sources of bauxite and hence most of the bauxite is imported, while the aluminum ingot is produced here. The earnings from the sale of the metals and the number of employees involved in the production are shown in Table 1.

The domestic sources, both mine and scrap, referred to in Fig. 1 represent our independence from imports and hence our self-sufficiency. Fig. 2 shows this in comparison with DOC data on the self-sufficiency of the USSR in selected metals.

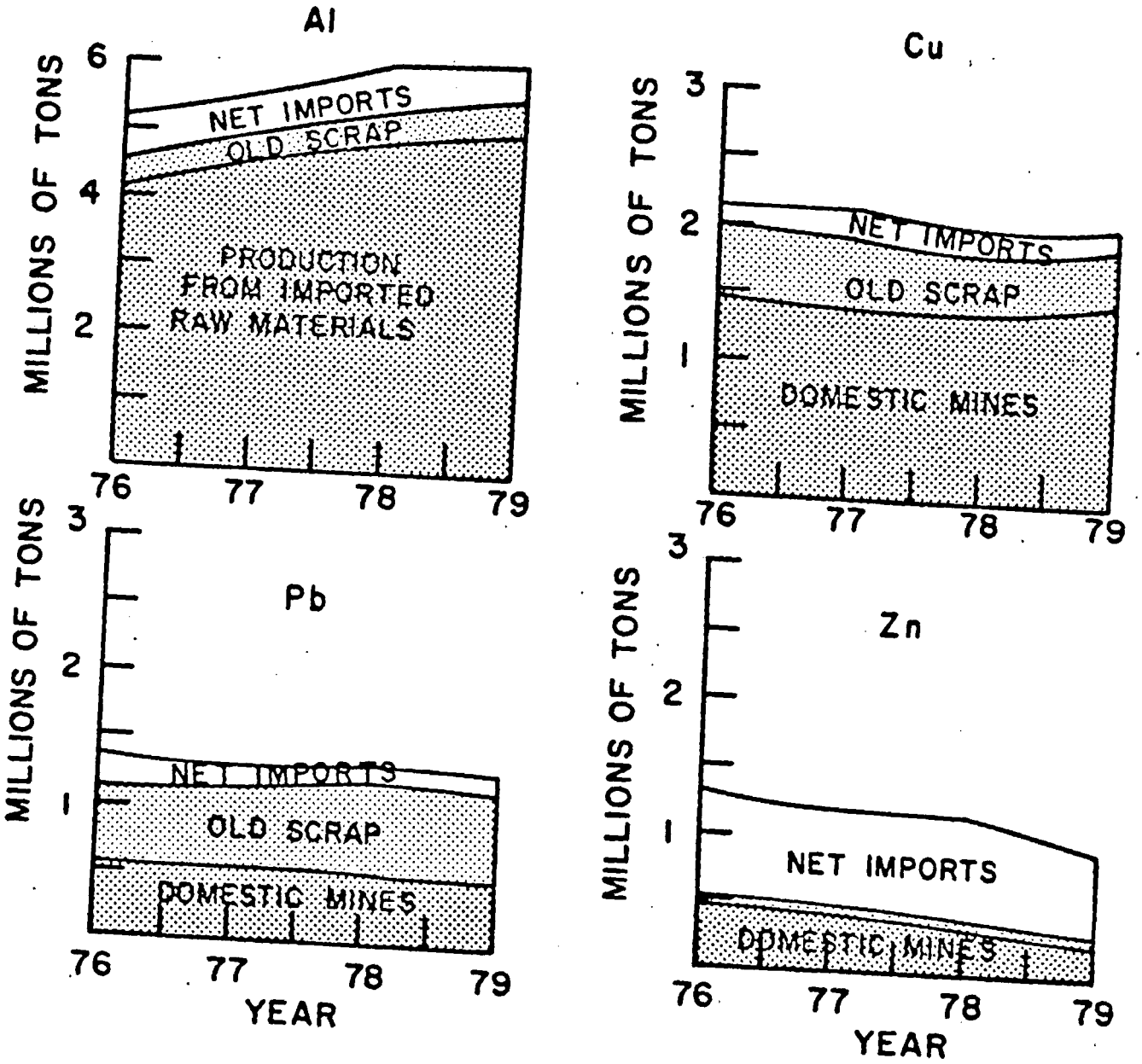

Fig. 1. U.S. production and consumption of principal nonferrous metals. Data from U.S. Bureau of Mines (ref. 3).

TABLE 1

Gross Sales of Primary Metal and Employment

		1976	1977	1978	1979
Al	$ millions	3,800	4,600	5,000	6,000
	employees	25,000	26,200	27,300	27,200
Cu	$ millions	2,250	2,000	1,970	2,900
	employees	29,700	24,900	26,400	27,500
Pb	$ millions	290	360	398	594
	employees	7,100	7,000	6,600	6,000
Zn	$ millions	355	318	212	215
	employees	10,800	10,700	9,800	9,000

Source: U.S. Bureau of Mines, Mineral Commodity Summaries, 1976-1980.

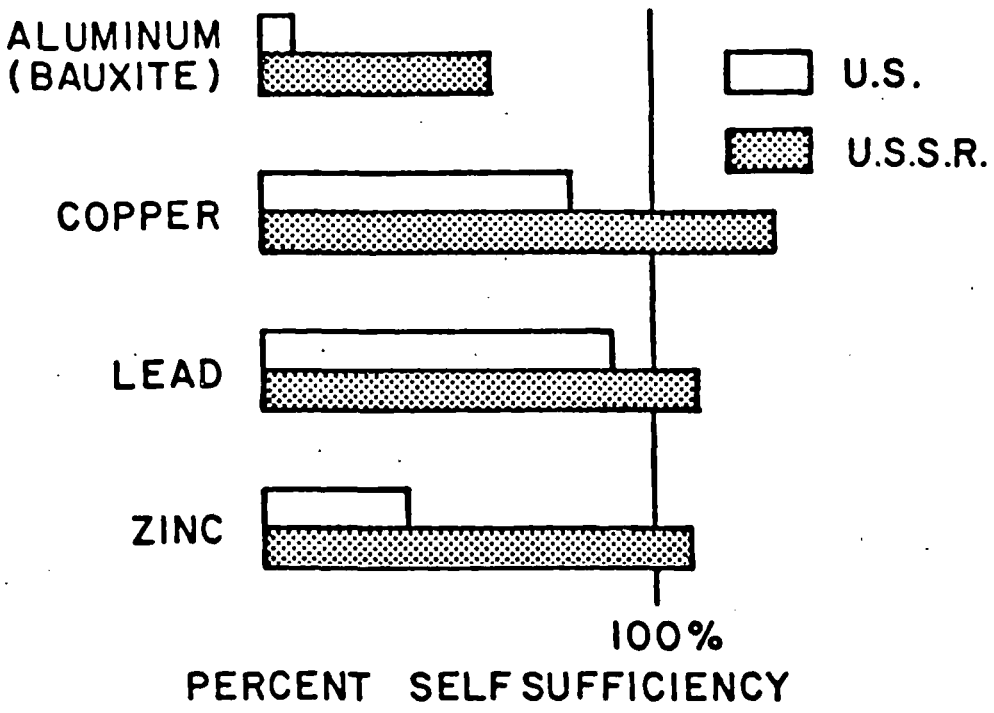

Fig. 2. Comparison of metal self-sufficiency of U.S. and U.S.S.R. U.S. data from Fig. 1. U.S.S.R. Data from Department of Commerce.

The relative economic health of the primary nonferrous metals industries is shown in Fig. 3. It is seen that the return on equity is considerably below that of the all-manufacturing average. Since the metals industries are very capital intensive -- e.g., a new plant may cost hundreds of millions of dollars -- the return on such an investment is not very attractive and resistance to change of method of operation is understandable. Compounding the difficulties are the environmental regulations and the dramatic increase in the cost of energy.

With prospects rather bleak for these industries in the U.S. it is important to examine the available data to find ways to ameliorate the situation. This examination will also reveal the paucity of data and thereby indicate where more specific data are required in order to optimize assistance to the industries.

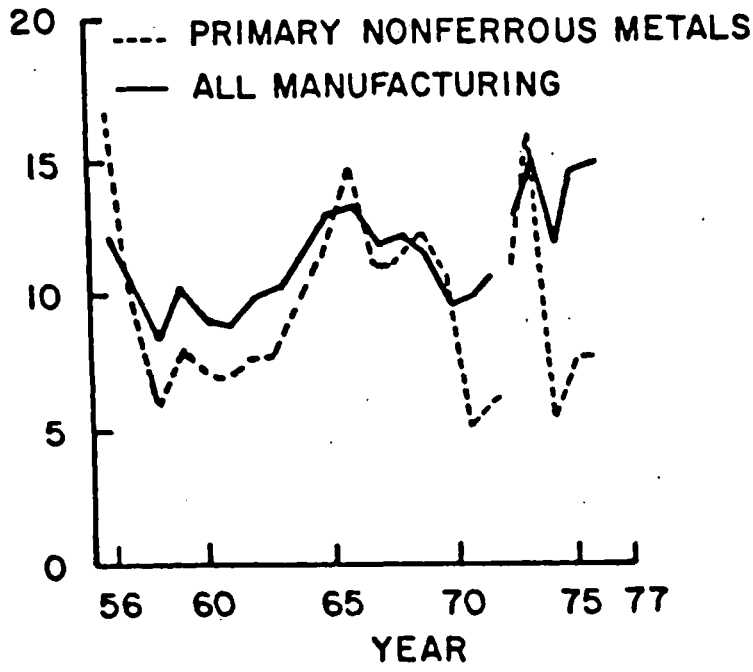

Fig. 3 Comparison of return on equity of the nonferrous metals industries with all manufacturing. Data from U.S. Bureau of Mines (ref. 4).

Comparison of R&D with Other Industries

The total R&D in some industries for the decade 1967-1977 is shown in Fig. 4. Only a few industries are shown for ease of reading the graph. One of the most active, electrical equipment and communication, is included for comparison. This is exceeded by aircraft and missiles but, because of the large DOD contribution to these fields, they are not considered representative. It should be noted that some of the disparities of R&D effort are to be expected. Communications devices is a very rapidly advancing industry with new introductions almost annually. Competition compels a large fraction of earnings to be reinvested. In capital intensive industries such as primary metals (steel is included in this term as well as nonferrous metals) changes are very slow, sometimes requiring decades. Thus, prior to the sudden and profound changes required by energy cost and environmental regulation, only a small amount of R&D was considered prudent. Curves of the type of Fig. 4 are also somewhat deceptive because they are of actual dollars. When they are corrected by the GNP deflator index to 1972 dollars, they take on the appearance of those in Fig. 5. We see that R&D for primary metals has remained essentially constant.

The total R&D of Figs. 4 and 5 consist of essentially two contributions, company funds and government funds. The company funds in dollars are shown in Fig. 6 and corrected to 1972 dollars in Fig. 7. The government contribution is shown in Fig. 8 and in 1972 dollars in Fig. 9.

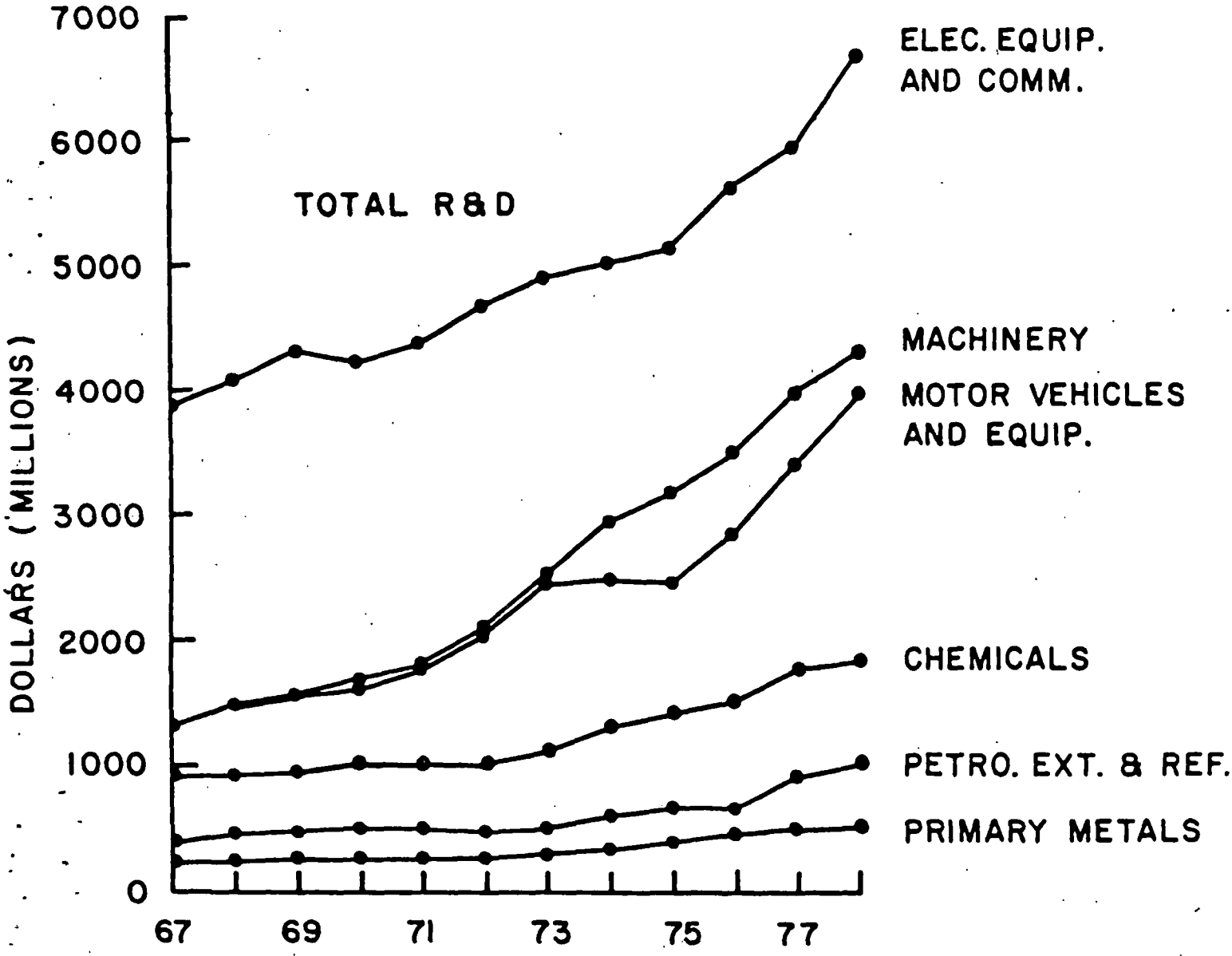

Fig. 4 Total R&D of various sectors in millions of dollars. Data from NSF (ref. 5)

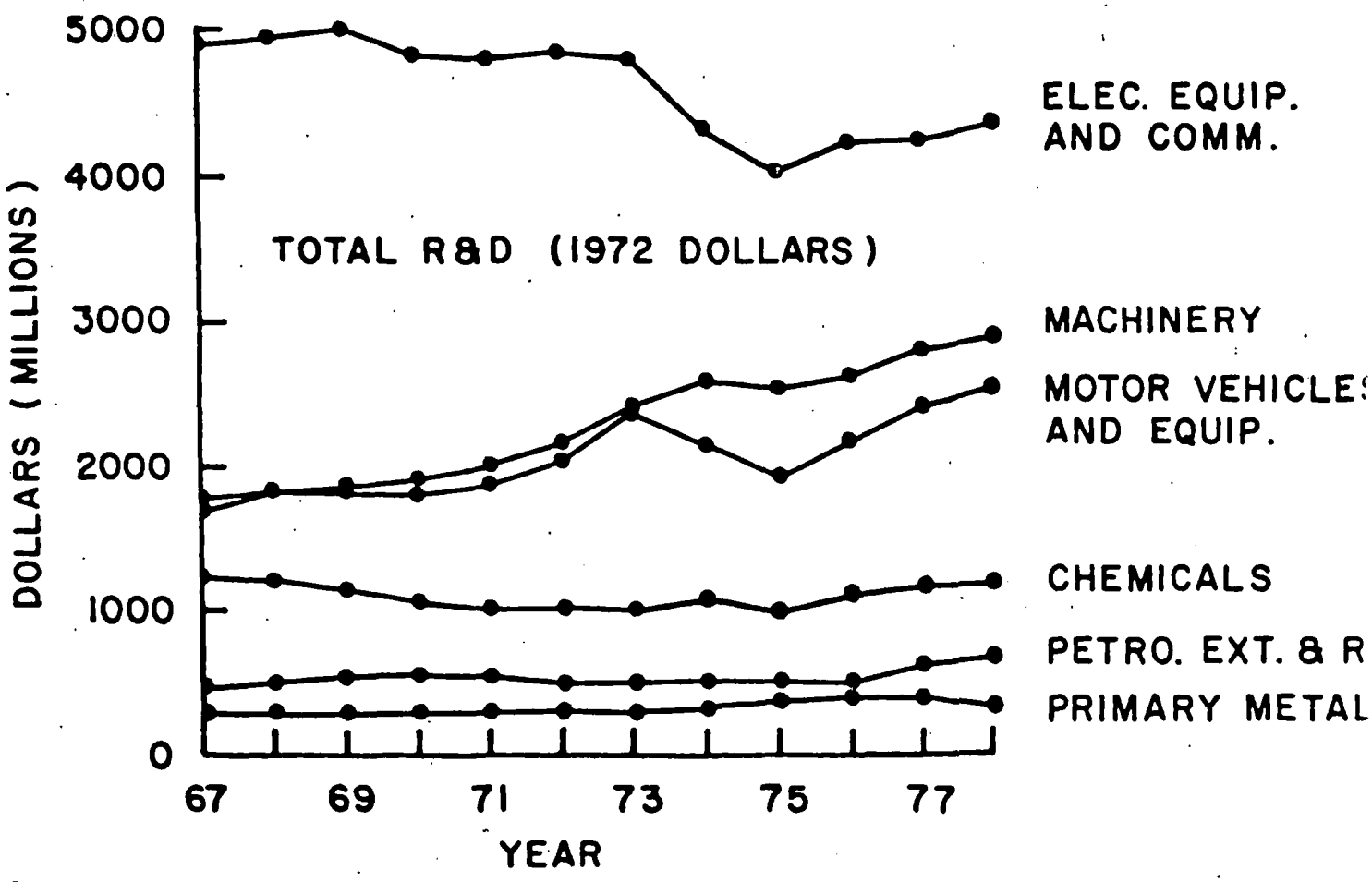

Fig. 5 Total R&D of various sectors in millions of constant 1972 dollars.

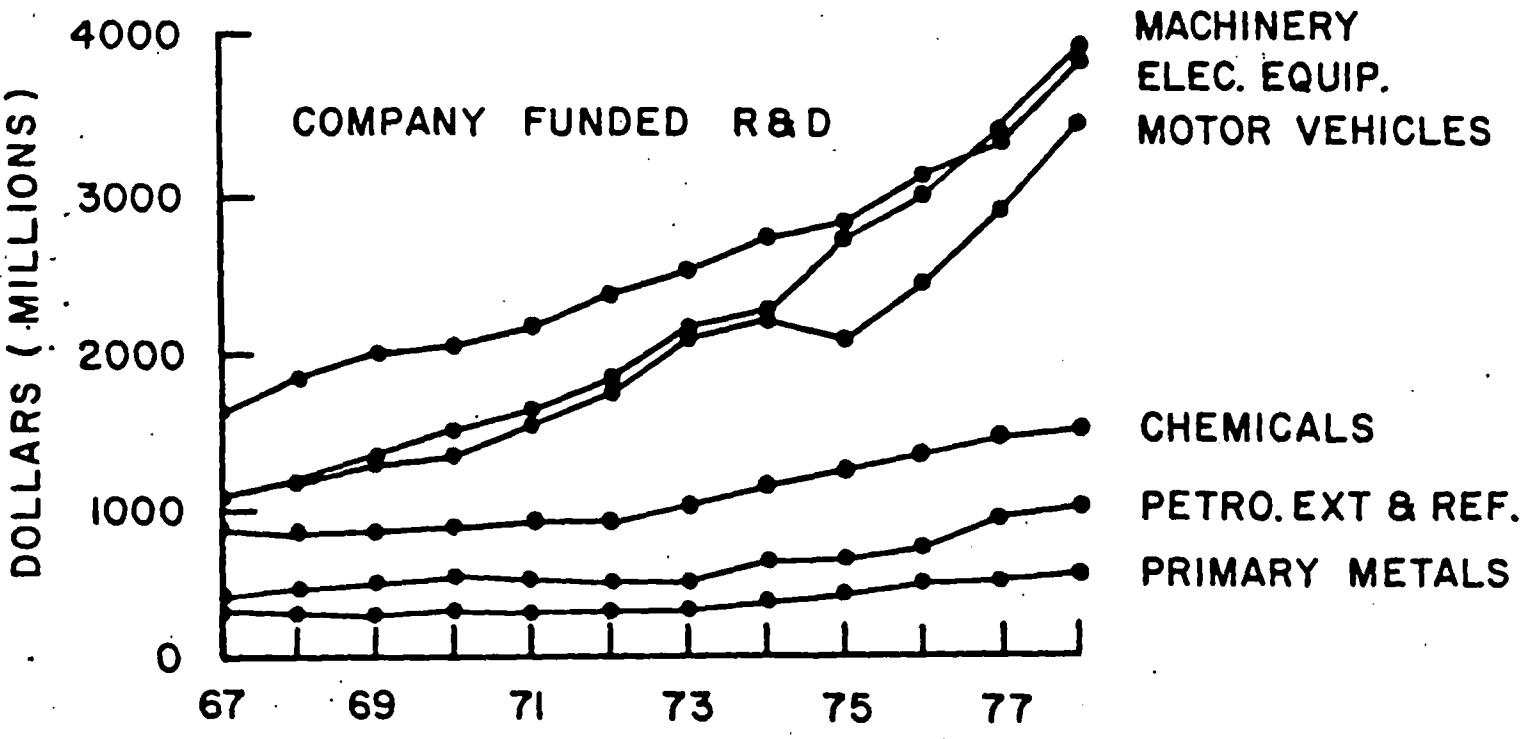

Fig. 6 Company funded R&D of various sectors.
Data from NSF (ref. 5).

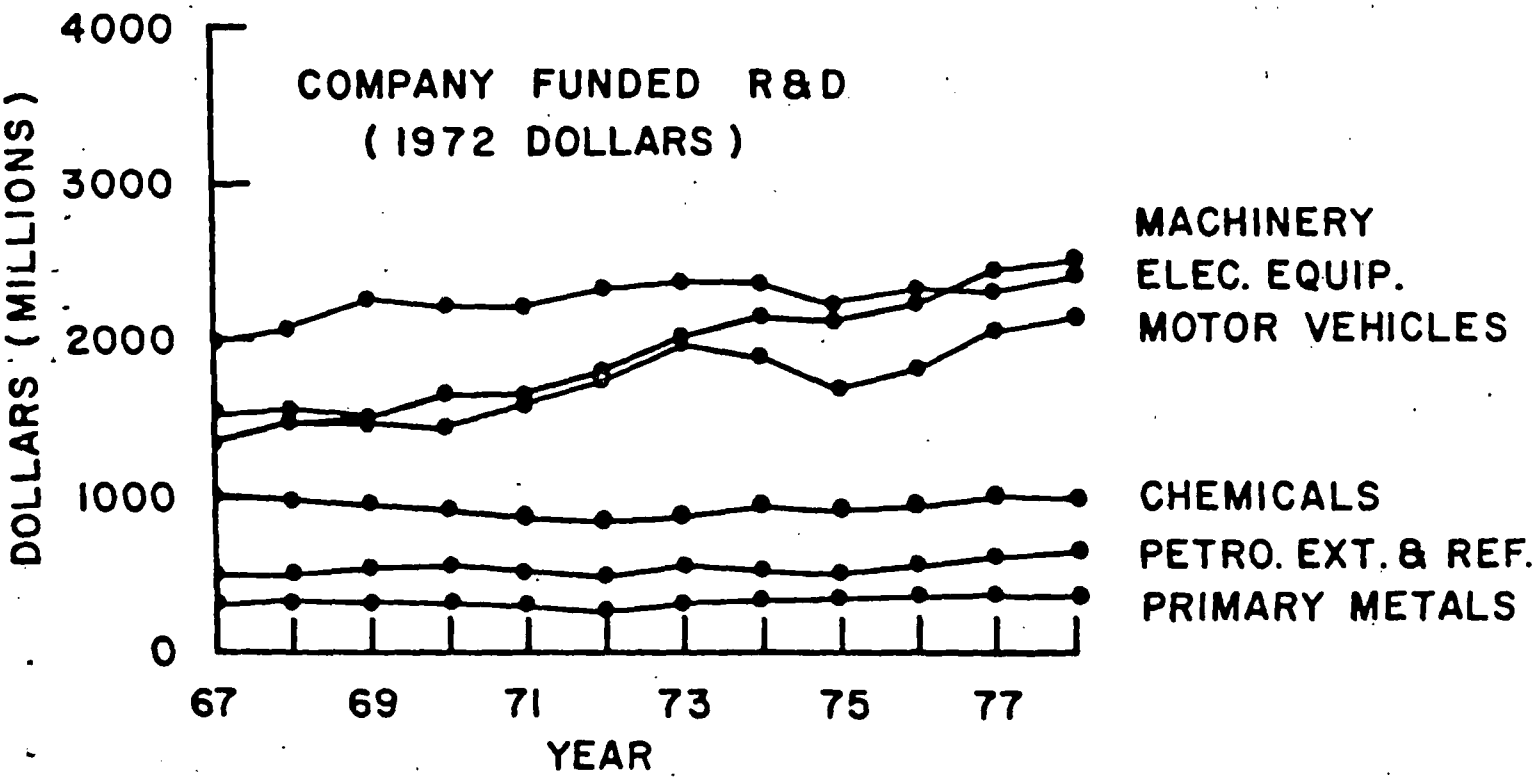

Fig. 7 Company funded R&D in constant 1972 dollars. GNP deflator index applied to data of Fig. 6.

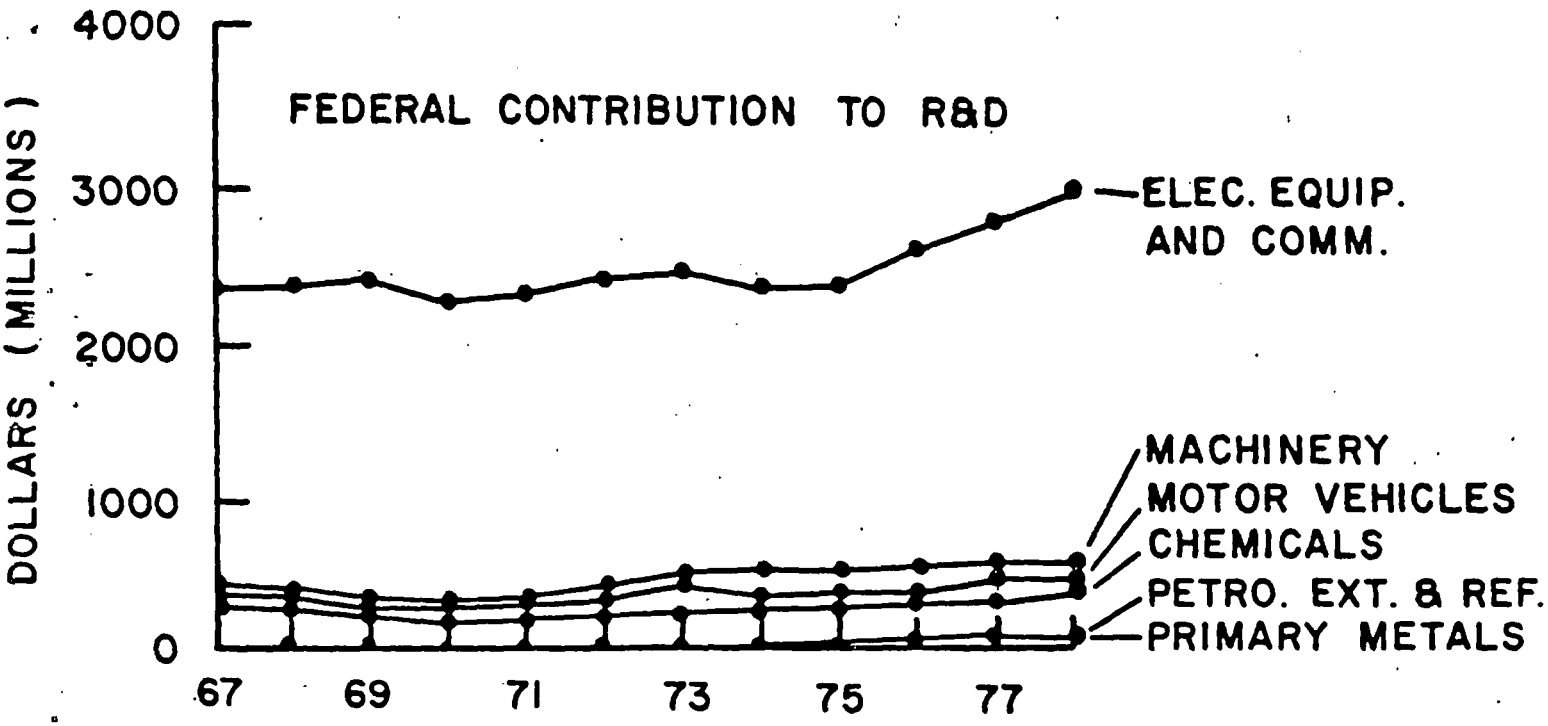

Fig. 8 Federal contribution to R&D of the sectors of Figs. 4-7. Data from NSF (ref. 5).

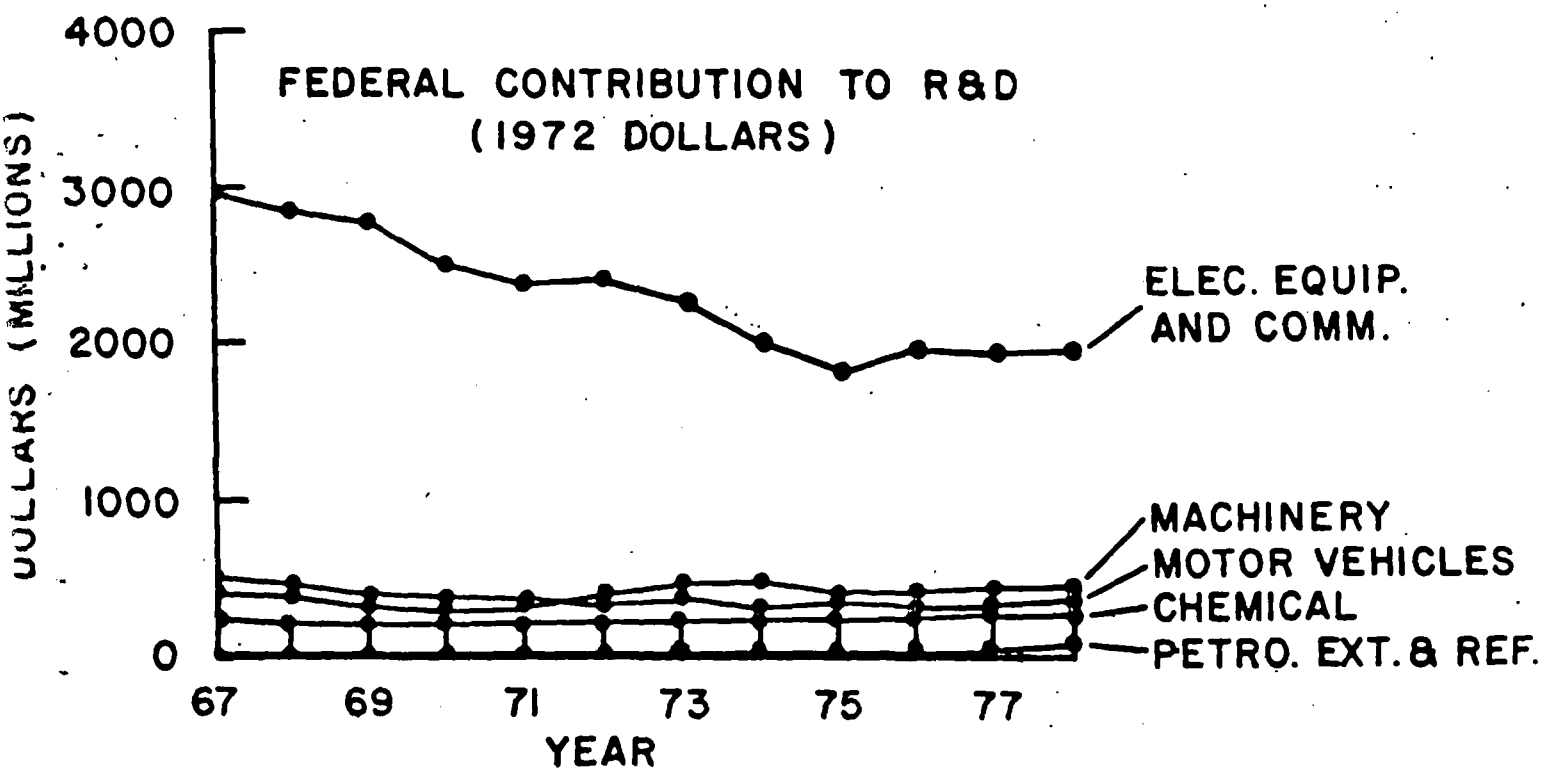

Fig. 9 Federal contribution to R&D in constant 1972 dollars. GNP deflator index applied to data of Fig. 8.

The percent of the federal contribution, i.e., the ratio of the data of Fig. 8 to that of Fig. 4, is shown in Fig. 10. (Note that the constant dollar ratio would be the same.) The important point to note in this figure is that the federal contribution to R&D for primary metals is lower than any of the others and almost insignificant compared to the company contribution. This neglect is even more strikingly shown for the nonferrous metals in Fig. 11. In this figure are plotted the total R&D expenditures, this value corrected to 1972 dollars, and the corresponding federal contribution (note the expanded scale of the ordinate.)

There are other comparisons of R&D efforts that can be made. If one examines R&D as a percentage of net profits, there is much less difference between industries. An average expenditure on R&D in the category of all-manufacturing is about 35% of net profits while in the nonferrous metals industry the average is about 25 to 30 percent[6]. The actual percent of net profits for companies that in some years show very small profits, or even losses, is meaningless. Some typical data are given in Business Week and are based on company 10K forms. (See Appendix A)

Since profits oscillate, a more realistic comparison may be made from company R&D expenditures as a percentage of net sales. Because sales of the steel industry are so large, their inclusion will distort the metals data. Therefore, Fig. 12 shows data for nonferrous metals only. It is again evident that, although R&D for nonferrous metals is at a relatively

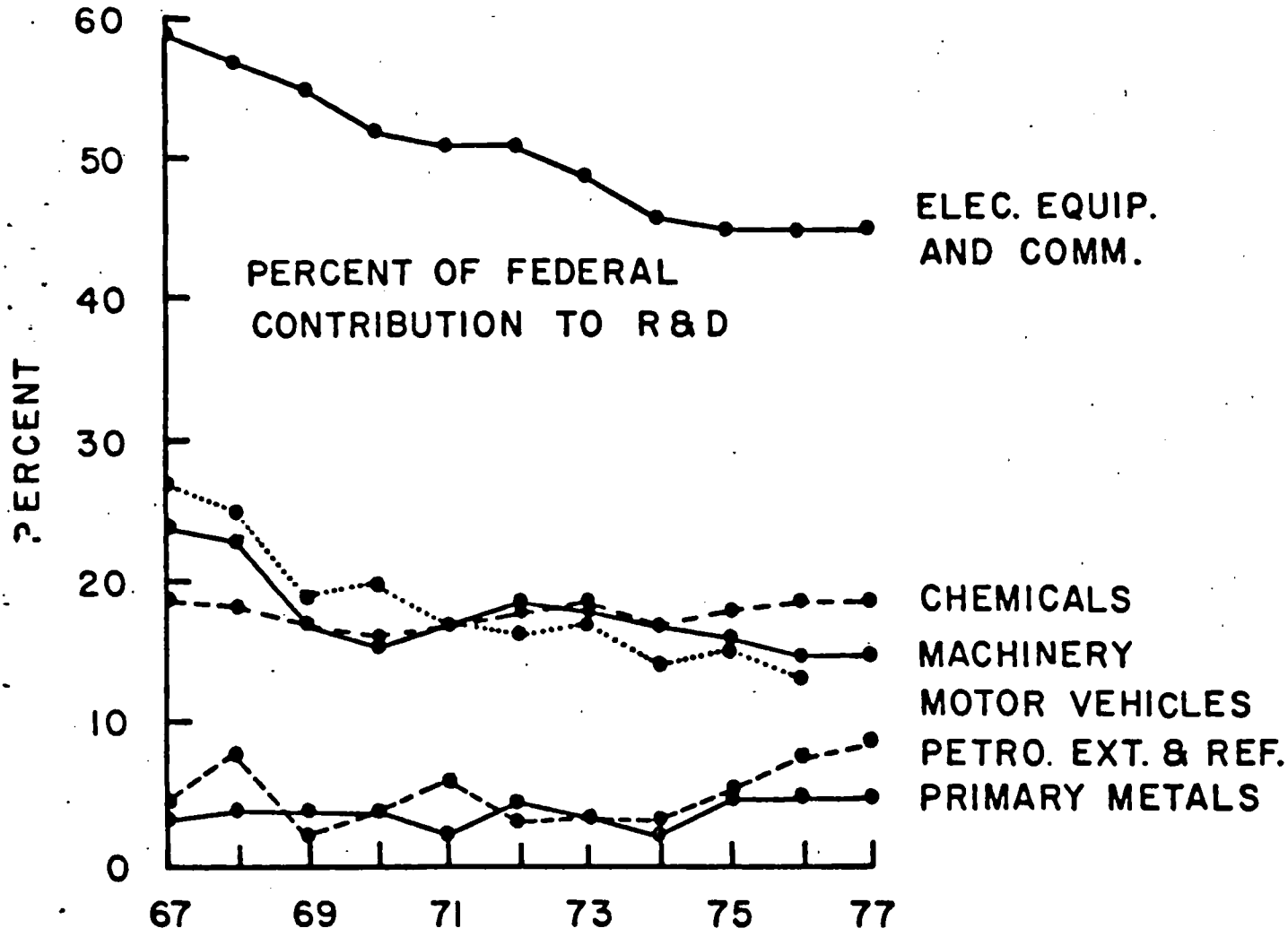

Fig. 10. Percent of federal contribution to total R&D of various sectors. Data from Figs. 4 and 8.

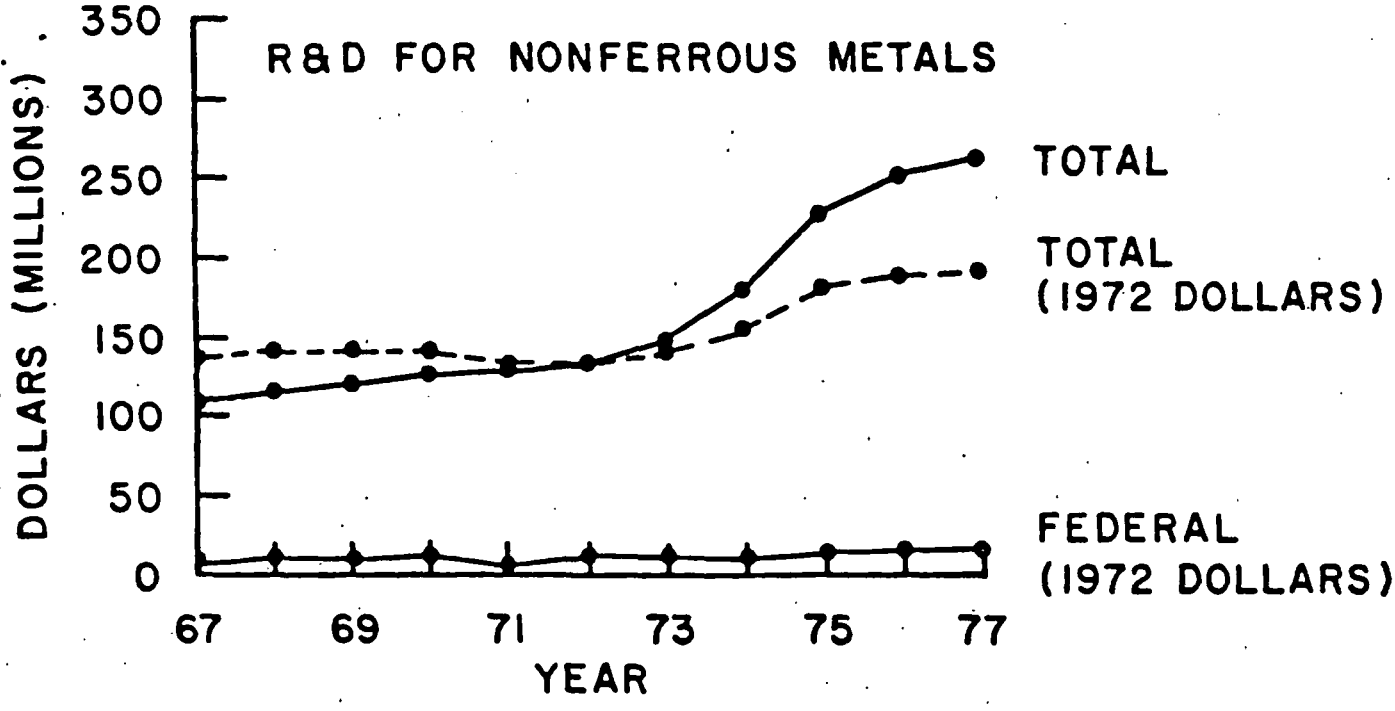

Fig. 11. R&D for nonferrous metals showing total in 1972 dollars, and federal contribution in 1972 dollars. Data from NSF (ref. 5).

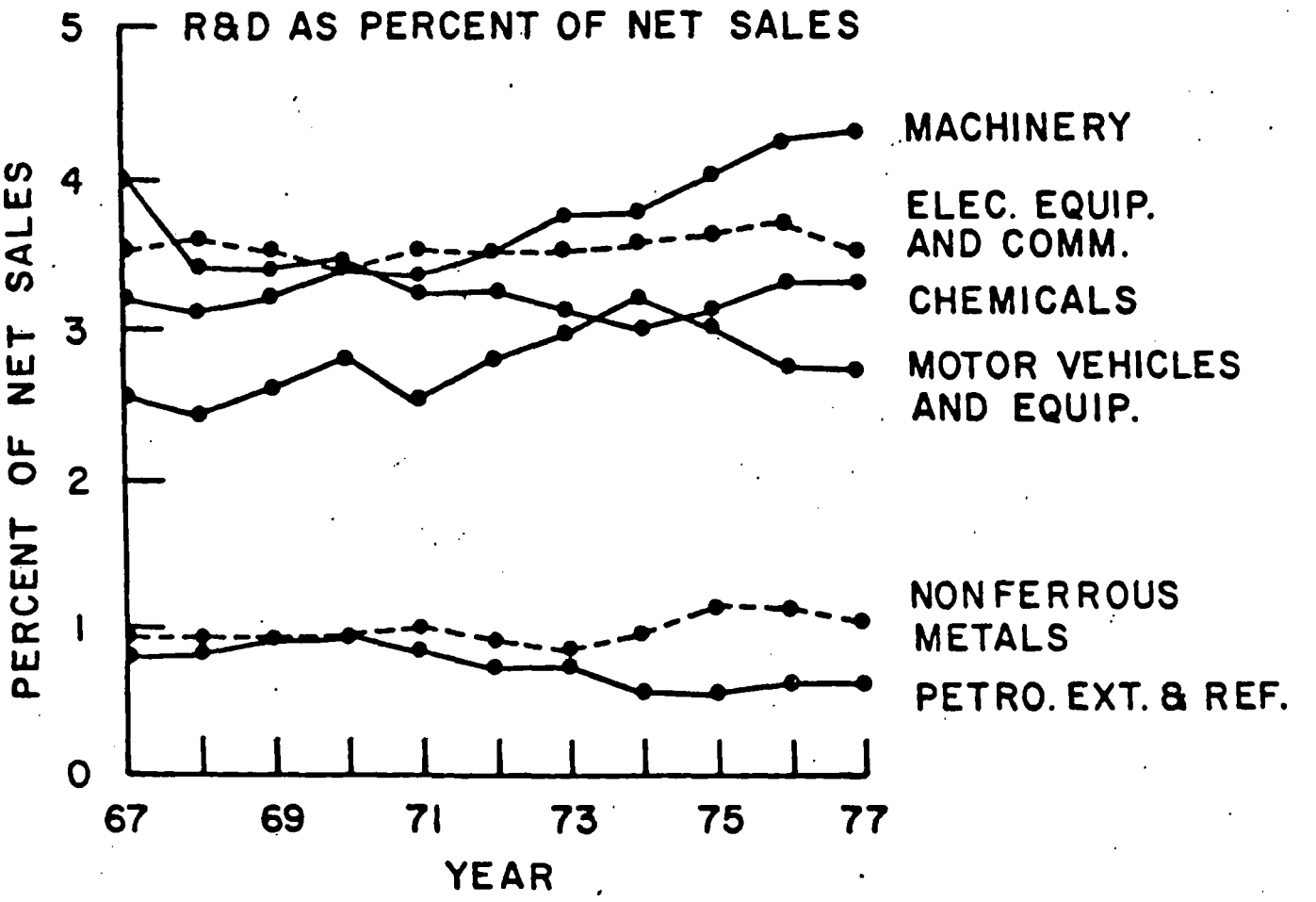

Fig. 12. Total R&D as percent of net sales. Data from NSF. (ref. 5).

low percentage, it is constant through the years. In a later section it will be shown that more than 75% of this R&D for non-ferrous metals and products is for the product improvement part in order to increase sales. Thus, less than 25% goes into exploration and primary processing, or about 0.25% of net sales.

Cooperative R&D

There are two types of cooperative R&D efforts to be considered, those between industries, and those between industry and government.

The aluminum, copper, and lead and zinc industries have cooperative trade associations. The latter three sponsor research and receive funds from domestic and foreign companies in proportion to the quantity of product sold the preceeding year. The aluminum companies' organization is based in Paris and is primarily concerned with increasing the uses of aluminum.

The copper industry cooperative has its office in New York City and is called the International Copper Research Association (INCRA). For the past two years its funds were $1.7 million each year but they are expected to be increased to $2 million this year. Most of their research is for product improvement, with an associated increase in use. About 12% goes into research, but this research is primarily a literature survey to develop handbooks of copper data. About 3% goes into laboratory research on thermodynamic properties of copper.[7]

A counterpart cooperative is the International Lead and Zinc Research Organization, also with its office in New York City. The current level of funding is $2 million per year for lead and $1 million for zinc. Again, most of this is for product improvement toward increase of sales. There is no basic research that is being supported, although 30% of the lead budget now goes for health studies both in the workplace and in the general population.[8]

Government-industry cooperation exists with both the Department of Interior and the Department of Energy.

The major DOE cooperative projects from mining through primary processing are the following, where the indicated sums are those already contracted for, not the total costs.[9]

1) with Kaiser Aluminum, to develop a wettable cathode to produce aluminum in Hall cells. Costs approximately $3,000,000. The cost-sharing formula is extremely complex, but if you regard it as 25% Kaiser 75% DOE you will not be far off.

2) with Alcoa, to develop an inert anode to produce aluminum in Hall cells. Cost approximately $11,000,000, shared 25% Alcoa 75% DOE.

3) with Alcoa, to develop a carbothermic direct reduction technology for aluminum. Cost approximately $4,000,000, shared approximately 30% Alcoa 70% DOE.

4) with Alcoa and General Electric, to develop a coal-fired aluminum remelt furnace. Cost approximately $4,000,000, essentially 100% DOE.

5) with a consortium put together by the University of Utah, to develop energy conservation opportunities represented by, and the technical and economic consequences of supporting, various process alternatives in the copper industry. Cost $340,000, 100% DOE.

The major cooperative programs between industry and the Bureau of Mines are listed in Table 2 in which a nickel and a tungsten program are included for completeness.[10]

There is another large project of the Bureau of Mines that should be included. It is the "citrate" process for removal of SO_2 from stack gases. It is of about 10 year duration and will cost the Bureau $10-15 million. They have worked with the copper, zinc and lead industries and an accurate breakdown

TABLE 2

MINERAL RESOURCES TECHNOLOGY

PROJECTS INVOLVING COOPERATIVE RESEARCH

PROJECTS	FY	FUNDING ($000) BUREAU	FUNDING ($000) OUTSIDE	NOTES ($000)
1. Ferric Chloride Leaching of Galena Concentrates/ Fused-Salt Electrolysis of Lead Chloride	80	250	200	$50 each from: Amax Lead and Zinc, Inc. ASARCO, Inc. COMINCO, Ltd. St. Joe Minerals Corp.
2. Alumina Miniplant	80	780	250	$50 each from: Aluminum Co. of Canada, Ltd. Anaconda Aluminum Co. Billiton International Metals Kaiser Aluminum and Chemical Co. Reynolds Metals Company
3. UOP, Inc.	Prior	1,917,780		
Nickel Laterite Pilot Testing	80	78,300		
	Total	1,996,080	398,467	
4. Tungsten Recovery from Searles Lake Brine	80	275	250*	Kerr-McGee * goods and services

of cost sharing in all aspects of development and demonstration is difficult, but it is estimated to be about 50-50.

In addition, the Bureau of Mines has numerous short-range studies with individual mining operators. While these studies are usually small, their aggregate is large and is a noteworthy activity of the Bureau of Mines.

Effects of Oil Industry's Investment in Minerals

Over the past few years a number of nonferrous mining companies, both in the U.S. and abroad, have been purchased by oil companies. With the oil companies' large capital resources and their commitment to R&D, it is anticipated that the R&D funding of their new minerals divisions will improve. In the course of the New York University survey, this question was posed directly. The general response was that the take-overs have been too recent to create a noticeable effect on the overall R&D expenditures. However, because the mining companies which were taken over often had negligible R&D programs prior to their takeover, on a percentage basis any increase would be extremely large. Such a quotation of figures would be misleading. The general response from knowledgeable officials was that increases were being carefully examined and probably would occur in the future.

Distribution of R&D Expenditures

Primary processing of metals involves several stages: exploration, extraction, comminution, beneficiation, and smelting or refining. Most studies apologize for the lack of data on the distribution of funding. However, it would be desirable to have detailed data on the amount of R&D expended for each, in addition to professional estimates of where increases of effort would be most useful. Estimates which emerge from the NYU survey on this point will be presented after a review of existing data.

Several barriers thwart the extraction of such detailed information from existing NSF data. For example, Fig. 11, based on NSF data, shows that in 1972 the total R&D for nonferrous metals and products was $130 million, while the detailed Battelle-Columbus study[11] showed that the R&D was $33 million for primary processing, recycling, pollution control and land reclamation. Thus, 75% of the R&D had gone into product development. A similar comparison can be made for 1977. NSF data show that $267 million was spent for R&D on nonferrous metals and products. The COMAT PhaseII study[12] shows that $48.3 million was spent for R&D in the following categories: exploration and extraction, production of finished material, new material development ($13.7 million), improved processing, recycling and recovery, and waste management. This represents 18% of the R&D and if the category of new material development is subtracted, then only $34.6 million has gone into R&D for exploration through primary processing, or only 13%.

Another barrier exists in the way companies classify development in their accounting procedures. For example, a mine brought into operation will be capitalized and R&D in exploration costs may become part of such capitalization on the financial balance sheet. R&D for a new technology will be labeled R&D until a new mill operation is built at which time the R&D may be capitalized. When the NSF questionnaire asked how much of the R&D expenditures in 1977 went for basic research in nonferrous metals and products, the total of the answers was $10 million, while the same question for applied research resulted in a total of $155 million. This illustrates the difficulties in achieving a uniform categorization.

Two studies have been made in an attempt to gain more details in the division of R&D funds in nonferrous metals industries from exploration through primary processing. The Battelle-Columbus Laboratory questionnaire[11] gave results for both the nonferrous metals industry as a whole and for the metals of interest in this present study. The results are shown in Table 3.

The data of Table 3 can be expressed as percentages and, for comparison, the percentages for the nonferrous metals industry (from the same Battelle report) are shown in Table 4.

It is evident from these data that each metal has its own requirements. Aluminum, for which nearly all the ore is imported, clearly has little need for mining or land reclamation research and primary processing and pollution control are its chief concerns. In contrast, the copper industry spends considerable funds for mining research.

TABLE 3

Privately Funded R&D Expenditures in 1972
(Millions of Dollars)

Metal	Al. & Mg.	Cu.	Pb. & Zn.
Exploration	0.066	1.16	0.014
Mining	0.007	1.5	0
Beneficiation	0.58	0.6	0.015
Primary proc.	7.2	3.05	1.3
Recycling	0.74	0.26	0
Poll. cont.	2.6	1.2	0.059
Land reclam.	0	0.05	0
Total	11.2	7.8	1.4

Source: Battelle-Columbus Laboratories, 1972.

TABLE 4

Percentage Division of R&D Funding for the Nonferrous Metals Industry and for Selected Metals (1972)

Stage	Industry	Al & Mg	Cu	Pb & Zn
Primary processing	53.2%	64	39	92.8
Pollution control	18.1	19.6	15.4	4.2
Beneficiation	10.2	5.2	7.7	1.1
Mining	7.9	0.06	19.2	0
Exploration R&D	6.4	0.6	14.9	1
Recycling	3.8	6.6	3.3	0
Land Reclamation	0.4	0	0.6	4.2

Source: Battelle-Columbus Laboratories, 1972

A later study by COMAT[12] (1977-1978) reports the results in somewhat different categories. These are shown in Table 5. These data may also be expressed in percentages and compared with the nonferrous metal total. This is done in Table 6.

TABLE 5

Annual R&D Expenditures by the Nonferrous Metal Industries
(1977-1978)
(Millions of Dollars)

	Al	Cu	Pb & Zn
Exp. & extr.	2.9	6.2	2.4
Prod. fin. mat.	13.2	2.3	1.7
New mat. dev.	7.7	1.0	0.6
Improved proc.	15.6	2.8	0.3
Rec. & recyc.	4.5	2.6	0.3
Waste mgmt.	1.5	0	<0.1
Unsp. & other	<0.1	0	0.1
Total	45.4	14.9	5.1

Source: COMAT, Phase II.

TABLE 6

Percentage Division of R&D Funding for the Nonferrous Metals Industries and for Selected Metals (1977-1978)

Stage	Industry	Al	Cu	Pb & Zn
Improved proc.	24.6%	34.4	18.8	5.9
Expl. & extract.	24.5	6.4	41.6	47
Prod. fin. mat.	22.4	29	15.4	33.3
New mat. div.	19.9	16.9	6.7	11.8
Rec. & recyc.	6.9	9.9	17.4	< 2
Waste mgmt.	1.4	3.3	0	< 2
Other	0.3	< 0.2	0	2

The New York University Survey

A need has arisen for greater detail in the various categories of R&D in the nonferrous metals industries. If an intelligent dialogue is to commence between government and industry for increased cooperation in generic or co-operative R&D efforts, all parties should have current information.

To accomplish this New York University sent out questionnaires to the companies with the greater R&D involvement in aluminum, copper, lead and zinc. The questions asked were: the level of R&D, government contribution, and the percentages of R&D for each metal in several categories. A sample copy of the questionnaire is shown in Appendix B.

It should be noted in examining the results that essentially all of the U.S. aluminum production is from foreign ore.

The response was excellent and indicated a willingness by the metal companies to cooperate with this project. The results of the questionnaire represent the amounts of U.S. production of these metals given in Table 7.

The large percentage in zinc indicates that either the Bureau of Mines forecast will be revised upward in their final commodities summary or that some companies misunderstood the request that only products from domestic sources be listed (except for aluminum).

TABLE 7

Quantity of Metal Production Represented by the New York University Questionnaire

	Tonnage (1000)	Bureau of Mines (Est.)	%
Aluminum	3,160	5,023	63
Copper	1,417	1,430	99
Lead	376	510	74
Zinc	414	260	159

Although all of the responding companies were willing to give a breakdown of the percentage of their R&D for each stage of processing of each metal, some declined to state the dollar amount. The missing amounts were imputed from earlier surveys, which did give funding level, by applying the GNP deflator factor. This method was used because Fig. 7 indicates that company-funded R&D in primary metals has been essentially constant in 1972 dollars. However, Fig. 11 shows that R&D for nonferrous metals has increased by 35% in constant 1972 dollars. Therefore, the imputation value is considered to be 65% reliable. If, in fact this total increase were in copper, then the total R&D funding would be 22% larger than that given in Table 7. The results of the survey for the four metals of interest are shown in Tables 8 and 9 where the results are given for the responding companies only.

TABLE 8

Results of New York University Survey in Thousands of Dollars

	Total R&D (in thousands)								
	Co. funded	Govt. funded	Exploration	Mining	Comminution	Beneficiation	Primary Processing	Alloying Fabrica.	Environmenta
Aluminum	72,000	5,400	----	----	----	----	37,000	25,800	13,100
Copper	31,500[a]	negligible	711	2,590	1,240	3,850	9,490	3,890	5,140
Lead	8,000[b]	300	260	210	0	356	2,120	----	50
Zinc	4,300[c]	negligible	320	50	0	180	1,300	720	380

(a) Imputation 28%; estimated at least 65% accurate

(b) Imputation 1%

(c) Imputation 2%

TABLE 9

Results of New York University Survey in Percent of Total R&D for each Metal

	Exploration	Mining	Comminution	Beneficiation	Primary Processing	Alloying and Fabrication	Environmental
Aluminum	---	--	----	---	47.7	33.2	17
Copper	2.2	8.2	3.9	12.2	30.1	16.3	12.3
Lead	3.2	2.6	0	4.4	26.5	0	0.6
Zinc	7.4	1.1	0	4.2	30.2	16.7	8.8

Comparison of Results of Battelle, COMAT, and New York University Surveys

The categories of the 1977 COMAT study of Table 5 are not quite the same as those of the 1972 Battelle study of Table 3. However, some comparison may be attempted. For example, in Table 5 exploration, extraction, improved process and production of finished material (although inclusion of the last category is questionable) may be considered as the sum of exploration R&D, mining, beneficiation and primary processing of Table 3. These may be compared with the sum of exploration through primary processing of Table 8, ignoring the magnesium contribution to aluminum. This comparison in dollars in shown in Table 10, and as a percent of total R&D in Table 11.

TABLE 10

R&D for exploration through primary processing ($ millions)

	1972[a]	1977-78[b]	1979[c]
Al and Mg	7.85	31.7	35.4
Cu	6.31	11.3	17.8
Pb and Zn	1.33	4.4	4.8

a) Battelle-Columbus 1972

b) Comat Phase II 1977

c) NYU 1979 (this report). Note that these data are from responding companies only.

TABLE 11

R&D for exploration through primary processing in percent of total

	1972	1977-78	1979
Al and Mg	70%	70%	47.5%
Cu	81	76	57
Pb and Zn	95	86	39

It can be seen in Table 11 that the R&D percentages for exploration through primary processing have remained reasonably constant over the period 1972-1979 for the metals under consideration. However, Table 11 shows that the percentage for these categories dropped in 1979. The reason for this is that while the dollar amounts for these categories have remained constant, the industries have been investing more in total R&D. This is seen by comparing Tables 3, 5 and 8. This is done in Table 12. The increased R&D has largely gone into product improvement (alloying and fabrication) and environmental.

TABLE 12

Total R&D in Dollars (millions) by industry for 1972-1979 (data from Tables 3, 5 and 8)

	1972	1977-78	1979
Aluminum	11.2	45.4	72.
Copper	7.8	14.9	31.5
Lead and Zinc	1.4	5.1	12.3

Environmental R&D

Congress enacted a series of laws in the past few years which was designed to correct the problems of increased pollution. The principal ones are the following:

Laws	Administering Agency
Clean Air Act	EPA
Federal Water Pollution Control Act	EPA
Occupational Safety and Health Act	OSHA
Resource Conservation and Recovery Act	EPA
Safe Drinking Water Act	EPA
Mine Safety and Health Act	MSHA

NSF has obtained data on the expenditures for R&D for pollution abatement for 1976, 1977 and has estimated the amount for 1978. Table 13 shows both amount and as a percent of R&D. Note that data are not available for motor vehicles. If the data of Table 13 are calculated as a percentage of net sales, a different order is obtained. This is shown in Table 14.

TABLE 13

R&D For Pollution Abatement in Dollars and as Percent of R&D

	1977		1978	
	$Million	Percent	$Million	Percent
Pet. Ext. & Ref.	61	6.6	72	6.7
Nonferrous Metals	12	4.4	13	4.6
Chemical	65	3.9	68	3.7
Machinery	33	0.8	41	0.9
Elec. Equip. & Comm.	20	0.3	19	0.3

Source: National Science Foundation

TABLE 14

R&D for Pollution Abatement as a Percent of Net Sales

	1977	1978
Chemical	0.14%	0.13%
Petrol. ref. and ext.	0.046	0.05
Nonferrous metals	0.044	0.041
Machinery	0.042	0.046
Elec. Equip. and Comm.	0.021	0.017

Source: National Science Foundation

We may collect the Battelle (Pollution control), the COMAT (waste management) and the New York University (environmental) data from Tables 3, 5 and 8 and consider these categories as similar, if not identical. These data are shown in Table 15. It is seen that there has been a significant increase in cost of R&D for environmental control between 1972 and 1979. The COMAT data does not appear to reflect the correct industry activity. Possibly their questionnaire was misinterpreted and pollution abatement research is contained in one of the other categories.

TABLE 15

R&D for Environmental Control ($ millions) and Percent of Total R&D

	1972	(Battelle)	1977-78	(COMAT)	1979	(NYU)
Aluminum	$2.6	19.6%	$1.5	3.3%	$13.1	17%
Copper	1.2	15.4%	0	0	5.14	12.3%
Lead and Zinc	0.06	4.2%	0.1	2	0.43	3.4%

Considerable pollution control technology is known for non-ferrous metals but the cost of compliance forces a business decision to be made. For example, a major copper smelter in Montana was recently closed with a resulting loss of 1500 jobs because it was decided that cost of compliance was too great for continued profitable operation. The sulfur dioxide and particulate regulations were followed by the closing of 9 of the 14 zinc smelters, or nearly one-fourth of the nation's zinc slab production capacity. "However, since the smelters which closed were somewhat obsolete and only marginally economic, it is difficult to place the blame entirely on the environmental regulation."[13] The lead industry may be particularly devastated. The current ambient air quality standard promulgated by EPA is being vigorously opposed by the industry. A study by the Charles River Association and the Research Corporation of New England carried out for the Lead Industries Association showed that compliance with the law would be virtually impossible.[13] Their conclusions are in Table 16.

Comparable data, Table 17, have been obtained in an analysis by various federal agencies.[14] Note, however, that in Table 17 the control costs have been estimated on an OSHA standard of 100$\mu g/m^3$ while the recently enacted standard is 50$\mu g/m^3$. The major upward revision of control costs and its effect on pricing lead has not been made.

TABLE 16

Impact on the Lead Industry of Attempting to Meet the EPA Ambient Air Lead Standard

Sector	Costs		Plant Closings
	Capital	Annual	
Primary Smelting	$190 m.	$35 m.	all seven
Secondary Smelting	$285 m.	$60 m.	40 of 50 (90% of loss of capacity)
Mining	not applicable		all non-Missouri Missouri (?)

Source: AIME, Lead-Zinc-Tin '80.

TABLE 17

Partial Environmental Impacts and Control Costs

	Copper	Lead
Min. & Ben.	686×10^6 tons waste and overburden. 170×10^6 tons toxic tailings	Acid mine drainage 8.4×10^6 tons toxic tailings
Processing	10% of national SO_2 emissions. 41×10^3 tons of particulates (0.4% of national total)	440-2740 tons/yr.. lead emissions
Control costs	Industry cost since 1970 $\$2 \times 10^9$ for SO_2 with another billion expected; 10-14% of production costs	$\$500 \times 10^6$ capt. costs 62% total plant costs
Price increase	12-15¢/lb..	16¢/lb.
Capacity loss	13-17%	$320\text{-}550 \times 10^3$ tons
Imports	9% increase	7% increase
Employment	5.5% decline by 1985	2240-8750 total jobs depending on degree of control

Source: Reference 14.

Effects of Energy Costs

There is a very large consumption of energy for the production of metals. Table 18 lists the energy required per net ton of product for the nonferrous metals under consideration and the total energy consumed for 1973[15].

TABLE 18

Summary Table of Energy Requirements for Metals Production in the U.S. in 1973

Metal	Primary Product	Energy in million per net Ton	Total Energy Required for U.S. Consumption in Trillion BTU
Al	ingot	244	1,408
Cu	refined copper	122	221
Pb	refined lead	27	24
Zn	elemental zinc	65	92

Source: Battelle-Columbus Laboratories, 1976.

Before primary processing can begin, crushing and grinding of the ores must take place. This comminution step is highly energy intensive because of low efficiency, often less than 1% in fine grinding. The energy consumed for comminuting Al and Cu is shown in Table 19.

It should be noted that as the grade of ores such as copper become lower, finer grinding is required to liberate the metal-containing fraction. It is a principle in communition that the energy increases rapidly with fineness of grind. This is reflected in the generalized curve of energy of extraction vs. grade of ore given by the U.S. Bureau of Mines and shown in Fig. 13.

The metal processing plants in the U.S. were largely built in the era of low concern for pollution control and energy costs. These processes could be replaced with more efficient ones from the energy standpoint and a change from pyro- to hydrometallurgical processes would be advantageous in some cases for pollution control. The energy situation has been studied in some detail by Battelle for the Bureau of Mines with the conclusions presented in Table 20.

TABLE 19

Energy Requirements for Crushing and Grinding
Al & Cu Ores

	Specific energy BTU/T*	% of total processing energy
Al	49	20%
Cu	2400	21%

*The conversion from KWH to BTU involves the Battelle Laboratory estimate of 32% efficiency of electrical generation with the result that 1KWH = 10^4 BTU.

Source: Battelle-Columbus Laboratories, 1975.

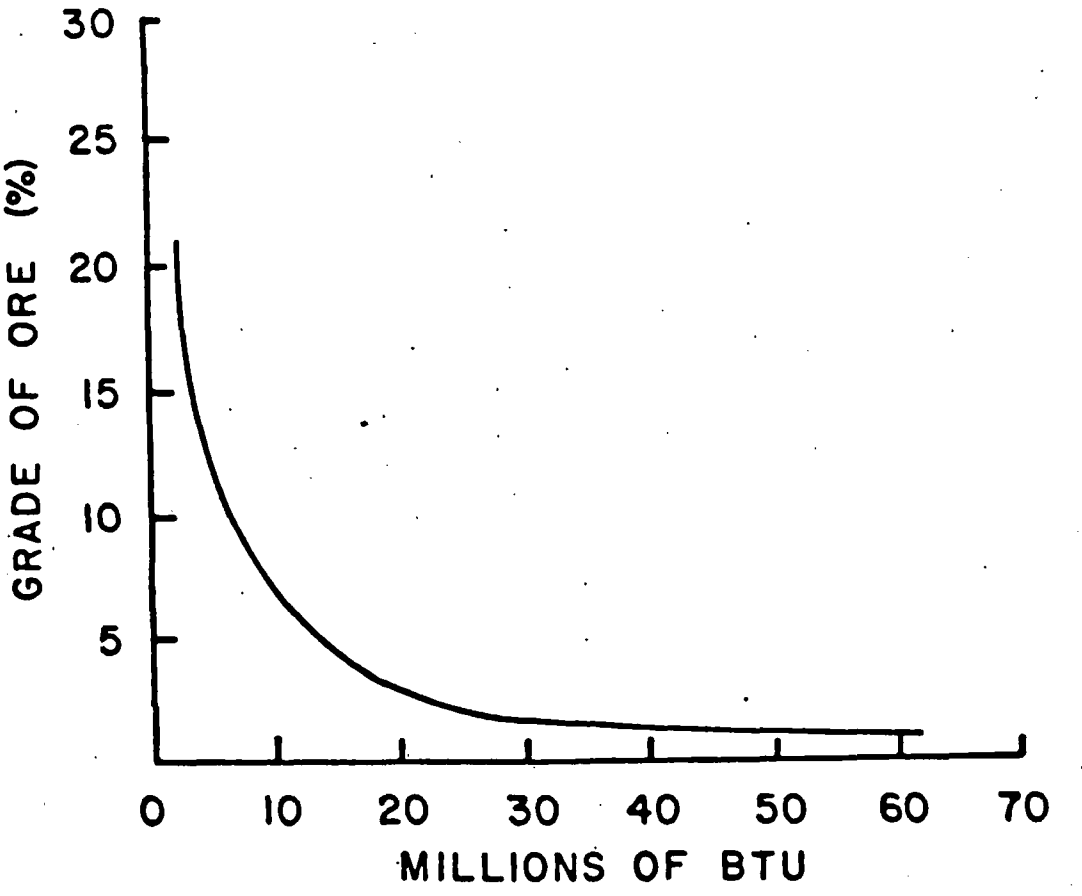

Fig. 13. Relationship between grade of ore, in percent of desired value, and the energy required to mine and beneficiate a net ton of primary product, (ref. 15.).

TABLE 20

Need and Principal Opportunities for Energy Savings Via Process Alternatives in the Production of Some Key Metals

Metal	Need for Replacement	Alternative Process	Estimated Energy Savings
Al	Highly desirable	Alcoa smelting process to replace Hall process	25%
Cu	Highly desirable	1) Flash smelting	10%
		2) Continous smelting	10%
		3) Blast furnace	10%
		4) Autogenous smelting	10%
Pb	Desirable	1) Single step smelting	30%
		2) Imperial smelting process	not known
Zn	Desirable	1) Imperial smelting process	approx. 7%
		2) Jarosite process	5-8%

Source: Battelle-Columbus Laboratories, Phase 9, 1976.

Competitiveness of the U.S.

Three important effects on the U.S. nonferrous metals position have been summarized:

1. National security and self-sufficiency
2. Pollution control
3. Increased cost of energy

Many foreign countries do not have as stringent environmental protection laws as those of the U.S. Furthermore, there is an increasing desire by LDC suppliers to produce finished metals within their countries rather than ship ore concentrates. The capital costs of new plant construction are given by Battelle in Table 21.

As an example, a new copper project in Colorado involves an investment of nearly $1 billion. With these considerations it is not unexpected that some companies choose to shut down plants in the U.S. and build overseas. Such action does not have a completely negative effect on the overall U.S. economic picture, for the energy used is not that of imported oil into the U.S. but oil imported into another country for the metals processing. The negative aspects are, of course, the loss of jobs and a decline in self-sufficiency.

The effects of environmental laws and of foreign assistance to their national metals companies have been assessed by Bureau of Mines specialists and have resulted in the prospects for the year 2000 given in Table 22.

TABLE 21

Capital Costs of New Plant Construction

Metal	Capital, dollars per annual ton
Al	2,400
Cu	6,000
Pb	1,400
Zn	1,600

Source: Battelle-Columbus Laboratories, 1979.

TABLE 22

Secular Changes in the Competitiveness of Selected U.S. Metal Industries, 1953-57 and 1973-77

Metal Industry	U.S. Production X10^3 Metric Tons			U.S. Producers Percent of U.S. Market			U.S. Producers Percen of World Market		
	1953-57	1973-77	2000	1953-57	1973-77	2000	1953-57	1973-77	200
Alumina ref.	1,457	3,181	4,900	100	72	39	44	22	9
Aluminum sm.	1,460	4,340	11,470	96	92	80	45	32	23
Copper min.	898	1,422	2,700	89	96	95	29	20	15
Copper sm.	1,000	1,408	2,860	79	94	95	30	19	16
Copper ref.	1,432	1,826	3,700	100	92	95	38	21	18
Lead min.	308	561	900	68	89	78	22	18	17
Lead sm.	903	1,192	1,100	71	94	89	22	18	17
Zinc min.	473	433	730	52	72	62	16	8	8
Zinc sm.	905	535	904	95	52	63	32	8	11

Source: Reference 10.

Opportunities for Improvement

The capital costs per annual ton for the construction of modern efficient plants were given in Table 21. Estimates of the operating price of a new facility excluding depreciation, and the calculated price including return on investment and taxes are compared to market prices in Table 23.

The operating costs are largely wages and energy and can be considered as tied to inflation. The volatility of pricing can be seen in the change in market prices. Thus, large capital investment for long-term requires either stability or some guarantees. This was reflected in the views of Battelle in their 1972 report[11] on needs of the industry. They were:

1. Tax incentives for funding of R&D programs.
2. Low interest loans for funding R&D to companies that have trouble generating the needed capital.
3. Cooperative R&D programs.
4. Accelerated amortization schedules for equipment and facilities devoted to R&D.
5. Federal insurance for companies testing expensive full-scale equipment.

Regarding item 5, it is obvious that one does not go from a laboratory bench model to a plant costing hundreds of millions of dollars. Various stages of pilot plants as well as full-scale demonstration plant must be operated, corrected for errors, and engineering personnel must be trained. This is a high-risk area and some incentive must be created for company expenditures of this stage.

TABLE 23

Operating and Calculated Prices for New Plants and Market Price of Product

Metal	Operating Cost	Calculated Price*	Market Price		
			July 76	Dec. 77	Oct. 80
Al	$ 0.37/pound	$ 0.66/pound	$0.44/pound	0.53	0.68
Cu	0.53	1.27	0.74	0.61	0.98
Pb	0.11	0.29	0.24	0.33	0.45
Zn	0.19	0.39	0.37	0.30	0.37

* Since this calculation was made in 1976, interest rates have increased by 50-70%.

Source: Battelle-Columbus Laboratories, 1979.

In 1977 the American Mining Congress requested a number of companies to list priority areas where government R&D was needed. They were:[13]

1. Safety
2. Upgrading low-grade ores
3. New and improved methods for mining.
4. Geological mapping and surveys.
5. Research in high-risk areas such as solution mining, ocean mining, and recovery of metal values from marginal deposits.
6. Methods of decreasing costs of meeting environmental standards.

Another series of recommendations was developed in 1978 through a workshop of industry and university experts held by the Committee on Mineral Technology of the NRC Board on Mineral and Energy Resources.[16] The committee recommended in general that "only a minimal technical effort should be expended on patching-up existing and old or potentially obsolete and costly procedures and processes. A maximal technical effort should be devoted to a re-evaluation and modification of existing procedures and processes and the rapid development of new procedures and processes which will satisfy likely future conditions under which the industry will be required to operate."

More specifically the Committee recommended that federal policy be directed toward the industry with the following objectives:

1. Provide for the professional development of competent R&D personnel.

2. Provide for the development of new technology through the establishment of demonstration projects and single industry consortia for R&D in new technologies.

3. Provide for incentives for the application of new technologies in the mineral industries through both tax incentives and increased protection above existing patent laws and antitrust policy and practice. Additionally government purchase programs based on the uses of new technologies for low-grade domestic ores would have a strong incentive.

A study was undertaken by Battelle Columbus Laboratories to determine the R&D needs for various minerals as perceived by knowledgeable people involved in such matters.[6] Although subjective opinions were gathered in this survey, they were in sufficient numbers to enable a ranking index to be formed. Opinions were solicited for the metals concerned, their processing stages and the urgency for R&D in short-term (0-5 years), intermediate-term (5-15 years) and long-term (greater than 15 years). Selected results are shown in Table 24 for the metals and processing stages of interest in this present review. In this Table the larger the number the greater the urgency.

TABLE 24

Estimated Indices of Urgency by Stage and by Metal
(Larger number means higher urgency)*

	Exploration			Mining			Minerals Processing			Recycling		
	ST	IT	LT	ST	IT	LT	ST	IT	LT	ST	IT	LT
Aluminum	4	5	6	3	4	4	2	3	4	3	3	4
Copper	3	4	4	2	3	3	2	2	3	2	3	3
Lead	2	3	3	1	3	3	0	1	1	1	2	2
Zinc	2	3	3	1	2	2	1	2	3	1	1	2

ST = Short Term 0-5 years

IT = Intermediate Term 5-15 years

LT = Long Term greater than 15 years

*Data from Ref. 6

Recent testimony of David Swan, Vice President of Kennecott Copper Co., amplifies these views.[17] He outlines the R&D process in four stages:

1. The generative stage is that which creates an adequate reservoir of basic science and knowledge.

2. The innovative or synthesis stage is that in which basic scientific findings are synthesized to find new and better ways of doing things.

3. The demonstration stage is that which demonstrates the utility and economic merit of a novel concept.

4. The transfer stage is that in which an innovative process is broadly applied.

This testimony develops these ideas further by pointing out that the federal government should increase its level of support in stages 1 and 3. Stage 1 is chosen as it is traditionally the area of university research. He suggests that federal policy for research emphasize long-term funding of projects at these institutions to establish a continuity of research on what are characteristically long-term projects. Stage 3, the demonstration stage, is expensive and is best done at the mine site. Often these demonstrations are of large-scale, high-risk, innovative projects which involve new technology developed in response to government-mandated regulation. Swan presents the mining industry view that the national program should provide mechanisms for a more effective federal contribution to demonstrating new technology.

In his testimony Swan emphasizes two further points:

a) that there be a review of policies which tend to inhibit cooperative industry R&D; specifically some of the antitrust provisions and interpretations.

b) that there also be a review of the current U.S. defacto policy which has the practical effect of denying large areas of the potentially most attractive mineral deposit areas in the U.S. to access for exploration.

The Concept of an Industry-Government Cooperative Program in Mining-Metals Research and Development

The nonferrous minerals industries have characteristics which inhibit rapid change. 1) The mining and beneficiation processes are restricted to the location of the ore body; costs of shipping necessitate that only concentrates can be shipped for refining. 2) The primacy of an ore body results in an international aspect of competition and is one of the forces for relocation of plants. 3) There is a large capital investment in the industry with a resulting reluctance to modify or build new technology. 4) Fluctuating price and demand results in cautious investment when long-term pay-off is required. 5) Concern over uncertainties in U.S. policy, laws and regulations inhibit innovation and investment.

A number of these problems can be alleviated by a better understanding of the solutions through increased research and development. The concept has developed that increased government-industry research, on a 50-50 funding basis, may be an effective method. With such cooperative programs the knowledge and experience derived would flow to all participants, generally in amounts far greater than could be achieved by individual corporate or federally supported project investment in R&D. The program would be of basic and applied research as well as advanced technology through pilot plant development.

Some example topics are given below:

1. Regional metallogenic studies which would integrate geochemical, geophysical and geological research.
2. Development of tonnage and grade frequency distributions.
3. Development of new down-hole and deep, high- resolution geophysical techniques.
4. Development of alternatives to excavation mining such as in situ leaching.
5. Effect of excavating mining on mechanical properties and integrity of underground rock.
6. Development of better techniques and/or equipment for in-mine handling of waste.
7. Development of beneficiation techniques that have greater flexibility with respect to ores.
8. Invention and/or development of nonpolluting alternatives to smelting.

These cooperative activities would be selected by those involved in the support and the site of the research activity would also be chosen. It could be in-house, in a government lab, or at one or more universities. A mechanism for carrying out the decision-making process would have to be established with agreement by industry.

This concept was tested by personal interviews with officials of 12 nonferrous mining and metals companies by Mineral Systems Inc.[18] The result was that nine were seriously interested and expressed and offered cooperation. Three had reservations, not to the concept, but rather to the mechanism of decision-making. Such conservativism is not unexpected, they simply would like to know more about how their money will be spent before they commit their funds.

Summary and Conclusions

This report has reviewed the patterns of R&D in the nonferrous mining-metals industry. Total annual R&D in this industry is below $300 million and for ferrous and nonferrous metals combined the total is about $500 million. This can be contrasted to the industrial chemical sector at $1.8 billion, machinery at $4.5 billion, electrical equipment at $6.7 billion and petroleum refining and extraction at $1.1 billion. The percentages of federal contribution to the R&D of these sectors are: electrical equipment 45%, chemicals 18%, machinery 15%, petroleum extraction and refining 8%, nonferrous metals 8%.

The nonferrous metals industry in the United States has had a series of severe pressures in the past few years. These have largely resulted from environmental and safety regulations, the high cost of energy and the current high interest rates. This review has shown that, compared to almost any other industry sector, the R&D has been low and federal contribution almost negligible. Nevertheless, the industry has been increasing its R&D funding.

The concept of government-industry cooperative research through the pilot plant stage has been proposed and tested for industry interest. The interest was found to be high. The important point in the survey was the necessity that the organization and control of such a program be acceptable to industry.

If the organization can be created acceptably to all, questions will arise as to the directions of research. Several surveys of industry representatives are quoted in this report concerning their views on priorities. In addition, the New York University Center for Science and Technology Policy has conducted a survey during October-November 1980 to determine the areas of R&D in which industry is spending its own money. This should serve as a useful guide to the cooperative program advisory members in the direction of funding of the program.

APPENDIX A

Reasons for the Omission of R&D Data from Business Week

A common source of R&D data by industry sector is Business Week. Once a year these data are published and frequently quoted by students and scholars. Business Week obtains their data from company annual reports and 10K forms. The annual reports and 10K forms of the companies surveyed in the present report were available during the report preparation as they were to Business Week. These had only limited usefulness. The Business Week summaries were not used for the following reasons.

1. Their data for the nonferrous metals industry includes companies that produce only minimally from ores.

2. There is no separation of R&D of foreign subsidiaries.

3. The reporting is inconsistent -- a company may be listed one year and not the next.

4. The annual reports and 10K forms give only limited information which is not selectively quoted or rejected, e.g., an oil company which owns a mineral company often reports total R&D with the mineral part not separated. In Business Week, the oil company R&D may be listed under oil R&D so that the mineral part is not listed.

5. In many company reports R&D is not a separate item, so the Business Week summary is incomplete.

6. The numbers given include R&D for consumer product improvement, which is often 75% of the total.

These objections are not the fault of the researchers at Business Week. The inaccuracies simply arise from incomplete or faulty data. Data of the quality in this report cannot be obtained from annual reports and 10K forms alone.

QUESTIONNAIRE ON R&D IN METALS & MINING INDUSTRY

A. Company or Appropriate Division: _____

("Division" when the metals business is a part of a parent corporation in other fields.)

B. Metals Produced and R&D Breakdown:

Metal	Production - in tons (1979)	R&D Funding: Corp. Funded	R&D Funding: Gov't. Funded	R&D Funding: Total	% of Total R&D Relevant to Stages of Production: Exploration	Mining	Comminution	Beneficiation	Primary Processing	Alloying	Fabrication	Environmental	Other
1. Copper													
2. Molybdenum													
3. Lead													
4. Zinc													
5. Aluminum													

C. R&D Activities in Pilot Plant Stages

Brief Title of Activity	Amount in 1979
1.	1. $
2.	2. $
3.	3. $

D. Other Specific Activities Not Covered by Above (e.g., exploration R&D in gold deposits)

Brief Title of Activity	Amount in 1979
1.	1. $
2.	2. $
3.	3. $

E. Approximate Amount of Direct Funding for University R&D (not including fellowships) $_____

F. Approximate Amount of Funding for Cooperative Research (e.g., trade associations) $

REFERENCES

1. United States President's Materials Policy Commission. Resources for Freedom, Washington (June 1952). U.S. Government Printing Office.

2. Material Needs and the Environment; Today and Tomorrow. Final Report of the National Commission on Materials Policy (1973) National Academy of Sciences.

3. Bureau of Mines, U.S. Department of the Interior, Mineral Commodity Summaries 1980.

4. Bureau of Mines, U.S. Department of the Interior, Minerals Yearbook.

5. "Research and Development in Industry, 1978 , Detailed Statistical Tables," Survey of Science Resources Series, NSF 80-307.

6. "The Problem Analysis Phase: Task 8 -- Assessing the Adequacy of R&D," report by Battelle-Columbus Laboratories to the National Science Foundation, February 23, 1979.

7. Private Communication from Dr. Charles Moore, Executive Director, International Copper Research Association.

8. Private Communication from Dr. Schrade Radtke, Executive Director, International Lead and Zinc Research Organization.

9. Private Communication from Dr. M.B. McNeil, High Temperature Processes Branch, Industrial Programs, DOE.

10. Private Communication from Dr. T.A. Henrie, Chief Scientist, Bureau of Mines.

11. "Survey of R&D in Private Industry in the Mining, Minerals and Metallurgical Fields," report by Battelle-Columbus Laboratories to the U.S. Bureau of Mines under Contract Number SOI 22048, October 13, 1972.

12. "Inventory and Analysis of Materials Life Cycle Research and Development in U.S. Industry, 1977," Phase II Report, COMAT (the Committee on Materials, a Federal Interagency Coordinating Committee), Thomas A. Henrie, Chairman, April 1979.

13. J.E. Cole, "U.S. Environmental Laws and Regulations as Applied to the Lead and Zinc Industries," Lead-Zinc-Tin '80, J.M. Cigan, T.S. Mackey, and T.J. O'Keefe, Editors, AIME, 1980,

14. "Report on the Issues Identified in the Nonfuel Minerals Policy Review (Draft for Public Review and Comment), U.S. Department of Interior, August 1979.

15. "Energy Use Patterns in Metallurgical and Nonmetallic Mineral Processing," Phases 5, 7, and 9. Battelle-Columbus Laboratories (1975, 1976).

16. Technological Innovation and Forces for Change in the Mineral Industry, Committee on Mineral Technology, Board on Mineral and Energy Resources, National Research Council 1978.

17. Hearings before the Committee on Science and Technology, U.S. House of Representatives, No. 103 Vol 4, October 23, 30, 1979.

18. Identification of National Needs with Industry Leaders Comments on Research and Development Needs in Minerals Extraction. A.Weiss, Mineral Systems Technology, 1980.

Economic Geology
Vol. 74, 1979, pp. 351–352

POTASH

JOHN C. DUNLAP AND ROBERT J. HITE

WHEN the request to organize a program on the geology of potash deposits for the 1978 Annual Joint Meeting of the Society of Economic Geologists and the Industrial Minerals Division of the Society of Mining Engineers of AIME was received, the convenors recognized that the program would have to be international in scope because most of the important new discoveries of potash have been made outside the United States.

The past 15 years have seen a tremendous acceleration in the generation of geologic and geophysical data pertinent to potash deposits. This has been due largely to the massive exploration efforts of the petroleum industry in all corners of the globe. These new data have resulted in the discovery of several new and important deposits as well as providing a better understanding of some occurrences already known. Because of this we decided to try to organize a program that would emphasize descriptions of some of the new findings and what their economic impact on the potash industry might be. Thus, although the collection of papers published in this issue of *Economic Geology* does not represent complete coverage of all the world's potash deposits, it does include papers describing most of the important newer discoveries.

Bedded deposits of potash associated with marine evaporites are now known to be much more common that geologists previously realized. Deposits are known at several localities on all continents except Antarctica and Australia and were deposited in all geologic periods except the Ordovician. Current world supplies come principally from mines in North America and in Europe, but potential new sources in other regions are being explored and because of favorable location or geology will doubtlessly become sources of supply in the future.

Six of the papers in this collection describe the regional geology of marine evaporites that contain potash deposits and illustrate very clearly the indispensable role played by the petroleum industry in discovering and in providing geological and geophysical information on the deposits. Two papers detail the geology of specific potash deposits, in one case from exposures in a new potash mine and in the other from cores and other data obtained during an evaluation program that is still in progress. Finally, a significant overall contribution is made by one paper devoted to an analysis and projection of future world supply and demand for potash salts and a discussion of economic and political factors that affect the potash industry.

Two of the regional papers describe different parts of the largest potash deposits in North America, and possibly the largest in the world, those of Middle Devonian age in the Williston Basin in the Great Plains region of Canada and the United States. Potash salts produced from these deposits in Saskatchewan, Canada, during 1977 were estimated to contain 5.9 million metric tons of K_2O equivalent, the largest production from any country in the western world. There has been no production from extension of these deposits into the United States. Here they are so deep it appears probable they can only be produced economically by solution mining.

Except for a very few cored and analyzed sections of some potash deposits, the two regional papers on the Middle Devonian evaporites are based upon interpretations of geophysical logs of several kinds recorded in wells drilled for petroleum. They represent excellent examples of multiple use of basic geological and geophysical data in natural resources investigations.

Details of the geology of a potash deposit of Mississippian age in the northern part of the Appalachian orogenic belt in New Brunswick, Canada, is the subject of one of the papers on a specific deposit. These evaporites have been deformed by both regional tectonics and salt flowage. In addition, there has been extensive solution of parts of these evaporites, which adds to the challenging problems facing the geologists at this continuing exploration project.

The third regional paper describes the upper Permian evaporites in the British sector of the North Sea and contiguous land areas, and thus adds another dimension to the famous Zechstein evaporites. Those deposits are now the source of potash salts produced at the new Boulby mine on the western shore of the North Sea at Saltburn, England. Details of the geology of the orebody at this mine is the subject of the second detailed paper. The very interesting structures in the area mined to date, the indicated paragenesis of the mineral suite, and the indicated paleomovement of brines and gases through the body of salts is better understood by the reader because of having the regional paper on the Zechstein to give perspective for the detailed geology of a relatively very small part of the larger body of salts.

The fourth regional paper describes evaporite deposits of Lower Cretaceous age that were deposited

in a linear basin 1,800 km in length along the western continental margin of Africa. These deposits are of particular interest, first because they include thick deposits of potash and rare magnesium salts; second, because of a scarcity of the less soluble carbonates and sulfates; and third, because of the similarities in structural environment, age, composition, and details of saline stratigraphy and mineralogy with evaporite deposits on the opposite side of the south Atlantic Ocean along the eastern continental margin of South America. The striking similarities in structure and stratigraphy in the two now widely separated regions have been explained as resulting from deposition in grabens caused by rifting that originally were contiguous and have since been separated to their present positions by the processes of plate tectonics. The scope of this paper is large, both in the geographic area covered and in the example it provides of the multiple use of basic geological and geophysical data. The information on stratigraphy and structure was originally obtained for use in petroleum exploration; it was then used to select an area for potash exploration and in considering geologic and geochemical problems in salt deposition; and most recently it has been used in evaluating the concept of plate tectonics.

Two potash-bearing evaporite deposits, of different ages and with distinctly different geology, located in Brazil, are covered by the fifth regional paper. One deposit, which is in the vast and almost inaccessible Amazon Basin of northern Brazil, is of Permo-Carboniferous age. This sequence consists of a large number of remarkably complete evaporite cycles, and the paper is the first documentation that they are potash bearing. The second occurrence described are those deposits of Lower Cretaceous age found along the northern Brazilian coast principally in the State of Sergipe. These deposits, which have been extensively explored for potash and may soon be developed for this resource, are in a complex structural setting and show evidence of a wide range of depositional environments and diagenesis. One of the world's largest deposits of the mineral tachyhydrite is found here. This mineral, which, until recently, was believed to be uncommon in an evaporite sequence, indicates extreme conditions of desiccation.

The sixth regional paper is a brief description of the newly discovered potash deposits of Cretaceous age on the Khorat Plateau of Thailand and Laos. The discovery of these deposits was somewhat of an exception to the rule, in that it resulted from a direct exploration effort in which bromine geochemistry played a major role. These deposits, which are very large and unbelievably shallow, contain an abundance of tachyhydrite and borate minerals and in this respect are strikingly similar to deposits of like age in coastal Brazil and the Gabon-Congo Basins of coastal Africa.

Economic Geology
Vol. 74, 1979, pp. 221–231

Phosphate Occurrences on the Western and Southern Coastal Areas and Continental Shelves of Southern Africa

A. O. FULLER

Abstract

Several different varieties of sedimentary phosphatic deposits of Neogene age occur on the southern and western continental margins of southern Africa. Their origin and distribution were influenced by major transgressions and regressions identifiable in offshore seismic reflection profiles and confirmed by onshore observations. Offshore deposits consist of nodules eroded from outcropping Neogene strata and mixed glauconite/apatite pellets. In addition concretionary masses occur on the South West African shelf associated with siliceous muds. On the western coastal plain the oldest deposit is a Miocene phosphatic sandstone which is unconformably overlain by a Pliocene unit containing reworked Miocene material. Small volumes of phosphate-cemented surface sands are found, and a number of deposits of aluminium phosphates occur in the vicinity of Saldanha Bay.

The deposits are of the platform type. No tectonic control of mineralization has been identified, but local topographic features have influenced the distribution of ores. Several modes of origin including direct precipitation, replacement, diagenesis, allochemical and lithochemical, have been identfied.

Offshore Phosphate Occurrences

Tertiary stratigraphy

During the past ten years marine geoscientists at the University of Cape Town have undertaken detailed investigation of the continental shelf off the southern and western coasts of South Africa by subbottom seismic reflection profiling and dredging (Dingle, 1971, 1973). The following summary of Tertiary stratigraphy in the offshore regions has been prepared from Dingle's work. It highlights the main features of the region, especially as they bear on phosphate deposits onland.

The continental shelf around the South African coast can be divided into contrasting western and southern parts that are separated by the Agulhas Arch, a region of elevated pre-Tertiary formations which lies in the western sector of the Agulhas Bank (Fig. 1). Widespread unconformities can be recognized so that the Tertiary can be subdivided into time-equivalent lithological sequences. Sufficient work has been done on dating material dredged from outcrops of these sequences to allow broad interpretation of their ages to be made as well as those of the major unconformities that separate them.

Seismic data shows that the western shelf is underlain by a more complex assemblage of Tertiary strata than its southern counterpart. The latter region was relatively stable during the Tertiary and the stratigraphic record is interrupted by only one major unconformity, of Oligocene age. The Oligocene break can be followed into the western shelf so that Dingle has been able to correlate the strata of the two regions on the basis of their position relative to the major hiatus.

The southern shelf contains two Tertiary sequences separated by the Oligocene unconformity. The lower (Dingle's T_L) rests on a Paleocene/early Eocene unconformity and contains sediments as young as upper Eocene. The upper (Dingle's T_U) has been dated, on the basis of the few ages available, as upper middle Miocene.

The widespread Oligocene unconformity allows the Tertiary succession underlying the western shelf to be divided into a lower sequence (T_1), assumed equivalent to T_L, and an upper equivalent to T_U, which can further be subdivided into three units (T_2, T_3, T_4). In contrast to the relatively straightforward Tertiary stratigraphy of the southern area, the western shelf succession is marked by many planes of erosion, rapid lithological change, and various structural attitudes, evidence of greater crustal mobility of the region.

The history of major transgressions and regressions interpreted from the offshore data is of particular importance with regard to the occurrence of onshore phosphorites. A major transgression occurred in early Tertiary time (Paleocene/Eocene). A major regression occurred at the end of Eocene time, eroding the bulk of early Tertiary sediments. This accounts for the paucity of Eocene sediments on land. A second major transgression occurred in Miocene time, possibly lower Miocene. At the end of the Miocene another regression occurred, accounting for an unconformity between Dingle's T_3 and T_4 sequences. A third transgression occurred in Plio-

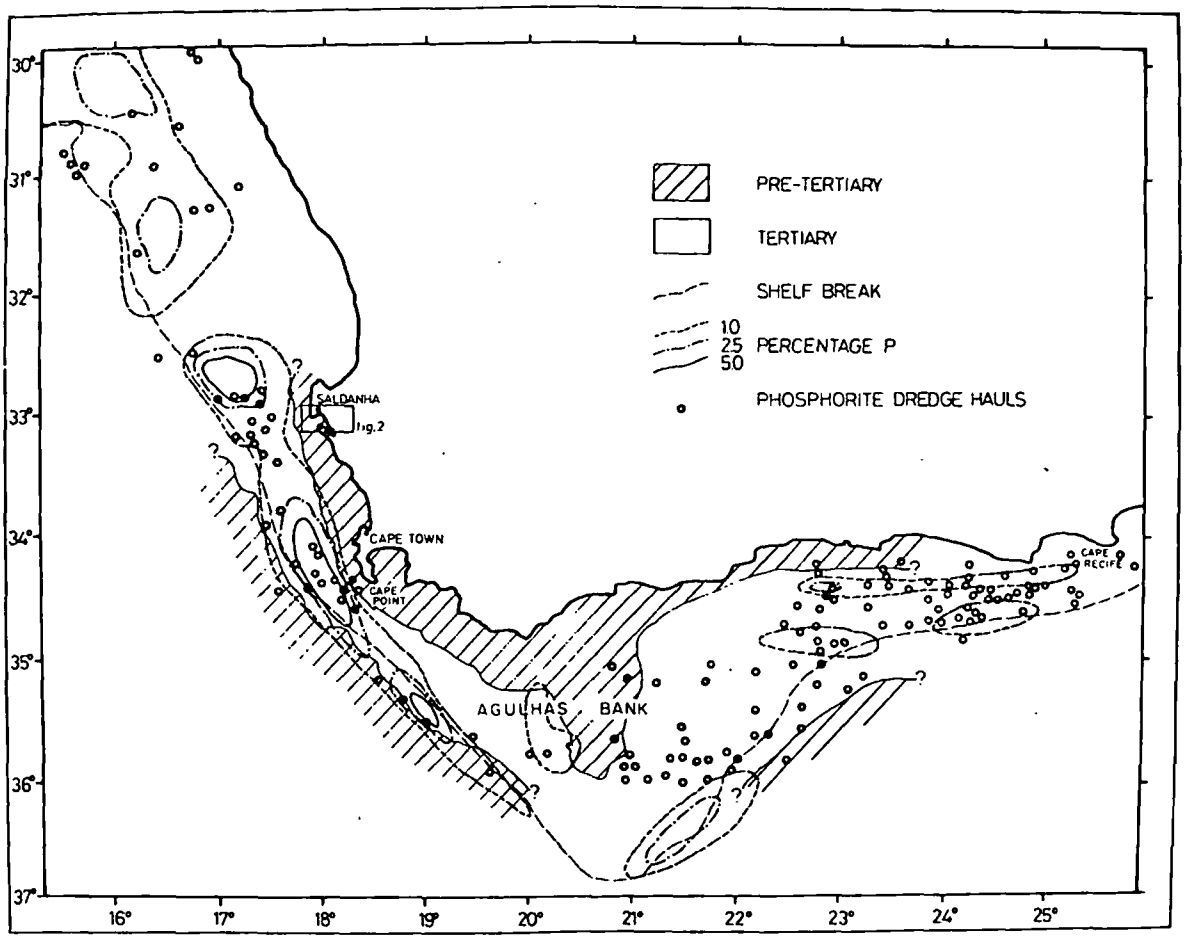

FIG. 1. Broad outlines of the geology of the southern and southwestern continental shelf as deduced from seismic survey and dredging.

cene time, followed by a regression. This sequence of events deduced from offshore seismic investigations agrees well with onland observations discussed elsewhere in the text.

Nodules

Historical note: Fragments of lithified phosphatic sediments, commonly referred to as nodules, were first recovered in dredgings from HMS Challenger (Murray and Renard, 1891). The samples came from localities on the upper, northwestern side of the Agulhas Bank (south of Cape Town) and from the the lower continental slope off the southwestern tip of the bank. Collet (1905) reexamined the Challenger material and described phosphorite collected by the Gazelle and Valdivia cruises. Cayeux (1934) and Haughton (1956) described material made available by the South African government and commercial trawling operations. Since 1967 investigation of the nodules has been carried out at the University of Cape Town as part of the Continental Margin Programme. This has resulted in a determination of their regional distribution, petrographic and geochemical characteristics, and a greater understanding of their lithogenesis (Parker, 1971, 1975; Parker and Siesser, 1972; Parker and Simpson, 1972; Summerhayes, 1973a, b).

Distribution: Phosphatic nodules are widespread on the continental shelf off the Cape coasts (Fig. 1). Nodules have been recovered from 107 stations off the west coast at depths between 200 and 500 m. The largest concentrations occur between Cape Point and Saldanha Bay and between Cape Agulhas and Cape Recife (Fig. 1).

Classification: Parker and Simpson (1972) and Parker and Siesser (1972) have recognized several nodule types and have suggested the following classification based on compositional and textural criteria. The scheme has been found useful in that it groups the major nodule types into only a few categories, but Birch (1975) points out that a continuous gradation in properties exists between one type and another.

The nodules are classified into two basic types—

nonconglomeratic (NC) and conglomeratic (C). Nonconglomeratic are further divided into three subtypes: NC1, composed of silt-size quartz and microfossils cemented by a collophane/micrite mixture (medium-grained packstones and wackestones); NC2, a brown microfossiliferous limestone cemented by a collophane/goethite/micrite mixture, the goethite imparting a distinctive brown color (medium- to coarse-grained packstones); and NC3, a composite of quartz, glauconite, and microfossil grains together with variable quantities of macrofossil fragments cemented together by a collophane/micrite mixture (fine- and coarse-grained packstones and wackestones).

The conglomeratic category is divided into two subtypes, C1, angular pebbles of NC1 and NC2 cemented by a matrix similar in composition to NC3, and C2, shell casts and macrofossils set in a NC3-type matrix depleted of glauconite and rich in microfossils.

Chemistry: Whole-rock chemical analyses of nodules (Table 1) show variations consistent with relative amounts of their dominant mineral phases: quartz, calcite, glauconite, and collophane (Parker, 1971).

Mineralogy: X-ray diffractograms of nodules show well-defined peaks corresponding to the dominant mineralogical species present: collophane, calcite, quartz, and glauconite. Birch (1975) reports that the ferruginous, nonconglomeratic varieties (NC2) produce diffuse reflections suggesting poor crystallinity. No positive identification of the iron oxyhydroxide has been made, but it is presumed to be goethite. Mixed-layer clays are ubiquitous and kaolinite was found in trace amounts in four samples. Plagioclase feldspar is present in all samples. K-feldspar is present only in nodules dredged in the vicinity of Cape Town.

The phosphate phase in all nodules analyzed, both from the western shelf and Agulhas Bank, is carbonate-fluorapatite (Parker, 1971). Birch (1975) has determined that the average CO_2 content of the apatites from western shelf nodules is 5.5 percent which agrees with the values of 4.8 to 6.1 percent found by Parker (1971) for Agulhas Bank samples.

Stratigraphic relationships: Phosphatized limestones of the nonconglomeratic nodule varieties and their pebble equivalents in the conglomeratic types are from the Agulhas Group (Siesser, 1972) of lower Miocene to Pliocene age which outcrops on the middle and the outer continental shelf off southern and southwestern South Africa (Dingle, 1973). The aerial extent of the conglomeratic category coincides with an elongate outcrop of Paleogene sediments on the inner Agulhas Bank parallel to the south coast (Dingle, 1974). The present distribution of nodules reflects the extent of their original outcrop when allowance is made for redistribution during Pliocene and Quaternary regressive episodes.

TABLE 1. Analyses of Nodules from the Agulhas Bank

	NC1–3		C1	C2
	Fe-poor	Fe-rich		
SiO_2	6.20	3.45	15.30	13.79
TiO_2	0.06	0.04	0.10	0.11
Al_2O_3	1.13	0.92	2.14	2.12
Fe_2O_3	1.40	25.80	5.58	7.34
MnO	0.01	0.06	0.01	0.02
MgO	0.97	1.49	1.34	1.45
CaO	47.02	33.42	37.04	36.54
Na_2O	0.62	0.34	0.78	0.73
K_2O	0.43	0.39	1.57	1.51
P_2O_5	14.82	10.26	17.89	16.82
S	0.31	0.21	0.46	0.45
F	2.12	1.42	2.21	2.04
LOF	25.52	23.24	16.15	16.89
Total	100.61	101.04	100.56	99.81
Less O	0.96	0.60	0.93	0.86
	99.72	100.44	99.63	98.95
No. of analyses	(3)	(3)	(8)	(4)

Analytical procedures:

X.R.F.: Si, Ti, Al, total Fe, Mn, Mg, Ca, Na, K, P, S.
Wet chemistry: CO_2, FeO, F.

Origin: Dingle (1974, p. 263) has summarized opinion regarding the origin of both the conglomeratic and nonconglomeratic varieties of nodules. Three considerations are:

1. All evidence suggests that diagenetic replacement of carbonate by phosphate was the principal mechanism of phosphatization. Numerous observations of surface to center decrease of phosphate content in individual limestone fragments support this conclusion.

2. Dingle (1974) states that "there is general agreement amongst workers on the Agulhas Bank deposits that the main source of phosphatising solutions is intimately connected with the high incidence of cold, nutrient-rich, ocean water upwelling, such as that now common along the south-west coast of southern Africa (Parker, 1971; Summerhayes, 1972, 1973a; Birch, 1973; Rogers, 1973). The affected areas have high pelagic biological activity, and the shelf and slope sediments are rich in organic carbon and biogenic carbonate. Phosphate-rich microenvironments are created in the sediment interstices by solutions derived from dead phyto- and zooplankton protoplasm. Under circumstances which bring these solutions into contact with a high surface area/volume ratio sediment susceptible to replacement (e.g., micrite), phosphatisation would proceed."

3. The conglomeratic nodules possess many features which suggest an interplay of several factors in their formation. These include poor sorting, large

periodic influx of iron-rich river waters which would have favored formation of glauconitized pelletal phosphorite types.

Onshore Phosphatic Formations

Exposures of Tertiary strata in the southern and western coastal regions of South Africa are not abundant because during the Pleistocene, when vast areas of the shelf were exposed, an extensive cover of eolian sand of Pleistocene age occurred.

Siesser (1972) has made a detailed study of formations which have their best exposure along the southern coasts. They consist mainly of calcarenites, both marine and eolian, commonly occurring in couplets typical of regressive sequences, i.e., dunes overlying beaches. Siesser (1972) has suggested the informal name, 'coastal limestones,' to replace previously used terms such as Alexandria Formation, Bredasdorp Formation, and Dorcasia Limestone. Although certainly of Tertiary age, precise dating has not been possible due to the poor state of preservation, and paucity, of microfossils. It is apparent that the oldest units are farthest inland and rest on marine terraces of highest elevation. These range from 670 to 370 feet above present sea level, most of the coastal limestones now lying below the water level. It is probable that these terraces correspond to the major transgressions which occurred in early Paleogene, early Neogene, and late Neogene time, but positive evidence is lacking. No significant phosphate mineralization is associated with these coastal limestones.

Information regarding Tertiary formations, apart from the coastal limestones, comes almost entirely from mining operations, drilling and quarrying, and is entirely restricted to the west coast. Eocene strata are known from only one locality (on the South West African coast; Siesser, 1977). It is likely that if at one time Eocene strata were more widespread, they were removed by erosion during the profound Oligocene regression. The earliest Tertiary strata widely represented are Miocene in age and they are followed unconformably by Pliocene units.

Miocene units—the Saldanha Formation

Four widely scattered occurrences of a thin phosphatic unit are located on the west coast, only one of which outcrops, the others being in pits and quarries. Tankard (1975) correlates these units and has proposed the name Saldanha Formation for them. He has selected as the stratotype the only natural exposure which is close to the town of Saldanha at Bomgat on Hoedjiespunt (Fig. 2). Tankard (1975) provides the following description of this occurrence. "The stratotype is 1.2 m thick on Hoedjiespunt. It is preserved in a basin on a granitic platform; the floor of the basin is 5.25 m above mean sea level. The lower 0.7 m of the stratotype consists of horizontally bedded microsphorite. The upper 0.5 m is a layer of granite boulders and cobbles supported in microsphorite which has been reworked. Bedding is not readily apparent in the upper layer. The unit consists in part of phosphatised microcoquina. The upper part of the stratotype represents more turbulent conditions in a shallow environment, probably due to regression, while the lower part is a quieter water deposit."

The formation is seen in relation to Pliocene deposits, which it unconformably underlies, in the floor of the New Varswater quarry at Langebaanweg east of Saldanha Bay (Fig. 2), the site of the only phosphate mining (excluding the small-scale exploitation of aluminium phosphates at Saldanha). The rock is a thin (1–1.5 m) brown phosphatic sandstone with an undulating polished surface, pitted by erosion and burrowed by marine animals. It is conglomeratic in places, containing phosphatic intraclasts. Petrographically it is described as a "fine-grained packstone with a matrix of microsphorite and finely-divided argillaceous and organic material. Anisotropic francolite has grown about the quartz-grain surfaces, while the voids are filled with isotropic collophane" (Tankard, 1975).

Neither the Hoedjiespunt nor Langebaan exposures contain sufficient suitable fossils to allow an age to be attributed with any confidence. But farther south, a few miles east of Cape Town at Ysterplaat, a layer of phosphatic sandstone was exposed in a quarry which contains an assemblage of gastropoda, bivalvia, bryozoa, echinoidea, chondrichthyes, and aves which is regarded as the Saldanha Formation and which is of Miocene age. The unit is thin (75 cm), made up of fine, medium and coarse sand lenses, and rests on latest Precambrian (Malmesbury) strata about 8.6 m above sea level. It is this unit which firmly places the Saldanha Formation in the Miocene, if Tankard's (1975) correlation of these scattered exposures is accepted.

The final exposure of this formation is on the Namaqualand coast in the vicinity of Hondeklipbaai (30°19'S; 17°16'E). The region is known for its production of alluvial diamonds. In the course of exploration a sequence of Tertiary strata has been exposed in boreholes and trenches. They were referred to by the mining fraternity as the E-Stage sediments. The lower E-Stage unit contains a 1 m thick phosphatic siltstone which on foraminiferal evidence is dated as late Miocene (A. J. Carrington; pers. commun.). It is regarded by Tankard (1975) as being a northward extension of the Saldanha Formation.

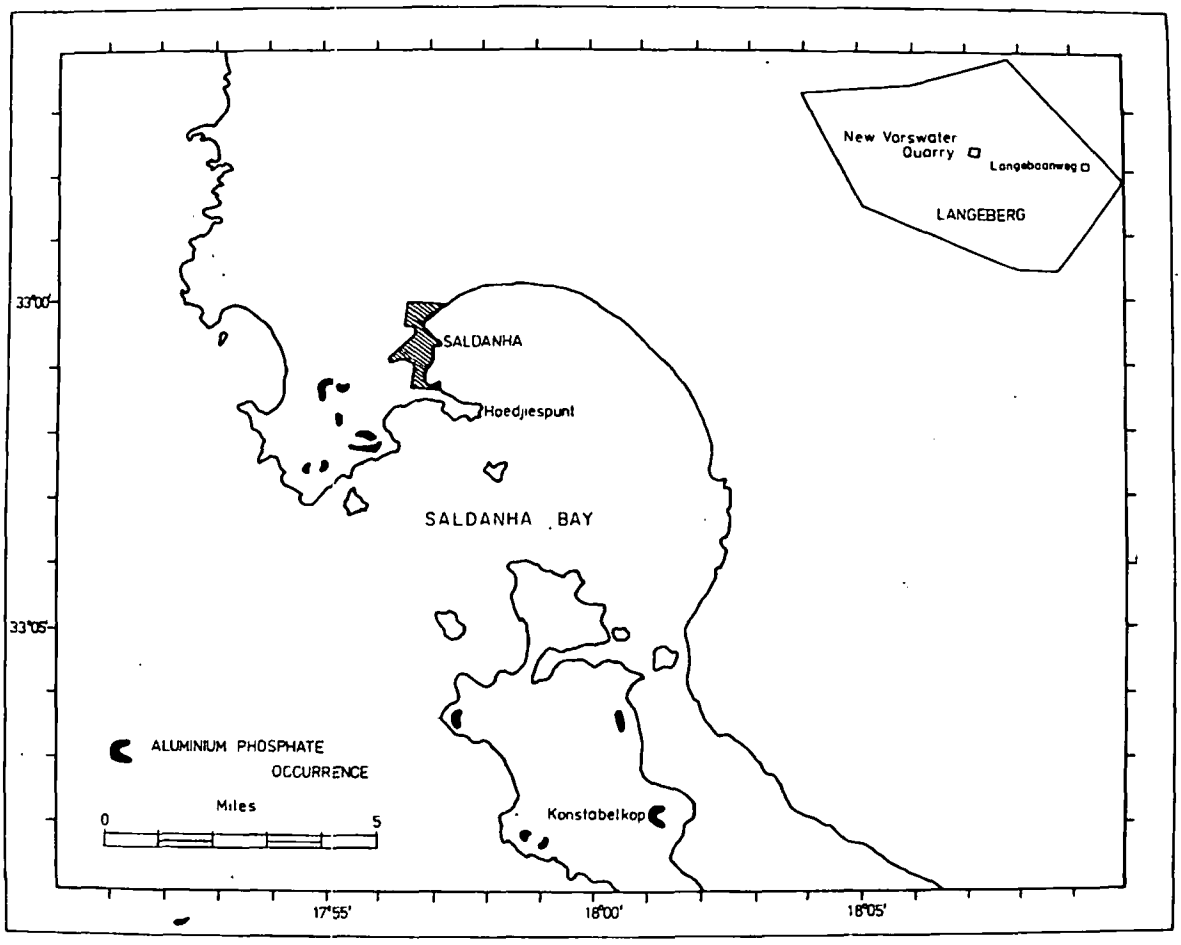

FIG. 2. Location plan of phosphate occurrences in the Saldanha area.

Tankard (1975) has provided chemical data (Table 2) for the Hoedjiespunt microsphorite (analyses 1 and 2) and Langeberg phosphatic sandstone (analyses 3 and 4). He interprets the low fluorine analysis 1 as indicating the hydroxyapatite dahllite, while analysis 2 is interpreted as francolite.

The origin of the Saldanha Formation is associated with the well-documented Miocene transgression. From the few exposures available it is apparent that although the unit is consistently thin, several facies representing various environmental conditions (e.g., water depth) are present. The formation is the only example of an in situ marine phosphorite known in the South African onshore coastal region.

Pliocene units—the Varswater Formation

For a number of years scientists at the South African Museum, Cape Town, have been studying a rich assemblage of fossil mammalian fauna recovered from the New Varswater quarry on the farm Langeberg at Langebaanweg east of Saldanha. Hendey (1974) has established that they are of Pliocene age. The fossils come from a unit in a sequence largely made up of fine-grained quartzitic sands. Hendey (1974) originally suggested the name Varswater Formation for this sequence. He included the basal marine phosphorite bed as part of the formation, but

TABLE 2. Chemical Analyses of the Saldanha Formation

	1	2	3	4
SiO_2	3.60	N.D.	59.92	35.16
Al_2O_3	1.83	N.D.	0.94	2.70
Fe_2O_3	0.27	N.D.	0.63	2.02
MgO	2.32	0.47	0.99	1.04
CaO	46.04	49.59	19.35	29.72
Na_2O	0.27	1.00	0.22	0.36
K_2O	0.06	0.05	0.32	0.18
P_2O_5	33.97	35.39	14.52	21.93
S	0.22	0.80	0.08	0.11
F	0.57	1.59	1.30	1.60
CO_2	3.28	4.08	0.75	1.84
H_2O^+	N.D.	2.24	N.D.	N.D.
H_2O^-	2.55	2.54	0.72	0.91
Total	96.13	97.75	99.79	97.74

Analysts:

1, 3, 4, Anglo American Research Laboratory.
2, General Superintendence Co.

Tankard (1974a) later demonstrated its unconformable relationship to the overlying Pliocene sequence, renamed it the Saldanha Formation, and restricted the name Varswater Formation to the Pliocene sequence.

The maximum thickness of the Varswater Formation is about 43 m. This thickness is not developed in the quarry from which it takes its name but has been determined from borehole logs prepared during extensive exploration for phosphate in the Saldanha area. The Formation originated during a Pliocene transgression which reached an elevation of about 55 m above present sea level. It contains both marine and fresh-water facies, the most important of which from an economic point of view being the Pelletal Phosphorite member, a 25 to 28 m thick unit occurring at the top of the sequence. Tankard (1974a) provides the following description of this member: "moderately sorted, fine phosphatic, quartzose sands. Quartz rounded to well-rounded, polished. Phosphate present as pelletal phosphorite which is largely subspherical in shape, medium to fine sand size. Occasional iron oxide staining of quartz and pelletal phosphorite. Lenses and concretions of phosphate sandstone common throughout demonstrating post-depositional phosphate mineralisation. Heavy minerals always less than 1 percent. Ilmenite constitutes about 97 percent. Shark teeth, marine mollusc shells and shell casts occur throughout, with limited terrestrial fossils at base. Microfauna: phosphatised foraminifera fragments, mainly Elphidium; echinoid spines; minute fish teeth; coprolites."

Tankard (1974a) has demonstrated on chemical and petrographic criteria that the phosphate pellets in the Varswater Formation were mostly derived from the erosion of the underlying Saldanha Formation during the Pliocene transgression.

Apart from the Saldanha area the Varswater Formation is not known with certainty to occur elsewhere in the western and southern coastal regions. Pelletal sands have however been reported from several localities and may represent extensions of the formation. Among these are the upper E-Stage sediments of the Namaqualand coast. It has already been noted that the lower E-Stage sediments are probably the equivalent of the Miocene Saldanha Formation, so it is possible that the E-Stage sediments represent an extension of the sequence developed at Saldanha.

Tankard (1974b) has tabulated seventeen partial chemical analyses of pelletal phosphorite concentrates from the Varswater Formation and provides a summary of average and ranges (Table 3). Analyses have been recalculated after exclusion of SiO_2, Al_2O_3, and K_2O which cannot be assigned to the apatite structures. Chemical and X-ray diffraction data identify the phosphate mineral as francolite.

TABLE 3. Partial Chemical Analyses of Pellet Concentrates from the Varswater Formation

Constituent	Average	Range
CaO	51.79	44.85–54.19
MgO	1.69	0.44– 7.62
Na_2O	0.82	0.77– 0.87
P_2O_5	37.80	36.63–39.01
CO_2	4.70	4.25– 5.54
SO_3	0.96	0.19– 1.84
F	3.85	3.15– 4.81
F/P_2O_5	0.10	0.08– 0.13
CaO/P_2O_5	1.37	1.15– 1.46

Analytical procedures:

MgO, CaO,	volumetric, E.D.T.A.
Na_2O,	flame photometric.
CO_2,	direct.
P_2O_5,	alkalimetric, molybdate.
SO_3,	gravimetric.
F,	spectrophotometric.

Phoscretes

Outcroppings of brown, massive, tabular collophane-cemented surface quartz sands occur at a number of localities in the western coastal regions (Visser and Schoch, 1973). They are referred to as phoscretes, their mode of origin being regarded as similar to related pedogenic materials such as calcrete and ferricrete. Little work has been done on these surface deposits, probably because their relatively small volume and thoroughly indurated state make them unattractive economically. Birch (1975) has compared them with other phosphorites in the area (both on- and offshore) and finds that although they are petrographically similar, they are easily distinguished by their higher levels of Al and/or Fe derived from terrigenous contaminants. That their origin is unrelated to marine processes is suggested by their elevations which frequently exceed 100 m above sea level. It is generally agreed that the phosphate was introduced by upward and/or lateral percolation of ground water and that precipitation occurred following evaporative concentration.

Aluminum phosphates

Deposits of aluminum phosphate occur at a number of localities in the granite hills both north and south of Saldanha Bay (Fig. 2). They were first described by Du Toit (1917). Tankard (1974c) provides a brief review of their main features and Visser and Schoch (1973) give field descriptions of the major deposits.

There is general agreement that the leaching of guano deposits and replacement of the granites and porphyries which form the bed rock account for the origin of these deposits. The bodies are highly irregular, mineralization having been controlled by joints and fractures in the granites along which solu-

tions could penetrate. Tonnages of ore are unlikely to exceed 1,000,000 tons in the largest deposit.

Visser and Schoch (1973) describe the ore as varying "from hard and compact to soft, friable and cellular. A concentration of hydrated iron oxides may locally cause bright reddish to brown colors, but the color commonly varies from shades of yellow to dark brown or light to dark grey. A dull greenish color often appears on weathered surfaces. Some of the ore is banded, streaky or spotted.

"Unaffected quartz grains are usually visible in the more compact fresh ore types. Altered feldspar grains may be present in less phosphatised varieties. The larger bodies are cut by numerous veins of aphanitic horny phosphate similar to that in the thin stringers which pervade all the phospatised rocks and which constitutes a major part of the dark brown resinous ore. In many cases similar material occupies master joints in the centres of narrow altered bands within fresh or solid quartz porphyry. This dense and horny phosphate is either light to dark brown with a dull resinous lustre, or chalky white to grey and even faintly banded in part, like chalcedony. Du Toit (1917) considered the chalky white material to have been veins of clay in the rock that are now phosphatised. As the differently colored varieties grade into each other, it would appear that the light colored type is the weathered and leached portion of the brown phosphate."

Du Toit (1917), on the basis of optical and chemical data, identified barrandite as well as wavellite or variscite which occur as minute yellowish crystals lining cavities.

Partial chemical data are provided by Tankard (1974c; Table 4). The material analyzed is described as phosphatized porphyry.

Apart from Du Toit's (1917) work and Visser and Schoch's (1973) field observations, no systematic study of these deposits has been undertaken.

Theories of Origin of Phosphate Occurrences

All workers who have studied phosphate occurrences around the South African coasts have stressed the applicability of the Kazakov-McKelvey hypothesis in accounting for their origin. Divergent upwelling along the west coast has been well documented and must have been effective throughout Tertiary time. Similarly the Agulhas Bank experiences strong dynamic upwelling. The regions are, and probably in general were, sites of low terrigenous input. This is particularly true of the western shelf.

The phosphate deposits described have affinity with the Florida type, lacking associated fine-grained dark shales and cherts. A possible exception is the deposit off the South West African shelf which has

TABLE 4. Partial Chemical Analyses of Phosphatized Porphyry

	Percent	Percent
SiO_2	59.20	65.40
Al_2O_3	8.32	6.78
Fe_2O_3	4.02	5.29
CaO	0.10	—
K_2O	0.60	0.48
P_2O_5	12.14	11.68
CO_2	—	—
F	Tr	Tr

coexisting siliceous oozes and strongly reducing muds.

Tectonically the deposits are of the platform type. The offshore varieties were probably derived from outcropping Tertiary strata deposited on a continental shelf which, particularly on the western margin, displayed a degree of instability throughout the period. Onland occurrences were controlled by major transgressions and regressions which although probably of eustatic origin were almost certainly influenced by seaward tilting of the shelf regions.

Nowhere has it been demonstrated that tectonic movements contemporaneous with sedimentation affected the site of phosphate accumulation. This may have been the case in offshore regions, but lack of direct information (from drilling) precludes analysis of this type. Emphasis has been on local topographic influences, as with the pelletal deposits of the Varswater Formation which are confined to erosional basins.

Varieties of deposits

Several different origins have been suggested to account for the varieties of deposits that have been discussed.

Direct precipitation types: phoscretes, phosphatic sandstones of Miocene age found onshore—the Saldanha Formation, and concretions on the South West African shelf: Among these the phoscretes are a special case. They are agreed to represent accumulations of phosphate introduced by circulating ground water in a phosphogenic province, mineralization occurring as a cement in quartzose sands.

The best documented example of an inorganic precipitation type of deposit is the Miocene phosphorite (Saldanha Formation) exposed in the floor of the New Varswater quarry at Langebaanweg. This is essentially a phosphate-cemented quartz sand, francolite occurring as drusy encrustations around quartz grains, the remaining voids being filled with a mixture of clays, organic matter, and collophane. The only evidence for replacement in this formation is seen in occasional phosphatized foraminifera and echinoid spines. Precipitation is thought to have occurred in shallow, warm embayments receiving an influx of upwelled water during periods of strong

divergence aided by prevailing offshore winds. Mass mortality of siliceous phytoplankton following the collapse of upwelling cells, and their subsequent decay and release of phosphate-rich protoplasm, resulted in the inorganic precipitation of phosphate in the sandy bottom sediments.

The concretionary phosphates in the siliceous muds of the South West African shelf are included here in the direct precipitation category although they differ from other examples in requiring a phosphatic nucleus for their growth. They also demonstrate diagenetic recrystallization as they mature. Clearly they are a special case and the physicochemical conditions they reflect differ from those required for true unseeded precipitation, especially with regard to temperature.

Replacement types: offshore nodules: The term nodule has been used in the account above to describe a wide variety of phosphatic material littering the southern African shelves. The term has traditionally been applied although the diversity of shapes it embraces, from large angular slabs to rounded masses, makes it something of a misnomer in many instances. The distribution of the nodules suggests that they have been eroded from outcropping Tertiary strata, although this must remain conjectural until drilling is undertaken on the shelf. Petrographic and chemical studies have clearly revealed that these rocks are microsphorites, mineralization being the result of diagenetic replacement of calcium carbonate.

Allochemical phosphorites: offshore glauconite/apatite pellets and pellets on the South West African shelf: Pelletal phosphorites on the South West African shelf are thought to have been derived from storm-wave disrupted inorganically precipitated semilithified collophane muds on the floors of shallow lagoons, subsequently redistributed into other regions of the shelf.

The mixed glauconite/apatite pellets of the southern African shelf are also allochems, being derived from disrupted semilithified microsphorite of replacement origin.

Lithochemical phosphorites: pelletal deposits onshore—the Pelletal Sand member of the Varswater Formation: Phosphate grains (pellets) in the Pelletal Sand member of the Varswater Formation were for the most part derived from the Saldanha Formation (Miocene), erosion of this unit occurring during a Pliocene transgression, detritus being trapped in shallow erosional basins.

Phosphatized bed rock associated with guano: aluminum phosphates: The aluminum phosphates of the Saldanha area clearly represent deposits formed by alteration of granite bed rock by solutions derived from guano accumulations. The high productivity of the region supported vast numbers of sea fowl which occupied topographic highs which formed islands in the Tertiary seas. These now form part of the mainland and although no trace of the original guano accumulations remains, numerous small deposits of aluminum phosphate testify to their former presence.

Acknowledgments

The author wishes to express his gratitude for cooperation received from colleagues in Marine Geoscience, University of Cape Town, especially R. V. Dingle, W. G. Siesser, G. F. Birch, and J. M. Bremner.

Department of Geology
University of Cape Town
Rondebosch 7000, South Africa
September 29, 1978

REFERENCES

Baturin, G. N., 1971, Recent authigenic phosphorite formation on the South West African shelf, *in* Delany, F. M., The geology of the East Atlantic continental margin: International Council Scientific Unions/Scientific Committee for Oceanographic Research, Inst. Geol. Sci. Rept. 70/16, p. 91–97.

Birch, G. F., 1973, Unconsolidated sediments off the Cape West coast: Joint Geol. Survey Univ. of Cape Town, Marine Geology Programme, Tech. Rept. 5, p. 48–67.

—— 1975, Sediments on the continental margin off the west coast of South Africa: Ph.D. thesis, University of Cape Town.

Cayeux, L., 1934, The phosphatic nodules of the Agulhas Bank: South African Museum Annals, v. 31, p. 105–136.

Collet, L. W., 1905, Les concrétions phosphatées de l'Agulhas Bank: Royal Soc. Edinburgh Proc., v. 25, p. 826–893.

Dingle, R. V., 1971, Tertiary sedimentary history of the continental shelf off southern Cape Province, South Africa: Geol. Soc. South Africa Trans., v. 74, p. 173–186.

—— 1973, The geology of the continental shelf between Luderitz and Cape Town (Southwest Africa) with special reference to Tertiary Strata: Geol. Soc. London Jour., v. 129, p. 337–363.

—— 1974, Agulhas Bank phosphorites; a review of 100 years of investigation: Geol. Soc. South Africa Trans., v. 77, p. 261–264.

Du Toit, A. L., 1917, Report on the phosphates of Saldanha Bay: South Africa Geol. Survey Mem., v. 10, p. 1–38.

Haughton, S. H., 1956, Phosphatic-glauconitic deposits off the west coast of South Africa: South African Museum Annals, v. 42, p. 329–334.

Hendey, Q. B., 1974, The Cenozoic carnivora of the Southwestern Cape Province: South African Museum Annals, v. 63, p. 1–369.

Kolodny, Y., 1969, Are marine phosphorites forming to-day?: Nature, v. 224, p. 1017–1019.

Kolodny, Y., and Kaplan, I. R., 1970, Uranium isotopes in seafloor phosphorites: Geochim. et Cosmochim. Acta, v. 24, p. 3–24.

Lloyd, A. T., and Fuller, A. O., 1965, Glauconites from shallow marine sediments off the South African coast: South African Jour. Sci., v. 61, p. 444–448.

Miller, A. K., and Furnish, W. M., 1956, Tertiary Nautiloids dredged near Cape of Good Hope: South African Museum Annals, v. 42, p. 327–328.

Murray, J., and Renard, A. F., 1891, Report on deep-sea deposits based on the specimens collected during the voyage of H. M. S. Challenger: Rept. Sci. Results of the Exploring Voyage of H. M. S. Challenger 1873–1876

(Deep-sea Deposits), London, Her Majesty's Stationery Office, p. 391–400.
Parker, R. J., 1971, The petrography and major element geochemistry of phosphorite nodule deposits on the Agulhas Bank, South Africa: South African Nat. Comm. for Oceanographic Research, Marine Geology Programme, Bull. 2, Univ. of Cape Town, 92 p.
—— 1975, The petrology and origin of some glauconitic and and glaucoconglomeratic phosphorites from the South African continental margin: Jour. Sed. Petrology, v. 45, p. 230–242.
Parker, R. J., and Siesser, W. G., 1972, Petrology and origin of some phosphorites from the South African continental margin: Jour. Sed. Petrology, v. 42, p. 434–440.
Parker, R. J., and Simpson, E.S.W., 1972, South African Agulhas Bank phosphorites: Phosphorus and Potassium, v. 58, p. 18–27.
Rogers, J., 1973, Texture composition and depositional history of unconsolidated sediments on the Agulhas Bank and the Orange-Luderitz continental margin: South African Nat. Comm. for Oceanographic Research, Marine Geology Programme, Tech. Rept. 4, Univ. of Cape Town, p. 44–59.
—— 1977, Sedimentation on the continental margin off the Orange River and the Namib Desert: Joint Geol. Survey/Univ. of Cape Town, Marine Geoscience Bull., v. 7, 212 p.
Siesser, W. G., 1971, Petrology of some South African coastal and offshore carbonate rocks and sediments: South African Nat. Comm. for Oceanographic Research, Marine Geology Programme, Bull. 3, 232 p.
—— 1972, Limestone lithofacies from the South African continental margin: Sed. Geology, v. 8, p. 83–112.
—— 1977, Late Eocene age of marine sediments at Bogenfels, South West Africa, based on calcareous nannofossils: South African Geol. Survey Bull. 60, p. 72–73.
—— 1978, Age of phosphorites on the South African continental margin: Marine Geology, v. 26, p. 17–28.
Summerhayes, C. P., 1972, Aspects of the mineralogy and geochemistry of Agulhas Bank sediments: South African Nat. Comm. for Oceanographic Research, Marine Geology Programme, Tech. Rept. 4, Univ. of Cape Town, p. 83–95.
—— 1973a, Distribution and origin of phosphate in sediments from the Agulhas Bank, South Africa: Joint Geol. Survey/Univ. of Cape Town, Marine Geology Programme, Tech. Rept. 5, p. 94–114.
—— 1973b, Distribution, origin and economic potential of phosphatic sediments from the Agulhas Bank, South Africa: Geol. Soc. South Africa Trans., v. 76, p. 271–277.
Tankard, A. J. T., 1974a, Varswater Formation of the Langebaanweg-Saldanha area, Cape Province: Geol. Soc. South Africa Trans., v. 77, p. 265–283.
—— 1974b, Chemical composition of the phosphorites from the Langebaanweg-Saldanha area, Cape Province: Geol. Soc. South Africa Trans., v. 77, p. 185–190.
—— 1974c, Petrology and origin of the phosphorite and aluminium phosphate rock of the Langebaanweg-Saldanha area, Southwestern Cape Province: South African Museum Annals, v. 65, p. 217–249.
—— 1975, The marine Neogene Saldanha Formation: Geol. Soc. South Africa Trans., v. 78, p. 257–264.
Visser, H. N., and Schoch, A. E., 1973, The geology and mineral resources of the Saldanha Bay area: South Africa Geol. Survey Mem. 63, p. 1–150.

Davis, S.N, 1969, Porosity and permeability of natural materials; in DeWeist (ed), Flow through porous media: Academic Press, NY, p. 54-59

1. Introduction

Few properties of natural materials have received more attention from hydrogeologists than porosity and permeability. Despite the vast amount of work expended in measuring these two properties in countless samples, reliable values can rarely be estimated on the basis of general geologic knowledge alone. The purpose of this chapter is to review the extent of our general knowledge concerning porosity and permeability and to relate this knowledge to the more analytical discussions which follow in subsequent chapters.

1.1. Porosity

Porosity, as used in this chapter, is defined as the ratio of pore volume to the total volume of a given sample of material. This definition is adequate for many purposes. Microscopically and submicroscopically, nevertheless, a complete gradation exists from large pores easily accessible to fluids to very small openings in minerals that are caused by minor lattice imperfections. The smallest openings contain fluids that are rendered essentially static by the close proximity of atomic force fields at the surfaces of the solids (Kemper *et al.*, 1964). Whether or not these submicroscopic openings are measured in the laboratory as part of the void space depends on the methods of the measurement employed. Techniques using heat, centrifuging, liquid saturation under a vacuum, and other conditions abnormal to near-surface rocks will certainly displace static fluid that might be best considered part of the solid rock.

A large number of terms have been introduced into the literature to describe various physical measures related to porosity. Moisture equivalent, effective porosity, specific retention, drainage coefficient, coefficient of storage, and specific yield are some of the terms used to qualify variables such as degree of saturation, forces applied to the sample, length of test, degree of interconnection of pores, and fluid chemistry. Besides simple porosity, the only other closely related term used in this chapter will be specific yield, which will be defined as the volume of water drained by gravity from an initially saturated sample divided by the total volume of that sample. Ideally, specific yield should be measured using samples having column lengths of more than 3 m to avoid excessive capillary effects. Drainage time should be measured in many years for clay-size material. As a result of these inconvenient requirements, few reliable measurements of specific yield of fine-grained materials have been made. Modern laboratories tend to rely on centrifuging to speed drainage and to overcome capillary effects. Strain

induced by centrifuging, however, makes the resultant specific yield values of fine grained materials open to question. This is particularly true of nonindurated silts and clays.

1.2. PERMEABILITY

Permeability is a measure of the ease with which fluids pass through a porous material. Permeability, or more properly, "intrinsic permeability," is a property of the solid material and is independent of the density and viscosity of the fluid. A common expression for permeability k is

$$k = -\frac{Q}{A}\frac{\mu}{\rho g}\left(\frac{\partial h}{\partial s}\right)^{-1}$$

in which Q is the volume of fluid discharged per unit time through a cross section having an area of A, μ is the viscosity of the fluid, ρ is the density of the fluid, g is the acceleration of gravity, and $\partial h/\partial s$ is the hydraulic gradient in the direction of flow s.

Permeability k has the dimensions of L^2. The darcy, which is almost universally used in the petroleum industry, will be used as the unit of permeability in this chapter. One darcy has the value of 0.987×10^{-8} cm^2. Units of hydraulic conductivity, which superimpose fluid properties on permeability and have the dimensions of LT^{-1} are most common in ground-water work. The "meinzer" is one of the popular units of hydraulic conductivity in the United States. It is related to a fixed viscosity and density of water (pure water at 60° F or 15.6° C). Media having a permeability of 1 darcy have a hydraulic conductivity of 18.2 meinzers.

Analytical work with single-phase flow of fluids almost universally assumes that permeability is constant with respect to time. Several important exceptions should always be kept in mind. Largest changes take place with changes of state or dissolution of minerals, as for example the slow formation of limestone caverns, the more rapid dissolution of gypsum, or the extremely rapid melting of granular ice as warm rain water percolates through a snow bank. Significant changes also take place in response to stresses associated with declining artesian pressures or with external compaction of sediments. If fluid chemistry changes, sedimentary materials will respond dynamically. Effects of partial or complete hydration which will cause clays, colloids, and some organic material to expand and close pore spaces are the most important of the responses to changing fluid chemistry. Permeabilities are largest with air and other nonpolar fluids. Partial hydration by brines will cause values to lower. Full hydration using distilled water as the measuring

fluid will cause a drastic reduction of permeability (Johnston and Beeson, 1945). These effects are greatest in fine-grained sediments and could account for permeability differences of several orders of magnitude in the sample.

Effects of measuring techniques on the permeability of fine-grained sediments and rocks is particularly striking. Young *et al.* (1964) have shown that increasing confining pressures of samples of argillaceous rocks in order to duplicate subsurface conditions produces a decrease in permeability of more than tenfold over results of unconfined tests. Permeability contrasts in some nonindurated materials may be even larger.

Natural material is commonly assumed to be homogeneous and isotropic with respect to permeability. In general, computational problems associated with heterogeneous aquifers are easier to deal with than those of nonisotropic aquifers. The measurement and/or estimation of the actual extent of heterogeneity is also much easier geologically than is the measurement of anisotropy. Further attention will be given to these matters in later sections of this chapter as well as in other parts of this volume.

2. Dense Rocks

2.1. Introduction

A large number of rocks have porosities of less than 2% and permeabilities of less than 10^{-2} darcy. Granite, dolerite, quartzite, slate, and gabbro are but a few of the common dense rocks which are abundant in the earth's crust. Of the major rock groups, most metamorphic, all plutonic igneous rocks, most volcanic rocks in near-surface intrusives, and many dense sedimentary rocks are grouped together as far as their gross hydrogeologic properties are concerned. Such rocks in their unmodified state will not yield fluids to wells nor will they store significant amounts of fluids in their limited pore spaces. Typical values of porosity and permeability for dense rocks are given in Table 1.

2.2. Weathering and Fracturing

Weathering and fracturing of dense rocks will increase overall permeabilities by two to four orders of magnitude (Table 2). Weathering will increase rock porosity from initial values generally less than 5% to final values of between 30 and 60% (Stewart, 1964). Fracturing alone,

TABLE 1

Rocks of Low Permeabilities and Porosities

Rock name	Porosity (%)	Permeability (darcys)	Reference
Chert	—	1.9×10^{-7}	Stuart *et al.* (1954)
Diabase	0.1	—	Brace (1965)
Dolomite	6.3	1.0×10^{-3}	Murray (1960)
	0.4	—	Brace (1965)
Granite	0.3	—	Brace (1965)
Graywacke	—	3.0×10^{-6} [a]	Stuart *et al.* (1954)
Limestone	8.4	1.0×10^{-3}	Murray (1960)
Marble	0.3	—	Brace (1965)
	0.6[b]	—	Manger (1963)
Mica schist	—	2.1×10^{-6}	Stuart *et al.* (1954)
Quartzite	—	1.9×10^{-6}	Stuart *et al.* (1954)
	0.6	—	Brace (1965)
Rock salt	0.6	7.3×10^{-6} [c]	Gloyna and Reynolds (1961)
Slate	—	1.3×10^{-6} [d]	Stuart *et al.* (1954)
	3.4[e]	—	Manger (1963)

[a] Median of 5 samples.

[b] Mean of 100 samples.

[c] Representative value taken from several different determinations. Permeability varied widely with confining pressure on specimen and with the type of fluid used.

[d] Median of 9 samples.

[e] Mean of 19 samples.

however, does not generally increase overall rock porosities by more than 2–5%. The size of fractures may range from large dislocations having open cracks of more than 1.0 mm to microfractures that develop throughout the rock prior to failure. Recent laboratory experiments (Brace *et al.*, 1966) have shown that initially dense rocks will gain from 0.004 to 3.6% in porosity after being compressed under moderately high confining pressures. Brittle rocks such as aplite will gain the least porosity, and slightly ductile rocks such as limestone will gain the most porosity. The hydrogeologic importance of this rock dilatancy under stress is yet to be investigated. It is possible that large volumes of otherwise dense rock will undergo small but significant increases in porosity near major faults and possibly even in zones of regional stress accumulation that are not broken by major faults.

Both weathering and fracturing are most evident within 20 m of the surface. In tropical countries weathering may extend to depths of more than 100 m, but most temperate regions have not experienced significant weathering of dense rocks below about 50 m.

TABLE 2

Porosity and Permeability of Originally Dense Rocks Modified by Fracturing and Weathering

Rock name	Type of test	Porosity (%)	Specific yield (%)	Permeability (darcys)	Reference
Quartz-mica schist, weathered	Laboratory	48[a]	20.6[a]	3.3×10^{-2}[a]	Stewart (1964)
	Field	—	0.61	0.97[b]	Stewart (1964)
Graywacke, fractured	Field	—	—	4.5×10^{-2}[c]	Lewis *et al.* (1966)
Metasediments fractured	Field	2.4 (estimated)	—	3.1×10^{-2}[d]	Lewis *et al.* (1966)
Iron formation	Field	—	—	5.5×10^{-4} (*minimum*) 5.8×10^{-2} (maximum)	Stuart *et al.* (1954)
Metabasalt	Field	—	2.0	1.9[e]	Meyer and Beall (1958)
Schist	Field	—	3.0	1.4[e]	Meyer and Beall (1958)
Marble	Field	—	0.4	18[f]	Meyer and Beall (1958)

[a] Median values for 21 samples.
[b] Assumed aquifer thickness of 70 ft.
[c] Median of 11 tests.
[d] Median of 6 tests.
[e] Assumed aquifer thickness of 200 ft.
[f] Assumed aquifer thickness of 160 ft.

Fracturing of rocks may extend to depths of several thousands of meters, and water has been encountered in some mines and tunnels at depths of more than 1000 m. Large excavations far below the surface, nevertheless, generally encounter little water (Samuelson, 1965).

Fractures of several types exist in dense rocks. Faults are extensive fractures that mark zones of differential movement within the earth's crust. They generally extend to an unknown depth below the surface. Some faults most certainly exist at depths of more than 10 km below the surface and hence penetrate all fluid-bearing zones of current economic interest. Fractures within the fault zones will tend to close with depth owing to the weight of overlying rocks. Joints are single fractures, commonly with planar surfaces along which macroscopic movement parallel with the surface is lacking. Joints arise from tensile stresses associated with the shrinkage of rocks during the drying, cooling, or chemical transformations; shearing stresses associated with the expansion of rocks during warming, hydration of minerals, or unloading; and compressive forces most commonly associated with

large-scale earth movements. Although, theoretically, some joints can propagate to great depths, the frequency of many joints decreases rapidly with depth (Jahns, 1943). Besides joints and faults, fractures of many origins are encountered near the surface. Landslides, impact effects, explosions, subsidence, and various human activities can disrupt rocks to depths of a few hundred meters.

2.3. Relation of Permeability and Porosity to Depth

The permeability and porosity of dense rocks decrease with depth. This decrease is not only caused by a smaller amount of rock weathering with depth but is also caused by the fact that many forces causing fracturing are localized near the surface. The rate of decrease varies widely from one locality to the next. As a rough generalization, however, both the porosity and permeability of originally dense rocks should be about 10 times greater at a depth of only 10 m than at a depth of 100 m.

Numerous ground-water studies have noted a decrease of yields with depth, which is related to the decrease of permeability and porosity with depth (Frommurze, 1937; Johnston, 1962; Le Grand, 1954; and Dingman *et al.*, 1956). Several possible sources of bias, nevertheless, are present in the water-well data. First, testing methods used are not uniform. Second, climatic conditions vary widely in regions used for comparison. Third, and probably most serious, wells started in areas of permeable rocks will be successful and therefore will be terminated at a shallow depth. On the other hand, wells drilled in areas of relatively impermeable rocks will tend to be drilled much deeper in unsuccessful attempts to reach water-bearing horizons. A comparison of wells within the entire region will show high water yields per foot of depth in shallow zones and a low yields per foot of depth in deeper wells. This may suggest falsely that permeability decreases with depth, whereas the variations of permeability are actually lateral rather than vertical.

Data from tests made on holes drilled for dam and tunnel site exploration have been studied in an attempt to evalute the possibility of bias in the water-well data (Davis and Turk, 1964). The depth and spacing of these holes are commonly determined before drilling, and many are positioned so as to intercept potentially permeable zones near the bottoms of the holes. Thus, the data are biased, if at all, in the direction of an increase in the permeability of rocks with depth. The data from hydrogeologic testing of the holes are also gathered in a more uniform manner, so that differences related to testing methods are not as important as in water wells. Results of the study showed essential agreement between test-hole and water-well data (Fig. 1); namely,

a rapid decrease with depth of the water that can be injected into the drillholes. The general conclusion is, therefore, that whatever biases exist in the water-well data, they are not important enough to mask the gross relationships of water yield and depth.

The relation between well depths and the yield of wells has been studied mostly for igneous and metamorphic rocks, and only to a minor degree for sedimentary rocks. Rather limited data suggest, however, that the same general type of depth-yield relationships holds for all dense rocks.

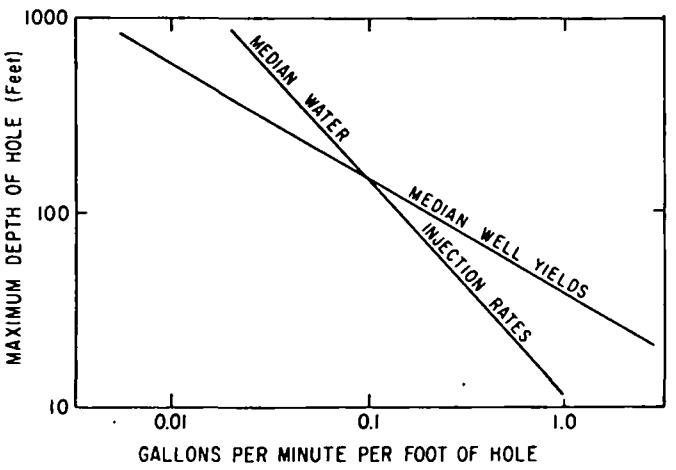

FIG. 1. The relation between depth, and yield and injection rates for granitic rocks of the Sierra Nevada (Davis and Turk, 1964).

Lack of detailed information on the actual configuration of flow in the vicinity of wells in dense rocks makes it difficult to relate well yields to gross permeabilities of the rocks. Tracer dilution tests require a prior knowledge of the local hydraulic gradient in the vicinity of the well. Conventional aquifer tests, if valid for dense rocks, require that the effective thickness of the aquifer is known. The common assumption, which is also made in compiling Table 2, is that the thickness of saturated rock in the well is equal to the effective thickness of the aquifer, so that the hydraulic conductivity can be obtained by simply dividing the transmissivity of the aquifer by the thickness of the aquifer. Pressure or packer tests are even more difficult to interpret because the shorter length of hole involved in the test will be influenced much more by the local fracture patterns developed in the rock. As a consequence of the foregoing uncertainties, most studies have given the relationship between

depth and well yield or injection rates rather than attempting to estimate the actual hydraulic properties of the rocks as a function of depth.

The relation of well yields to well depths would suggest that a close relation must exist between the local topography and well yields. This is borne out by a number of studies (see a review in Davis and De Wiest, 1966). In general, recharge from streams and production of water directly from alluvium within valleys strongly favor large well yields in valleys. Valleys also tend to form along lines of structural weakness that may contain fractured and permeable rocks. After valleys, the next best water yielding areas are found on flat uplands. Here, erosion is slow, so that weathered rocks that are permeable and porous tend to accumulate. Inasmuch as the underlying rocks have a low permeability, water will tend to accumulate within the basal part of the weathered material. Valley walls and sharp-crested hills and ridges are the least favorable localities for water-well development. These areas have maximum rates of erosion with bare, dense rock at or near the surface. In addition, opportunities for recharge are minimal. Relative yields of wells suggest that rocks 5–50 m below the surface average from two to three times more permeable under broad upland areas than at or near tops of steep hills.

2.4. Importance of Rock Type

The influence of rock type on gross permeability of rocks is not as large as one might expect (Davis and De Wiest, 1966). Maximum yields of domestic wells ranging in depth from 10 to 100 m will generally be between about 40 and 80 liters/min. This is true of granite, diorite, dense basalt, gneiss, schist, and many other rocks of diverse origin. Softer metamorphic rocks such as serpentine and some slates and phyllites will tend to have lower well yields, generally from 10 to 40 liters/min. Marble and dolomite will have somewhat greater maximum yields, generally from 50 to 150 liters/min. Truly large differences in well yields between areas having different rock types are usually due to differences in the histories of weathering and/or of fracturing of the rock rather than to lithologic differences. As an example, rocks in a thrust sheet may be more than 100 times more permeable than similar rocks in an adjacent autochthonous mass, yet in another region the two rock types may have nearly identical permeabilities.

2.5. Effects of Solution on the Permeability and Porosity of Dense Rocks

All minerals are soluble to some extent. Water circulating through minor cracks can, if given enough time, open the cracks and increase

greatly the permeability. Abundant evidence of this type of permeability increase is so well known from limestone, dolomite, and marble that it would hardly seem worth more than passing mention. A number of fascinating problems concerning solution permeability, however, remain to be investigated. Factors controlling the initiation and selective development of solution openings are poorly understood (Davis, 1966). Structural control of solution is almost always present but details are puzzling. For example, a cavern may follow a joint for several meters and suddenly come to a dead end or turn abruptly along another intersecting joint. The apparent randomness is such that even if joint and fault patterns are mapped in detail at the surface, the exact position of subsurface solution openings cannot be predicted with confidence. Another interesting question concerning solution openings is the extent to which they develop in rocks that are ordinarily thought of as being rather insoluble. Tolman (1937) suggested several years ago that solution of siliceous rocks was important, but little work has been done to test his hypothesis.

Water in equilibrium with the minerals in basaltic rocks will contain about 60 ppm (parts per million) silica, calculated as SiO_2. Water in equilibrium with the minerals in granite will have from 15 to 30 ppm, and water in equilibrium with quartz will have only about 10 ppm silica (Davis, 1964). Rain water has less than 0.5 ppm silica, so that if it entered directly into cracks, a significant amount of silica should be removed in solution. A hypothetical example is now given.

Assumptions:

Water passes through quartzite (nearly pure SiO_2).

A single set of parallel joints receives per year 10 liters of water for every meter of joint. This would represent 1.0% of a 1000 mm/year rain in joints spaced 1.0 m apart.

Recharge water increases uniformly in silica content from 0.0 ppm at the surface to 10.0 ppm at a depth of 10 m.

Calculations:

Area of joint being considered is 10.0 m^2.

Annual removal of silica is 100 mg.

Silica removed in 10^5 years is 10^4; this would represent a rock volume of about 3.8×10^3 cm^3.

Under the assumptions made, the crack marking the joint would be widened by 0.38 mm in 10^5 years.

The widening of a crack by 0.38 mm is very significant from the

standpoint of fluid flow. Normal cracks along joints are mostly less than 0.1 mm wide (Davis, 1966), and the discharge of ground water along the cracks is a function of the width of the crack cubed. This assumes that the flow through cracks can be approximated by the equations for the flow between parallel plates. Thus, even if the increase in an exceptionally large cracks were only from 1.0 to 1.3 mm (representing slightly less than the 10^5 years solution in the previous example), the discharge through the rock would be more than doubled, providing the hydraulic gradient remains constant.

Several factors, however, argue against the rapid opening of cracks in crystalline rocks by solution. First, considerable silica is taken into solution as the water passes through the soil horizon (Davis, 1964; Laney, 1965), so that water moving downward into the underlying rock will be much nearer saturation than rain water. Second, surface and subsurface runoff will tend to bypass the rather tight joints without significant circulation of ground water through the joints. Third, unlike most carbonate rocks, the average silica-rich rock will have large amounts of insoluble residue such as iron, aluminum, and titanium oxides that will tend to clog the small cracks in the rock.

Large initial permeability of the rock and a high water temperature both would favor rapid solution enlargement of primary openings in silica-rich rocks. Hot springs in crystalline rocks may have discharges of more than 100 liters/min (Waring, 1965). Many of these springs are probably localized along fault zones. Such large discharges would suggest that solution openings have developed in the rocks. This is logical inasmuch as silica is almost as soluble in boiling water as limestone is in the average near-surface ground water.

2.6. Anisotropic Characteristics

Reliable measurements in the field of the extent of anisotropy in dense rocks is virtually lacking. Stuart *et al.* (1954) made aquifer tests in low grade metamorphic rocks of the iron mining district of Michigan and found the transmissivity of the rocks to be roughly twice as large along the strike as perpendicular to the strike. Similar results were obtained by Stewart (1964) in tests of higher grade metamorphic rocks of Georgia in which the permeability was greater in the direction of the schistocity than perpendicular to the schistocity. On the other hand, Yokota (1963) compared theoretical flow nets under a dam with the actual head measurements made after the construction of the dam and concluded that for the rock studied, which was granite, isotropy could be assumed with very little error.

PdO on the concentration of hydrogen chloride it follows (fig. 3) that change in the hydrogen chloride content of the mixture from 10 to 30 vol. % increases the degree of chlorination by almost twice. Further increase in the concentration of hydrogen chloride does not have a significant effect on the rate of the process. The order of the reaction in hydrogen chloride was determined and was equal to half.

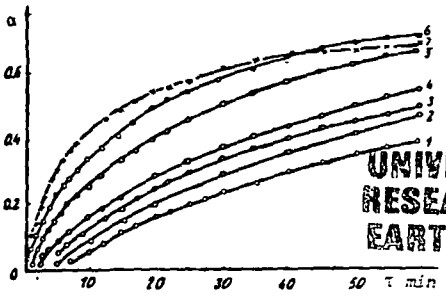

Fig.3 The dependence of the degree of chlorination of PdO on time at HCl concentrations (vol.%): 1 - 10, 2 - 13.5, 3 - 15; 4 - 20, 5 - 30, 6 - 40, 7 - 100. Temperature 450°C. Consumption of gas mixture 10 litre/h.

The effect of water vapour on the chlorination of PdO was also investigated. It was shown that variation of P_{H_2O} from 2 to 10mm Hg has practically no effect on the reaction of PdO with HCl (zero order in H_2O); i.e. the reaction product does not retard the chlorination process. It can be supposed that the reaction of PdO with HCl at 400-475°C is complicated by diffusion of the reagents through the layer of reaction product $PdCl_2$, and the process probably occurs in the intermediate region.

At temperatures above 500°C, where the decomposition of $PdCl_2$ which forms becomes appreciable, the reaction of PdO with hydrogen chloride occurs in two stages:

$$PdO + 2HCl \rightarrow PdCl_2 + H_2O$$

$$PdCl_2 \rightarrow Pd + Cl_2$$

and the final product from the reaction of the oxide with the gas is the metal. It was shown that the controlling stage of the high-temperature reaction of PdO with HCl is the decomposition of $PdCl_2$. Thus, at 750°C the process is characterised initially by a sharp increase in weight, indicating chlorination of PdO to $PdCl_2$, and then by a uniform decrease in weight to a value corresponding to metallic palladium.

Conclusions

1. It was shown that palladium hardly enters into reaction with hydrogen chloride at all in the range of 20-1000°C even in an extremely reactive form (spongy metal).
2. At temperatures up to 500°C palladium monoxide reacts vigorously with hydrogen chloride to form the chloride. The activation energy of the reaction in the range of 400-475°C amounts to 24kcal/mole (101kJ/mole). At higher temperatures the reaction product is the metal, since the $PdCl_2$ which forms decomposes.
3. It was shown that the order of reaction (1) is half in HCl and zero in H_2O.
4. The decomposition of $PdCl_2$ in a stream of hydrogen chloride begins at 500°C and takes place similarly to the decomposition in a stream of inert gas (argon). The apparent activation energy for the thermolysis of palladium chloride amounts to 31kcal/mole (130kJ/mole).

References

1) G Brauer (Ed.): Manual of preparative inorganic chemistry: IL, Moscow 1965, p. 724.
2) Yu V Karyakiv and I I Angelov: Pure chemical substances: Khimiya, Moscow 1974, p. 187.
3) I S Shaplygin and V B Lazarev: Fifth All-Union Conference on thermal analysis: Novosibirsk 1973. Summaries of Reports, Nauka, Moscow 1973, p. 142.
4) L I Tolokonnikova et alia: Fifth conference on kinetics and mechanism of chemical reactions in the solid. Summaries of reports. Chernogolovko 1973, p. 3,
5) B V Erofeev: Dokl. Akad. Nauk. SSSR 1946, 52, 515.

UDC 669.2

Rate of transfer of electric charges across the platinum–V_2O_5–V_2O_4 melt interface and the capacitance of the electric double layer

A S Churkin G A Toporishchev and N Ya Kondyurina (Urals Polytechnical Institute - Department of the Theory of Metallurgical Processes)

Summary

An electrochemical method was used to investigate the transfer of electric charges across the interface between a platinum electrode and a V_2O_5–V_2O_4 melt. The nature of the processes which occur was studied, the thermodynamic parameters were calculated, and the capacitance of the electric double layer was determined.

The results show that the transfer of electric charges across the interface between platinum and a semiconducting melt can be investigated by electrochemical methods.

UDC 546.98+546.92

Precipitation of palladium and platinum from aqueous solutions with ozone

A F Chudnov (Kuzbass Polytechnical Institute - Department of General and Inorganic Chemistry)

The wide use of palladium and platinum in catalysis has created the problem of their regeneration. The spent catalysts are most often treated with acids, and the palladium and platinum are extracted from the obtained solutions with extractants or by ion exchange or are precipitated as thiocyanates or sulphides[1-3]. It is possible to remove these metals directly from the ground catalysts as volatile chlorides by high-temperature chlorination[4]. The variety of subjects, compositions and conditions exclude the possibility of the existence of a universal method, but the high cost of these metals makes the problem of their recovery urgent.

We studied the possibility of the precipitation of palladium (II) and platinum (II) from aqueous solutions with ozone in the form of poorly soluble tetravalent derivatives (oxides or complex chlorides). The work was carried out on normal laboratory apparatus by bubbling an ozone-air mixture (8mg O_3/l) at a rate of 4 l/h through solutions of the divalent derivatives of palladium and platinum at room temperature.

The initial derivatives $K_2[PdCl_4]$ and $K_2[PtCl_4]$ were synthesised according to published data[6]) and were subsequently identified by their UV spectra (on an SF-16 spectrophotometer). The other reagents were used in the chemically pure grade without additional purification.

The concentration of the hydrochloric acid solutions of $K_2[PdCl_4]$ was determined by means of their intrinsic colour by a photocolorimetric method (FEK-M instrument, 20ml cuvette, green filter, fig. 1). The solutions of $K_2[PtCl_4]$ and $K_2[PtCl_6]$ were analysed according to published data[6]). The degree of oxidation of the palladium and platinum in the ozonolysis products was established by characteristic qualitative reactions[5]) and by UV spectroscopy (SF-16 instrument).

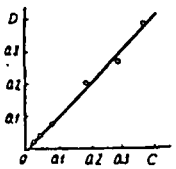

Fig.1 Calibration curve for the determination of the concentration of hydrochloric acid solutions of $K_2[PdCl_4]$ on an FEK-M photocolorimeter. D is the optical density, and C is the concentration of Pd^{2+} g-ion-1.

The experiments show that the precipitation is affected by the nature of the medium, the pH value, and the concentration of the reagents. Ozonisation of the initial aqueous solution of $K_2[PdCl_4]$ (3.10^{-4}-8.10^{-3}M, pH = 4-5, volume of sample 30-60ml) is accompanied by a rapid change in colour; from the characteristic yellow of palladium (II) the solution becomes brown, and after only 10 min a black sol. of the palladium (IV) derivative is formed. Presumably, it has the composition $K_2[Pd(OH)_nCl_m]$, were n + m = 6. On heating to 80-90°C or prolonged standing (10-12h) in the presence of a reducing agent (acetone), a voluminous black precipitate of hydrated palladium oxide separates. In more concentrated initial solutions (>2.10^{-3}M) $K_2[PdCl_6]$ appears in the precipitate, and the palladium is precipitated almost completely.

If the initial solution of $K_2[PdCl_4]$ is made alkaline to a total alkalinity of 0.1N, a brown precipitate of hydrated divalent palladium separates. During ozonisation it is rapidly oxidised, and a fine black suspension is formed. It separates as a compact readily filtered precipitate of palladium dioxide. On standing the dioxide is reduced in the solution to the oxide.

During ozonisation in a sulphuric acid medium (0.2-1.0M H_2SO_4) the colour of solution changes from bright-yellow after 10-15 min to a greenish colour and then to dark-brown. A dark-brown precipitate of palladium (II) and (IV) oxides is formed. Thus, in a neutral, alkaline, and sulphuric acid medium ozone precipitates palladium (II) almost completely as oxides.

In nitric acid medium (0.2-2.0M HNO_3) a dark-brown suspension appears at the beginning of the ozonisation of $K_2[PdCl_4]$. It then dissolves in the solution, and the amount of precipitate decreases with increase in the nitric acid concentration. In 5M nitric acid there is none at all, and water-soluble derivatives of palladium (IV) are formed.

During ozonisation of $K_2[PdCl_4]$ (3.10^{-4}M) in 1-2M hydrochloric acid the solution soon becomes red (the $[PdCl_6]^{2-}$ ion), but there is no precipitate of the chloride on account of the low concentration of the salt. Hydrochloric acid solutions of palladium (IV) are unstable and are rapidly reduced to palladium (II), depending on the concentration in the absence of ozone. Thus, the period for the reduction of half the palladium (IV) in 2M hydrochloric acid amounted to 360 min with a palladium (IV) concentration of 0.306g-ion/l, 220 min for 0.180g-ion/l, 90 min for 0.120g-ion/l, 40 min for 0.082 g-ion/l, and 10 min for 0.036g-ion/l. The solutions of $[PdCl_6]^{-2}$ obtained by chlorination are more stable, since the dissolved chlorine, in contrast to the readily decomposed ozone, stabilises the palladium (IV).

The best results were obtained during the precipitation of palladium (II) with ozone in a hydrochloric acid medium (0.5-2.0M HCl) in the presence of 10-15% potassium chloride (ammonium chloride is less effective). Here a compact red crystalline precipitate of $K_2[PdCl_6]$ is formed and is readily separated from the solution on a filter. Typical experimental data are given in fig. 2. It is seen that the degree of precipitation of the palladium (II) amounts to 98-99%, and the consumption of ozone (during the precipitation of the bulk of the palladium) amounts to approximately a gram per gram or 2 moles of ozone for a gram-ion of palladium.

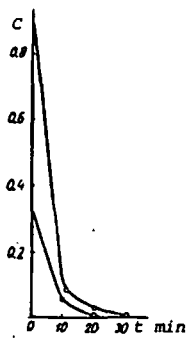

Fig.2 The effect of the ozonisation time on the precipitation of Pd^{2+} in the form of $K_2[PdCl_6]$ (volume of sample 36ml): t is the ozonisation time min, C is the concentration of Pd^{2+}, g-ion/l.

Under these conditions a series of experiments was set up on the extraction of palladium from spent APK-2 catalyst. [Its characteristics were given in the literature[4])]. The catalyst was ground to a powder and kept in 20% hydrochloric acid for 24h. The solution(red-brown) was filtered, a 15% solution of potassium chloride was added to the filtrate, and the solution was ozonised. The red salt $K_2[PdCl_6]$ soon separated, and the solution became colourless, i.e. palladium (II) was fully precipitated. After separation of $K_2[PdCl_6]$ on a filter the filtrate was returned for the extraction of palladium from the next batch of spent catalyst.

Ozonisation of solutions of $K_2[PtCl_4]$ with concentrations of 2.10^{-4}-2.10^{-3}M under analogous conditions showed that in HCl, H_2SO_4, and HNO_3 media platinum (II) is oxidised to form water-soluble derivatives of platinum (IV); in alkaline and neutral media colloidal solutions of hydrated platinum dioxide with $K_2[PtCl_6]$ as impurity are formed. As in the case of palladium, the most complete precipitation of platinum (II) occurs in hydrochloric acid medium (0.5-2.0M HCl) in the presence of 10-15% of potassium chloride as a finely crystalline compact precipitate of $K_2[PtCl_6]$. Typical results are given in fig. 3.

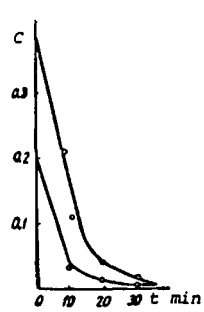

Fig.3 The effect of the ozonisation time on the precipitation of Pt^{+2} in the form of $K_2[PtCl_6]$ (volume of sample 42ml). t is the ozonisation time min, C is the concentration of Pt^{+2} g-ion/l.

It is seen that more complete precipitation is achieved for platinum than for palladium, and this is clearly due to the higher stability of platinum (IV) in the solution. Ozone can evidently be used instead of the traditional chlorine as a more convenient oxidising agent for the preparative synthesis of $K_2[PdCl_6]$ and $K_2[PtCl_6]$.

Comparison of the experimental data on the precipitation of palladium (II) and platinum (II) by ozone shows that these metals can be separated by ozonisation in a sulphuric acid medium. During the ozonisation of solutions of 0.5-2.0M sulphuric acid containing equal amounts of $K_2[PdCl_6]$ and $K_2[PtCl_6]$ (3.10^{-4}M for each) a dark-brown precipitate of palladium dioxide is formed. According to analysis[6], the precipitate separated on the filter contained 98-99% of palladium and 1-2% of platinum. Most of the platinum was present in the filtrate with palladium as impurity.

References

1) French Patent No. 2251364 1975, Ref. Zh. Khim. 22L106P 1976.
2) Japanese Patent No. 49-16357. Ref. Zh. Khim. 2L99P 1975.
3) V Sh Barkan: Tsvetnye Metally 1977, 1, 21.
4) Ya I Ivashentsev and A V Nechepurenko: Izv VUZ Tsvetnaya Metallurgiya 1976, 3, 87, 143.
5) I I Cheryaev et alia (editors): Synthesis of complexes of metals of the platinum group: Nauka 1964.
6) S I Ginzberg et alia: Analytical chemistry of platinum metals: Nauka, Moscow 1972.

UDC 669.332.2:536.3

Investigation of heat exchange in a reverberatory furnace with allowance for the scattering and absorption of radiation

Yu A Zhuravlev, E V Bogdanova and V G Lisienko (Krasnoyarsk Institute of Nonferrous Metals - Department of Metallurgical Furnaces)

To solve the problem of further improvement in reverberatory smelting (the use of effective heating schemes, the conversion to automatic control of the thermal operation of the furnace, etc) it is necessary to investigate the effect of the main operational parameters and conditions of fuel combustion on the characteristics of the thermal of the thermal operation of reverberatory furnaces. Experimental investigation of the thermal operation of these furnaces is extremely difficult, and we therefore resort to theoretical analysis by means of mathematical models of heat exchange in the working zone.

In the development of complex mathematic models of heat exchange in the reverberatory furnace, however, it is necessary to use a series of simplifying assumptions, i.e., disregard of the scattering of radiation by dust particles, constant chemical composition of the charge slag, uniformity of charging of the banks, etc. It is therefore of practical interest to solve the problem of external heat exchange with allowance for the scattering of radiation as applied to the real conditions in the reverberatory furnace. In addition, experimental verification of the mathematical model of heat exchange on an actual plant is important.

In the literature [1-4] etc) the effect of scattering on radiant heat transfer was investigated for comparatively simple radiating systems (a flat layer, an isothermal medium with uniform radiation characteristics, black walls, the limiting cases of a weakly absorbing or optically dense medium etc). To investigate the role of the scattering of radiation in radiant heat exchange processes in the working zone of the reverberatory furnace in the present work we used an algorithm which we developed for the zonal solution of the problem of external heat exchange with allowance for the scatterin of radiant energy by statistical trials[5]. This algorithm is based on the determination of the free path of the photons $r_{fr}(m)$ by means of random numbers:

$$r_{ff} = \frac{1}{K_s} \ln \gamma \qquad (1)$$

where: K_s = the scattering factor m^{-1}
γ = a random number distributed uniformly in the interval (0;1)

A detailed description of the algorithm and the flow chart for the calculation of the generalised angular coefficients of the radiant heat exchange with allowance for the scattering were given in the literature[5]. The calculations were performed on the basis of the previously developed zonal mathematical model of heat exchange, which corresponded to the circumstances of the reverberatory copper-smelting furnace of the NGMK plant, heated by natural gas[6]. The working zone along the length of the furnace was represented in the form of eight working sections 3.125m in length. In each section we isolated the volume zone of the flames (combustion products) and three surface zones (lining, slag, and charge banks).

The role of the scattering of radiation was investigated for a thermal load of 60.5MW, a flame length of 7.5m, and an oxygen content of 21% in the blast. To calculate the radiation characteristics the average diameter of the dust particles d_{av} was taken as 50μ on the basis of published data[7]) for a reverberatory furnace (table 1). For particles of such size (coarse particles) the scattering characteristic can be taken as spherical, and the diffracted radiation can be taken as transmitted[8]). In this case the dimensionless attenuation factor K' is equal to unity, and the effective attenuation cross-section $k = F_{av}/4$ (where F is the average specific surface area of the particles, m^2/g[6]). In addition, for dust particles of the indicated size with specific values of the optical constants (the refractive index and absorption coefficient) characteristic of the dust formed in flame-type smelting furnaces the scattering factor amounts to 60% of the full attenuation factor[8]).

Table 1: The screen analysis of the dust from the reverberatory furnace[7])

Point where dust sample taken	Amount of dust (%) on total weight with particles measuring mm			
	0.127	0.063-0.127	0.05-0.063	Less than 0.05
Below boilers and flues	19.6	24.2	8.6	47.6
From chimney stack	4	3.1	1.9	91.6

The average specific surface area of a spherical form was calculated by means of the equation (10):

$$F_{av} = \frac{6}{\gamma_d \cdot d_{av}} \qquad (2)$$

where: γ_d = the specific gravity of the dust, calculated for the following chemical composition (%): 20 Cu_2S, 25 FeS, 8 FeO_2, 25 Fe_2O_3, 10 SiO_2, and 12 others, and is equal to $4 \cdot 10^6$ g/m^3
d_{av} = the average diameter of the particles, $5 \cdot 10^{-6}$m.

Then,

$$F_{av} = \frac{6}{4 \cdot 10^6 \cdot 5 \cdot 10^{-6}} = 0.030 \text{ m}^2/\text{g}$$

The dust content of the gases in the working zone of the reverberatory furnace under normal conditions amounts on the average to 30-50 g/m^3, reaching 100-200 g/m^3 during charging. The calculations were performed for the limiting concentration of dust in the working zone of the furnace, equal to 200 g/m^3. For the actual conditions with the gases in the furnace at a temperature of 1500°C the concentration of dust is equal to

$$\mu = \frac{200}{1 + \frac{1500}{273}} = 30.817 \text{ g/m}^3$$

PILOT-PLANT TESTS OF FLOTATION OF PULPS FROM NICKEL-PYRRHOTITE CONCENTRATE AUTOCLAVE LEACHING

UDC 622.765

V. V. Yakovlev, M. I. Mantsevich, V. A. Shcherbakov, and A. I. Glushnitskaya

The chemical concentration technology [1, 2] which has been developed for processing nickel-pyrrhotite sulfide concentrates includes the separation of non-ferrous metal sulfides and elementary sulfur from iron oxides by flotation.

The physical and chemical properties of the pulp entering the flotation process depend to a considerable extent upon conditions in the hydrometallurgical operations. If the pulp temperature during leaching and precipitation of the non-ferrous metals does not reach the melting point of elementary sulfur, most of the sulfur-sulfide material is present as fine formations.

When the pulp temperature rises as a result of disturbances in these operations or the inclusion of an aggregation operation in the processing scheme, the particles of elementary sulfur coagulate and form drops which wet and occlude the sulfides. After cooling, these drops solidify as granules ranging in size from 0.1-0.2 to 2-3 mm of an "alloy" or elementary sulfur and sulfides.

Classification of the material by size is required to extract these prior to flotation. Two methods were tested under pilot-plant conditions: screening on a vibrating screen and hydraulic classification. The latter proved to be more reliable. The results of particle-size analysis of the classification products indicate that the granule separation process is fairly efficient (Table 1).

Depending upon the yield of granules (sands from classifier II), 15-30% of the valuable constituents pass into them ished sulfur-sulfide product and are sent for further proc action of the valuable constituents is practically complete.

PPTF

Pulp flotation after separation oduct followed a continuous routine in a 59-5L machine with a , using a scheme including rougher and control operations and s (see Figure). The flotation machine was made from steel perceptible signs of corrosion in five years of use).

The capacity of the flotation u 0 liters/hr in the course of the tests; the operations, taki -filling factor adopted of 0.75, were of the following du a 13-18 min, control flotation 22-30 min, and recleanings (total) 30-40 min. Pulp density is not more than 1.28-1.35 g/cm^3 at pH = 3-4.5. The optimum flotation machine unit was established; as a whole it was 0.224-0.18 m^3/ton/day, including 0.08-0.065 in rougher flotation, 0.044--0.035 in control flotation, and 0.1-0.08 m^3/ton/day in the recleanings.

Butyl Aerofloat at the rate of 200-300 g/ton (in terms of active constituents), T-66 frother up to 100 g/ton, and kerosene up to 300 g/ton in certain cases were used for flotation of the sulfur-sulfide product.

Flotation of the oxidized pulp is characterized by high froth product yields and considerable mechanical extraction of finely-dispersed ferric hydroxide into the froth products. The latter factor requires considerable dilution of the crude concentrates in the recleaning operations with fresh or recirculating water to raise the level of hydroxide removal from the concentrate. The high flotation activity of the sulfur-sulfide material is appaeent in thsse circumstances; it ensures 95-97% nickel extraction in recleaning I and II and copper extraction of about 95%, while the copper and nickel content of the recleaning tailings is similar in most cases to the waste tailings content of these elements. Thus, the sulfur-sulfide concentrate recleanings are a kind of flotation-washing operation.

Processing pyrrhotite-bearing concentrates in a scheme without an aggregation operation from material containing 2.6% Ni and 1.6% Cu yielded a sulfur-sulfide concentrate containing 8.8-9.0% Ni, 5.1-5.6% Cu, and up to 40% S (element). Nickel and copper extraction into the concentrate reaches 90-92%.

Table 1
Particle-Size Characteristics of Classification Products

Products	Yield of size classes, %		
	+0.15 mm	−0.15+0.074 mm	−0.074 mm
Classifier I feed	19.6	6.0	74.4
Classifier I overflow	31.5	16.4	52.1
Classifier I sands	47.7	19.5	32.8
Classifier II overflow	2.4	14.6	83.0
Classifier II sands	78.6	18.3	3.1
Wet cyclone sands	30.0	15.3	54.7
Wet cycl.feed (flot.feed)	1.0	2.1	96.9

[1]The granule separation scheme includes rough (I) classification and washing of sands from that operation in spiral classifiers and control classification of overflow (I) in a wet cyclone.

Results of Sulfur-Sulfide Flotation (without aggregation)

	% concentrate	% tailings	% feed
Yield	27.8	72.2	100.0
Content:			
Ni.....	8.8/8.82	0.22/0.28	2.61/2.66
Cu.....	5.14/5.25	0.1/0.18	1.57/1.59
Fe.....	18,8	47.7	39.8
S_{total}....	56.8	2.4	17.5
S^o.....	39 7	Traces	11.0
Extraction:			
Ni.....	91.9/92.4	6.2/7.6	98.1/100
Cu.....	90.1/92	4.6/8.0	97.6/100
Fe.....	13.3	86.7	100
S_{total}....	90.0	10.0	100
S^o.....	100	Traces	100

Note: The numerator shows the content and extraction in the solid phase, the denominator the calculated content and extraction, taking into account the content in the liquid phase.

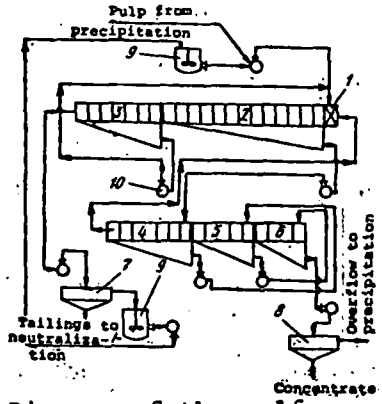

Diagram of the sulfur-sulfide flotation process stage layout: 1 - intake cell; 2 - rougher flotation (13 cells); 3 - control flotation (7 cells); 4 - recleaning I (7 cells); 5 - recleaning II (5 cells); 6 - recleaning III (4 cell cells); 7 - thickener for tailings (1.8 m diameter); 8 - thickener for concentrate (1.8 m diameter); 9 - collecting tank (volume 11.4 m^3); 10 - sand pump.

When an aggregation operation was introduced to the process, a classifier overflow containing 2.8-3.1% Ni and 1.1-1.5% Cu was fed to the flotation process. A sulfur-sulfide concentrate containing 12.6-13.0% Ni and 5.1-6% Cu was obtained in these circumstances (Table 2).

The higher quality of the concentrate is due to separation of a substantial part of the copper sulfides, the incompletely decomposed pyrrhotite, and the elementary sulfur into the granules.

Slime and chemical analyses of the flotation tailings (Table 3) showed that most of the sulfides were present in the fine classes and losses of sulfides with the tailings were attributable to the -20μ classes. With satisfactory classification of the material prior to flotation there are almost no metal losses with the +74μ class, but when relatively coarse inclusions enter the classification overflow, the losses of valuable constituent attributable to this class rise sharply.

On average, the non-ferrous metals content of the tailings is 0.2-0.3% Ni and 0.1-0.2% Cu. A definite proportion of the losses is attributable to the tailings liquid phase; this is due to incomplete precipitation of copper and more particularly nickel, and to the reverse passage of non-ferrous metals into solution due to sulfide oxidation during the pumping of pulp in flotation.

Table 2
Sampling Results from the Sulfur-Sulfide Flotation Tailings

Products	Yield	Content					Extraction				
		Ni	Cu	Fe	S_{tot}	S^o	Ni	Cu	Fe	S_{tot}	S^o
Rougher flotation feed	100.0	2.83	1.13	44.29	12.05	5.47	100	100	100	100	100
Rougher flotation concentrate	35.65	7.64	2.99	37.4	31.2	15.34	96.2	94.7	31.1	92.4	100
Rougher flotation tailings	82.48	0.23	0.10	48.3	2.55	Traces	6.6	7.7	93.1	16.8	Tr.
Recleaning I concentrate	24.55	10.95	4.29	31.7	44.0	22.4	95.0	93.5	14.7	85.0	100.6
Recleaning I tailings	15.05	0.45	0.14	49.6	2.98	Tr.	2.3	1.9	16.9	3.7	Cu.
Recleaning I concentrate	22.14	12.35	4.85	23.6	46.7	23.53	96.7	95.3	11.8	86.2	102.6
Recleaning II tailings	3.95	0.79	0.20	49.1	3.52	0.96	1.1	0.7	4.4	1.2	0.6
Recleaning III concentrate	20.6	12.9	5.08	22.2	48.8	26.56	93.9	92.8	10.3	83.8	100
Recleaning III tails	1.54	5.01	1.81	41.0	18.5	9.12	2.8	2.5	1.5	2.4	2.6
Control flotation concentrate	3.05	0.49	0.18	48.8	2.24	Tr.	0.5	0.5	3.4	0.6	Tr.
Control flotation tailings	79.4	0.22	0.10	50.0	2.45	»	6.1	7.2	89.7	16.2	»

Sulfide oxidation was particularly marked when a non-continuoss metal precipitation process was used; this gave rise to the need to store pulp prepared for flotation over a 2-4 hr period. The shift to a continuous precipitation schedule reduced nickel and copper dissolution. Nevertheless, the nickel content of the tailings liquid phase reaches 100-200 mg/liter, the copper content 100 mg/liter, and the cobalt content 10-20 mg/liter, which usually accounts for 1.5-2% of the content of these metals in the initial feed.

The main ways to reduce metal losses in the liquid phase are by improving the process of metal precipitation and eliminating sulfide oxidation in all possible ways, particularly by reducing the number of pulp-pumping operations, cutting down pulp storage time in vessels, increasing the speed of sulfide flotation, etc. The non-

ferrous metals which have oone into solution can be re-extracted by using ionic flotation[3] and also by sorption processes

The pilot-plant tests confirmed the results of laboratory and larger-scale investigations and were used as the basis in developing an autoclave technology project.

REFERENCES

1. V. I. Goryachkin, I. M. Nelen', V. A. Shcherbakov, et al, Tsvetnye Metally, 1974, No. 9, 1-6.
2. V. A. Shcherbakov, V. V. Yakovlev, I. V. Fgorov, and A. M. Panfilov, Tsvetnaya Metallurgiya (Byul. Inst. Tsvetmetinformatsiya), 1975, No. 1, 24-27.
3. S. I. Mitrofanov, S. S. Semeshkin, M. A. Shevelevich, et al, Tsvetnye Metally, 1973, No. 12, 72-74.

PILOT-PLANT TESTS OF A PULSATING ADSORPTION COLUMN FOR THE EXTRACTION OF GOLD FROM NON-CLARIFIED SOLUTIONS

UDC 662.342:661.183.12

E. I. Zakharov, B. E. Ryabchikov, N. G. Rudenko, L. K. Mikheev, and B. E. Beskrovny

Ion-exchange processes have gained wide acceptance in the gold-extraction industry since they provide for a higher recovery and the production of high-purity metals.

In gold-extraction plants, there are numerous nonclarified solutions, containing up to 0.02-0.5% of suspended particles. Such solutions may be recycling solutions, waste waters, or thickener overflows. Pachuca tanks, currently employed in pulp processes, are not suitable for the processing of such solutions since they require a large number of series-connected apparatus, which consume a great deal of air and involve complicated maintenance.

Industry today has developed a novel PSK pulsating adsorption columns [1-3], which have been found to be well suited to the processing of various solutions and pulps [3-8]. They do not require large investments nor large operating costs; they have simple designs and are much more economical than Pachuca tanks.

The specific features of the ion-exchange gold-extraction process are low speed (the period to onset of equilibrium runs up to 350 hours) and the favorable ratio between the flux of resin and solution, both passing through the column: $n = W_r/W_s = 1:2000-1:3000$. However, these conditions required the design of an improved pulsating column to ensure a long and controlled period during which the sorbent will remain in the column. Such a design was developed and is being marketed under the trade name PSK-T mobile pulsating column [1, 6, 8].

The Kuranakha Plant assembled and installed an installation (Fig. 1) consisting of an adsorption column, 200 mm in diameter and 10 mm high, a container for the starting solution, a feed pump, rotameters, pulsating elements, and two separators for the collection of resins.

A pump 2 is used to feed the solution from the buffer container 1 through the rotameter 4, rising upward, then is expelled through control separator 5. Grade AM125 sorbent is fed manually to the top zone of the column. Resin, saturated in the column, is removed downwards -- with an air-lift pump -- into separator 6, where it is allowed to remain for a certain time. The solution is recycled to the bottom part of the column.

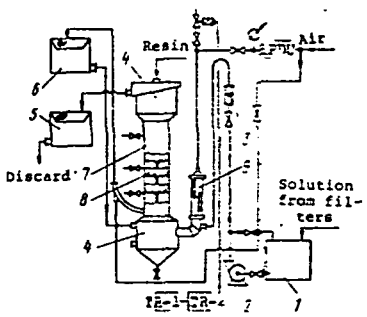

Fig. 1. Schematic diagram of adsorption tower (column):
1 - buffer container; 2 - pump; 3 - rotameter; 4 - top and bottom settling zones; 5 - control separa or; 6 - separator; 7 - column; 8 - packing; 9 - pulsation chamber; 10 - BPDU by-pass remote control; TR-1 and TR-2 - time relays

Column 7 contains specially-designed perforated plates (trays) with clearances of 100 mm; their cross-section was so selected that when the solution feed rises the flow velocity in the plate holes is larger than the entrainment rate of the largest resin particles. During top feed of resin, it is retained at the plate where it forms a fluidized-bed layer. For downward movement of the ionite, the direction of the solution flow is reversed by air pulsation; this is achieved as follows: air is slowly fed to the pulsation chamber during the operation. An electromagnetic solenoid valve is then opened to remove air from the pulsation chamber; the solution in the column is thus forced into the the pulsation chamber and its level in the column drops sharply. Pulsation amplitude depends on the "flash" time. By varying the pulsation amplitude and frequency, we were able to control the resin flow and its residence time in the column.

At the very instant that the direction of solution flow is reversed, the resin particles move together with the solution from one plate to the other. The amount of transferred sorbent depends on the amplitude of reverse solution flow.

In technological tests, gold was extracted from solutions containing 0.8-4.4 mg/l Au, 2-12 mg/l Zn and other impurities; adsorption was conducted with type AM-2B resin in the form of OH^- and Cl^- ions.

The first tests were conducted on regenerated type AM-2B resin following its extended use in pulp processing.

Determination of the operating schedule for the extraction column was effected

using laboratory data on the hydrodynamic kinetic and static features of the process in type PSK-T columns.

The tests were performed under the following conditions: a throughput of 830 l/hr (specific load of 28 $m^3/m^2 \cdot hr$); resin throughput of 300 ml/hr; resin-to-solution flow ratio n = 1:2800; pulsation frequency 1 pulse/hr; pulsation amplitude 45 mm; sorbent residence time in column 100 hours; solution residence time 20 minutes.

The test lasted 118 hours. To accelerate the onset of steady-state conditions for the column, its top 20 plates were quickly filled with resin and the rated pulsation amplitude established. Concentration of Au in the solution was varied during the tests (Fig. 2a), reaching an average of 1.5 mg/l; the average Zn content was 8 mg/l. The waste solution contained 0.1-0.5 mg/l Au (about 0.37 mg/l on average), corresponding to a recovery of about 75%. Resin saturation was about 6 mg/l. The calculated number of contact stages (CCS) was 2.5-3 and the VETS factor [Translator's note: VETS is the Russian designation for the height of that part of the column in which the concentration of the material being extracted reaches equilibrium] is 3-4 m.

The second test was conducted (Fig. 2b) at a smaller load (24-26 $m^3/m^2 \cdot hr$) and throughput (710-730 l/hr). Since the starting solution had a high gold concentration (3.3 mg/l Au on average) and a high Zn concentration (12 mg/l), the flow rate was raised to n = 1:2400. The tests were conducted with fresh AM-2B rsin in a Cl^- form. The pulsation parameters remained unchanged.

The test lasted 136 hours, with 100 m^3 of solution processed during the tests. The waste solution contained 0.4 mg/l Au on average; its concentration was varied synchronously with the gold content in the feeding solution (Fig. 2b). Recovery reached 83%; resin saturation was 10 mg/l for Au and 21 mg/l for Zn. The number of CCS was 2.5-3.

Results obtained from both tests were in good agreement with the theoretical data.

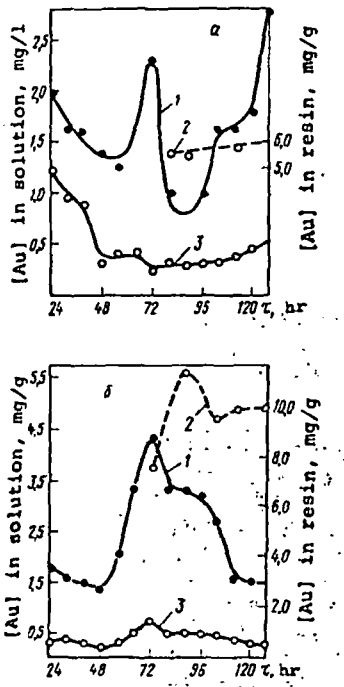

Fig. 2. Indices for gold adsorbed with unregenerated resin (a) and with fresh resin (b):
Gold content: 1 - in starting solution, mg/l; 2 - in saturated resin, mg/l; 3 - in gold-free solution mg/l.

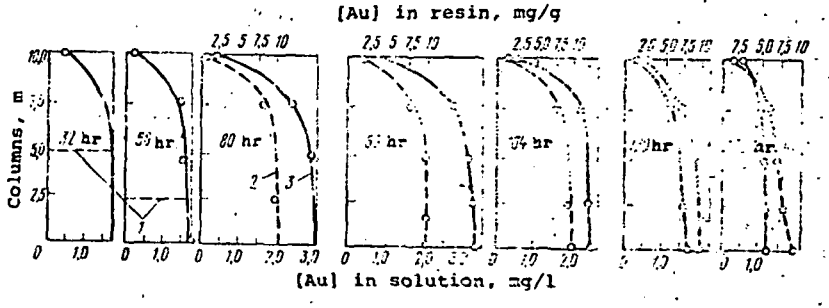

Fig. 3. Gold content in resin and solution over the column height:
1 - resin level in column, m; 2 - gold content in resin, mg/l; 3 - gold content in solution, mg/l.

During the tests, we regularly took samples from resin and solutions over the height of the column; from the sampling data, we plotted the concentration curves (Fig. 3) corresponding to the different time intervals of column operation. As is evident from the curves, the principal changes in concentration occur in the top part of the column over a 2.5-m height, i.e., during the first 25 hours of contact between the resin and the solution. During the subsequent 74 hours, the changes in solution and resin concentration are insignificant.

Such concentration [saturation] curves usually correspond to the situation in which the sorbent is saturated to its equilibrium capacity in the top part of the column; any additional contact period with fresh solution will bring no significant changes in saturation. On the other hand, Au adsorption develops in two stages: external and internal diffusion. During the initial period the process rate is limited by external diffusion and then later by internal diffusion. Under static conditions, the first stages require about 75 hours of contact while the second stage needs 180-250 hours. We tend to improve the mixing of the phases in the column so that the first stage takes 25 hours. The second stage cannot be accelerated so that, as be-

using laboratory data on the hydrodynamic kinetic and static features of the process in type PSK-T columns.

The tests were performed under the following conditions: a throughput of 830 l/hr (specific load of 28 $m^3/m^2 \cdot hr$); resin throughput of 300 ml/hr; resin-to-solution flow ratio n = 1:2800; pulsation frequency 1 pulse/hr; pulsation amplitude 45 mm; sorbent residence time in column 100 hours; solution residence time 20 minutes.

The test lasted 118 hours. To accelerate the onset of steady-state conditions for the column, its top 20 plates were quickly filled with resin and the rated pulsation amplitude established. Concentration of Au in the solution was varied during the tests (Fig. 2a), reaching an average of 1.5 mg/l; the average Zn content was 8 mg/l. The waste solution contained 0.1-0.5 mg/l Au (about 0.37 mg/l on average), corresponding to a recovery of about 75%. Resin saturation was about 6 mg/l. The calculated number of contact stages (CCS) was 2.5-3 and the VETS factor [Translator's note: VETS is the Russian designation for the height of that part of the column in which the concentration of the material being extracted reaches equilibrium] is 3-4 m.

The second test was conducted (Fig. 2b) at a smaller load (24-26 $m^3/m^2 \cdot hr$) and throughput (710-730 l/hr). Since the starting solution had a high gold concentration (3.3 mg/l Au on average) and a high Zn concentration (12 mg/l), the flow rate was raised to n = 1:2400. The tests were conducted with fresh AM-2B rsin in a Cl^- form. The pulsation parameters remained unchanged.

The test lasted 136 hours, with 100 m^3 of solution processed during the tests. The waste solution contained 0.4 mg/l Au on average; its concentration was varied synchronously with the gold content in the feeding solution (Fig. 2b). Recovery reached 83%; resin saturation was 10 mg/l for Au and 21 mg/l for Zn. The number of CCS was 2.5-3.

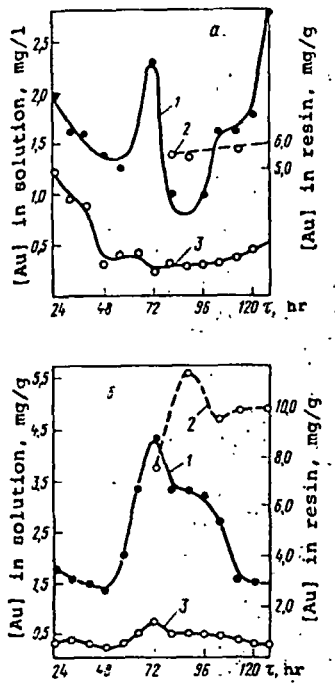

Fig. 2. Indices for gold adsorbed with unregenerated resin (a) and with fresh resin (b):
Gold content: 1 - in starting solution, mg/l; 2 - in saturated resin, mg/l; 3 - in gold-free solution mg/l.

Results obtained from both tests were in good agreement with the theoretical data.

During the tests, we regularly took samples from resin and solutions over the height of the column; from the sampling data, we plotted the concentration curves (Fig. 3) corresponding to the different time intervals of column operation. As is evident from the curves, the principal changes in concentration occur in the top part of the column over a 2.5-m height, i.e., during the first 25 hours of contact between the resin and the solution. During the subsequent 74 hours, the changes in solution and resin concentration are insignificant.

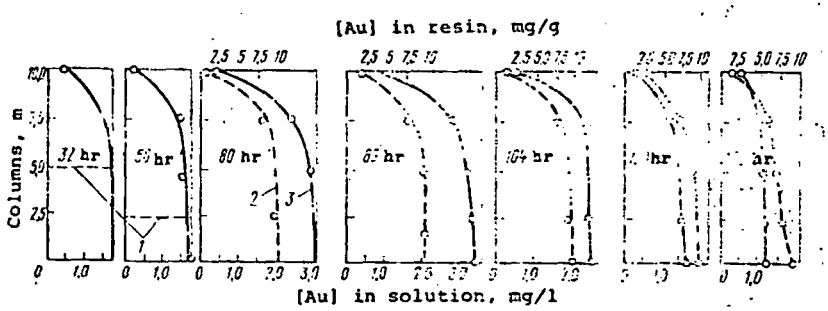

Fig. 3. Gold content in resin and solution over the column height:
1 - resin level in column, m; 2 - gold content in resin, mg/l; 3 - gold content in solution, mg/l.

Such concentration [saturation] curves usually correspond to the situation in which the sorbent is saturated to its equilibrium capacity in the top part of the column; any additional contact period with fresh solution will bring no significant changes in saturation. On the other hand, Au adsorption develops in two stages: external and internal diffusion. During the initial period the process rate is limited by external diffusion and then later by internal diffusion. Under static conditions, the first stages require about 75 hours of contact while the second stage needs 180-250 hours. We tend to improve the mixing of the phases in the column so that the first stage takes 25 hours. The second stage cannot be accelerated so that, as be-

fore, it requires 180-250 hours, i.e., to obtain a fully-saturated resin we have to ensure a contact period of 200-270 hours. This may be obtained by the installation of two series-operating columns. Discharge concentrations may also be lowered since sorbent saturation increases by 20-30%, i.e., the process contributes to extracting the remaining gold from the solution.

Gold extraction to any desired figure at the given sorbent saturation may be obtained by increasing the resin throughout. We thus entrain a larger part of the column into the mass-transfer process (Fig. 3).

CONCLUSIONS

The results of our pilot-plant tests show the high efficiency of pulsation columns in systems with very slow exchange kinetics (load 30 $m^3/m^2 \cdot hrs$; VETS - 3-4 m; time to equilibrium - 250-300 hours); use of such columns substantially improves the engineering-economy figures for the gold-extraction processes.

Our test results, as well as data from industrial employment of large-size pulsation columns were decisive in the design of a plant for the processing of 3000 m^3/hr of nonclarified gold-bearing solutions.

REFERENCES

1. B. E. Ryabchikov and E. I. Zakharov. Equipment for Ion-Exchange. Moscow. "Tsvetinformatsiya," 1974; ill.
2. S. M. Karpacheva, L. S. Rachinskii, V. M. Muratov, et al. Pulsation Apparatus. Moscow, "Tsintikhimneftmash," 1971, 68 pp.; ill.
3. S. M. Karpacheva, E. I. Zakharov, V. N. Koshkin, et al. "Extraction and Sorption in the Metallurgy of Molybdenum, Tungsten, and Rhenium." Moscow, "Tsvetmetinformatsiya," 1971, p. 182-193.
4. B. E. Ryabchikov, E. I. Zakharov, and D. I. Trofimov. In the book: Problems in Atomic Science and Techniques. Pulsation Apparatus. Moscow, "TsNIIatominform," 1972, pp. 63-76.
5. E. I. Zakharov, V. S. D'yachkov, N. Koshkin, et al. In the book: Problems in Atomic Science and Techniques. Pulsation Apparatus. Moscow, "TsNIIatominform," 1972, pp. 77-83.
6. E. I. Zakharov, B. E. Ryabchikov, V. N. Koshkin, et al. In the book: Development and Use of Pulsation Apparatus. Moscow, Atomizdat, 1974, pp. 171-188.
7. S. M. Karpacheva, S. F. Medvedev, and S, M. Balakirev. Tsvetnye Metally, No. 7, pp. 10-14.
8. F. V. Rauzen, E. I. Zakharov, B. E. Ryabchikov, et al. Atomnaya Energiya, 1974, vol. 34, No. 1, pp. 27-31.

METALLURGY

ALUMINUM, ALUMINA, AND ELECTRODES

PRECIPITATION OF SULFATE COMPOUNDS IN CONCENTRATING SOLUTIONS FROM ALUMINUM PLANT GAS CLEANING

UDC 669.713.1

V. A. Morozova and E. P. Rzhechitskii

Supplying industrial enterprises in non-ferrous metallurgy with recirculating water is a major trend in organizing the efficient utilization of water resrouces and in protecting reservoirs from pollution. Sodium sulfate is the main constituent preventing the utilization of slime waters in shop recirculating water in aluminum plant cryolite regeneration sections. The most effective way is to organize the extraction of sodium sulfate from industrial gas cleaning solutions, where its concentration reaches 70-90 g/liter.

We demonstrated previously in [1] that it was possible in principle to extract sodium sulfate in the form of Glauber's salt $Na_2SO_4 \cdot 10H_2O$ by cooling the mother liquor to 0° C after precipitation of the secondary cryolite and the conditions required for the process. For installations of small capacity the best system is crystallization of sodium sulfate in the form of the double salt $NaF \cdot Na_2SO_4$ by evaporation of clarified gas cleaning solutions.

Crystallization of Sulfate Compounds in Evaporation of Solutions

Test no.	Solution	Chemical composition, g/liter: solution NaF	solution Na_2SO_4	solution Na_2CO_3	solution $NaHCO_3$	filtrate NaF	filtrate Na_2SO_4	filtrate $Na_2CO_3+NaHCO_3$	Na_2SO_4 passage into precipitate, %	Phase composition of deposit
7	Clarified gas-cleaning solution	13,9	44,8	12,3	18,7	22,4	66,5	66,7	35,1	$NaF \cdot Na_2SO_4$
6		13,9	44,8	12,3	18,7	21,8	62,3	96,9	52,4	$NaF \cdot Na_2SO_4$
170		10,0	50,4	9,3	16,0	9,7	109,3	108,0	52,0	$NaF \cdot Na_2SO_4$
6a		13,9	44,8	12,3	18,7	20,2	52,4	124,2	68,5	$NaF \cdot Na_2SO_4$
11		17,0	46,3	10,1	24,4	23,3	51,7	138,0	76,2	$NaF \cdot Na_2SO_4$
25		14,8	49,7	10,6	22,7	16,8	49,3	150,7	82,3	$NaF \cdot Na_2SO_4$; $Na_2CO_3 \cdot 2Na_2SO_4$
9		17,0	46,3	10,1	24,4	21,6	45,4	157,7	85,5	$NaF \cdot Na_2SO_4$; $Na_2CO_3 \cdot 2Na_2SO_4$
14		28,0	35,5	6,3	25,9	18,4	57,7	120,7	66,0	$NaF \cdot Na_2SO_4$; NaF
16	Mother liquor	5,0	44,0	29,7	5,5	8,0	125,3	134,7	34,2	$NaF \cdot Na_2SO_4$
19		5,0	44,0	29,7	5,5	7,2	132,7	149,5	35,7	$NaF \cdot Na_2SO_4$ $Na_2CO_3 \cdot 2Na_2SO_4$
29		3,05	49,6	28,6	5,0	3,6	170,3	181,0	50,8	$NaF \cdot Na_2SO_4$; $Na_2CO_3 \cdot Na_2SO_4$

When solutions containing sodium fluoride, sulfate, and carbonate are evaporated, crystallization of the salts $NaF \cdot Na_2SO_4$ and $Na_2CO_3 \cdot 2Na_2SO_4$ takes place [2,3]. Industrial solutions for secondary cryolite production at aluminum plants have the following composition, g/liter: 5-25 NaF; 50-90 Na_2SO_4; 5-40 Na_2CO_3; 5-30 $NaHCO_3$.

Gas cleaning solutions after clarification and mother liquors after cryolite precipitation were taken for extraction of accumulated sodium sulfate in the form of the compounds indicated.

The solutions were evaporated under laboratory conditions, in a thermostatically controlled metal reactor at 70-80° C with mixing, at atmospheric pressure and in vacuo. When the solutions are concentrated in vacuo the heat input is reduced, but encrustation of the reactor surface increases substantially. The precipitates produced were washed with an alcohol solution (50% alcohol and 50% water).

A chemical analysis of the solutions and the solid phase composition are given in the Table.

The phase composition of the precipitates was found by qualitative X-ray diffraction and crystal optical analysis methods. The X-ray diffraction patterns for the precipitates in experiments No. 9, 11, and 14 are given in Fig. 1.

The refractive indices of the products are:

$NaF \cdot Na_2SO_4$ . . . . . $n_o = 1.436$ $n_e = 1.439$

$Na_2CO_3 \cdot 2Na_2SO_4$ . . . . . $n_g = 1.492$ $n_p = 1.450$

NaF . . . . . $n = 1.324$

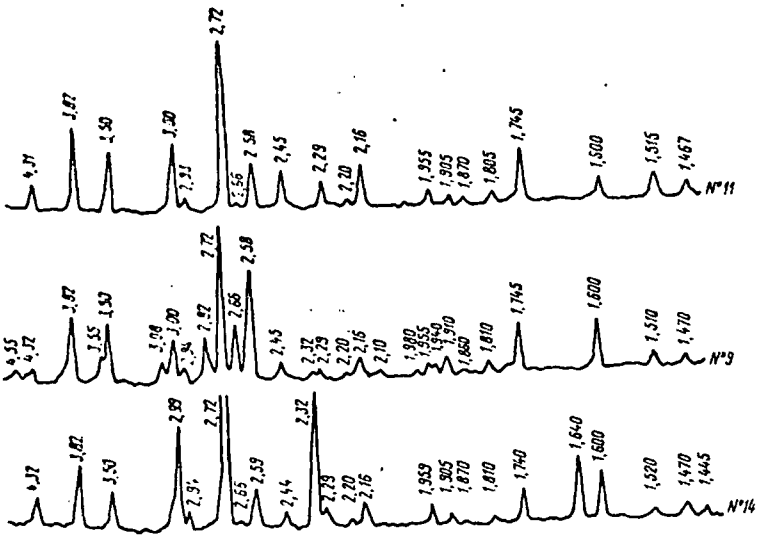

Fig. 1. X-ray diffraction patterns for precipitates: $NaF \cdot Na_2SO_4$ (experiment 11); $NaF \cdot Na_2SO_4$ and $Na_2CO_3 \cdot 2Na_2SO_4$ (experiment 9); $NaF \cdot Na_2SO_4$ and NaF (experiment 14).

The double salt $NaF \cdot Na_2SO_4$ crystallizes in the form of rhombohedral and hexagonal lamellar crystals 30-150μ in size and forms radiating concretions. The relative density of the salt is 2.611.

The $NaF \cdot Na_2SO_4$ thermogram is given in Fig. 2; the effect of fusion of the salt at 790° C is apparent.

As was shown by the results of experiments on the evaporation both of clarified solutions and mother liquors containing a comparatively small amount of sodium fluoride (3-5 g/liter), the double salt separates out into the solid phase first, then the burkeite or NaF, depending on the chemical composition of the initial solution.

Crystallization of $NaF \cdot Na_2SO_4$ by concentrating clarified gas cleaning solution may be used to extract sodium sulfate from industrial solutions. The degree of evaporation is determined by the concentration of soda and sodium bicarbonate, which must remain dissolved.

It is apparent from the Table that $NaF \cdot Na_2SO_4$ separates out in concentrating a clarified gas cleaning solution up to a total sodium carbonates content of not more than 140 g/liter. With further evaporation, burkeite separates out into the solid phase. When the sodium fluoride content of the initial solution is considerable (experiment 14) it crystallizes with the $NaF \cdot Na_2SO_4$.

Sulfate compounds should not be separated from the mother liquors, because when the $NaF \cdot Na_2SO_4$ crystallizes the passage of sodium sulfate from solution to precipitate is comparatively small in extent (~34%), and with more complete evaporation a mixture of $NaF \cdot Na_2SO_4$ and $Na_2CO_3 \cdot 2Na_2SO_4$ is precipitated. The product cannot be used, and separation of the mixture is difficult.

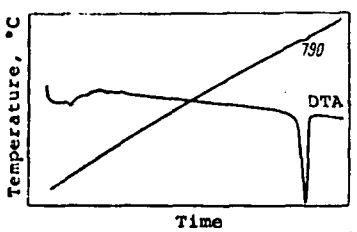

Fig. 2. Thermogram of double salt $NaF \cdot Na_2SO_4$.

To precipitate sulfate salts, therefore, they should be extracted as $NaF \cdot Na_2SO_4$ by the evaporation of clarified gas cleaning solutions containing 13-17 g/liter NaF and 45-70 g/liter Na_2SO_4. The filtrate is used in the cryolite production system after removal of the precipitate. The extracted salt can also be used for the production of cryolite.[1] It is best to transport the double salt from several plants to one plant, where it can be processed to obtain cryolite and sodium sulfate. This plant must operate a more complex installation for the extraction of sulfates from gas cleaning solutions by cooling them to low temperatures: from +5 to -2° C. The double salt may be used for other purposes in the national economy, for example, for the fluoridation of water.

CONCLUSIONS

Sodium sulfate should be extracted as the double salt from clarified gas cleaning solutions by evaporation to a total sodium carbonates content of 130-140 g/liter. Under these conditions 65-76% of the sodium sulfate separates out into the solid phase.

REFERENCES

1. V. A. Morozova, E. P. Rzhechitskii, and V. P. Klimenko, Tsvetnye Metally, 1973, No. 9, 28-31.
2. A. A. Furman and S. S. Shraibman, The Preparation and Purification of Mother Liquors, Moscow, Khimiya, 1966, 245 pp., illustrated.
3. T. M. Zlokazova, M. G. Zolotareva, P. D. Katsenelenbogen, et al., Inventor's Certificate No. 196745, Izobreteniya, Promyshlennye Obraztsy i Tovarnye Znaki, 1967, No. 12, 18.

[1] U.S. Patents No. 2925324 and 2925325, 1960.

THE PRESENT SITUATION IN HYDROMETALLURGY AND PROSPECTS FOR THE DEVELOPMENT OF HYDROMETALLURGICAL PROCESSES[1]

UDC 669.2.053.4

B. N. Laskorin

During the past twenty years there has been rapid development in hydrometallurgical methods and a steady expansion in their fields of application in the metallurgy of the non-ferrous metals.

The inevitability and regularity of the transition to hydrometallurgical methods arises primarily out of the necessity to make full use of the valuable constituents in raw materials being processed and to prevent damage to the environment by gaseous industrial waste.

The particularly favorable conditions which have contributed to the extensive development and industrial utilization of these methods are due to major successes in inorganic and physical chemistry in the study of heterogeneous reactions (the mechanism and kinetics of leaching processes and oxidiation-reduction reactions) and of inorganic reactions taking place under pressure at temperatures above 100° C, i.e., the chemistry of autoclave leaching processes and of autoclave methods of depositing pure metal powders from solution using gaseous reducing agents.

The greatest advances in production technology for compounds and non-ferrous metals of high purity in recent times have been made by using ion-exchange and solvent-extraction technology, based primarily on the use of filterless methods or methods of sorption from pulps, as well as sorption and solvent extraction from clarified solutions and membrane technology.

Various countries have now gained great industrial experience in the use of autoclave processes, bacterial leaching, and sorption and solvent-extraction technology in the hydrometallurgy of the non-ferrous metals.

A continuous autoclave leaching process has long been in use at many plants producing alumina.

Acid, carbonate, and ammonia autoclave leaching are widely used in processing oxidized and sulfide nickel-cobalt and tungsten-molybdenum concentrates and middlings. Sulfuric acid autoclave leaching of lateritic nickel-cobalt ores has been successfully used over a long period at the Moa Bay enterprise in the Republic of Cuba. This experience is undoubtedly of great importance in the further development of acid autoclave processes.

The Mekhanobr Institute has developed and introduced on an industrial scale an autoclave-soda process for the production of tungsten anhydride from low-grade scheelite-molybdenum concentrates, for the first time in world practice; this process is now being used successfully by many enterprises in the USSR and in other countries.

An autoclave method is in use at many foreign nickel enterprises, for example, at the Sherritt Gordon Plant in Canada. Autoclave methods are being developed for processing sulfide nickel, copper, molybdenum, zinc, and various bulk polymetallic concentrates. Thus 12 of the 42 papers in the autoclave section at the First All-Union Conference on Hydrometallurgy were devoted to the study of autoclave processing of Noril'sk pyrrhotite concentrates.

It can be stated that an optimal solution to the problem of integrated processing of complex copper-nickel material, producing elementary sulfur and giving a high rate of extraction of all valuable constituents, can be found primarily in the use of hydrometallurgical autoclave-sorption or solvent-extraction technology.

The work on high-temperature hydrolysis as a method for chemical concentration and processing of solutions is worthy of attention. Reaction speeds increase substantially at the high temperatures that can be reached in the autoclave treatment of solutions, and products can be obtained with a structure that ensures accelerated solid and liquid phase separation. Thus the products of hydrolysis of aluminum and titanium salts obtained at room temperature, or even at 100° C, are usually gelatinous, difficult to wash free of impurities, and giving very poor results in filtration or thickening. The corresponding metal hydroxides separated from solution at 220° C filter very well and can be produced in the pure state.

Considerable advances have been made in the industrial assimilation of the autoclave separation of copper, nickel, and cobalt powders from aqueous solutions using gaseous reducing agents. The most widely used reducing agent is hydrogen, but the possibility of using carbon monoxide, converted natural gas, and various freely

[1]Based upon a paper read at the First All-Union Conference on Hydrometallurgy.

available liquid organic reducing agents is not excluded. This method will undoubtedly find more extensive industrial application in the immediate future in the production of copper, gold, silver, and the platinum metals, and may possibly be used later to produce iron powder.

By no means all metals can be produced by autoclave reduction; radical improvements are therefore planned for electrochemical methods as a result of adoption of continuous processes, and particularly by using selective ion-exchange membranes.

Autoclave leaching is not always the only method or the best method even for sulfide ores and concentrates of non-ferrous metals. There are other effective methods for the overwhelming majority of mixed ores, and particularly for oxidized ores; the characteristics of these methods are lower unit capital investment and good technical and economic results. Of these methods, only some potential applications of bacterial leaching were discussed at the abovementioned conference.

A detailed analysis made by the Interdepartmental Commission on Development of Hydrometallurgical Methods set up by the State Committee for Science and Technology showed that, as a rule, pyrometallurgical methods of processing have limited possibilities compared with hydrometallurgical methods, especially as regards the complete utilization of raw materials. Hydrometallurgical processes predominate in zinc and tungsten production. The limited possibilities of pyrometallurgy arise from the physicochemical essentials of the processes; they are limitations of principle, not determined by the state of development of this or that method. In addition, substantial unit capital investment is usually a feature of pyrometallurgical methods, and they are energy-intensive, requiring the consumption of large amounts of fuel or electric power to melt and superheat all the charge constituents.

More than 1.5 million tons of sulfur and up to 2 million tons of iron are lost every year in the USSR alone in the pyrometallurgical processing of various copper ores and concentrates. Every year some 70,000 tons of zinc are lost with the slags and dust in smelting Urals copper-zinc concentrates. The discharge into the atmosphere of large amounts of toxic gases and aerosols is an essential disadvantage of modern pryometallurgical methods. In a number of cases, an effective way of obtaining much greater efficiency at existing pyrometallurgical enterprises is to redesign them on the basis of combining pryometallurgical and hydrometallurgical methods, i.e., to separate out a certain part of the concentrate with a high percentage of metal (to be sent for hydrometallurgical processing) at the concentration plants using a simplified scheme ensuring maximum extraction and to use the bulk middlings for the hydrometallurgical process stage.

Purely hydrometallurgical schemes which can be used to process low-grade bulk concentrates with a high level of technical and economic efficiency will have considerable advantages for most of the newly built enterprises. This provides prospects for considerable improvements to concentration plant schemes, with a simultaneous increase in the extraction of all the valuable constituents.

The copper industry provides an example of the rapid and widespread development of hydrometallurgical methods. At present a total of about 6.0 million tons of primary copper is being produced annually in the capitalist and the developing countries, more than 800,000 tons of which is hydrometallurgical copper.

There are some 50 enterprises throughout the world using hydrometallurgical methods to produce copper, 19 of them in the United States. From 1963 to 1973, copper production in the United States by hydrometallurgical methods rose from 7 to 20%, with a total production of 1.5-1.7 million tons per year.

The solvent extraction of copper from ammonia and sulfuric acid solutions has been mastered. The extractants used are solutions of alkyl- or benzyloxyoximes in kerosene (Lix-93 and Lix-94) and, more recently, Kelix-100 and Kelix-120, which are alkyloxyquinoline derivatives. The first plant operating a solvent extraction scheme was started up in the United States in 1968. There are now 12 enterprises in operation using solvent extraction technology in various countries (besides the USSR).

According to the forecast for the United States, in 1975 15% of all copper will be produced by solvent extraction. Copper produced in this way is 12.9 cents per kg cheaper than when the cementation method is used. The economic efficiency of the solvent extraction system will increase substantially with the production of copper powder from the reextract by hydrogen reduction in autoclaves.

The development by a number of firms in America, England, and India of hydrometallurgical schemes for processing sulfide copper concentrates is a major advance; these schemes are destined for large-scale industrial implementation in the near future. These methods will provide radical solutions to the problems of environmental protection. Having regard to the atmospheric pollution that is already taking place, the United States government was forced to pass a law (as long ago as 1970) under which a fine ranging from 2 to 20 cents is imposed for each kilogram of sulfur discharged into the atmosphere by an enterprise, making operation unprofitable in a number of cases.

According to forecasts by a number of foreign researchers, hydrometallurgical methods will undergo further development during the next decade; it is assumed in particular that hydrometallurgical production of copper will increase substantially.

As has already been observed, the greatest advances in hydrometallurgy in the past 20 years have been based upon the use of ion-exchange and solvent-extraction technology.

The manufacture of selective sorbents and extractants has been developed and mastered, and schemes for processing the ores and concentrates of non-ferrous, rare, and dispersed metals and gold have been perfected. Sorbents for sorption from pulps and solutions have been created, and the industrial production of the strongly basic gel-form anion exchangers AM, AMP, VP-1A, and VP-3A and the macroporous anion exchangers AM(p), AMP-p, and VP-1A(p) on the same basis, the bi- and polyfunctional anion exchangers AM-2B, EDE-10p, and AN-2f, the moderately basic anion exchangers AM-3 and VP-1P(p), as well as the extremely promising carboxyl ampholytes AMK, AMK-2, and VPK, and various phosphorus-bearing and phosphorus-nitrogen-bearing ion exchangers (the ampholytes AFI-5, AFI-7, VPF-1 and VPF-2) has been mastered. These ion exchangers are of high mechanical strength, which ensures minimum losses under the most severe operating conditions.

In correlating the large amount of work published in the world on the mechanism of non-ferrous metal sorption by ion exchangers, a clear relationship can be seen between the basicity of an ion exchanger and its affinity for various metal complexes.

In an overwhelming number of cases, macroporous ion exchangers have advantages over the corresponding gel forms in terms of sorption kinetics. In a number of cases the effect of stereochemical factors is clearly apparent; this can be determined by using copolymers produced from α-, β-, or γ-vinylpyridine with divinylbenzene.

Anion exchanger VP-3A(p), which is produced from α-vinylpyridine, has the most favorable matrix structure, ensuring high sorptive capacity in the whole range of concentrations by comparison with anion exchangers based upon α-β-vinylpyridines. This is characteristic of the sorption of vanadium, molybdenum, tungsten, and other metals which form large complex or polymer ions in solution.

The use of AM-3(p) and VP(p) moderately basic porous anion exchangers for vanadium, molybdenum, tungsten, columbium-tantalum, and other ores and concentrates has great potential value. Since these elements form polymer ions in solution, the kinetics of their sorption are determined to a substantial extent by the nature of the porosity and are particularly sensitive to structural stereochemical factors.

The development in 1953 of a process of metal sorption from pulps and sorption leaching was a great event in hydrometallurgy and ion-exchange technology. This process exceeds the traditional and classic filtration methods in intensity by hundreds of times, and by thousands of times in a number of instances.

The efficiency of sorption from pulps increases significantly when it is combined with leaching. In these circumstances improvements in leaching kinetics, reduced reagent consumption, and substantial increases in metal extraction are observed in many cases.

The sorption leaching method has been successfully used for over five years in the Kizil-Kum at the large Muruntau auriferous ore processing enterprise.

A sorption leaching process has been perfected for all the main types of auriferous ore, and it was adopted in 1972-1973 at the Kuranakh and Matrosov Plants. As a result, gold extraction rose by 15-20% at the Matrosov Plant and by 8-10% at the Kuranakh Plant by comparison with the filtration schemes previously used. Conversion of all the main hydrometallurgical enterprises in the gold-mining industry to sorption leaching is planned in the immediate future.

Sorption or solvent-extraction recleaning processes are used to produce metallic gold containing 99.99% Au. Pure cathode gold, from which high-purity metal is obtained, is separated out from the desorbate or reextract.

A sorption technology for processing copper, nickel-cobalt, molybdenum, and tungsten ores and concentrates has been developed and tested at pilot-plant level.

Various ampholytes of AMK, VPK, VPG, etc. type can be successfully used for copper sorption from solutions obtained by heap leaching and leaching in place, as well as for sorption leaching of oxidized copper ores and the removal of copper from nickel electrolyte.

A direct analogy exists between sorption and solvent-extraction processes, i.e., between solid and liquid ion exchangers. Physical and chemical forces of the same nature operate in sorption and in solvent extraction. However, the different states of aggregation of the absorbers involve great variations and produce specific characteristics in each of these processes.

The successive development of this viewpoint has made it possible to utilize the enormous amount of factual material on the chemistry and technology of ion-exchange

processes to create new types of extractant (liquid ion exchangers) and to develop a series of new specific solid sorbents by analogy with liquid absorbers or extractants.

Comparative evaluation of sorption and solvent-extraction processes has made it possible to define the most effective and optimal fields of application for each of these processes.

Liquid cation and anion exchangers or extractants containing ionogenic cation-exchange, anion-exchange, or chelatophoric groups are used in non-ferrous hydrometallurgy. The great potential of polydentate liquid polymer (oligomeric) extractants, produced for the first time in the USSR on a phosphate compound base (polyalkylphosphonitrilic acids), should be particularly noted. The organic diluent is an important factor in all cases in which liquid ion exchangers are used.

Many researchers have established that the absorbing power of an ion exchanger is intensified when the degree of basicity of the phosphoryl group increases and on transition from monodentate to polydentate absorbers, i.e., in the end to polymers.

Of the neutral organophosphorus compounds, phosphine oxides are the most efficient absorbers of heavy metals. The high distribution coefficients, steep isotherm, and great selectivity of phosphine oxides make them suitable for solving various difficult problems in hydrometallurgy.

The properties of a large class of phosphine oxide compounds and their various derivatives have been studied in detail. It has been established that removal of the electronegative substitute from the phosphorus atom intensifies the complexing properties of phosphine oxides.

A further increase in their effectiveness is achieved by the introduction of electropositive groups or radicals which intensify the basicity of the phosphine oxides. The aminophosphine oxides and phosphoric tris-amides are examples of such compounds.

Further improvements in solvent-extraction technology primarily involve the development of a process of extraction from pulps of various densities. The opportunity of varying selectivity within wide limits as a result of altering the structure of the hydrocarbon radical and the nature of the diluent is an advantage of liquid ion exchangers; they also have great potential by virtue of their kinetic characteristics.

For the present, processes of solvent extraction from solutions cannot compete with sorption from pulps, especially in concentrating valuable elements from extremely dilute solutions.

The high level of losses of liquid ion exchangers (extractants) is the main cause of the poor technical and economic characteristics of the process. The main task in improving the solvent-extraction process is to develop economic and effective methods of regenerating the extractant and solvent, i.e., to reduce specific losses substantially.

New opportunities are arising in hydrometallurgy as a result of the creation of processes which combine the advantages of sorption and solvent extraction.

One such combined method is the use of porous granules impregnated with an organic solvent and processes of solid ion exchanger desorption with liquid ion exchangers or neutral extractants.

Further developments in hydrometallurgy can be achieved by the extensive use of membrane technology methods, particularly electrodialysis using selective ion-exchange membranes. The problems of reducing the consumption of chemicals, improving the hydroelectrometallurgical processes, increasing the efficiency of oxidation-reduction reactions, and separating elements with similar properties are being solved successfully.

IN SITU, 1(1), 37-73 (1977)

PERMEABILITY FROM SINGLE AND MULTIPLE DETONATIONS IN BOREHOLES

C. R. McKee
Department of Mineral Engineering
University of Wyoming
Laramie, WY 82071

M. E. Hanson and R. W. Terhune
Lawrence Livermore Laboratory
University of California
Livermore, CA 94550

ABSTRACT

Relationships describing the permeability enhancement caused by explosive detonations in boreholes have been derived and combined to yield

$$k = k_c \frac{r_d^{-3f-3}}{(r_d^{-f-m} + n_o/n_c)^2} + k_o ,$$

for the case in which the stress decays asymptotically as a power law; k_c and n_c represent permeability and fracture density at the edge of the pulverized region near the cavity wall; f is a geometric attenuation factor; m is the dissipation due to real material effects; k_o is the original permeability, n_o the initial fracture density, and r_d the scaled radius. This relationship has been compared with available measurements from the American "Hardhat" nuclear shot, the French nuclear events in Hoggar granite, and a chemical explosive shot in coal near Kemmerer, Wyoming. Significant correlation between theory and experimental measurements is observed. A comparison between single and multiple detonations shows that permeability enhancement falls off steeply near the shot; however, enhancement can be considerable midway between two shots spaced 10 cavity radii apart. The degree to which enhancement can be significant depends on material properties and initial fracture density. Porosity distribution from the explosive is the dominant parameter in permeability enhancement.

INTRODUCTION

We are currently in the midst of an energy crisis, and it is generally recognized that a mineral crisis also looms on the horizon. Recent productivity trends in U. S. surface mining show the industry losing ground in comparison with other industries at home and abroad in competing for capital[1]. This is primarily a result of the fact that increases in equipment handling capacity have been more than offset by the need to turn to lower-grade ores. This situation has been further complicated by inflation and other factors[2]. Greater attention is, therefore, being focused on in situ processes for mineral recovery[3,4].

Methods of in situ recovery fall into three categories. First, an ore body may possess sufficient native permeability for direct in situ recovery through boreholes[5]. Secondly, if the natural permeability is low, stimulation by hydraulic fracturing, explosive detonation, or some other means will be necessary. Finally, the formation may be so impermeable that a modified in situ process involving partial mining and the use of explosives will be required to generate permeability sufficient for processing[6,7].

Considering the convenience and potential lower cost of borehole recovery, it would be very desirable to render as many deposits as possible amenable to this technique. For low-permeability deposits, an array of explosively loaded wellbores offers the possibility of creating a distribution of many fractures not achievable by other techniques. If fractures with sufficient porosity to create permeability can be generated, then a viable in situ recovery process may be possible.

Explosives are often discussed in the context of in situ recovery. However, only recently have serious attempts been made to understand the mechanisms controlling enhancement of permeability by means of explosives. See [8] for dicussion of previous theories.

THEORY

Many permeability models have been proposed[9,10]. The most widely accepted one is the Blake-Kozeny-Carmen[11] theory, in which the medium is viewed as a bundle of capillary tubes. Because permeability through fractures interests us here, we postulate a parallel arrangement of fractures instead. The flow from a single fracture of uniform width (w) and aperture (a) (see Fig. 1) is [12].

$$Q_f = - \frac{wa^3 \rho g}{12\mu} \frac{dh}{dr} \qquad (1)$$

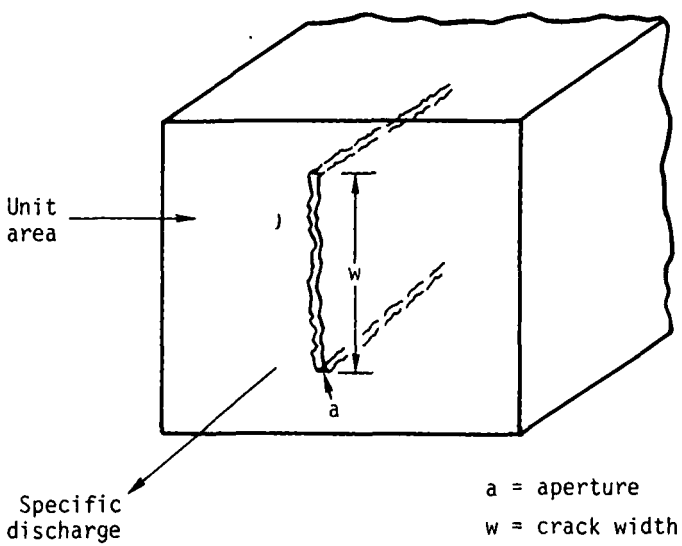

FIG. 1

Unit channel for calculating flow through a fracture. By considering a number of such channels penetrating the block, one derives a Blake-Kozeny-Carmen formula for fracture permeability.

The porosity (ϕ) from a group of fractures having similar properties is

$$\phi = naw \ , \tag{2}$$

where n is the fracture density (number/unit area). Multiplying equation (1) by n and eliminating a, the flow from a group of fractures is

$$a = -k \frac{\rho g}{\mu} \frac{dh}{dr} \ , \tag{3}$$

where the permeability (k) is given by

$$k = \frac{\phi^3}{12Tn^2w^2} \ , \tag{4}$$

and the tortuosity (T) is defined as

$$T = \left(\frac{\text{actual channel length}}{\text{direct distance between channel and points}} \right)^2 . \tag{5}$$

The tortuosity concept was first introduced by Kozeny and later modified by Carmen[10]. It accounts for the fact that pore (or fracture) channels are not straight. The ratio of actual to direct length appears twice, since it affects both the head gradient and fluid velocity. The fracture-density-width product in equation (4) can be expressed in terms of specific surface (fracture surface area/unit volume of solids) as

$$S = \frac{2nw}{1-\phi} \ . \tag{6}$$

Substituting into equation (4), we obtain

$$k = \frac{\phi^3}{CT(1-\phi)^2S^2} \ , \tag{7}$$

where C = 3 for fractures.

When fractures are pervasive (w = 1), then from equations (6) and (7), we obtain

$$k \propto \frac{\phi^3}{n^2} \ . \tag{8}$$

For a fixed porosity, equation (8) implies that increasing the fracture density will strongly decrease permeability.

To link explosion effects to either of the permeability equations above, the process must be somewhat idealized. We view the explosion as occurring in two stages, the first dominated by a large-amplitude stress wave, and the second involving an expansion of the cavity by high-pressure gases from the detonation. The effects of the first stage on the medium are of a dynamic nature, while those of the second stage extend over a much longer time interval and can be regarded as a quasistatic process. To obtain a description of permeability, these processes must be related to the fundamental equations for permeability.

According to Kutter and Fairhurst[13], the principal role of the stress wave is to initiate fractures. Griffith[14] postulated a failure criterion for real materials. From tensile tests, he learned that the average stress at rupture was small compared with the theoretical strength of the solid. He concluded that energy in the test piece was not uniformly distributed. At points where the cracks originate, high concentrations of strain energy must exist. We assume that these concentration points are macroscopic flaws in the material. A real geologic medium will contain a distribution of flaws having variations in length and orientation. We view flaws to be nucleation sites for fracture generation.

If similar specimens of a given material are subjected to failure tests, they do not all fail at the same stress. A distribution of breakage strengths will be found[15]. It can, therefore, be interpreted that the material contains a distribution of flaw strengths. Variation in stress levels from an applied load at flaw tips is proportional to the square root of their lengths[16]. Longer flaws will, therefore, have a higher probability of extending under a given applied stress.

The dynamic stress wave will cause all flaws whose strengths are less than the magnitude of the locally applied stress to extend. A relation between the growth of flaws or the increase in specific surface and energy can be obtained from comminution theory. Several comminution relations have been proposed. The one most applicable to our situation is Rittinger's Law, which states that an increase in specific surface area is directly proportional to the energy input:

$$S \propto E \, . \tag{9}$$

Rittinger's Law has been substantiated by the general scaling laws of Langefors and Kihlstrom [17] which have been verified for burden dimensions varying between 0.01 and 10 m with a 10^7 variation in explosive charge. Rittinger's Law has been further substantiated by Felts and others [18] in the laboratory and theoretically by Rose [19].

Creating fractures does not in itself generate permeability. This is because the stress wave propagates at the compressional-wave velocity (c_p), while fractures can grow in a rectilinear path at a maximum velocity of 1/3 c_p. Hence, the stress wave will inevitably outrun the fractures it generates. New fractures will then be initiated on other flaw sites in the material. At this moment in the process, the medium consists of a noninterconnected system of fractures with essentially no new porosity.

The second stage of the essentially continuous explosion process is dominated by the quasistatic expansion of the gas in the cavity. The cavity void space is produced by irreversible pressure-volume work of the explosive gases. Void space is created by irreversible radial compression and by the tangential tension of the surrounding rock. The fracture porosity will be proportional to the first invariant of the strain tensor [20],

$$\phi \propto \Delta \, , \tag{10}$$

where Δ is the first invariant and contributes to porosity only when it assumes positive values (dilatation). In stating equation (10), we have considered only explosion-induced porosity. Furthermore, the quasistatic, radial displacement and tangential stress caused by the gas pressure will result in linking a portion of the fractures created by the passage of the dynamic stress wave. Also, gas fracturing may contribute to linking of fractures.

Figure 2 shows the postshot configuration. The cavity's initial radius is r_o. The explosion springs the cavity to a larger radius r_c. The material initially between r_o and r_c has been compressed into a narrow region beyond r_c. This material, in trying to recover a fraction of its original size, is locked in. The tangential stress in the locked-in region gives rise to a compressive radial stress or effective pressure.

The two stages, dynamic and quasistatic, must now be given mathematical form. As mentioned earlier, the dynamic phase is responsible for creating surface area, a fraction of which is subsequently linked in the quasistatic cavity expansion stage. To obtain an expression for surface area, we must find the energy input per unit volume from Rittinger's Law. The power input per unit is[21]

$$P = T \cdot \dot{u} \ , \tag{11}$$

where T is the stress tensor and $\dot{u}$ is the particle velocity or time derivative of the displacement. The time average energy applied is determined by integrating equation (11) over a time interval $t_o \leq t \leq t_1$ to obtain

$$E = \int_{t_o}^{t_1} P \, d \, t \ . \tag{12}$$

Since fracture surface energy is so small, it is probably not possible to separate its energy from the much larger amount deposited irreversibly as strain energy and heat. We, therefore, assume that only a small fraction of the energy input acts to nucleate new

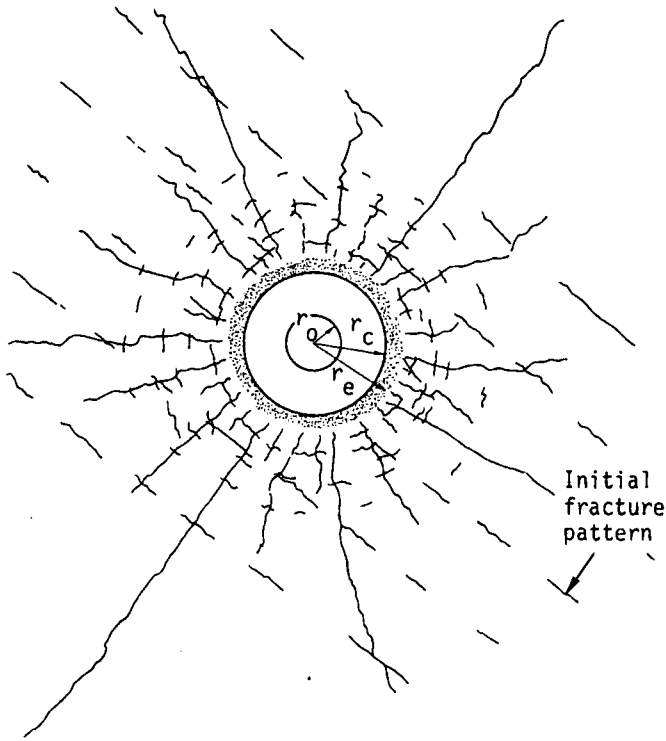

FIG. 2

An illustration of the post-shot configuration for an explosive fired in a borehole. The sketch includes an initial fracture pattern with the explosive patterns. The preshot radius is r_o, the post-shot radius is r_c, and the limit of significant compaction is r_e.

fractures or surface area. To simplify matters, we use the mean value theorem for integrals on equation (12) to obtain

$$E = \bar{P} (t_1 - t_o) , \tag{13}$$

where $\bar{P}$ is an average power input over the specified time interval.

The power for plane harmonic waves [20] and for cylindrical or spherical waves with dissipation [22] can be expressed in terms of particle velocity or stress squared. We may, therefore, write

$$E \propto \bar{\dot{u}}^2 \propto \bar{T}^2 . \tag{14}$$

Even for high stress levels, equation (14) is still a good approximation.

The contents of proportionality in equation (14) are immaterial, since we are only trying to determine functional dependence. The time interval is regarded as fixed. Hence, equation (14) may be used in Rittinger's Law to predict the incipient fracturing or surface area dependence with distance from the shot. The functional dependence can be predicted by applying the nonlinear continuum models to obtain the decay rates for particle velocity or stress. We must also include the effect of existing fractures. To be included with the explosion-induced fractures, the natural fractures should be pervasive and unhealed. Other critieria will be discussed below. For the case of pervasive fracturing ($w = 1$) and small porosity, surface area is directly proportional to fracture density or

$$S \simeq 2n . \tag{15}$$

Denoting the explosion-induced fractures by n_e and the naturally occurring ones by n_o, the total specific surface or fracture density becomes

$$n_t = n_o + n_e , \tag{16}$$

where

$$n_e = bE \tag{17}$$

and b is a constant of proportionality.

The second or quasistatic stage can be satisfactorily treated by using the bilinear elastic static solutions for dilatation around a pressurized cavity[24], which can be substituted into equation (10) to yield

$$\phi \propto \frac{f - \alpha}{r^{1 + \alpha}}, \tag{18}$$

where f = 1, 2 for cylindrical and spherical symmetries, respectively, and

$$\alpha = f - \varepsilon, \tag{19}$$

where ε is a small positive number related to the ratio of elastic constants in compression and tension (24).

If no bilinearity in the elastic constants is present, then from equations (18) and (19), dilatation, and hence porosity, would be identically zero. Bilinearity implies the existence of cracks and flaws that are necessary to create permeability.

The use of equations (18) and (19) is supported by displacement measurements reported by Borg[23]. These measurements were taken around a 61-kt nuclear explosive fired in granodiorite. Measured and calculated displacement follows a $1/r^2$ decay. Strain is proportional to the spatial derivative of the displacement and justifies the use of these equations. As discussed above, the effective pressure used as the boundary conditions for the analytic solutions arises from locked-in stresses caused by compressing material around the cavity (Fig. 2). Effective radius for the pressure is taken to be r_e.

Combining equations (8), (10), (16), and (17), we obtain the expression,

$$k_e \propto \frac{\Delta^3}{(n_o + bE)^2} \tag{20}$$

for the explosively created permeability. The effect of preshot permeability is included by adding to it the explosively generated permeability to obtain

$$k_t = k_e + k_o \ , \tag{21}$$

where k_o is the preshot permeability. If open fractures are present and contribute to permeability, then they should be included in k_o. Only pervasive, unhealed fractures having negligible porosity should be used to determine n_o.

Some limiting cases to equations (20) and (21) are evident. From equation (21), if initial permeability is high, then the explosive's contribution to the total permeability can be negligible. Secondly, if initial fracture density is large compared to that generated by the explosion, then substituting equations (18) and (19) into (20), we obtain

$$k_e \propto 1/r^6 \text{ (cylindrical geometry)} \tag{22}$$

$$k_e \propto 1/r^9 \text{ (spherical geometry)} \ , \tag{23}$$

where ε is small compared to f.

Hence, the effect of the explosive decays strongly with distance. On the other hand, if the material is relatively competent or if explosion-induced fractures dominate the initial fracture density, we obtain

$$k_e \propto \frac{\Delta^3}{E^2} \ . \tag{24}$$

From Selberg[25], energy decays asymptotically in the elastic limit as

$$E \sim 1/r^2 \text{ (dynamic, spherical geometry)} \tag{25}$$

$$E \sim 1/r \text{ (dynamic, cylindrical geometry)} \tag{26}$$

Substituting for dilatation from equation (18), we find (for $n_e >> n_o$ and in the elastic limit)

$$k_e \propto 1/r^4 \text{ (cylindrical geometry)} \tag{27}$$

$$k_e \propto 1/r^5 \text{ (spherical geometry)} \ . \tag{28}$$

In the general case, energy will obey a power law decay

$$n_e = bE \sim 1/r^{f+m} , \tag{29}$$

where f is defined as before (f = 1, 2 for cylindrical and spherical geometry, respectively). In the perfect elastic case, m = 0 (asymptotic limit). However, in general, m is greater than zero. For a competent formation ($n_e >> n_o$), permeability will have the form

$$k \propto \frac{r^{2m}}{r^{3+f}} . \tag{30}$$

If m = 0, then we recover equations (27) and (28). Real materials will exhibit dissipation and deviate from elastic behavior (i.e., m will be greater than zero). From equation (30), we see that explosion-created permeability can decay much more slowly than for the perfectly elastic case or for the case where the initial fracture pattern dominates. A physical interpretation of this is readily apparent. For the perfectly elastic case, we note that fractures must exist as continuous rays emanating from the cavity. On the other hand, a real material will exhibit a fracture pattern having a distribution of fracture lengths. For a dissipative material, fracture density decreases more rapidly with distance from the cavity than in the elastic limit. There is always competition between fracture density and porosity. When fracture density decreases with distance from the borehole, as in a real material, surface area declines more rapidly tending to compensate for the decrease in porosity. Hence, the result is a slower decrease in permeability away from the explosive cavity. This results because an increase in surface area increases drag and, hence, resists flow. On the other hand, making porosity larger increases the cross-sectional area to flow, thus decreasing resistance.

EXPERIMENTAL RESULTS FROM SINGLE EXPLOSIVE DETONATIONS

Hardhat (Spherical Geometry)

The Hardhat event was a 5-kt nuclear explosion in granite. Boardman and Skrove[26] performed extensive air permeability measurements around the Hardhat nuclear chimney. Their raw data shows considerable scatter, some of it attributable to their measurement techniques. We have applied a selection criterion[24] to their data to obtain a consistent set. As discussed in reference [24], the stress wave decayed approximately as the elastic case. Initial fracture density was taken to be small compared to explosively created fractures. Borg[23] reports that preshot material was broken by fractures, faults, and shear zones, most of which were healed (cemented by minerals of a later origin). She further states that the consensus among geologists is that joints and fractures are shortlived, i.e., terminated within a few yards. The typical flaw size is, therefore, small compared to the cavity radius (20 m) and justifies ignoring the effects of the existing fractures. Figure 3 shows the comparison between permeability measurements and equation (28), the theoretical prediction for an elastic material. Preshot permeability measurements were not performed. We, therefore, assume $k_o \simeq 0$. Agreement between the theoretically predicted slope and the experimental data is quite good.

Hoggar (Spherical Geometry)

Delort and Supiot [27] report results of permeability measurements at the French Hoggar test site in the Sahara. Their measurements give a detailed picture of the permeability distribution around the postshot cavities and resulting chimneys. They analyze a number of detonations of varying yields and present the results in terms of scaled radii. We will not compute the dilatation

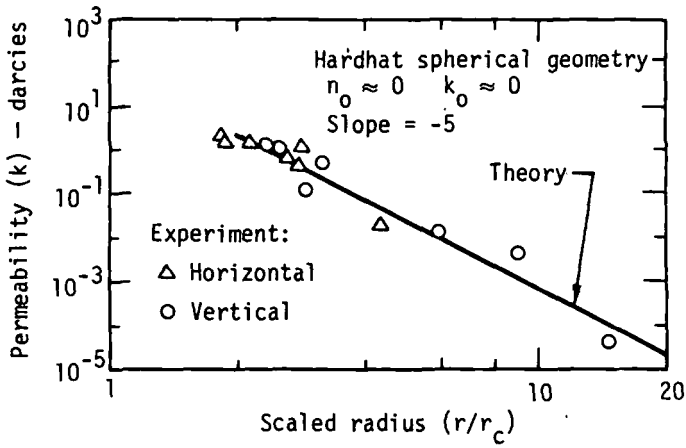

FIG. 3

Comparison of theoretical and measured permeability, k, as a function of distance scaled in terms of the cavity radius r_c. Permeability was measured in both horizontal and vertical holes and is independent of direction. The experiment was Hardhat, a 5-kt nuclear explosion in granite at the Nevada Test Site.

(and, hence, the porosity dependence) near the chimney relief zone. Instead, we will use their data from the region unaffected by chimney relief so that our pressurized cavity solution, equation (18), will be valid.

The preshot fracture density is reported to be on the order of 1 to 0.5 per m [28]. Explosion-induced fractures near the cavity wall are closely spaced, producing particles having dimensions characteristic of sand or gravel[27]. Fracture density decreases from the crushed zone to a distance of 3.6 cavity radii, at which it is 20 times greater than the natural fracture density[28]. Beyond this distance, drill cores separate into thin disks, indicating the presence of appreciable residual stresses. This

phenomenon occurs to approximately 5 cavity radii. Fracturing in this zone is difficult to quantify, and we assume that it continues to decline in accordance with equation (17). Various investigators have taken great pains to quantify various fractured zones. However, permeability data in the events we discuss do not appear to exhibit a discontinuous behavior. We, therefore, assume that fracture density, or at least that portion responsible for permeability, decays in a continuous manner as predicted by equation (17). This is not surprising, in view of the fact that most natural geologic materials contain a distribution of flaws or weak points so that a unique tensile strength cannot be given. No two volumes of rock will, therefore, fail at the same stress. This results in a blurring of the boundaries between regions displaying different fracturing effects, giving rise to a continuous fracture density dependence with distance from the cavity.

In view of the fact that explosion-induced fractures are much more numerous than the natural fracture density, we ignore n_o in equation (16). Beyond 4 to 5 cavity radii, the explosion-induced fractures will, with increasing distance, blend into the natural fracture system by using equation (21). The undisturbed permeability appears to be on the order of 5×10^{-3} μm^2 (5 md) [27].

Explosion-created fracture density can be predicted by combining equations (14) and (17) to obtain

$$n_e \propto \dot{u}^2 . \tag{31}$$

Terhune's analysis[29] indicated that particle velocity attenuates with distance as

$$\dot{u} \sim 1/r^{1.6} , \tag{32}$$

in agreement with Hoggar measurements.

Equation (32) is an asymptotic result, valid for distance greater than 1.5 cavity radii. Nearer the explosive, attenuation is more rapid. The implications of this will be discussed below.

Substituting equation (32) into equation (31), we find that the fracture density should decay asymptotically as

$$n_e \propto 1/r^{3.2} , \tag{33}$$

which corresponds to a value for m of 1.2 from equation (21). We recall that m > 0 implies greater energy dissipation due to inelastic effects.

Substituting equation (33) into equation (30), with f = 2, m = 1.2 yields

$$k_e \propto 1/r^{2.6} . \tag{34}$$

Substituting into equation (21) with k_o = 5 millidarcies (md) and scaling r with respect to the cavity radius, we find

$$k_t = k_c \left(\frac{r_c}{r}\right)^{2.6} + 5 \text{ (in md)} , \tag{35}$$

where k_c is the intercept at the cavity wall. An approximate fit to the Hogger data given by Delort and Supiot[27] gives a value of

$$k_c = 1700 \text{ md} . \tag{36}$$

The predictions of this theory are in good agreement with the few available observations as is shown in Fig. 4. Data points were taken from reference[27].

We anticipate that energy decay rates will be higher at distances less than 1.5 to 2 cavity radii. In particular, if energy decays more rapidly than $1/r^{4.5}$ ($m \geq 2.5$), the permeability decay by equation (28) (f = 2, spherical geometry) must flatten and decrease as the cavity wall is approached. A decrease in permeability near the crushed zone was reported by Derlich [30]. We have not carried out the numerical calculations in this close-up region to predict the slope. Additional energy absorption due to phase changes also occurs in this region. It is not clear

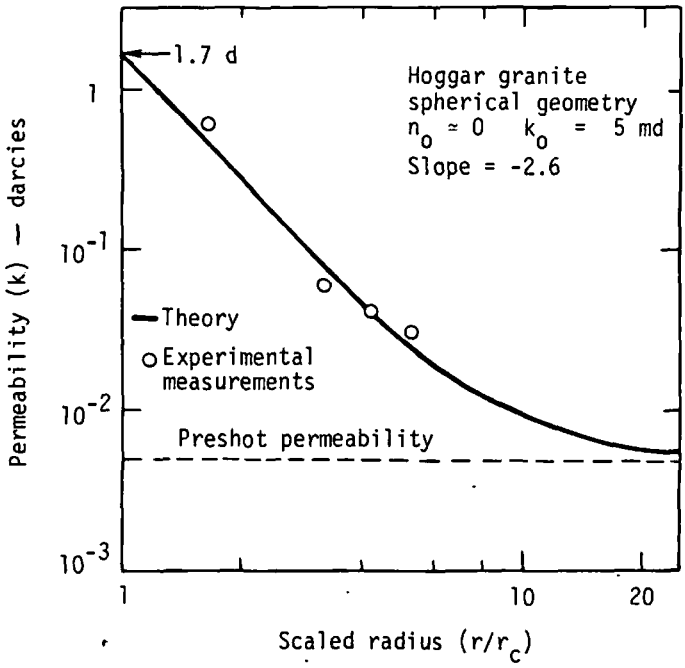

FIG. 4

Comparison of theoretical and measured permeability values. The log of permeability, k, is given as a function of distance scaled in terms of cavity radius r_c. The data is taken from a series of nuclear detonations in the Sahara by the French. The medium was granite.

that Rittinger's Law will hold in such an extremely nonlinear regime. However, such extreme conditions are significant only within 1 to 2 cavity radii near nuclear detonations and are of minimal importance with chemical explosives.

Kemmerer Coal (Cylindrical Geometry)

As part of a coal gasification program, the Lawrence Livermore Laboratory conducted an explosive test in a coal outcrop

near Kemmerer, Wyoming [31]. A cylindrical, high-explosive charge (Teledet*), 5.5 m long, 0.1 m in diameter, and weighing 59 kg, was detonated in a vertical borehole. The center of the explosive charge was buried 15 m below the ground surface in a 26-m-thick, subbituminous coal seam. The postshot cavity radius was estimated from calculations to be 17 cm. The coal outcrop was highly jointed, with two joint sets normal to each other. The coal seam was bedded with the bedding dipping at 18°. Logs indicated that bulk elastic properties of the undisturbed coal did not vary from hole to hole. All permeability tests were conducted in situ using packers. Pressure testing was performed using water injection until a quasisteady condition was attained. Permeability was then measured at steady state.

In Fig. 5, the horizontal bars in the boxes are values of repeat measurements in the same hole. They represent the uncertainty in permeability. Width of the boxes along the radial direction is a measure of drill hole deviation from the vertical. Further details concerning the experiment can be found in the works of Hearst[31] and Butkovich[32].

Preshot permeability as well as initial and postshot fracture frequency measurements displayed considerable scatter. No velocity or stress attenuation measurements or calculation near the explosive have been reported. Because of these factors, we compare the postshot permeability to the linear elastic solution, equation (27), for cylindrical geometry. This equation does not include the initial fracture density or permeability. Indeed, one can find some measurements of preshot permeability higher than some postshot measurements [31]. Given the data, one cannot significantly improve upon this estimate. However, if initial fracture density is negligible (a fact which is not at all clear), one would expect the permeability to decay less rapidly. Equation (3) with $m > 0$ (inelastic behavior, $n_o = 0$) predicts a slower

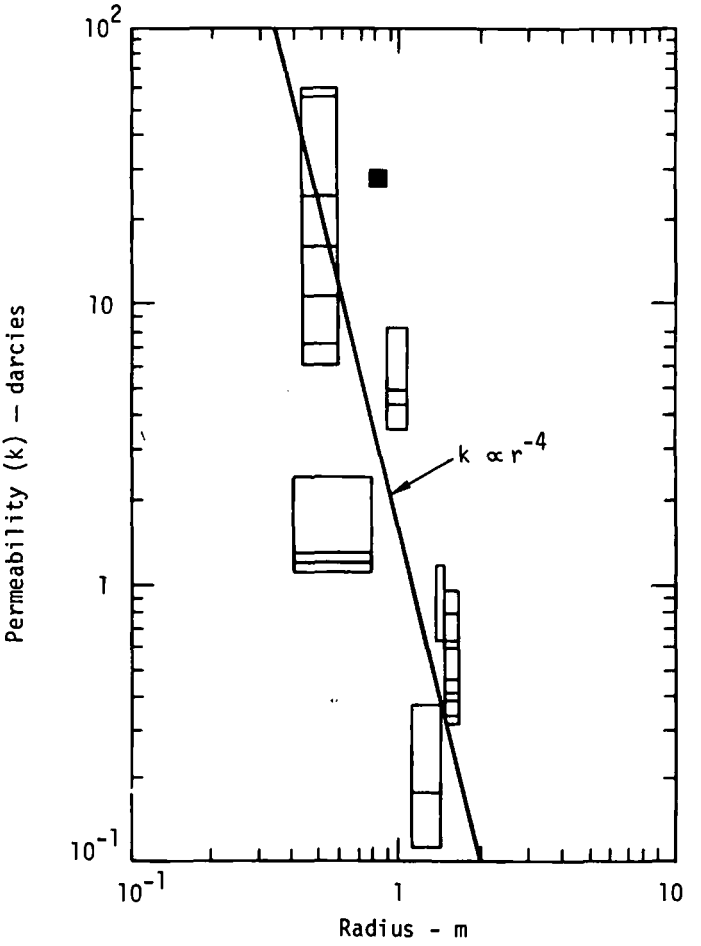

FIG. 5

Post-shot permeability vs radius for a chemical explosive detonated in a coal seam. The emplacement geometry possessed cylindrical symmetry. Permeability is in darcies, while the radial distance in meters is measured from the axis of symmetry. The small box on the upper right represents two measurements in the same borehole.

decay. In fact, a least squares fit to the data, assuming that measurements are scattered lognormally, results in the fit

$$k = \frac{427}{(r/r_c)^3} . \tag{37}$$

The exponent 3 is less than the elastic limit, corresponding to $m = 1/2$ in equation (30). It implies that particle velocity should decline as $r^{-0.75}$ as opposed to $r^{-0.5}$ for the linear elastic case. This is in agreement with the trend for real materials to display higher attenuation than the ideal elastic case.

In view of the experimental scatter, it is risky to assign a definite slope to the entire permeability distribution. It is entirely possible for more than one mechanism to operate, resulting in a continuously changing slope as in the Hoggar example above. This can occur depending on the relative importance of initial permeability, fracture density, and energy dissipation. These are not precisely known because of the high scatter in the measurements.

THEORETICAL COMPARISON OF SINGLE AND MULTIPLE DETONATIONS

The effect of multiple detonations is a straightforward extension of the theory for single charges if certain assumptions are made. These are: (1) that energy fluxes from a number of detonations can be superimposed, (2) that the fracture surface area is directly proportional to cumulative energy input, and (3) that the elastic potential can be superimposed from many cavities to result in a total dilatation which, when positive, is proportional to the porosity increase. The third assumption is not strictly correct unless the bilinear effect is small. The three explosive events discussed above (Hoggar, Hardhat, and Kemmerer coal) tend to substantiate assumption three. We can conclude, therefore, that dilatation, to a close approximation, behaves linearly and that superposition is valid.

We will not attempt to treat this subject in exhaustive detail. We will rather limit our discussion to the case of two explosives, cylindrical charges separated by a distance of 10 cavity radii between their lines of center. We further assume that their length is large compared with the separation distance.

Other implied assumptions are the same as for single charges: (1) that gravitational stresses are small compared to the residual strains induced by the explosive, (2) that free surface relief effects are unimportant, and (3) that the cavity does not depart from symmetry assumptions used in deriving the appropriate solutions for porosity or energy.

To calculate fracture density, porosity, and permeability from two charges, we first compute their functional dependencies for a single charge. Constants for these equations will be normalized to the cavity wall for a single explosive. Increases due to effects of another nearby explosive will be observed by comparison with the effects due to a single explosive.

The fracture density from equations (16), (17), and (29) is

$$n = n_o + \frac{n_c}{r_d^{(f+m)}}, \tag{38}$$

where

$$r_d = r/r_c \tag{39}$$

and n_c is the fracture density at $r = r_c$ (cavity wall) due to the explosive. Equation (29) for radial dependence is in general an asymptotic law valid when $r > \sqrt{2}\, r_c$ (r is measured from the center of the cavity). Since the energy dissipation rate may be higher as r approaches r_c, we expect that the actual fracture density will be greater than n_c, thus causing a reduction in permeability near the cavity wall below that shown in Figs. 6 and 8. However, n_c will still be correct for the bulk of the explosively effected region, and it will, therefore, be instructive to observe its enhancement due to a nearby detonation. Values of k_c, n_c must,

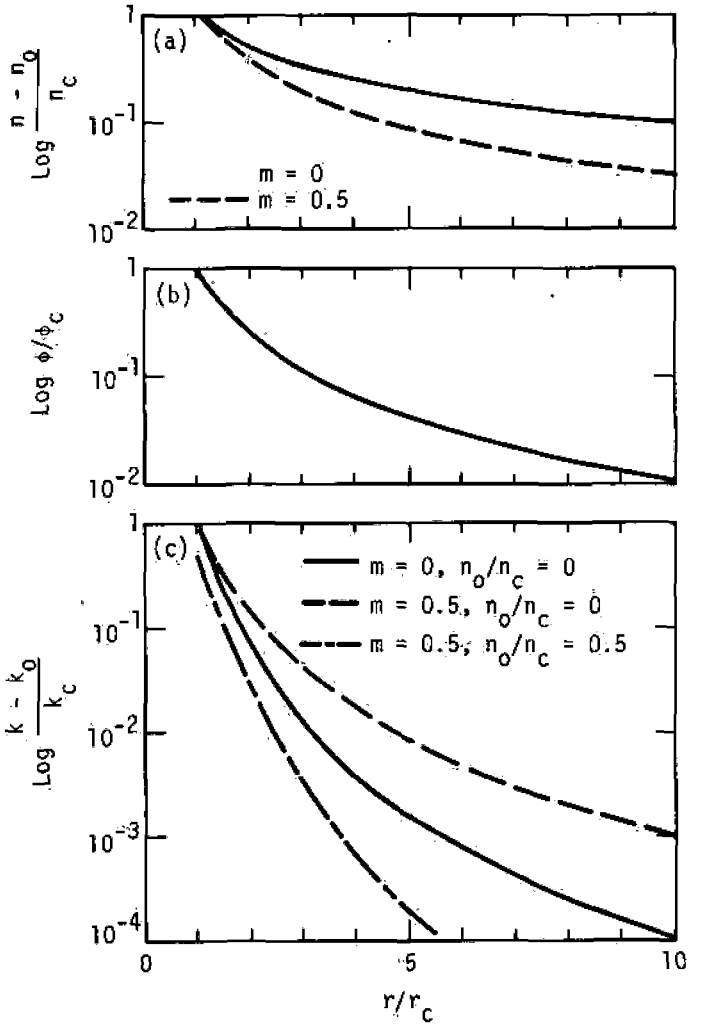

FIG. 6

(a) Explosion-induced fracture-density enhancement, normalized to the fracture density at the cavity wall as a function of scaled distance. The solid curve represents a semielastic medium (m=0) and the dashed line a dissipative media (m=0.5). (b) Explosion-induced porosity, normalized to porosity at the cavity wall as a function of scaled distance. (c) Explosion-induced permeability enhancement, normalized to the permeability at the cavity wall. Three cases are shown: (1) a semielastic medium with zero initial fracture density, (2) a dissipative medium (m=0.5) with zero initial fracture, and (3) a dissipative medium with an initial fracture density of half the explosion-induced fracture density at the cavity wall (m=0.5).

lead one to expect a more gradual decline in permeability with distance, which is incorrect.

All three curves show a slight decrease in permeability as the cavity wall is approached. In Fig. 8c, it is only noticeable in the bottom curve. The decrease for the top two curves in Fig. 8c is due to the fact that porosity decays more rapidly than fracture density, resulting in a higher contribution to surface area as each explosive is approached. The decrease in permeability for the bottom curve is due to increased surface area from the presence of an initial fracture density. The values at $r/r_c = 5$ are doubled over that for a single charge for the top two curves. However, permeability for the bottom curve is enhanced by a factor of 5. This is due primarily to the increased porosity from the second explosive. Enough porosity is added to compensate for initial fracture density.

If detailed calculations were performed, permeability should flatten due to increased energy dissipation as the cavity walls are approached. While this can be calculated, extending our analytic solution for porosity into the region would be tenuous since it is in this locked-in zone that the boundary condition is created for the analytic solution. Porosity in this crushed region is not likely due to random rotation of grains.

The optimum permeability distribution from Fig. 11c is produced in a dissipative medium with small initial fracture density. Such an effect can be expected in a competent formation.

DISCUSSION

Most of the key equations, such as (14), (17), (18), and the superposition arguments have been based on the assumption that the medium behaves in an approximately elastic manner. We would, therefore, expect the results to be valid for rocks which fail in the brittle region due to response from an applied load. Rocks which respond in a ductile manner may have large pore space com-

paction and exhibit cataclystic flow in which individual grains are rotated and fractured. As mentioned above, it is not clear whether Rittinger's Law would hold under such extreme conditions. Also, a significant loss in porosity would invalidate equation (32), which assumes that preshot and explosion-created permeability could be superimposed. In ductile response, it is likely that most of the preshot porosity would be removed, thus severely reducing preshot permeability. While this effect may be corrected by multiplying k_o by the ratio of postshot to preshot porosity function contained in equation (7), the remainder of the theory can only be expected to furnish a crude approximation at best.

It is also interesting to note that dilatation must always be identically zero in the absence of a bilinear effect. Under such circumstances, porosity cannot be produced from any number of stressed boreholes.

Although permeability declines fairly rapidly, appreciable permeability can still be achieved. Referring back to Fig. 11c, we note that if k_c were 100 darcies, permeability at $r_d = 5$ for the best case (top curve) would be 158 millidarcies. Depending on the application, this could be a substantial permeability. If drill holes having a 0.3-m (1-ft) diameter were drilled and sprung by an explosive by a factor of 3 (varies with depth), drill holes separated by a distance 10 r_c would then be 15 ft apart. Wider separation would produce lower permeability enhancement, which may still be acceptable for many in situ processes.

The theory we have developed does not distinguish between simultaneous and sequential detonations. The role of the stress wave is to nucleate flaws into fractures, which are connected in the expansion phase. If the medium possesses flaws having sufficient length and number for this purpose, then producing additional cracks in a medium by one explosive for the other to act on will have little effect. However, in a competent material with low-

flaw-density, sequential detonation may have an important effect on permeability. This is one of the factors that must be addressed in future experiments.

In order to implement this theory, accurate calculations of stress or particle velocity decay are required. It is especially true for the case of low initial fracture density. This is because equation (35) (low n_o) combined with equation (42) involves the particle velocity to the inverse fourth power. A small error in its exponent (± 0.2) would result in an exponent for permeability decay which is off by nearly 1 in the exponent. Over a distance of 10 cavity radii, the predictions could be in error by a factor of 10. Most numerical calculations of particle velocity exhibit higher attenuation than is actually observed. This is due to the fact that artificial dissipative mechanisms are introduced to stabilize the calculations. This effect can increase the decay to as much as $1/r^{1.25}$ instead of $1/r$ in the elastic limit (spherical geometry), resulting in considerable error. Hence, checking numerical calculations against experimental measurements of particle velocity is highly desirable.

SUMMARY

Several theories of permeability were first discussed and analyzed. These theories were deficient in that they correlated permeability only with the degree of damage or fracture density. They were not based on any fundamental equations related to permeability, and they ignored porosity. Our investigation demonstrated that permeability should be inversely proportional to the fracture density squared rather than directly proportional as previous workers had supposed. The significance of porosity was clarified and quantified.

The theory of McKee and Hanson[24] was extended to include the effects of preshot fracture density, inelastic dissipation, and multiple explosive charges. This theory divides the explosion process into a dynamic and quasistatic stage. The dynamic part is responsible for generating a distribution of fractures. Fracture density was related to energy flux through Rittinger's Law. Fractures are linked by hoop stress induced by the continuing quasistatic expansion of the cavity by high-pressure gases, and by initial momentum imparted to the cavity wall from the shock wave.

Existing preshot fractures having negligible porosity and a characteristic dimension several times larger than the cavity were added to the explosively created fractures. Fractures smaller than the cavity were regarded as part of the native flaw distribution, which furnishes nucleation sites for stress-wave-generated fractures. Guidelines for treating natural fractures having porosity comparable to that induced by the explosive were also suggested.

Fracture density generated by explosives was expressed in equation (28) in terms of energy flux as

$$n_e = bE \ .$$

As indicated in equation (25), energy was found to be proportional to particle velocity or stress squared.

Porosity was viewed as being deposited and sustained by irreversible compression of rock into a stressed or locked-in region concentric with the cavity. This effect was satisfactorily represented by a static analytic solution for a pressurized cavity. We remarked that elastic constants must exhibit different values in compression and tension to produce a non-zero dilatation. In equation (21), porosity was taken to be proportional to dilatation. Porosity decays as $1/r^2$ and $1/r^3$ around a cylindrical and spherical cavity, respectively.

Permeability from a single charge was found to have the form,

$$k = k_c \frac{(\phi/\phi_c)^3}{(n/n_c)^2} + k_o .$$

Additionally, we found that if stress obeys a power law relation, permeability will decline as

$$\frac{k - k_o}{k_c} = \frac{r_d^{-3f-3}}{(r_d^{-f-m} + n_o/n_c)^2} ,$$

where f = 1, 2 (cylindrical or spherical geometry) and m represents inelastic dissipation. This equation will be true for most explosives beyond a distance of 1.5 to 2 cavity radii measured from the axis of symmetry.

Various limits of this equation were explored. It was noted that a low initial fracture density and increased energy dissipation (m > 0) tended to produce a permeability distribution with a more gradual decline. The worst case is obtained when the medium possesses a natural fracture density comparable to that induced by the explosive. Then, permeability declines as $1/r^6$ in cylindrical and $1/r^9$ in spherical geometry. Such an effect may occur in a poorly cemented or loosely consolidated sandstone and in other friable materials.

The case of multiple explosives was then analyzed, and it was found that fracture density and porosity could be directly superimposed. However, resulting fracture density and porosity must be combined into one permeability formula. If the explosives are identical, these quantities can be substituted directly into equation (54). Various cases involving dissipation and initial fracture density were examined.

It was concluded that while permeability will decrease strongly, in many cases, substantial permeability can still be achieved provided fracture density and shot spacing are closely controlled.

ACKNOWLEDGMENT

The authors wish to thank Iris Borg for her many enlightening discussions concerning the pre- and postshot fracturing phenomena around the nuclear shots. The authors also acknowledge discussions with Dave Leach, Joe Hearst, and Ted Butkovich concerning the chemical-explosive experiment in coal near Kemmerer, Wyoming. This work was performed under the auspices of the University of Wyoming, and under ERDA Contract No. W-7405-Eng-48.

FOOTNOTES

*Reference to a company or product name does not imply approval or recommendation of the product by the University of Wyoming or the University of California or the U.S. Energy Research and Development Administration to the exclusion of others that may be suitable.

REFERENCES

1. Michaelson, S. D. Wanted: new systems for surface mining. Engng Min. J. 175 (10), 63 (1974).

2. Bailly, P. A. The problems of converting resources into reserves. Min. Engng 28 (1), 27 (1976).

3. Aplan, R., McKinney, W., and Pernichole, A. Solution Mining Symposium, AIME, New York (1974).

4. Laswell, G. W. Wanted: rotary drilling technology for in situ mining systems. Min. Engng 28 (1), 22 (1976).

5. White, L. In situ leaching opens new reserves in Texas. Engng Min. J. 176 (7), 73 (1975).

6. Lang, L. and Morrey, W. Scientific blasting for in situ leaching proves successful at Agnew Lake mines. Engng Min. J. 177 (1), 100 (1976).

7. Fletcher, J. In-place leaching-Miami mine-Miami, Ariz. Soc. Min. Engrs AIME, Trans., 250, 310 (1971).

8. McKee, C. R., Hanson, M. E., and Terhume, R. W. "Permeability from Single and Multiple Detonations of Explosive Charges. World Mining and Metals Technology, 1, Alfred Weiss, Ed., AIME, 365 (1976).

9. Scheidegger, A. The Physics of Flow Through Porous Media, 3rd ed. 124-150, Univ. of Toronto Press, Toronto (1974).

10. Bear, J. Dynamics of Fluids in Porous Media, 162-175, Amer. Elsevier, New York (1972).

11. Carmen, P. Fluid flow through granular beds. Trans. Inst. Chem. Engrs, London 15, 150 (1937).

12. Lamb, H. Hydrodynamics, 582, Dover Publ., Inc., New York (1945).

13. Kutter, H. K. and Fairhurst, C. On the fracture process in blasting. Int. J. Rock Mech. Min. Sci. 8, 181 (1971).

14. Griffith, A. A. Theory of Rupture. Proc. First Int. Cong. Appl. Mech., 55-63, Delft, The Netherlands (1924).

15. Weibull, W. A statistical theory of the strength of materials. Ingvetensk Aka. Handl. No. 149 (1939).

16. Sneddon, I. N. and Lowengrub, M. Crack Problems in the Classical Theory at Elasticity, 29, John Wiley and Sons, Inc., New York (1969).

17. Langefors, U. and Kihlstrom, B. The Modern Technique of Rock Blasting, John Wiley and Sons, Inc., New York (1967).

18. Felts, L., Clark, G., and Yancik, J. A laboratory method of determining the thermodynamic efficiency of high explosives. Trans. AIME, 318 (Mar. 1956).

19. Rose, H. E. A comprehensive theory of the communition process. Proc. 2nd European Symposium on Size Reduction (1966), Verlag Chemie, Amsterdam (1967). Decema-Monograph No. 993-1026.

20. Jaeger, J. C. and Cook, N. G. W. Fundamentals of Rock Mechanics, 199, Champman and Hall, London (1969).

21. Achenbach, J. D. Wave Propagation in Elastic Solids, 166, North Holland, New York (1973).

22. Hanson, M. and McKee, C. SAFE (Synergetic Acoustic Fracturing Effect), Rept. UCRL-51822, Lawrence Livermore Laboratory, Livermore, CA (1975). To appear in AIME Trans.

23. Borg, I. Y. Some Shock Effects in Granodiorite to 270 Kilobars at the Piledriver Site, Vol. 16, Geophysical Monograph Series AGU, Washington, D.C. (1972).

24. McKee, C. and Hanson, M. Explosively created permeability from single charges. Soc. Pet. Eng. J. 15, 495 (1975).

25. Selberg, H. L. Transient compression waves from spherical and cylindrical cavities. Arkiv for Fysik 5, 97 (1952).

26. Boardman, C. R. and Skrove, J. Distribution in fracture permeability of a granitic rock mass following a contained nuclear explosion. Trans., AIME 237, 619 (1966).

27. Delort, F. and Supiot, F. Nuclear stimulation of oil reservoirs, Proc. Symposium on Engineering with Nuclear Explosives, CONF 700101, Vol. 1, 649, Amer. Nuc. Soc., Hinsdale, Ill. (1970).

28. Faure, J. Research on Geologic Effects of Underground Nuclear Explosions in a Sahara Granite Massif, translation, Lawrence Livermore Laboratory, Livermore, CA (Feb. 1972).

29. Terhune, R. W. Comparison of Computer Model Predictions of Nuclear Explosion Effects in Hoggar Granite with Experimental Measurements, Rept. UCRL-74306, Lawrence Livermore Laboratory, Livermore, CA (1972).

30. Derlich, S. Underground nuclear explosion effects in granite rock fracturing. Proc. Symposium on Engineering with Nuclear Explosives, CONF 700101, Vol. 1, 505, American Nuclear Society, Hinsdale, Ill. (1970).

31. Hearst, J. R. Fractures Induced by a Contained Explosion in Kemmerer Coal, Rept. UCRL-51790, Lawrence Livermore Laboratory, Livermore, CA (1975).

32. Butkovich, T. Correlations Between Measurements and Calculations of High-Explosive-Induced Fracture in a Coal Outcrop. Int. J. Rock Mech. Min. Sci. 13, 45 (1976).

NOTICE

subcontractors, or their employees, makes any warranty, express or implied, or assumes any legal liability or responsiblity for the accuracy, completeness or usefulness of any information, apparatus, product or process disclosed, or represents that its use would not infringe privately-owned rights."

METALLURGY

HEAVY NON-FERROUS METALS

THE PRESENT SITUATION AND PROSPECTS FOR THE DEVELOPMENT OF ELECTROLYSIS OF AQUEOUS SOLUTIONS

UDC 669.2:621.357.1

A. L. Rotinyan and V. L. Kheifets

Electrochemical processes in aqueous solutions are used in metallurgy for electrolytic refining of metals or for extracting them from solution (electroextraction).

Electrochemical refining is economically advantageous for, e.g., the separation of gold and silver from copper, removing platinoids from nickel, and for the production of high-purity metals.

Processes of electroextraction from solutions after leaching make it possible to organize a reagentless closed circuit producing metal of high purity.

The high purity of the cathode metal is usually regarded as due to the high separation factor value characteristic of electrochemical processes, due to differences in the standard and equilibrium potentials of the electrode reactions. However, the following must be borne in mind when selecting process conditions in complex cases of separation.

The joint discharge of any two types of ion takes place at a common cathode potential. The view is accepted [1,2] that equality of the sum of the equilibrium potential and the overvoltage in the joint reactions is the condition which determines the possibility of joint discharge. It is accepted here that the equilibrium potential of a given type of ion is constant for a given solution composition, and the condition for joint discharge is written as follows [1,2]:

$$\varphi^{0'} + \frac{RT}{z'F} \ln a' + \eta' = \varphi^{0''} + \frac{RT}{z''F} \ln a'' + \eta'', \quad (1)$$

where ϕ^0 are the standard potentials, z are the valences, a are the activities of the ions, and η are the respective reaction overvoltages.

This is not a precise statement. In the joint discharge of two types of ion which crystallize in a common lattice their activity in the evolving alloy is not unity and equation (1) should be written as follows:

$$\varphi^{0'} + \frac{RT}{z'F} \ln \frac{a'_{soln.}}{a'_{alloy}} + \eta' = \varphi^{0''} + \frac{RT}{z''F} \ln \frac{a''_{soln.}}{a''_{alloy}} + \eta''. \quad (2)$$

Attention should be given to the fact that both magnitudes (activity in the alloy a_{alloy} and the overvoltage for metal evolution η) are interdependent, because they are functions of partial current density; this functional link is linear for the alloy metal content and logarithmic for the overvoltage. Thus the relationship expressed by equation (2) proves to be much more complex than is apparent at first glance.

It is very easy to calculate the metal content of an alloy for the idealized case in which both metals are discharged without chemical and concentration polarization if the equilibrium potentials are known and the alloy which forms is ideal. However, such a calculation cannot even be regarded as provisional. Assessment of the composition of the alloy is made even more complicated by the fact that the functional link between the activity of a constituent and its concentration may take various forms, depending upon whether a solid solution or intermetallic compounds are formed.

When an intermetallic compound is formed, the depolarization effect may become so great that there may be joint discharge of the ions of two metals which are far apart in the voltage series.

Thus it is impossible in principle in the cathodic evolution of metals to achieve absolute separation of the two constituents.

The practical possibility of separation will be determined by the ion concentrations in the solution, the standard potentials, and the overvoltages, as well as by the composition and properties of the solid phase.

The following are the substantial advantages of electrochemical methods:

ecologically clean cycles can be set up;

associated elements can be separated from the main metal fairly completely, to obtain intermediate products suitable for further processing.

Electrochemical refining and electroextraction are now widely used in the production of copper, zinc, nickel, and lead. Methods of producing pure manganese, cobalt, antimony, and chromium by electrolysis have been developed and put into practice in recent decades.

In addition to its great advantages, the electrolytic method of producing metals also has substantial drawbacks:

the process is of relatively low intensity;

there are great difficulties in the way of integrated mechanization and automation;

it is highly energy-intensive.

It is therefore natural that ways of developing aqueous solution electrolysis processes in metallurgy must first involve the elimination of these drawbacks, although the prospects for adoption of electrochemical methods, even in their present form, are quite good [3,4].

It must be remembered that any improvement to the process must not affect its main advantage: the production of cathode metal of high purity.

The process of electrolysis can be intensified by increasing the number of electrodes in a box-type cell by bringing them closer together, or by raising the current density. The former method has already led to definite improvements, but its prospects are limited. The potential of the latter method calls for more detailed examination.

When the current density is raised in a periodic process in ordinary box-type cells, the time for the cathode to build up to the prescribed thickness (regulated by the quality of the cathode deposit and the distance between the electrodes) is reduced. As a result the number of service operations on the cell increases, reducing working time and consequently making intensification less effective.

All other conditions being equal, a rise in current density leads to increased probability of formation of dendritic deposits.

A higher rate of access of discharging ions to the cathode must be maintained in order to obtain a high-grade (fairly smooth) cathode deposit at increased current density. This higher rate can be achieved either by increasing the concentration of these ions in the electrolyte (which is limited by the solubility of the salt) or by reducing the thickness of the catholyte diffusion layer by creating a high rate of electrolyte circulation, or by combining the two factors. One of the effective ways in the particular case of copper electrorefining is current reverse. Experiments on the electrodeposition of copper, zinc, and nickel [5-12] have shown that high-grade deposits can be obtained at current densities up to 40,000 A/m^2 with high speeds of electrolyte travel along the cathode. However, this leads to enormous electrolyte flows in the system and makes the process unprofitable. In addition, the relationship between the maximum current density at which high-grade deposits can still be obtained and the speed of electrolyte flow is usually expressed as

$$I_{max} = kV^x, \qquad (3)$$

where $x < 0.5$ for laminar flow and $x < 1$ for turbulent flow. Consequently, the further increase in I_{max} becomes slight at very high V values. This relationship is clearly apparent in the Figure, which shows the results of experiments in producing nickel deposits from sulfate-chloride electrolyte at 60° C. The great difference between the curves is due to the fact that deposition of nickel in powder form begins at a current density much lower than the critical density.

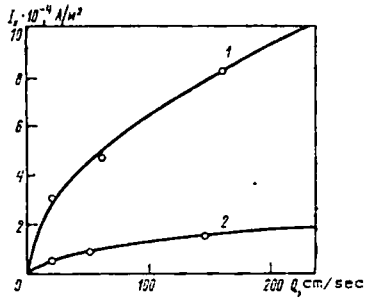

Relationship between speed of circulation and cathodic current density in deposition of nickel.

The curves should be closer to each other in electrodeposition of metals which evolve with low polarization (copper, zinc), when powder deposits are formed at current densities close to the critical density; however, some discrepancy is practically inevitable.

Intensification of the process by raising the current density makes it necessary to examine the effect of this factor upon the purity of the cathode deposit.

There are two possibilities. If an electropositive metal (copper, gold, or silver) is being deposited, most of the impurities, which have substantially more electronegative potentials, are not in practice discharged with the main metal and there is no fear of excessive contamination of the cathode deposit. If, however, an electronegative metal is being deposited, particularly one which evolves with considerable polarization, most of the impurities are discharged at the critical current [13]. In this case the relationship of cathode deposit contamination by the impurity Ai to various factors with the electrolyte circulating through the cell at speed Q (liters/hr) will be expressed by the following equation [14]:

$$A_i = \frac{DQC_{init.}}{I(Q\delta + DS)},$$

where D is the diffusion coefficient, δ is the thickness of the diffusion layer, C_{init} is the impurity ion concentration in the incoming electrolyte, I is the cathode current density, and S is the cathode surface.

It follows from this equation that increasing the cathodic current density when Q = const, for example, by increasing the main metal concentration, leads to an increase in the purity of the cathode deposit. However, as was stated above, increasing cathodic current density when Q = const is limited by the solubility of the main metal in the electrolyte and by increases in losses and in incomplete production, and cannot lead to any substantial intensification.

There is an increase in the diffusion of impurity ions at the same time as the diffusion of the main metal to the cathode surface increases. When the rise in the maximum current density (to produce a high-grade deposit) lags behind the increase in diffusion there is increased metal contamination by the impurity, because it is deposited at the critical current. The quantitative relationship flows from the following.

Let us express the speed of electrolyte circulation and the thickness of the diffusion layer by the equations

$$Q=k_1V \tag{5}$$

and

$$\delta=k_2V^{-y}, \tag{6}$$

where V is the linear flow velocity.

By substituting equations (3), (5), and (6) into (4) we obtain

$$A_i=\frac{Dk_1C_{init}^{1-x}}{kk_1k_2V^{1-y}+k_1DS}=\frac{C_{init}V^{1-x}}{K_1V^{1-y}+K_2}. \tag{7}$$

Since x < y for metals of nickel type both in laminar and in turbulent flow, the impurities content of the metal will increase as the process increases in intensity under conditions for high-grade deposit formation; to produce metal with the permitted impurities content when the whole volume of electrolyte is purified will call for a higher degree of purification.

However, x ≈ y for metals which are discharged with low polarization, when I_{max} is close to I_{crit}, and where $K_1V^{1-y} >> K_2A_i$ it does not depend upon the linear velocity of electrolyte flow.

The thickness of the diffusion layer can be reduced by creating a high rate of electrolyte flow along the electrode surface and by other methods, for example, by applying ultrasonic vibrations [15], using a cell with a moving or vibrating cathode, or by raising the electrolyte temperature.

Intensification by applying ultrasonic vibrations does not differ in principle from the electrolyte-flow method as regards altering the extent of cathode deposit contamination, because when the power of the ultrasonics is not very great its only effect is greatly to reduce the thickness of the diffusion layer.

According to formula (4), the application of ultrasonic vibrations will increase A_i if the rise in I (equal to I_{max}) lags behind the reduction in δ. A similar relationship is obtained when the reduction in diffusion layer thickness is produced by moving the cathode relative to the solution.

Raising the electrolyte temperature makes it possible to obtain high-grade deposits of a number of metals at substantially higher current densities. It was therefore proposed that the process should be carried out in autoclave-type cells at temperatures > 100° C. In these circumstances the cell voltage is reduced due to the rise in the specific conductivity of the electrolyte and the reduced polarization.

Which of these ways of intensifying the electrolysis process will be applied in practice?

There is no doubt that controlled electrolyte flows and some increase in circulation in a box-type cell with a periodic cycle may lead to an increase in cathodic current density of almost twofold (and has already led to such an increase in the electrorefining of copper [16]).

However, the advantages of high speeds of electrolyte flow (an increase in current density of not less than one order of magnitude) can be fully utilized only by transition to a continuous electrolysis cycle, and this is possible only with simultaneous organization of continuous metal discharge and the use of continuous (powder) anodes or by moving from a refining scheme to schemes for non-electrochemical dissolution and electroextraction of metal. Thus the best alternative is simultaneous utilization of the principles of high circulation speed and a moving cathode.

Although there have been several attempts to create electrolytic cells of drum and slotted type with a continuous cycle, they have not yet emerged from the pilot-plant stage. It is therefore not yet clear whether they are economical in use.

There is apparently little prospect of using ultrasonics for tonnage production, because of the difficulty of organizing the process and because ultrasonic vibrations have a dispersing effect upon the anodes.

As regards electrolysis at high temperatures in autoclave-type cells to produce compact metal, the necessity for very complicated apparatus will undoubtedly make it unprofitable.

Production of metal in powder form may be a promising way of organizing a continuous process [17]. Metals with low surface tension (Cu, Zn, Ag, Cd) tend to form powdery dendritic deposits in ordinary electrolytes without surface-active additions. In this case powdery deposits can be produced with high current efficiency at current densities practically equal to the critical diffusion current.

When electropositive metals are deposited in compact form (for example, copper or silver), electronegative impurities form practically no part of the cathode deposit as a result of joint discharge. A transition to electrolysis at critical current (powder deposit) will lead to codeposition of impurities also at the critical current routine. Consequently a powdery deposit will contain substantially more impurities than compact metal.

However, when electronegative metals such as zinc, cadmium, and nickel are deposited in compact form, many impurities are deposited at the critical current and the cathode deposit proves to be richer in impurities than the solution. In this case electrolysis at the critical current will lead to a situation in which the relationship between the constituents in the deposit will become equal to their relationship in the solution, i.e., the powdery deposit will be purer than the compact deposit.

The flowchart for production of powdery deposits appears to be simpler than that for an intensified process producing compact metal. In a number of cases, however, the transition to production of metal powder will require radical changes in electrolyte composition. Thus the catholytic layer is alkalinized and hydroxide is included in the deposit when nickel is produced in powder form from the usual sulfate-chloride electrolyte. It therefore becomes necessary to use a solution with ammonium chloride added.

Intensification of electrolytic metal production processes by increasing the current density involves the solution of various problems: the permissible degree of electrolyte acidification, its supplementation with discharging ions, removal of impurities from the new electrolyte composition, and so on.

In practice these problems remain when soluble anodes are used, because at high current densities there is a strong probability of anode passivation and it becomes necessary to separate the anode and the cathode space. Otherwise the electrolyte will be heavily contaminated by impurities when the crude anodes dissolve.

Thus there must be simultaneous and integrated solution of the problems of supplementing the electrolyte with ions of the metal to be deposited, electrolyte purification, the electrolytic cell heat balance, and the like in industrial electrolysis in any form. Correct organization must ensure a closed process circuit and an economical process.

REFERENCES

1. N. P. Fedot'ev, N. N. Bibikov, P. M. Vyacheslavov, and S. Ya. Grilikhes, Electrolytic Alloys, Moscow, Mashgiz, 1962, 311 pages, illustrated.
2. Applied Electrochemistry, edited by A. L. Rotinyan, Leningrad, Khimiya, 1974, 536 pages, illustrated.
3. Non-Ferrous Metallurgy in the Industrially Developed Capitalist Countries and the Developing Countries, edited by T. M. Petelina, Moscow, Tsvetmetinformatsiya, 1973, 272 pages, illustrated.
4. M. L. Navtanovich and V. L. Kheifets, Tsvetnye Metally, 1974, No. 1, 14-16.
5. W. A. Wesley, Ind. Engrg. Chem., 1952, 44, 957-961.
6. V. A. Popov, in: Material from a Conference on Zinc Electrolysis at High Current Densities, Moscow, Metallurgizdat, 1960, 214-216.
7. T. X. Carlin, Plating, 1966, 53, 10-14.
8. L. Krushev, Izvestiya na Instituta po Fiziko-Khimiya (Bulgarian Academy of Sciences), 1967, No. 6, 71-76.
9. A. I. Levin and V. N. Kocherov, Inventor's Cert. No. 183949, Byull. Izobr. i Tov. Znakov, 1966, No. 14, 57.
10. H. L. Brenner and C. I. Werulund, J. El. Chem. Soc., Modern Electroplating, 1942.
11. D. Krupkowa, Prace Inst. Hutn., 1964, 1, 16-21.
12. V. L. Kheifets, Trudy Inst. Gipronikel', Leningrad, 1968, Issue 38, 63-69.
13. V. L. Kheifets and A. L. Rotinyan, Zhurnal Vsesoyuznogo Khimicheskogo Obshchestva im. Mendeleeva, 1971, No. 16, 705-709.
14. A. L. Rotinyan and V. L. Kheifets, Trudy Inst. Gipronikel', Leningrad, 1958, Issue 3, 309-316.

15. S. M. Kochergin and G. Ya. Vyaseleva, Electrodeposition of Metals in an Ultrasonic Field, Moscow, Vysshaya Shkola, 1964, 111 pages, illustrated.
16. A. I. Levin, Tsvetnye Metally, 1970, No. 5, 44-49.
17. O. A. Khan and G. N. Sosnovskii, Tsvetnye Metally, 1966, No. 4, 42-46.

LETTERS TO THE EDITOR

THE PRESENT SITUATION AND PROSPECTS FOR THE USE OF SOLVENT EXTRACTION AND SORPTION IN ZINC AND CADMIUM PRODUCTION

UDC 669.536.66

L. S. Getskin

Solvent-extraction and sorption processes are used in industry for indium, cadmium, and thallium extraction in zinc production and for tellurium extraction in lead production. The adoption of these schemes has provided an opportunity for substantial increases in the extent of utilization of polymetallic materials and has yielded great benefits to the national economy.

Unfortunately, these trends were not reflected in the paper.

One cannot agree with the statement by the authors that "...raising the temperature and concentration of acid, using the jarosite and goethite processes, and the use of new filtering equipment do not give a radical improvement in valuable constituent utilization, fuller use of raw material, or greater process efficiency in spite of their effectiveness". This proposition contradicts all the existing practices and trends in the technical development of zinc hydrometallurgy. The adoption of a hydrometallurgical method for zinc cake processing, high-temperature leaching of zinc cake, a single-stage leaching scheme for roasted zinc concentrates, a three-stage scheme for removal of copper and cadmium from zinc solutions, continuous counterflow washing of zinc cake in thickeners, and other improvements have made radical changes to the existing zinc production technology, increasing the extent of raw material utilization and yielding great technical and economic benefits for the national economy.

The statement that "...sorption purification in cadmium production will reduce the number of operations, cut production costs, and increase cadmium extraction" is extremely controversial. A hydrometallurgical method for removal of nickel and cobalt from cadmium solutions which is more efficient than the methods suggested by the authors of the paper has now been implemented at the Leninogsk Polymetallic Combine on an industrial scale.

When considering the use of sorption processes for zinc production effluent purification and the use of various equipment, the authors give no specific recommendations: which sorbents and which equipment should be used to implement these processes?

The adoption of "...a scheme for bulk sorption of indium, germanium, and gallium with subsequent separation by elution in stages or subsequent selective solvent extraction and sorption" is proposed as a matter of high priority. This proposal is somewhat controversial, especially as regards indium, because solvent extraction of indium is widely used in Soviet practice and has shown itself to be highly effective technically and economically.

Finally the authors suggest a range of various solvent-extraction and sorption schemes for extraction of associated elements in zinc production, without touching upon the basic zinc and cadmium production technology. Thus the paper is written solely from the point of view of removing impurities from zinc solutions and extracting associated rare elements, not as a radical improvement in zinc hydrometallurgy.

The authors' proposals for expanding the production of ion-exchange resins and industrial manufacture of highly efficient solvent-extraction and sorption apparatus are expressed as general slogans and are not specifically defined. The operation of industrial pulsating columns at one of the zinc plants is of great interest, but this is not even mentioned in the paper.

The paper makes no new contribution to the choice of ways of solving the main problems of technical progress in zinc and cadmium metallurgy. The 'Main Trends in the Development of the USSR National Economy for 1976-1980' provide for increasing the extraction of non-ferrous metals from ores and fuller use of raw materials, and the adoption of highly efficient ore-dressing schemes and hydrometallurgical and other advanced processes.

Economic Geology
Vol. 74, 1979, pp. 389–396

Potash at Salt Springs, New Brunswick

JOHN P. ANDERLE, KEITH S. CROSBY, AND DAVID C. E. WAUGH

Abstract

A tectonically disturbed sequence of Mississippian-age evaporites located between Sussex and Saint John in southeastern New Brunswick, Canada, has been investigated by geologic, geophysical, and drilling programs. Eighteen of twenty-two drill holes have penetrated 10 to 140 ft of sylvinite in an evaporite sequence underlying 2,000 to 3,000 ft of conformable red beds. Stratigraphic studies involving lithological characteristics, bromine, borate, and geophysical data have facilitated improved understanding of the structure of the salt deposit. The salt sequence has been affected by flowage, which is represented by major and minor folding. In the more structurally disturbed areas, the sylvinite interval has been extensively subterraneanly eroded at the upper anhydrite-salt contact.

Introduction

THE Salt Springs salt and potash reservation covers an area of approximately 77 sq miles in Kings County, New Brunswick, Canada, about 35 miles northeast of the port of Saint John and approximately 15 miles southwest of Sussex.

In 1972 the Mineral Resources Branch of New Brunswick, under a cooperative agreement with the Federal Department of Regional Economic Expansion, and following geological and gravity surveys in the Salt Springs area which defined a circular structure interpreted as a body of salt, drilled the Salt Springs No. 1 borehole. This hole was terminated at a depth of 3,000 ft after encountering a thick section of salt and high-grade sylvinite.

In March 1975 the Government of New Brunswick, sole owner of salt and potash mineral rights, conducted a public bidding through which International Minerals and Chemical Corporation (Canada), Ltd., received the right to explore and develop salt, potash, and underground storage within the area of the Salt Springs reservation. The company began its exploration program in September 1975. This program has consisted of geological, geophysical, and geochemical investigations and an extensive drilling program. The principal results obtained with respect to potash occurrence in the Salt Springs area are the subject of this paper.

Exploration Program

A N 59° E base-line grid system consisting of 14 cross lines at approximately one-half-mile spacing and totaling 43 miles of line was constructed in the north central portion of the property. Gravity readings were taken at 500-ft intervals with a Worden master gravimeter. Scintrex proton magnetometer readings and Crone very low frequency-electro magnetic readings were taken on the same grid at 100-ft intervals. Also, a multiple frequency McPhar induced polarization system, Model P660, with a dipole spacing of 1,000 ft was used to record apparent resistivity readings at 1,000-ft intervals. Detailed geologic mapping of 100 sq miles comprising the salt and potash reservation and surrounding area was completed. This mapping, together with geophysical information, provided an early understanding of the stratigraphy and structure of the Salt Springs area, facilitating the positioning of the boreholes during the initial exploration phase.

Twenty-two holes have been drilled in the Salt Springs property with approximately one-half-mile spacing. Eighteen of these holes encountered sylvite mineralization ranging from 10 to 140 ft in apparent true thickness and grade of approximately 28 percent K_2O. The drilling has defined a sylvinite bed in an area 4,000 ft wide by 14,000 ft in length.

Geological Setting

The Carboniferous sediments of eastern Canada were deposited in a large graben or rift structure, the Fundy epieugeosyncline (Kelly, 1970). The Fundy epieugeosyncline extends from southern Nova Scotia to White Bay, Newfoundland. It is bordered to the north by the New Brunswick Platform and to the south by the Meguma Platform in Nova Scotia and consists of several subbasins. The Moncton subbasin of southern New Brunswick is characterized by a thick sequence of Carboniferous sediments.

Geology of the Marchbank syncline

The Marchbank syncline is the most southerly part of the Moncton subbasin. It has a length of approximately 20 miles and lies between the Caledonian Mountains on the southeast and the Clover Hill fault on the northwest (Fig. 1). It contains Carboniferous sediments, as indicated by geophysical

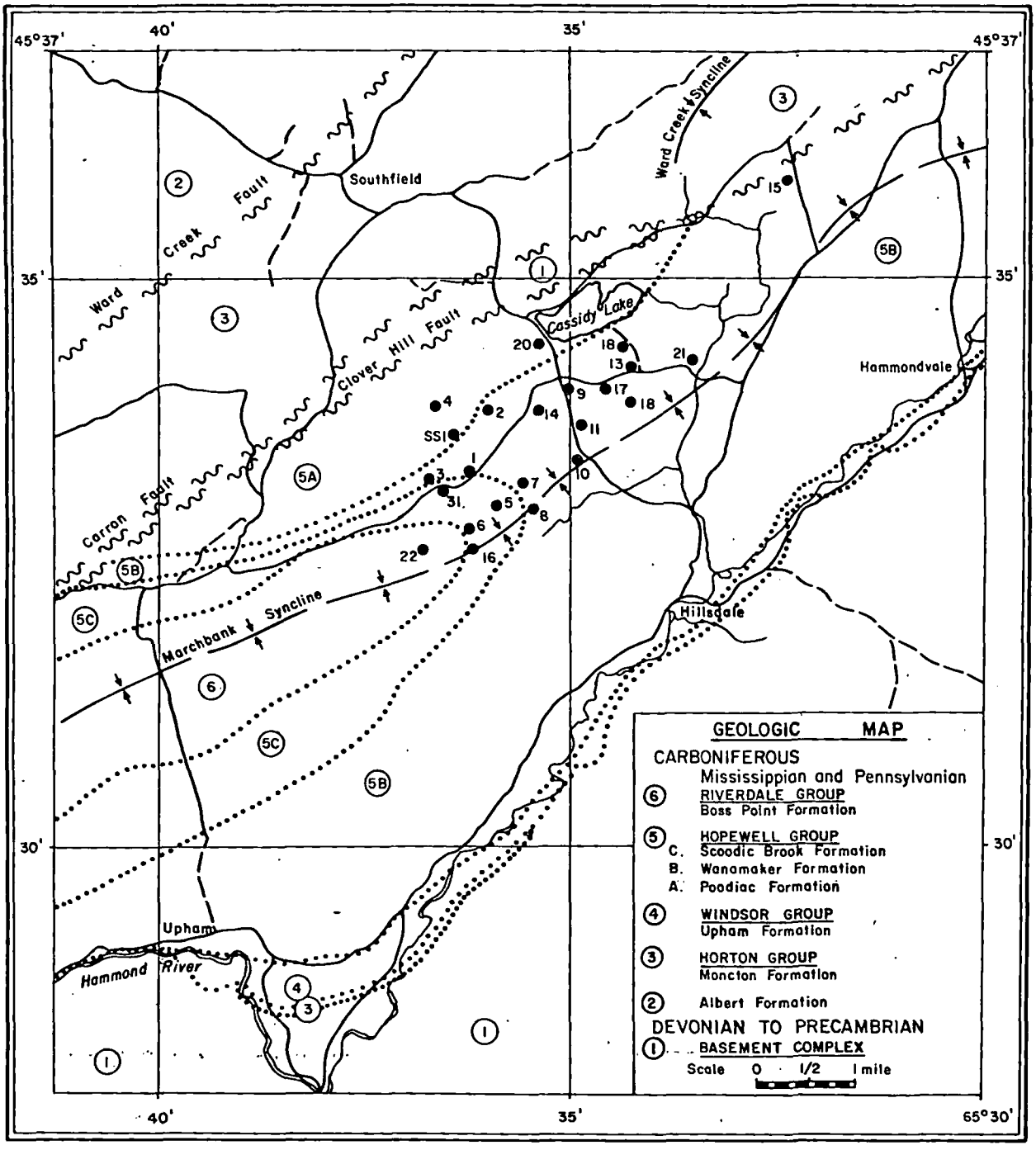

FIG. 1. Geologic map, Salt Springs, New Brunswick.

surveys and drilling, with a maximum thickness of about 6,000 ft. As shown in Figures 1 and 3 these sediments have been divided into the Horton, Windsor, Hopewell, and Riverdale Groups. Information obtained by the International Minerals and Chemical Corp. during the exploration program has provided a basis for subdividing the Windsor and Hopewell Groups. The stratigraphy of the clastic rocks is complicated by rapid and numerous facies changes and pinchouts and by a scarcity of marker fossils. For these reasons the authors have utilized lithostratigraphic terminology in subdividing sediments in the area explored. Additional stratigraphic studies will be required before reliable correlations can be made with Carboniferous sediments in other parts of the Fundy basin or subbasins.

The surface geology shows that the Marchbank syncline is somewhat asymmetric; bed rock on the northwest limb dips 10° to 15°, whereas that on the southeast limb dips 20° to 25°. Dips as steep as 40° are found locally at the southern margin of the syncline.

The Clover Hill fault is interpreted as being a thrust fault; the dip at the surface is approximately 80° northwest but is interpreted as decreasing with depth. The fault zone is 500 to 1,500 ft in width with a known vertical displacement of 3,000 ft. Formations on opposite sides of the fault are characterized by discordant structures. The direction of movement of the block on the northwest side of the fault is upward and eastward.

Stratigraphy of the Windsor Group

The Windsor Group lithologies are composed of anhydrite, limestone, halite, sylvinite, and/or carnallite with red-brown to gray claystone and sandstone in varying proportions and sequences depending on the location in the Fundy basin. In the Moncton subbasin as a whole the Windsor Group is represented largely by the low order evaporites, limestone and anhydrite, but in the March bank syncline the high order evaporites, halite and potash salts, are dominant. The carbonate, sulfate, and chloride phases are all preserved in the stratigraphic record of the Marchbank syncline, which now are well known from data derived from more than 46 exploration holes and from surface exposures. Data from both sources were used in subdividing the Windsor Group into the formations, members, and beds shown in Figure 2 and described briefly below.

Upham Formation

The Upham Formation consists of the Devine Corner Member overlain by the Upperton Member. The former is characterized by light-colored laminated to massive limestone which locally contains oolites, stromatolites, and brachipods. The Upperton Member is composed principally of anhydrite which usually is massive, although it is locally laminated. The formation is underlain disconformably by the Moncton Formation.

Cassidy Lake Formation

This formation contains the high order evaporites of the Windsor Group which occur only in the subsurface. The salts have been divided into four members as described below.

Basal Halite Member: Consists of very light, gray to clear, medium to coarsely crystalline halite that characteristically contains dark argillaceous halite bands of interstitial gray-green anhydrite claystone. These bands vary in thickness from 4 to 20 in., marked by diffused boundaries with clean halite intervals separating the argillaceous bands. The argillaceous bands become more numerous in the upper segment of the number. White nodules (0.5 mm) of danburite have been recognized in this member at the lower contact.

The Basal Halite Member varies in true thickness from 5 ft near the southern margin to more than 500 ft in the central part where folding and salt flowage obscure the true thickness. Repetition of beds due to folding makes the true thickness difficult to identify because of the homogeneous nature of the Basal Halite Member. At most places the contact with the underlying Upperton anhydrite is conformable and is usually gradational across 8 in. of strata; however, cores from some exploratory holes showed a marked angular unconformity, representing décollement salt flowage along a more competent lithology.

Middle Halite Member: This member consists of very light brown to light brown, medium-grained crystalline halite, which is characterized by dark gray to dark brown argillaceous halite bands consisting of interstitial gray-green anhydritic claystone and red-brown claystone. These alternating bands of argillaceous and clean halite vary in thickness from 4 to 20 in. with diffused boundaries.

The Middle Halite Member varies from a minimum of 80 ft along the southern margin to a maximum of more than 250 ft in the central part of the deposit. This member is in gradational contact with the underlying Basal Halite Member, with an interval of interbedded, clear to very light gray and light brown halite over several feet to 150 ft.

Potash Member: During the exploration program, the Potash Member has been defined arbitrarily as the halite unit between the Middle Halite and Upper Salt Members which contains the principal sylvite mineralization in the Salt Springs area. Data that will permit rigorous identification of this halite unit, regardless of whether or not potash salts are present, are needed before final definition of the member is made. As defined, it consists of two submembers, the Sylvinite bed above and the Lower Gradational bed below (Fig. 2). The base of the latter is placed at the lowest occurrence of red-rimmed crystals of sylvite in the orange or light brown halite that overlies the Middle Halite Member; it varies in thickness from 10 to 70 ft. Observations indicate that variations in thickness of the Lower Gradational bed and the Sylvinite bed are inverse, although not rigorously so, suggesting they may, in part at least, be time equivalents.

The Sylvinite bed is characterized by sylvite mineralization greater than 15 percent KCl, consisting entirely of sylvinite and halite with no potassium-magnesium salts. This bed is mainly composed of

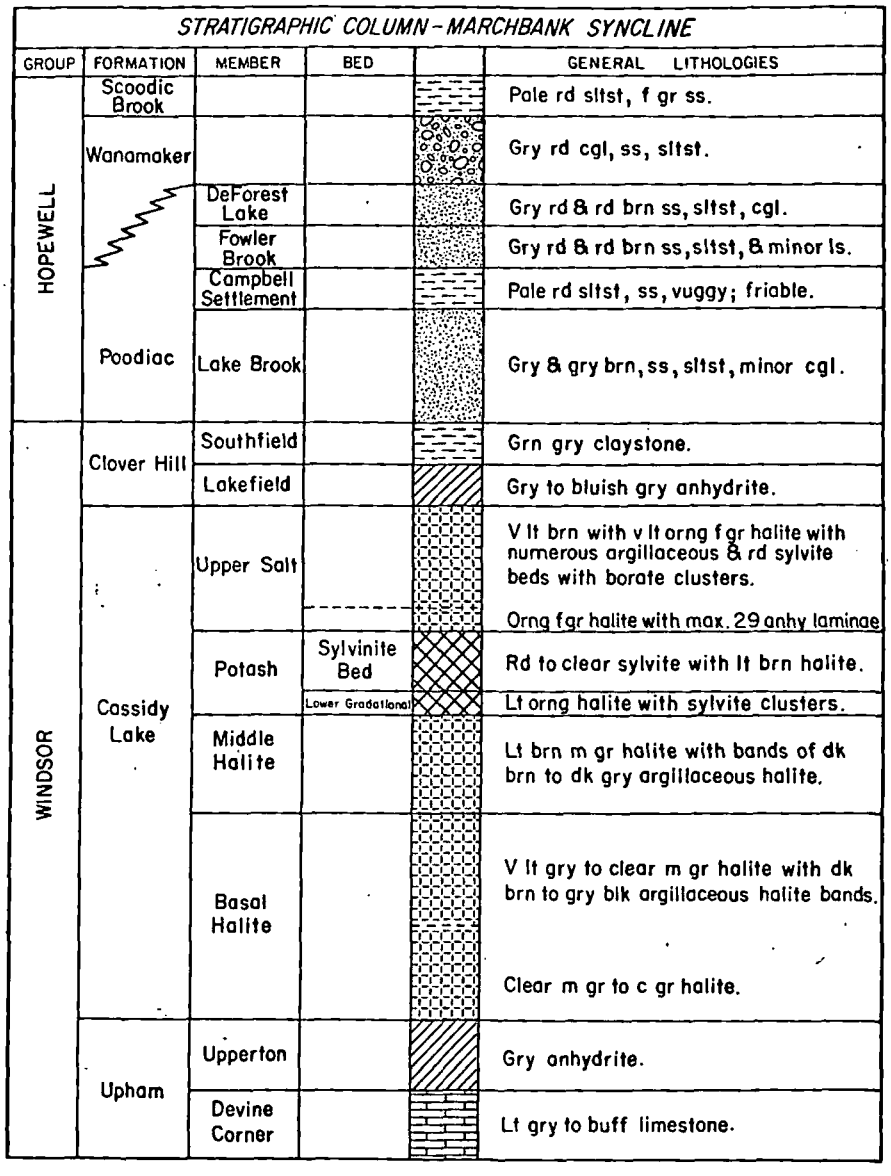

FIG. 2. Stratigraphic column of the Marchbank syncline.

brick-red to blood-red sylvite crystals, 2 to 5 mm in diameter, in a matrix of dark brown to dark orange finely crystalline halite, the dark color being due to trace quantities of disseminated clay. The lower part of the bed contains more clear sylvite and this, together with lighter colored halite, gives a lighter color to the whole rock. Holes IMC-2 and SS-1 penetrated a gray to dark gray sylvinite bed below the red sylvinite.

The Sylvinite bed is not homogeneous but is interrupted by barren halite and low-grade sylvinite beds, 1 to 12 in. thick. Although locally there appears to be a correlation of these beds over several thousand feet, it has not yet been possible to trace any bed within the Sylvinite bed over the entire property.

The true thickness of the Potash Member varies between 60 to 150 ft. Assuming that the thickness, taken to be the true thickness of the Potash Member, is correct, and not the unrecognized result of salt flowage, there appears to be considerable variation in the original thickness of the potash salts deposited. Further investigations are required, however, to determine whether these variations are primary.

Upper Salt Member: The Upper Salt Member is very distinctive. Unlike the homogeneous lithologies of the Middle and Basal Halite members, the Upper Salt member is a heterogeneous unit. It is characterized by orange, brown, colorless, and argillaceous halite beds; red sylvinite beds and laminae;

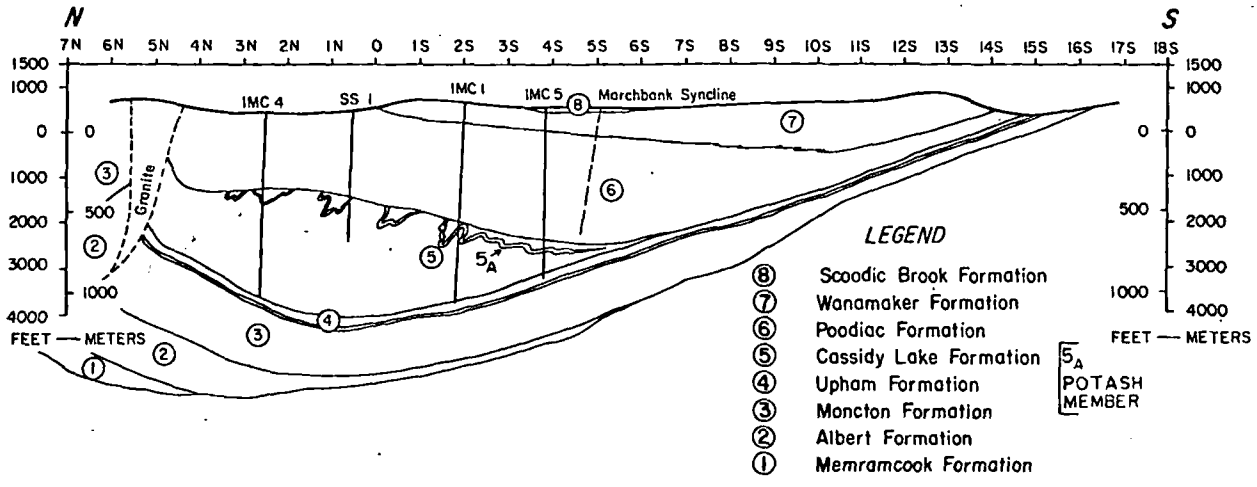

FIG. 3. Geologic cross section, Salt Springs, New Brunswick through IMC-4, SS-1, IMC-1 and IMC-5 (IMC = International Minerals and Chemical Corp.; SS = Salt Springs).

claystone and gray anhydrite laminae; and by the presence of certain borate minerals.

Attempts at detailed subdivision of the Upper Salt Member have met with little success due to the absence of persistent marker beds. As in the Potash Member, marker beds can be recognized between neighboring holes only. However, it is possible to subdivide the Upper Salt Member very generally into three parts which have obscure gradational contacts that are often difficult to recognize. The upper part consists of light brown to light orange finely crystalline halite with disseminated gray-green claystone, red sylvinite beds and laminae, and gray-green claystone laminae with numerous borate clusters and laminae. Generally there are no anhydrite laminae within this interval. The borates are often associated with laminations of claystone and sylvite. They occur as disseminated crystals varying from 1 to 4 mm in diameter, in clusters with a maximum diameter of 1 cm, and as distinct laminations. They are, in order of decreasing abundance, boracite, hydroboracite, hilgardite, szaibelyite, and trace ulexite (Murowchick and Gricius, 1977).

The middle part of the member is characterized by light brown to light orange (minor bright orange) and colorless finely crystalline halite with clayey halite beds, red sylvite beds, and laminae with a maximum of 24 anhydrite laminae (1 mm to 1 cm), and by minor claystone laminae. Borate crystals occur as described in the interval above.

The lower part of the Upper Salt Member has the most consistent lithology of the three subdivisions. It generally consists of orange colored finely crystalline halite with gray anhydrite laminae and no clay. No borate crystals were observed. This unit varies in thickness from 9 to 30 ft with approximately 5 to 29 anhydrite laminae, ranging in thickness from 0.5 to 2 mm. It is in gradational contact with the underlying Potash Member.

The thickness of the Upper Salt Member varies. In the vicinity of IMC holes 5, 6, 7, and 11, a maximum thickness of 210 ft has been drilled. South of these holes the member thins to 40 to 60 ft. At present the decrease in thickness in the southern part of the deposit is believed to be depositional because lithology typical of the upper subdivision of the member is found at the top of the thinner sections. The thickness also decreases toward the north, but in that direction the thinning is caused by suberosion. From 0 to 100 ft of Upper Salt Member was found in holes located over the central part of the salt deposit where maximum suberosion has taken place. From the lithology of the member it was obvious that the upper part was missing in this area (Fig. 3).

Clover Hill Formation

This formation consists of the Lakefield and Southfield members. The former member is characterized by gray, massive to bedded anhydrite. Frequently the anhydrite is entirely or partly brecciated, with a thickness of about 25 ft. The contact of the Lakefield anhydrite member with the underlying Upper Salt Member is represented by a 4- to 20-in minutely laminated bed of anhydritic claystone, called the residual bed. Analysis of this bed indicates the presence of halite, sylvite, borate minerals, claystone, and anhydrite found in the Upper Salt Member and is probably a residue resulting from suberosion of the salt beds at the contact.

The Southfield Member consists of gray-green claystone 10 to 44 ft thick, in gradational contact with the overlying red clastics of the Hopewell Group. The red and gray-green claystones are interbedded

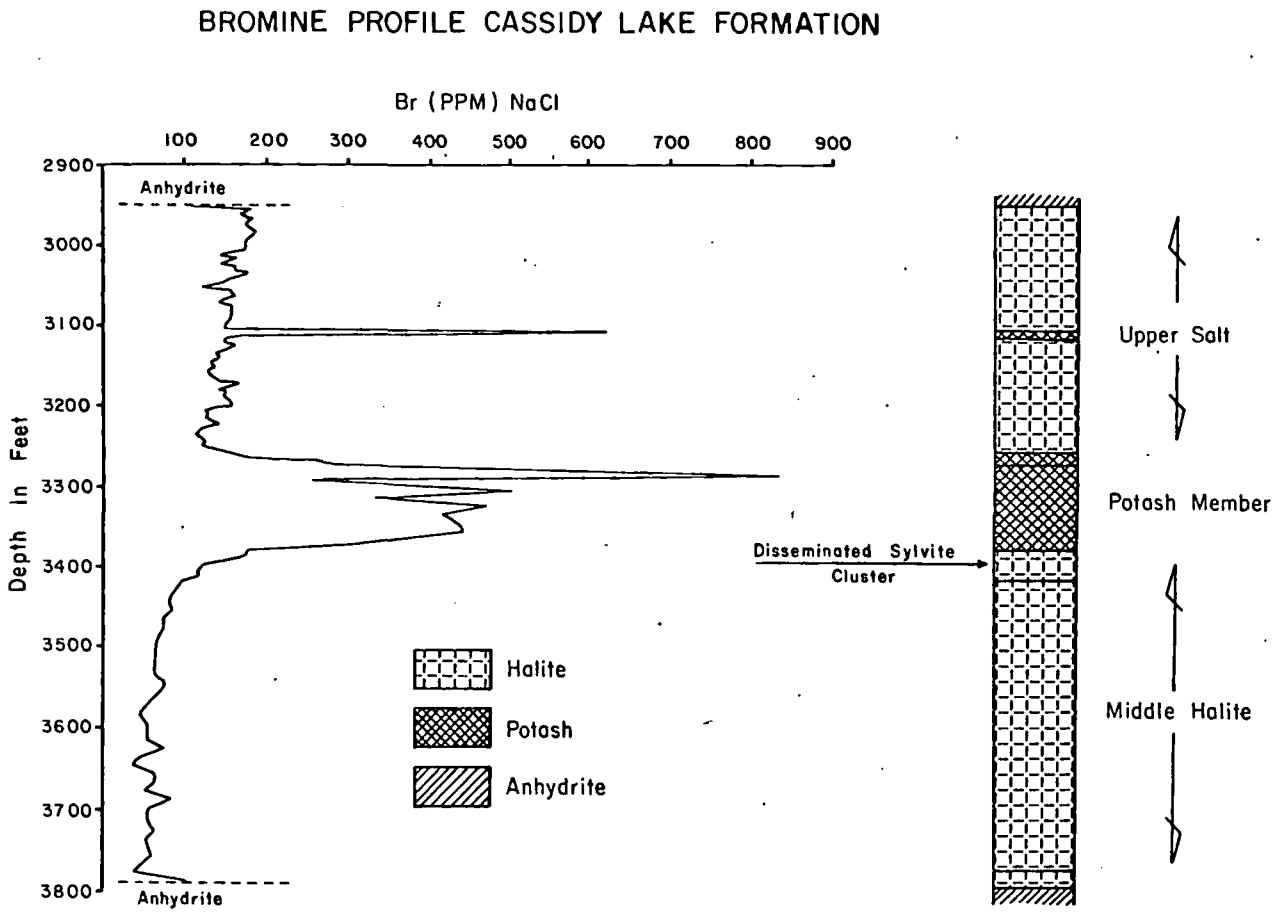

FIG. 4. Bromine profile, Cassidy Lake Formation.

over a 20-ft interval. The contact with the underlying anhydrite member is conformable and distinct.

Stratigraphy of the Hopwell Group

In the Marchbank syncline the Hopewell Group has been subdivided into several new formations and members during exploration of the Salt Springs potash deposit. Each of the three new formations possesses a variance in lithologic homogeneity and the boundaries display significant and distinct lithologic changes. The three are shown in Figure 2 and are described briefly below.

Poodiac Formation

This formation consists of red-brown to gray-brown siltstones and sandstones in gradational contact with the underlying marine claystone of the Clover Hill Formation. The Poodiac Formation attains a maximum thickness of about 3,000 ft along the Marchbank syncline axis where four distinct members are recognized. These are the Lake Brook, Campbell Settlement, Fowler Brook, and DeForest Lake Members as shown in Figure 2.

Wanamaker Formation

This formation is composed of generally gray-red, poorly sorted, granular to boulder conglomerates, with sandstone and minor siltstone. The conglomerate is the predominant lithology on the southern and eastern margin of the syncline, becoming finer and thinner northward. The Wanamaker Formation, which is in excess of 1,000 ft thick at the south margin and only 400 ft thick in the drilling area, may be, in part at least, laterally a coarser equivalent of the Poodiac Formation.

Scoodic Brook Formation

This formation consists of pale red siltstone with minor sandstone in conformable contact with the underlying Wanamaker Formation and the overlying Riverdale Group, Boss Point Formation. The Scoodic Brook Formation has a maximum thickness of about 300 ft along the Marchbank syncline.

Bromine Study

Approximately 280 samples for bromine analysis were taken of salt cores from the Cassidy Lake for-

mation, handpicked at 5- to 20-ft intervals. Hole IMC-6, which has a complete stratigraphic succession, represents a typical bromine profile (Fig. 4).

The Basal Halite Member averages about 48 ppm bromine, the Middle Halite averages about 71 ppm, whereas the Lower Gradational bed of the Potash Member averages 124 ppm. The Upper Salt Member ranges from 113 to 187 ppm, averaging 150 ppm bromine.

It is apparent that a gradual increase in bromine occurs from the Basal Halite to the Sylvinite bed and continues high through the Upper Salt Member. This characteristic profile is consistent over the deposit and was used to verify the stratigraphic interpretation in holes complicated by folding. One uninterrupted evaporite cycle is also indicated by these bromine profiles.

Evaporite Tectonics

The salt body in the Marchbank syncline is approximately 6 miles long, in a northeast to southwest direction, and 2 miles wide, with a probable maximum thickness of 2,500 ft, thus forming an elongated lens as opposed to a diapiric shape. The top of the evaporite sequence conforms with the inclination of the overlying clastic sediments. The thick salt section between holes IMC-1 and IMC-4 (Fig. 3), representing the center of the gravity anomaly, must be explained by a depression in the pre-evaporite rocks because the top of the salt mass is nearly flat in this area.

As stated in the description of the thickness of the Upper Salt Member, there is stratigraphic evidence from the cores of much solution of the upper part of the salt in the central part of the deposit. There is also evidence of solution from structural data because the conformable contact between the Poodiac and Clover Hill Formations is often in great contrast to the strong angular relationship between the latter formation and the underlying salt and potash. Inclination in the salt varies from 10° to 90° but generally averages 40° to 55°. Intersections along the south flank average 20° to 30°.

The direction and time of salt flowage are difficult to discern at this stage of development but probably are influenced by movement on the Clover Hill fault. It is apparent, however, that folding occurred with relatively low stress, as schistosity in the salt cores has not been observed except very locally.

Small-scale asymmetrical folds, observed in most cores, usually vary from 1 to 10 ft across. Their relationship to the major folds is not fully understood from observations to date.

Initial drilling intersected only one limb of the major folds, and consequently no repetition or major inclination changes were observed. However, study

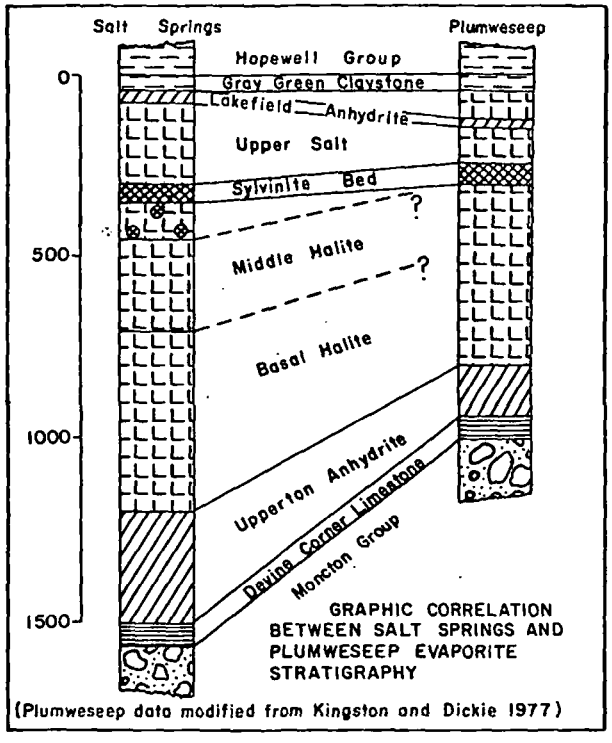

FIG. 5. Graphic correlation between Salt Springs and Plumweseep evaporite stratigraphy.

of cores from holes IMC-7, IMC-3, IMC-31, and IMC-13 indicate several tentative conclusions. (1) Overturned folds of 150- to 500-ft amplitude are present. (2) The strike of the major folding in the evaporite is probably northeast to southwest, similar to the general strike in the Marchbank syncline and to the major structural trend of Carboniferous rocks in the Moncton subbasin. The shape of the evaporite body is elongated in this direction, therefore the folding is inferred to have a similar strike. (3) The direction of inclination of the axial planes is uncertain, but a north dip is regarded as most probable. This attitude would parallel the axial plane of the Marchbank syncline and would best fit the observations to date.

Summary of Evaporite Deposition

The end of deposition of continental clastics of the Moncton formation was marked by transgression of the Windsor Sea and the deposition of carbonate sediments. Restricted circulation resulted in increased salinity, followed by sulfate sedimention; with continued evaporation of the sea under the influence of a restricted but continuous influx, halite and potash deposition occurred. The deposition of these evaporites was probably widespread and simultaneous throughout the Moncton subbasin, with minor variations caused by topographic restrictions and local irregularities on the floor.

The Salt Springs stratigraphic sequence in the Marchbank syncline is very similar to the evaporite stratigraphy at the Plumweseep deposit, in the Dunsinane syncline (Fig. 5). Similarities are apparent in lithologies, colors, texture, thickness, and sequence (Worth, 1972; Kingston and Dickie, 1977).

Both deposits have a sequence of homogeneous lower halite in contact with basal anhydrite and limestone. Only one main sylvinite bed is present with consistent mineralogy and thickness. The Upper Salt is a heterogeneous sequence consisting of halite, sylvinite beds, anhydrite laminations, and borate minerals. This sequence of evaporites (Sussex I Evaporites) is overlain in both deposits by an upper anhydrite that probably represents the beginning of a second evaporite cycle (Sussex II Evaporites) in the Moncton subbasin. In the Plumweseep deposit a 75-ft bed of halite overlies this anhydrite.

The retreat of the Windsor Sea is represented by a gray-green, marine claystone which covers the evaporites in both deposits. A sequence of transitional sedimentation of deltaic to fluvial flood-plain deposition followed.

Salt flowage was initiated with burial and was further influenced by the most recent movement of the Clover Hill fault which occurred during late Pennsylvanian to early Permian time.

Acknowledgments

The preparation of this paper has been made possible through the cooperation of the International Minerals and Chemical Corporation. I am grateful for permission from M. A. Upham, president, and P. O. Sandvik, director, to use data from the corporation. Gratitude is extended to S. R. McCutcheon and J. C. Dunlap for critically reviewing the manuscript.

J. P. A. AND K. S. C.
J. P. ANDERLE, LTD.
P. O. Box 1554
FREDERICTON, NEW BRUNSWICK E3B 5G2, CANADA
D. C. E. W.
INTERNATIONAL MINERALS AND CHEMICAL CORPORATION
P. O. Box 99
NORTON, NEW BRUNSWICK E0G 2N0, CANADA
November 10, 1978

REFERENCES

Kelly, D. G., 1970, Geology of southeastern Canada, geology and economic minerals of Canada, *in* Douglas, R. J. W., ed., Economic geology report: Queen's Printer for Canada, no. 1, p. 284–296.

Kingston, P. W., and Dickie, C. E., 1977, Geology of New Brunswick potash deposit: Canadian Inst. Mining and Metallurgy Conf., Ottawa, 1977, 19 p.

Murowchick, B. L., and Gricius, A., 1977, Mineral identification of evaporite samples from Salt Springs, New Brunswick: Bartow, Florida, International Minerals and Chemical Corp., internal rept.

Worth, J. K., 1972, Final report on drilling, Sussex area, New Brunswick (1971): New Brunswick Dept. Nat. Resources, Mineral Resources Br., Topical Rept. 72-3.

Economic Geology
Vol. 74, 1979, pp. 358–376

Potash Salts in the Williston Basin, U.S.A.

SIDNEY B. ANDERSON AND ROBERT P. SWINEHART

Abstract

The potash deposits of North Dakota and Montana are extensions of the rich deposits now being mined in Saskatchewan. These deposits underlie 28,500 km² (11,000 sq miles) in northwestern North Dakota and 7,800 km² (3,000 sq miles) in northeastern Montana. The Middle Devonian potash deposits occur in beds within the Prairie Formation, an evaporitic sequence composed primarily of halite. The Prairie Formation evaporites were deposited within the Devonian Elk Point Basin, which extended from northwestern Alberta to the northwestern North Dakota–northeastern Montana area. On the U.S. side of the border, the Prairie Formation salt reaches a maximum thickness of 168 m (550 ft) in Burke County, North Dakota, whereas in Saskatchewan it exceeds 213 m (700 ft). North Dakota's potash ranges from 1,707 m (5,600 ft) deep near its eastern limit in northwestern Bottineau County to over 3,660 m (12,000 ft) in eastern McKenzie County. In Montana, the deposits range from 2,530 m (8,300 ft) in Daniels County to 3,500 m (11,500 ft) in Richland County. Three potash zones can be identified in Saskatchewan and North Dakota; two, in Montana. In North Dakota, the two major beds, the Esterhazy and Belle Plaine, reach a combined gross thickness of 25 m (83 ft) and a net thickness of 17 m (55 ft). In Montana they reach a combined thickness of 19 m (61 ft) gross and 13 m (43 ft) net.

Introduction

THE potash deposits of North Dakota and Montana are extensions of rich deposits now being mined in Saskatchewan. The potash deposits underlie 11,000 sq miles (28,500 km²) in northwestern North Dakota and 3,000 sq miles (7,800 km²) in northeastern Montana. They are of Middle Devonian age and occur in beds within the Prairie Formation (Fig. 1), an evaporitic sequence composed primarily of halite, but also potash and anhydrite. The formation conformably overlies the Winnipegosis Formation and is conformably overlain by the Dawson Bay Formation. Both formations are of Devonian age and are composed primarily of carbonates.

The evaporites of the Prairie Formation were deposited in the Devonian Elk Point Basin, a large trough which extended southeastward from the Northwest Territories and northwestern Alberta to its southern terminus in northwestern North Dakota and northeastern Montana (Fig. 2).

Geologic History of the Potash Units

During deposition of the Winnipegosis Formation, reefs, which restricted inflow of waters from the open sea, formed in Alberta in the northern part of the Devonian Elk Point Basin. Circulation within the basin was further restricted by reefs that formed on structural highs in the northwestern part of the basin and along the basin margins (Saskatchewan Dept. Min. Resources, 1973). These restrictions, coupled with arid conditions, caused concentration of brines within the Elk Point Basin, resulting first in deposition of gypsum, then of halite, and finally of potassium salts. Periodic influxes of fresh sea water into the basin caused deposition of alternating beds of halite and potash. Potash deposition was restricted to the southern part of the Elk Point Basin, an area that covers parts of Saskatchewan, North Dakota, Montana, and a small part of Manitoba adjacent to the Saskatchewan border.

Initial evaporite deposition of the Prairie Formation in North Dakota and Montana is represented by a basal anhydrite (Fig. 3). Deposition of anhydrite on the U. S. side of the international boundary appears to have been restricted to North Dakota and extends 60 to 65 miles (96 to 104 km) east of the present salt limits of the Prairie. The anhydrite may indicate the original extent of the salt. Solution is known to have occurred along the eastern salt margins in western Bottineau, eastern Renville, and northeastern Ward Counties, North Dakota, but whether salt extended as far east as the anhydrite is unknown. The eastern edge of the basal anhydrite is farther east than the eastern edge of the overlying Prairie salt, which may indicate a westward tilt of the Williston Basin in early Prairie time with a resulting westward shift in deposition. Westward tilting of the basin is also indicated in Saskatchewan (Holter, 1969).

Following deposition of salt of the Prairie Formation, the Dawson Bay carbonates were conformably deposited. A reddish argillaceous bed known as the "second red" that occurs at the base of the section

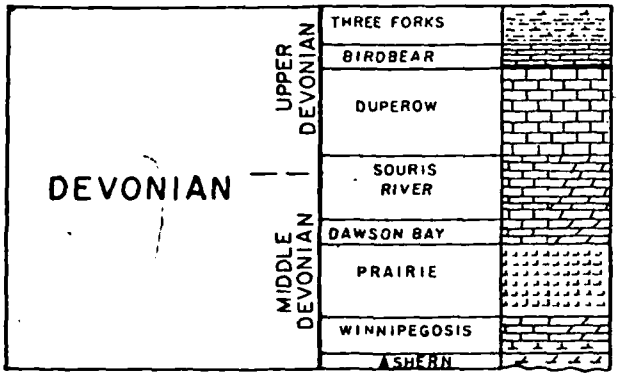

FIG. 1. Stratigraphic section of the Devonian system, Williston Basin, U. S. A.

probably kept waters of the Dawson Bay Sea from coming in contact with the salt.

Geology of the Deposits

The present limits of the Prairie salt in the United States are from western Bottineau County in north-central North Dakota to Daniels County in eastern Montana and as far south as northern Dunn County in west-central North Dakota (Fig. 4). Evidence of solution is indicated along both the eastern and western margins as well as in three other areas in eastern Montana. Thickness of the salt ranges from a feather-edge along the margins to over 500 ft (150 m) in Burke County, North Dakota. In Montana, the thickest section is in east-central Sheridan County where the salt has a thickness of slightly more than 300 ft (90 m).

On the U. S. side of the international boundary, as in Saskatchewan on the Canadian side, three potash beds are present (Fig. 5). The Esterhazy and Belle Plaine Members, the lower beds, are present in both North Dakota and Montana and continue across the international boundary. The upper bed, termed the "Patience Lake Member" in Saskatchewan and the "Mountrail Member" in the U. S., is discontinuous and cannot be traced across the boundary; however, the two members are probably correlative. The Mountrail Member is not known to occur in Montana.

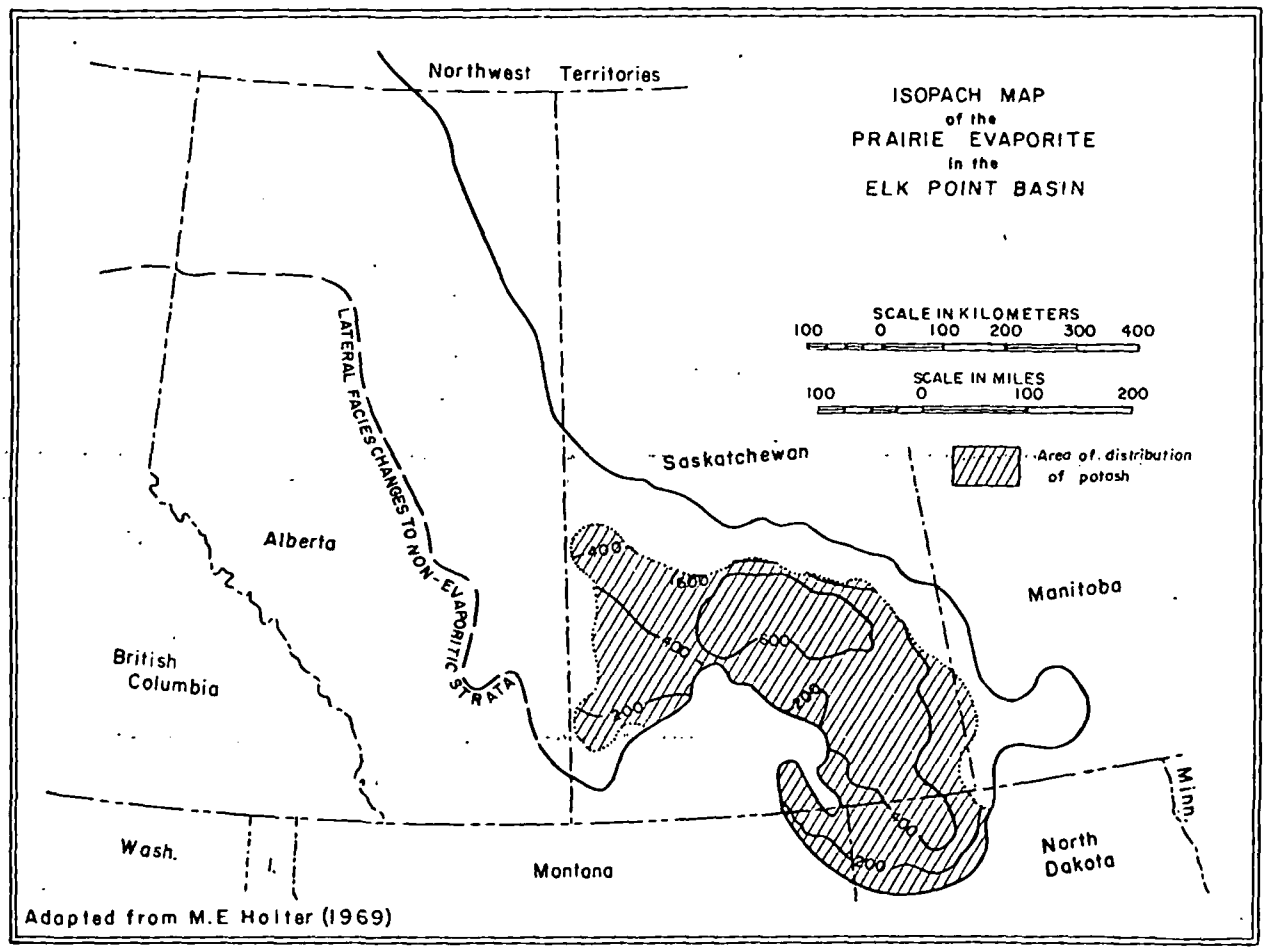

FIG. 2. Devonian Elk Point Basin.

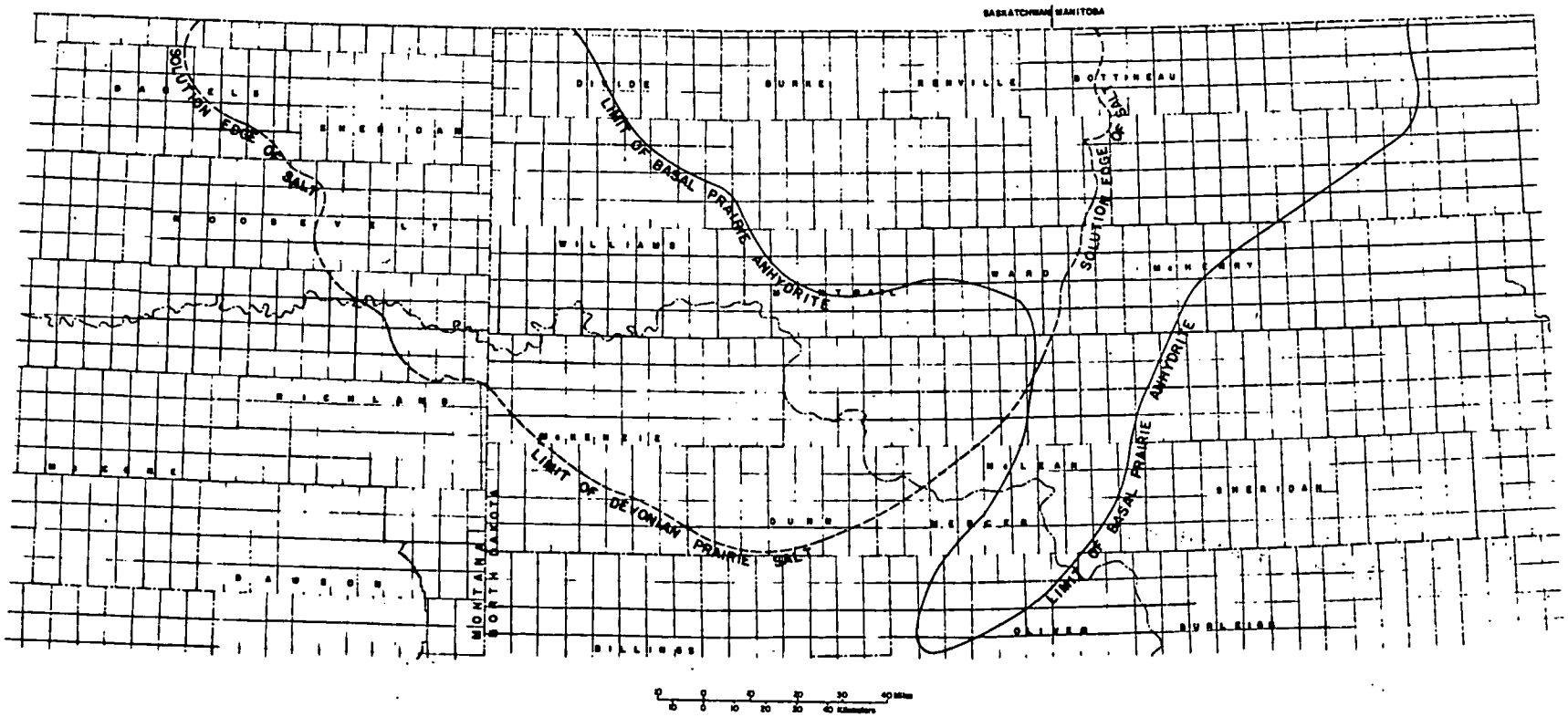

FIG. 3. Extent of the basal Prairie anhydrite and Prairie salt in northwestern North Dakota and northeastern Montana.

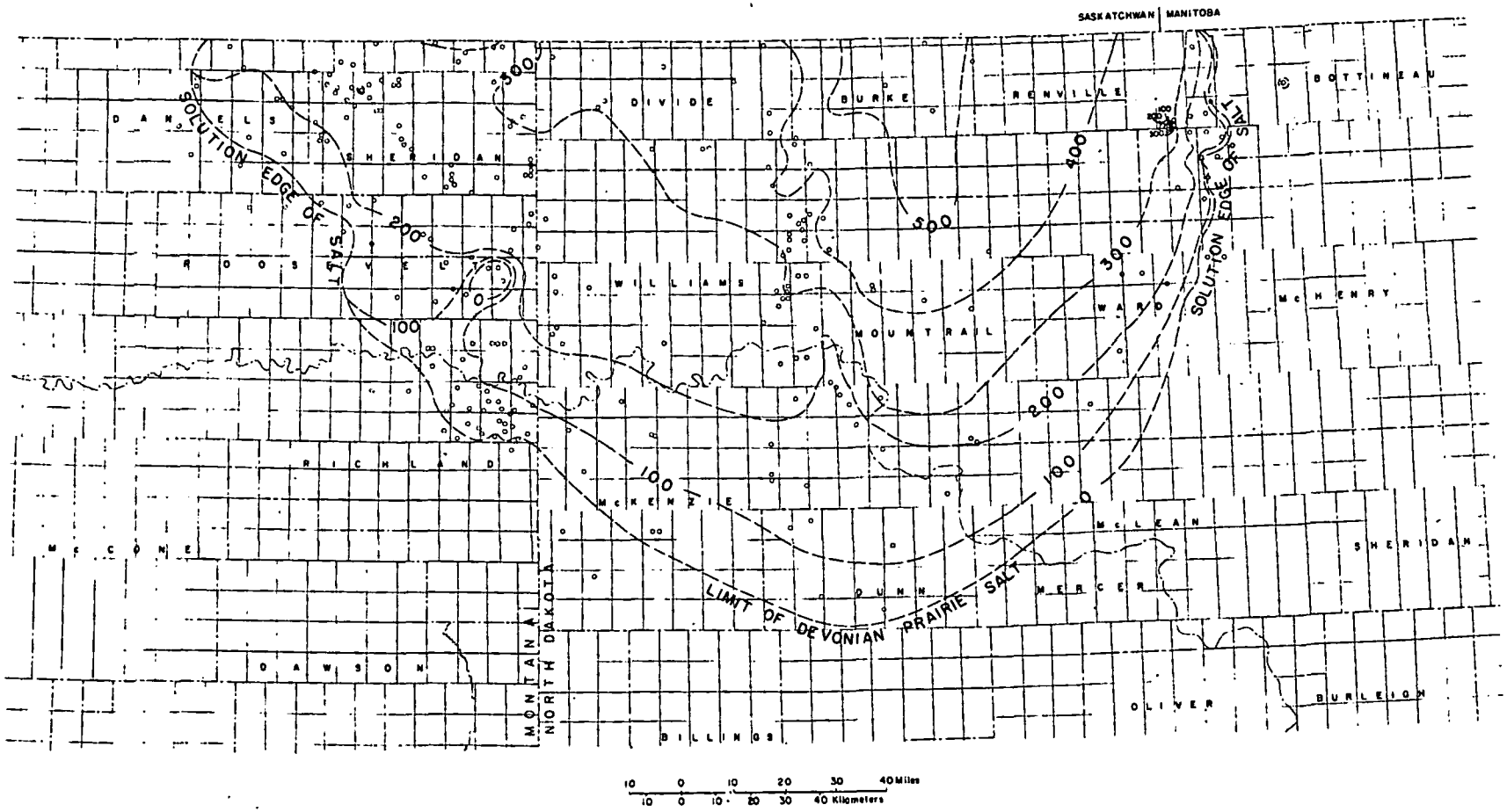

FIG. 4. Prairie salt isopach in northwestern North Dakota and northeastern Montana.

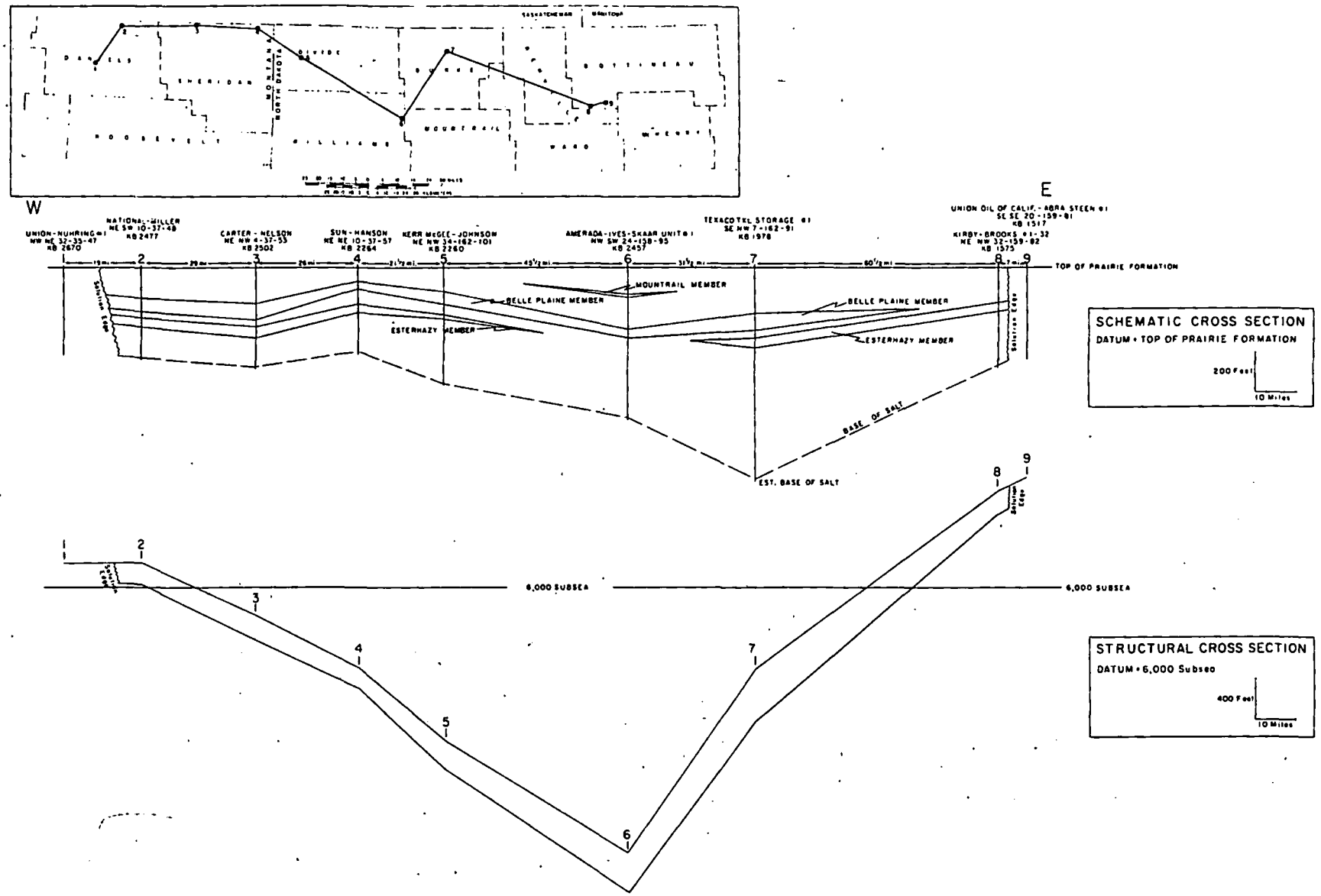

FIG. 5. Schematic and structural cross sections of the Prairie Formation, northwestern North Dakota and northeastern Montana.

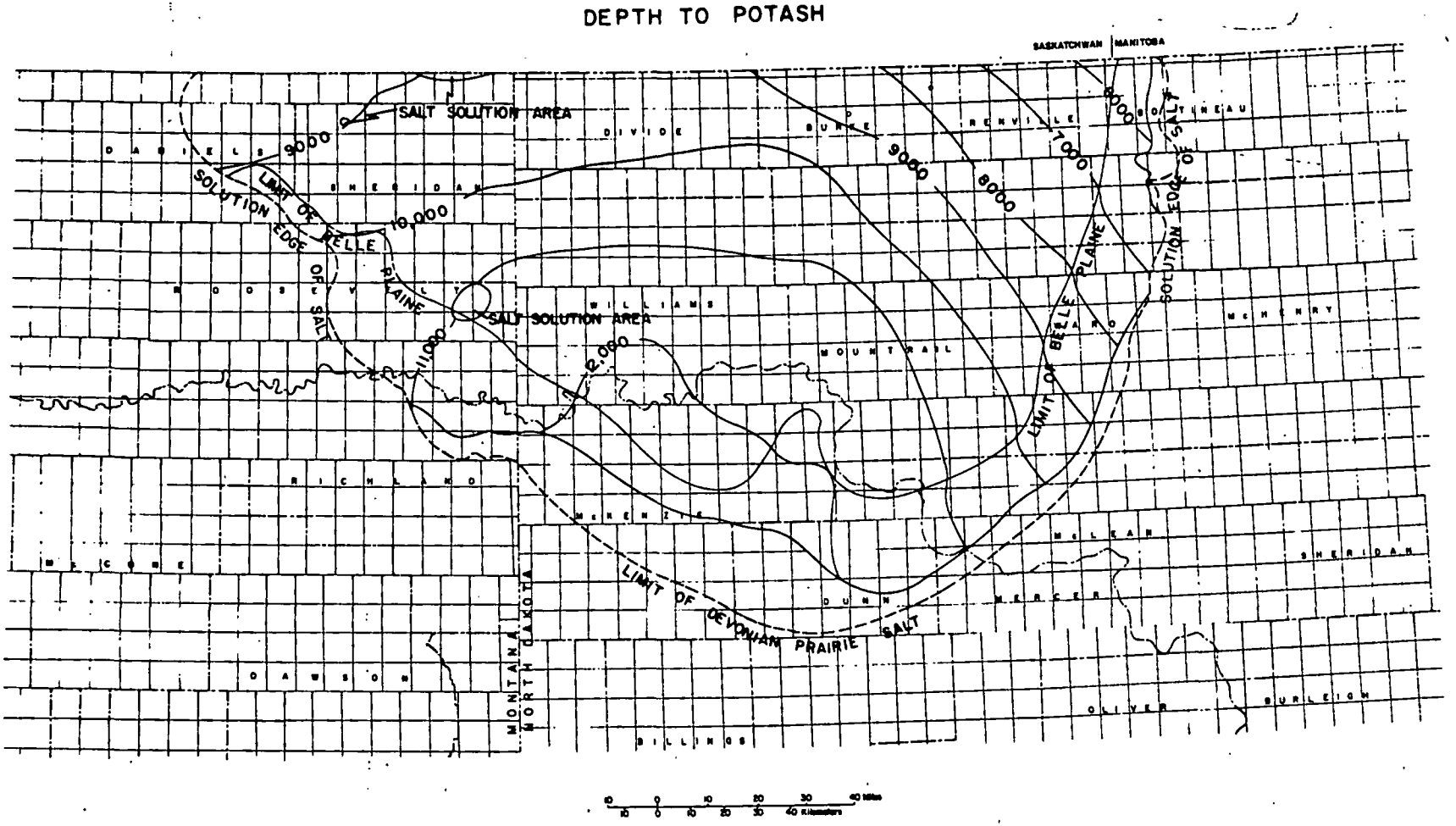

FIG. 6. Depth to potash in northwestern North Dakota and northeastern Montana.

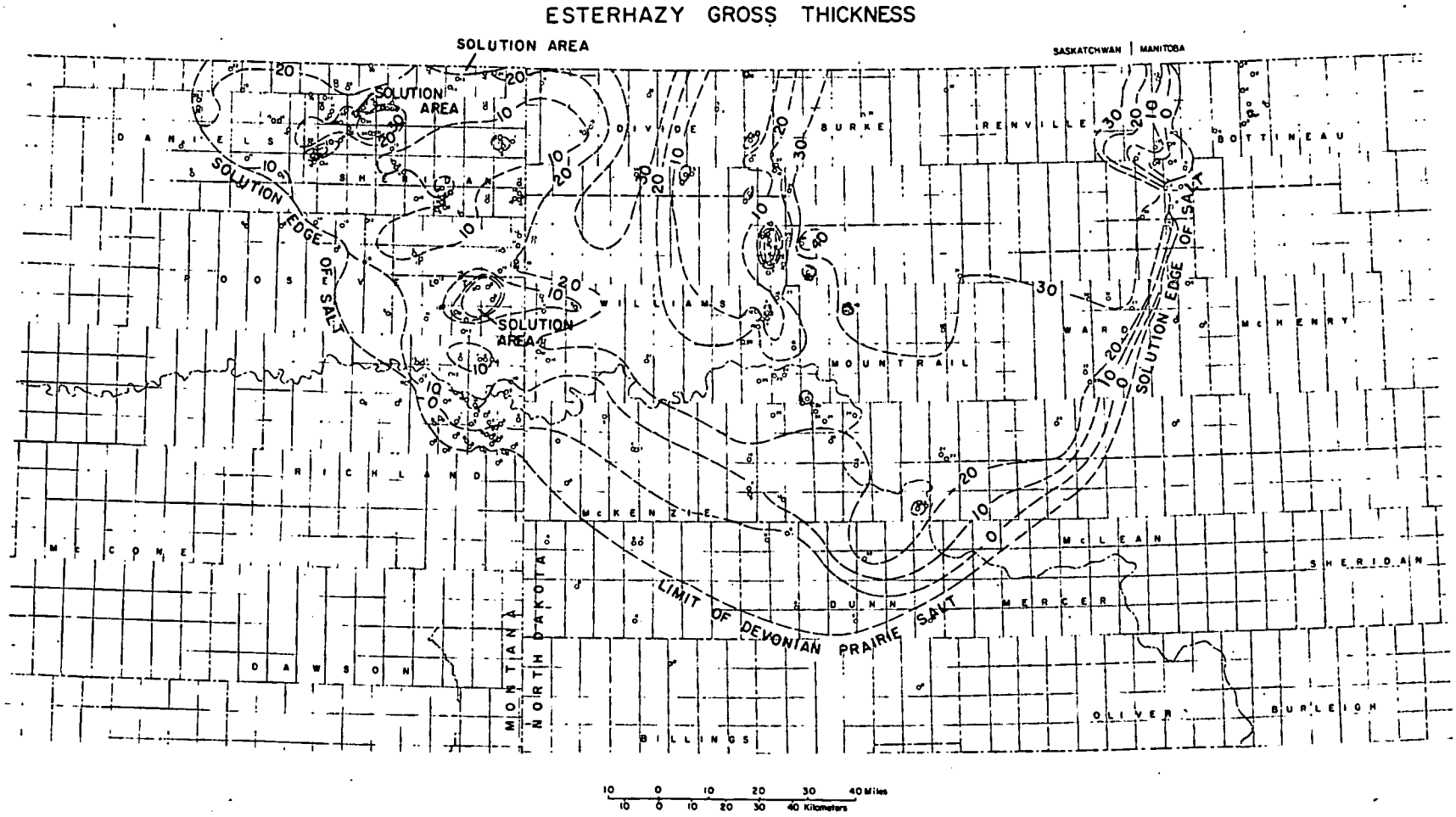

FIG. 7. Gross thickness of the Esterhazy Member of the Prairie Formation in northwestern North Dakota and northeastern Montana.

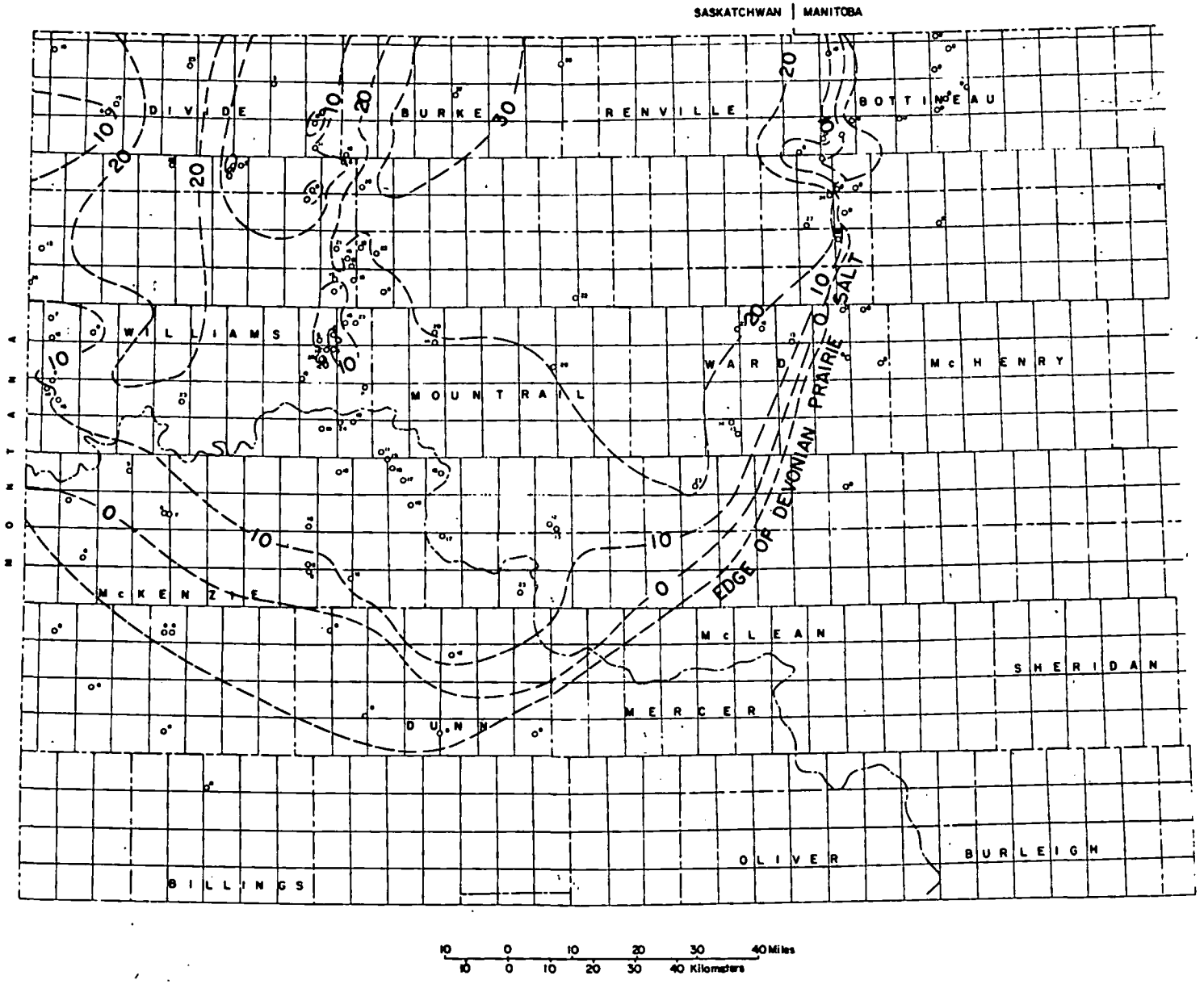

FIG. 8. Net thickness of the Esterhazy Member of the Prairie Formation in northwestern North Dakota.

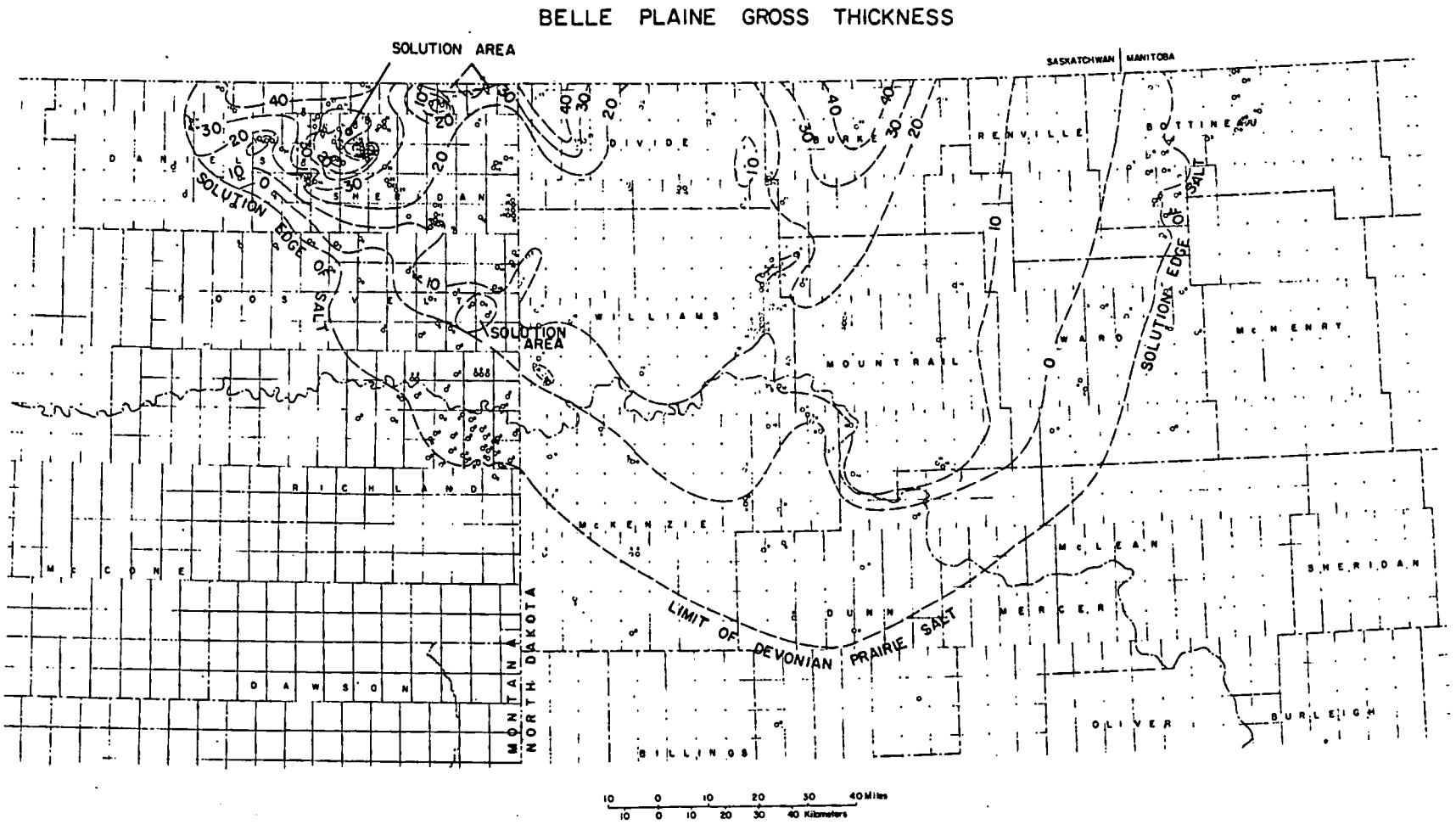

FIG. 9. Gross thickness of the Belle Plaine Member of the Prairie Formation in northwestern North Dakota and northeastern Montana.

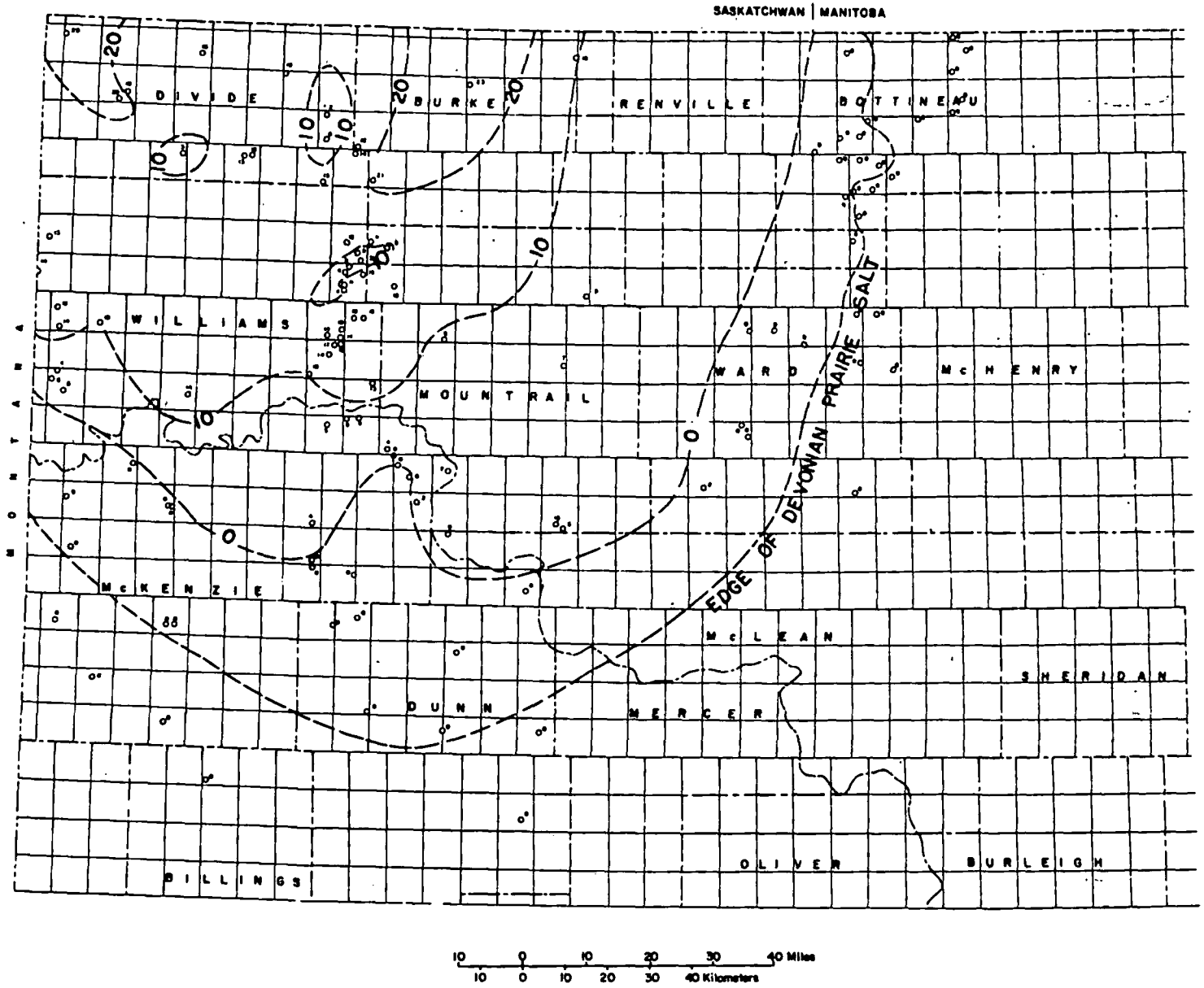

FIG. 10. Net thickness of the Belle Plaine Member of the Prairie Formation in northwestern North Dakota.

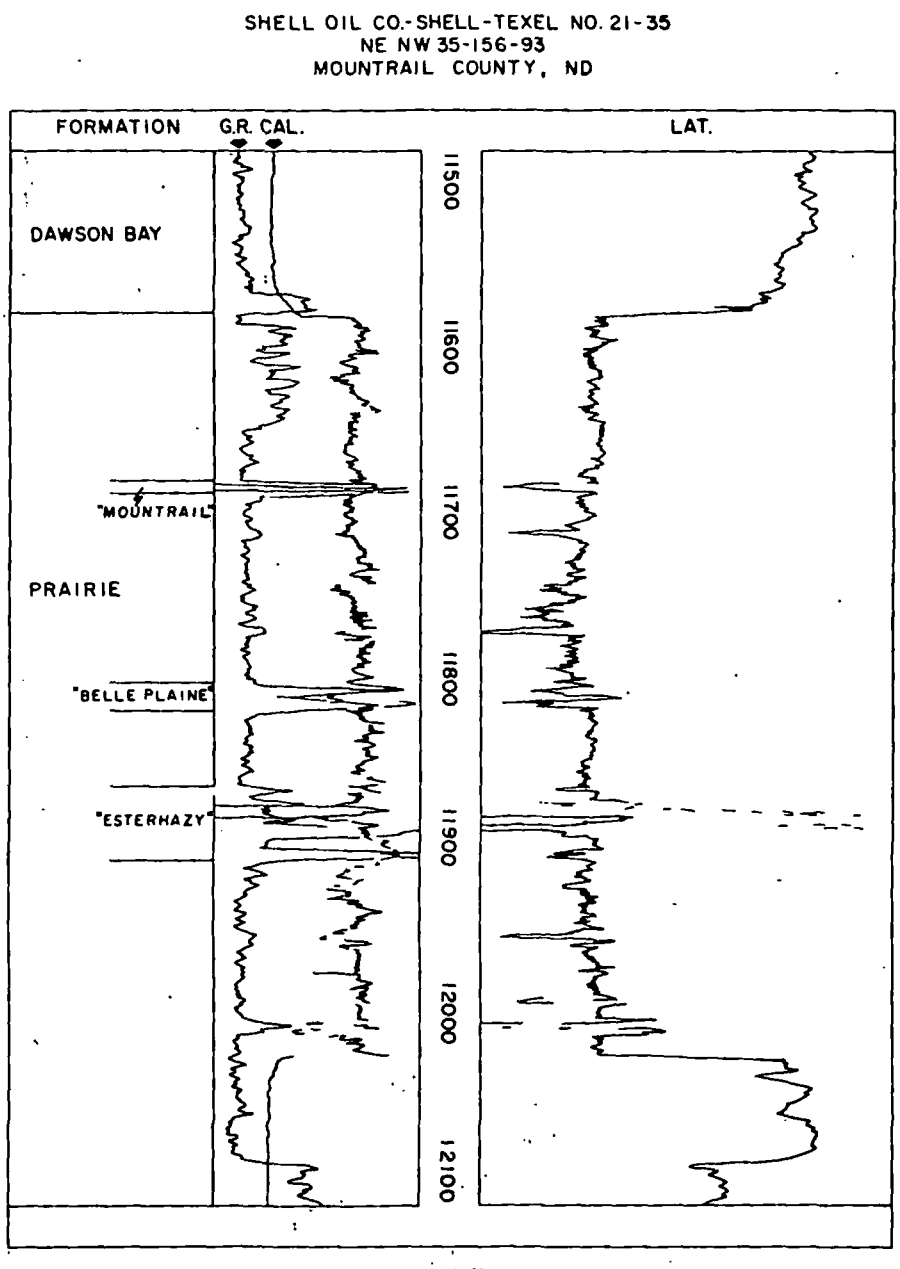

FIG. 11. Log section of the Shell Oil Company–Texel No. 21–35 well, Mountrail County, showing the Prairie Formation.

The two major beds, the Esterhazy and Belle Plaine Members, reach a combined gross thickness of 83 ft (25 m) and a net thickness of 55 ft (17 m) in North Dakota. In Montana they reach a combined thickness of 61 ft (18.5 m) gross and 43 ft (13 m) net.

This study is based on apparent potash-bed thicknesses from gamma ray logs. The thicknesses were determined by selecting characteristic points on the well logs; however, actual minable thicknesses may be less because of the gradational contacts of halite and sylvite.

The potash deposits of North Dakota and Montana occur at depths exceeding 3,500 ft (1,065 m), which precludes the possibility of conventional shaft-mining and makes solution-mining the only viable method

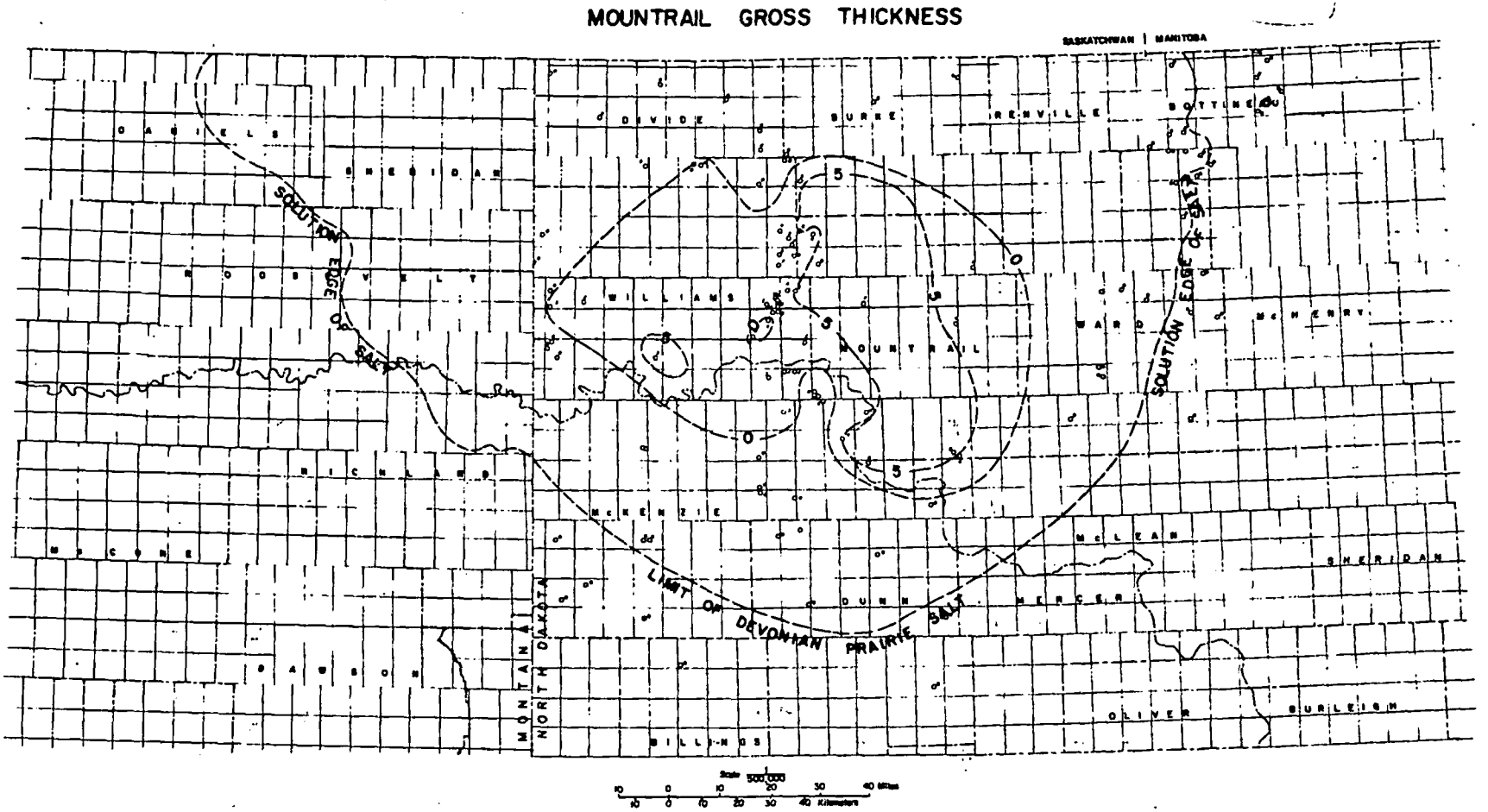

FIG. 12. Gross thickness of the Mountrail Member of the Prairie Formation in the study area.

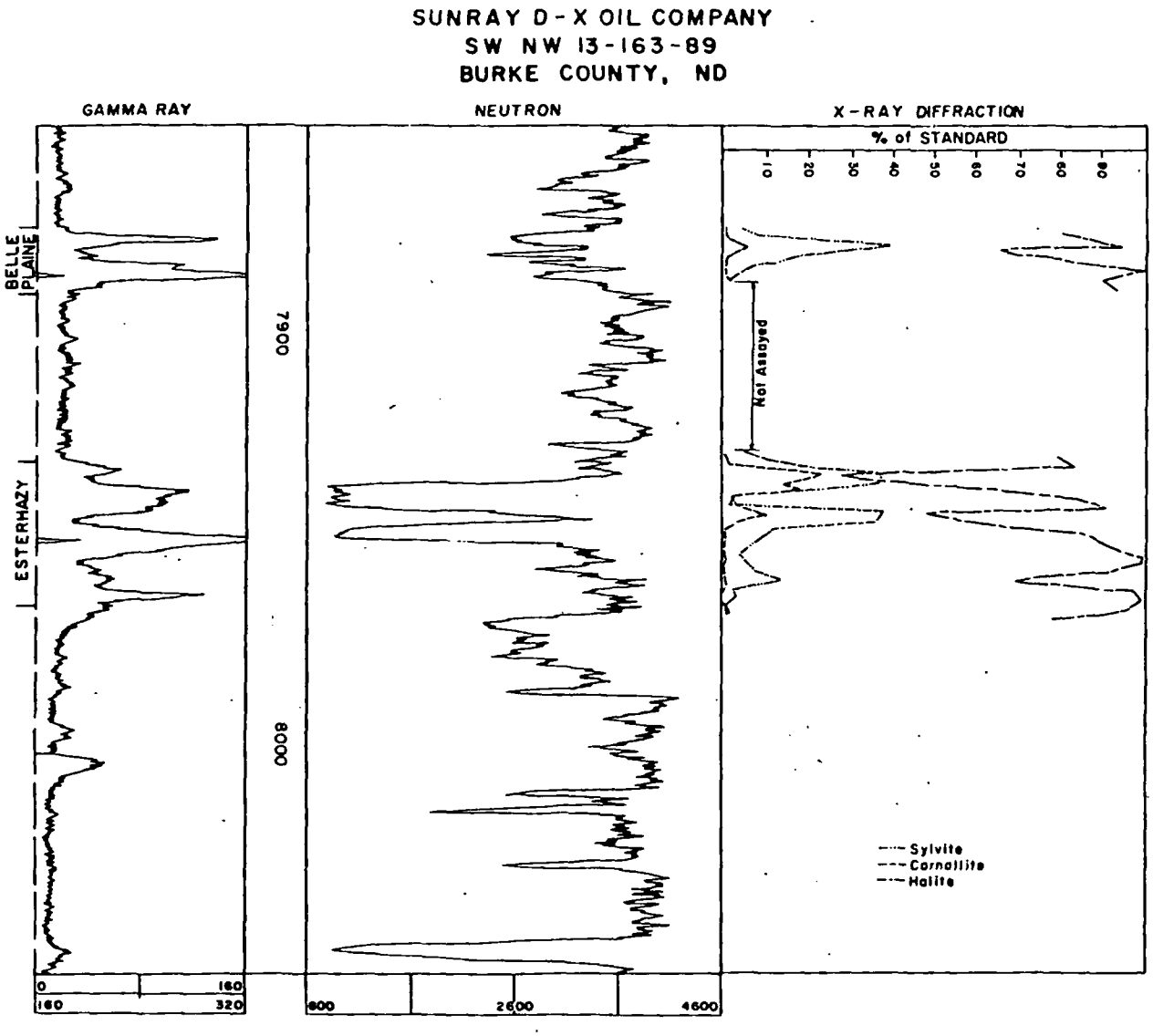

FIG. 13. Log section of the Prairie Formation in the Sunray D-X well in northeastern Burke County, North Dakota, with X-ray analysis.

(Fig. 6). In North Dakota depths range from 5,600 ft (1,700 m) near the eastern limit in northwestern Bottineau County to over 12,000 ft (3,650 m) in southern McKenzie and northern Dunn Counties. Depths in Montana range from 8,300 ft (2,530 m) near the western limit in Daniels County to 11,500 ft (3,500 m) in Richland County (Fig. 6).

Esterhazy Member

The Esterhazy Member is the most extensive potash bed in the U. S. portion of the Williston Basin (Fig. 7); extending westward from western Bottineau County, North Dakota, to Daniels County, Montana, and south from the international boundary to northeastern Dunn County, North Dakota. This member is also the lowest stratigraphically and the shallowest. The Esterhazy Member occurs at a depth of 5,632 ft (1,717 m) in northwestern Bottineau County, which is the shallowest known occurrence of potash in the U. S. portion of the basin.

In North Dakota, the Esterhazy Member has a maximum known gross thickness of 44 ft (13 m) at a depth of 11,800 ft (3,600 m) in west-central Mountrail County. In eastern and central Burke County,

North Dakota, gross thicknesses of 38 to 39 ft (12 m) are developed at depths of 7,900 ft (2,400 m) to 7,000 ft (2,130 m). In Montana, gross thicknesses of 31 ft (9.4 m) to 34 ft (10 m) are developed in west-central Sheridan County at a depth of about 9,000 ft (2,750 m). Three areas without potash occur in eastern Divide County, North Dakota, and another in southeastern Williams County. These areas occur where the potash is generally less than 10 ft (3 m) thick. The possible explanations are: (1) the Nesson anticline may have influenced deposition; (2) the area may have been higher than surrounding areas during deposition of the potash; and (3) fresher water may have entered the area and dissolved the potash soon after deposition.

In North Dakota the maximum net thickness known is 32 ft (10 m) in north-central Burke County (Fig. 8). The net thickness equals the gross thickness of the potash member minus the thickness of the interfingering halite beds. Other areas in North Dakota with substantial net thicknesses are: central Divide County, 29 ft (9 m); northeastern Burke County, 28 ft (8.5 m); and southwestern Bottineau County, 27 ft (8 m). In Montana the maximum net thickness is 22 ft (7 m) in northwestern Sheridan County.

Belle Plaine Member

The Esterhazy and Belle Plaine Members are separated by an interval of halite that ranges from

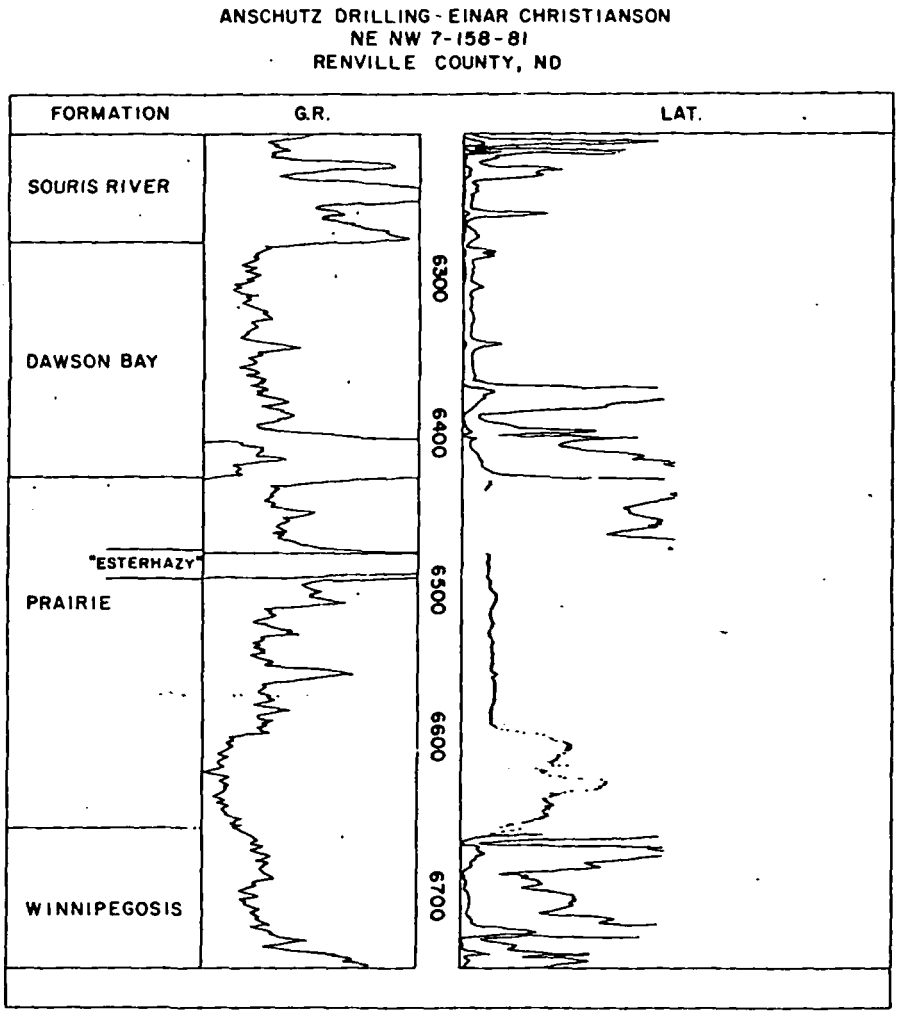

FIG. 14. Log section of the Prairie Formation in the Anschutz Drilling-Einer Christianson well in Renville County, North Dakota.

less than 15 ft (4.5 m) to more than 50 ft (15 m) thick. The Belle Plaine Member, which is not as extensive as the Esterhazy Member, extends from western Bottineau County, North Dakota, west to central Daniels County, Montana, and south from the international boundary to northeastern Dunn and east-central McKenzie Counties, North Dakota (Fig. 9). The greatest known gross thickness in the U. S. portion of the Williston Basin is in west-central Sheridan County, Montana; here the member attains a thickness of 46 ft (14 m) at a depth of slightly more than 9,000 ft (2,750 m). In North Dakota, the greatest known thicknesses are in northwestern Divide County where the gross thickness reaches 45 ft (14 m) and in central Burke County where it reaches 44 ft (13 m). Net thicknesses in North Dakota reach maximums of 29 ft (8.8 m) in Divide County and 23 ft (7 m) in central Burke County (Fig. 10). In Montana they are as much as 38 ft (12 m) in northeastern Daniels County and 30 ft (9 m) in northwest Sheridan County.

Mountrail Member

The Belle Plaine Member is overlain by another potash member that has not been named; it is here informally named the Mountrail Member. Between the Belle Plaine and Mountrail Members is an interbed of halite that ranges in thickness from 40 ft

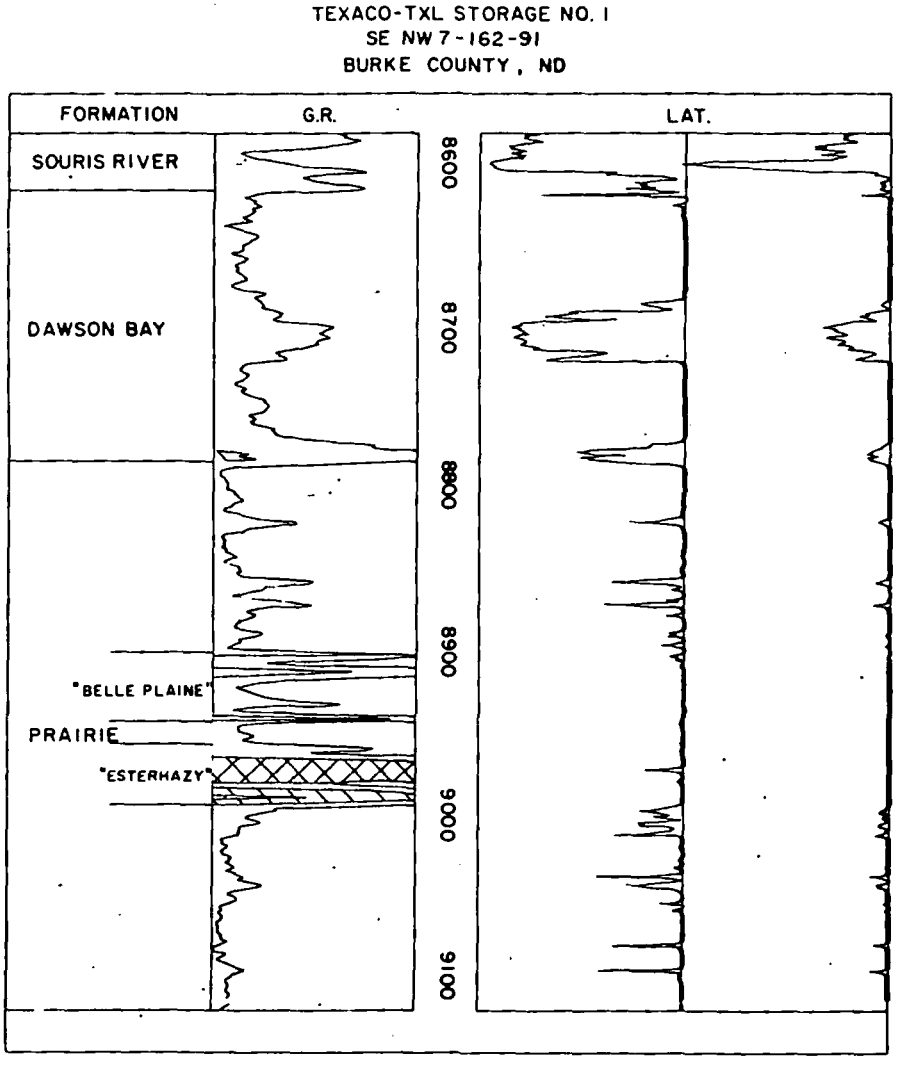

FIG. 15. Log section of the Prairie Formation in the Texaco-TXL Storage No. 1 well in Burke County, North Dakota.

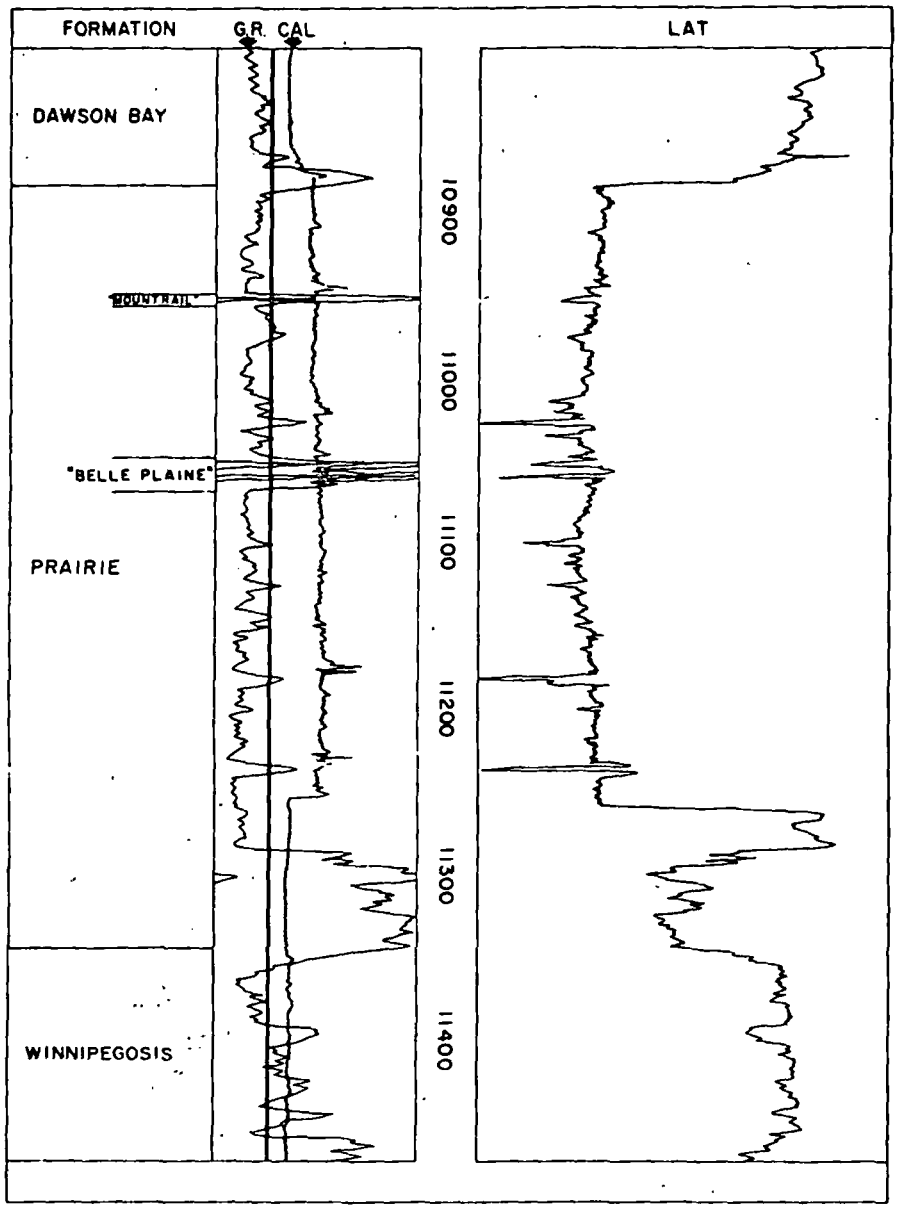

FIG. 16. Log section of the Prairie Formation in the Amerada Ives-Skaar Unit No. 1 well in Williams County, North Dakota.

(12 m) to 130 ft (40 m). The Mountrail Member is established for the potash bed between depths of 11,680 ft (3,560 m) and 11,687 ft (3,562 m) in the Shell-Texel No. 21–35 well located in the NE¼NW¼ of sec. 35, T 156 N, R 93 W, Mountrail County, North Dakota (Fig. 11).

The Mountrail Member is thinner and covers a smaller area than the Esterhazy or Belle Plaine Members. The Mountrail Member attains a maximum thickness of 8 ft (2.4 m) in south-central Mountrail County (Fig. 12). The member occurs near the top of the Prairie salt section; however, it probably has

TABLE I. Structural Cross-Section Data

CROSS SECTION NUMBERS AND DISTANCE BETWEEN WELLS

9 ← 7 mi → 8 ← 60 1/2 mi → 7 ← 31 1/2 mi → 6 ← 45 1/2 mi → 5 ← 21 1/2 mi → 4 ← 26 mi → 3 ← 29 mi → 2 ← 19 mi → 1 — DISTANCE BETWEEN WELLS

W-E STRUCTURAL CROSS SECTION DATA

WELL NAMES AND LOCATION	PRAIRIE SALT		POTASH MEMBERS		NOTES
	TOP OF SALT	BOTTOM OF SALT	THICKNESS AND TOP OF BELLE PLAINE	THICKNESS AND TOP OF ESTERHAZY	
Union-Nuhring #1 NWNE 32-35-47 KB 2670	NOT		PRESENT		Base of 2nd Red Bed at -5782
National Miller NWSE 10-37-48 KB 2477	-5759'	-5981'	38' at -5831'	22' at -5831'	
Carter Nelson NENW 4-37-50 KB 2502	-6273'	-6525'	46' at -6365'	28' at -6420'	
Sun-Hansen NENE 10-37-57 KB 2264	-6788'	-6997'	26' at -6814'	24' at -6874'	
Kerr McGee-Johnson NENW 34-162-101 KB 2260	-7522'	-7823'	37' at -7580'	6' at -7642'	
Amerada-Ives-Skaar #1 NWSW 24-158-95 KB 2457	-8624'	-9006'	11' at -8785'	NOT PRESENT	Mountrail Member 3' at 8690'
Texaco TXL Storage #1 SENW 7-162-91 KB 1978	-6804'	-7339'	44' at -6920'	39' at -6978'	Well TD in salt
Kirby-Brooks #1-32 NENW 32-159-82 KB 1575	-5041'	-5283'	NOT PRESENT	28' at -5123'	
Union-Steen #1 SESE 20-159-81 KB 1517	NOT		PRESENT		Base of 2nd Red Bed at 6418'

no economic value because of vertical separation from the Belle Plaine and Esterhazy Members and because it is so thin.

Mineralogy of the Potash Deposits

The sparse mineralogical data about the Prairie Formation, on the U. S. side of the basin, indicate that it is similar to the Prairie in Saskatchewan and includes halite, sylvite, and carnallite, as well as the insolubles anhydrite, clay, and dolomite (Fig. 13).

Carnallite in Saskatchewan is restricted largely to the northern and eastern margins of each of the three potash members (Holter, 1969). In apparent contrast, though based primarily on neutron logs, carnallite in the U. S. portion of the basin seems to be largely, but not entirely, restricted to the Easterhazy

Member. The mineral occurs where the member is thick and buried deeply. On its eastern margin in North Dakota and in Montana the Esterhazy Member appears to be relatively free of carnallite.

Favorable Areas for Potash Development

In North Dakota the most favorable areas for potash development appear to be: central Burke County, where the depth to potash is 8,300 ft (2,650 m) to 9,000 ft (2,745 m); western Divide County, where the depth is from about 8,900 ft (2,715 m) to 9,200 ft (2,800 m); and western Bottineau, eastern Renville, and central Ward Counties, where the depth is 6,000 ft (1,830 m) to 7,500 ft (2,285 m). Figures 14 through 17 illustrate selected log sections in these areas of the Prairie Formation.

In Montana, the northeast portion of Daniels County and the northwest portion of Sheridan County appear to be the most favorable areas for potash development. In northeast Daniels County depths range from 8,300 ft (2,530 m) to 8,900 ft (2,715 m) and in northwest Sheridan County depths range from 8,600 ft (2,620 m) to 9,000 ft (2,745 m).

Potash Resources

The total potash resources in the U.S. portion of the Williston Basin are estimated to be approximately 60 billion tons; North Dakota has an estimated 50

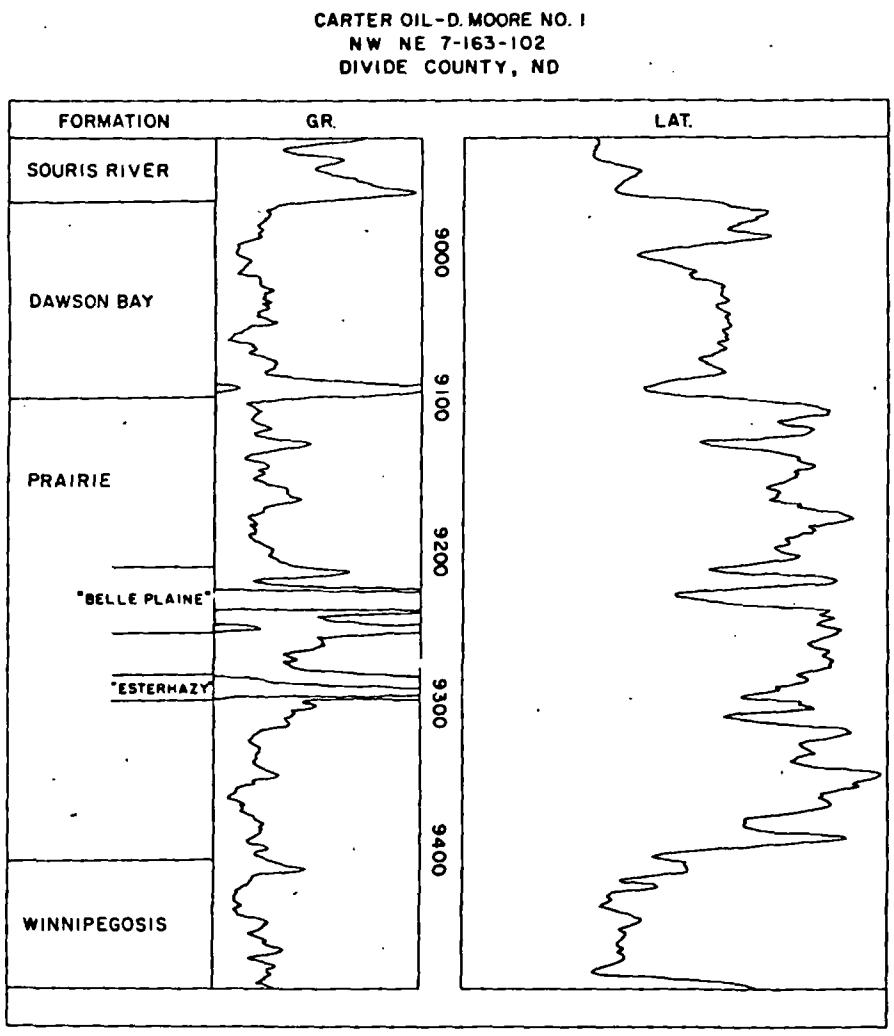

FIG. 17. Log section of the Prairie Formation in the Carter-D. Moore No. 1 well in Divide County, North Dakota.

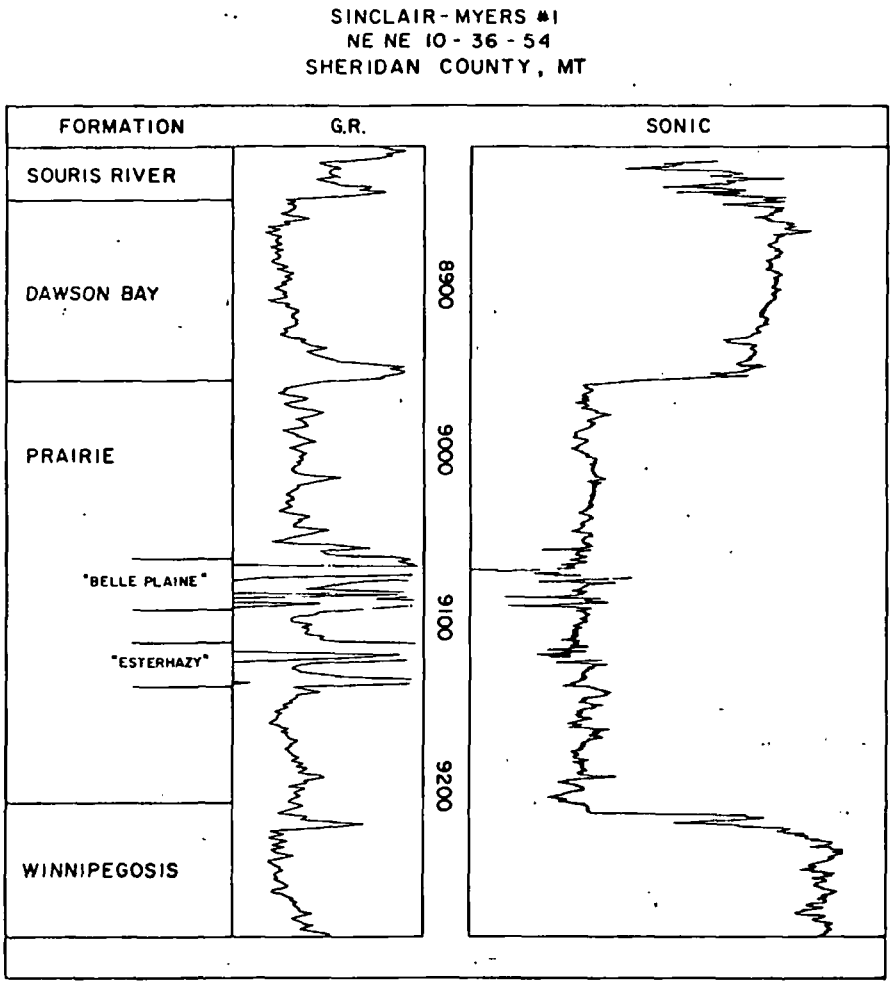

FIG. 18. Log section of the Prairie Formation in the Sinclair Myers No. 1 well in Sheridan County, Montana.

billion tons and Montana, 10 billion tons. We do not have an estimate of recoverable resources.

S. B. A.
NORTH DAKOTA GEOLOGICAL SURVEY
UNIVERSITY STATION
GRAND FORKS, NORTH DAKOTA 58202
R. P. S.
BURLINGTON NORTHERN INC.
904 FIRST NORTHWESTERN BANK CENTER
BILLINGS, MONTANA 59101
November 10, 1978

REFERENCES

Anderson, S. B., 1964, Salt deposits in North Dakota, *in* Mineral resources of North Dakota: Grand Forks, General Extension Div., Univ. North Dakota, p. 62–65.

Bannatyne, B. B., 1960, Potash deposits, rock salt, and brines in Manitoba: Manitoba Dept. Mines Nat. Resources, Pub. 59-1, p. 1–15.

Carlson, C. G., and Anderson, S. B., 1966, Potash in North Dakota: North Dakota Geol. Survey Misc. Ser. 26, 12 p.

Holter, M. E., 1969, The Middle Devonian Prairie Evaporite of Saskatchewan: Saskatchewan Dept. Min. Resources, 134 p.

Saskatchewan Department of Mineral Resources, 1973, Potash in Saskatchewan: 34 p.

Economic Geology
Vol. 74, 1979, pp. 195–220

Petrology of the Tertiary Phosphorite System of Florida

STANLEY R. RIGGS

Abstract

Four basic types of macroscopic phosphorite have been recognized within the Florida stratigraphic section. Orthochemical and allochemical phosphorite are primary marine sediments formed within the environments of deposition. The authigenic microcrystalline phosphorite mud (microsphorite) which precipitates in situ either biochemically or physicochemically is orthochemical phosphorite. If the microsphorite mud is subsequently modified into discrete clastic particles, then it is considered to be allochemical phosphorite. The muds may be torn up by biological or physical processes to produce the intraclastic allochems or ingested and excreted by organisms to form the pelletal phosphorites; if there is sufficient energy, the muds may also aggregate around a nucleus grain to form the oolites or pseudo-oolites. A fourth type of allochemical grain is the fossil skeletal material which rains into the sediment system. The bulk of the phosphate macrograins deposited during the Miocene phosphogenic system consisted of these orthochemical and allochemical phosphorites. Subsequent processes modified some of the primary phosphorites to produce the other two varieties of macroscopic grains. Any phosphorite which is later reworked into a younger sediment system is called lithochemical phosphorite. Subaerial weathering processes chemically and mineralogically change the phosphorite to produce the metachemical grains.

Microscopically, most of the phosphate macrograins are true aggregates composed of a complex mixture of various mineralogical and biological components. The primary component is the cryptograined carbonate fluorapatite matrix with various types and amounts of disseminated cryptograined coloring matter. Also, there is a multitude of micrograined included material which represents a mixture of everything that was in the environment at the time of precipitation of the orthochemical mud. The inclusions consist primarily of bacteria-like rods and rod aggregates, microorganism fossil hash, dolomite rhombs, and terrigenous sand and clay. Consequently, each phosphate macrograin is a complex sedimentary rock, the chemical composition and physical characteristics of which are totally dependent upon the specific types of inclusions and their abundances.

Introduction

AGRICULTURAL resources, followed closely and now intimately by energy, are the most basic of all resources to man. As the world population continues upon its exponential explosion, we become more and more dependent upon a highly intensive fertilizer and energy-based agriculture. According to the U. S. Bureau of Mines statistics (Stowasser, 1975), the United States produced 42.1 million short tons of phosphate rock in 1973, 98.6 percent of which was utilized for fertilizer production. About 82 percent of this production came from the Atlantic Coastal Plain deposits in Florida and North Carolina, with by far the greatest proportion coming from Florida. These coastal plain deposits represent the single most important phosphate resources in the world, accounting for 32 percent of the total world production in 1973. The phosphate resource and reserve potential of Florida, as well as the entire Atlantic Coastal Plain, are still very, very large. However, major land use and environmental pressures continue to mount in Florida causing a vast array of speculations about the future availability of phosphate reserves, as well as expansion of the mining district in the world's most important deposits. The location of the known deposits and phosphate districts of the southeast Atlantic Coastal Plain are presented in Figure 1.

The origin and mechanisms of phosphorite formation, the processes and environments of deposition, the secondary or supergene alteration, and the internal makeup of the phosphorite itself have been evasive objects of study. The problems of sedimentary phosphorite have not been easily solved for three main reasons. The first and foremost factor is the small size of the phosphorite crystallites. They are on the order of several hundreds of angstrom units and exceedingly difficult to analyze texturally, structurally, and mineralogically. Second, most phosphorite macrograins or sedimentary particles are aggregates of phosphate crystallites complexly mixed with other cryptograined and micrograined constituents in varying amounts; thus, most individual phosphorite macrograins are complex rocks. The different physical and chemical components which comprise each phosphorite macrograin must be recognized and then techniques developed to separate

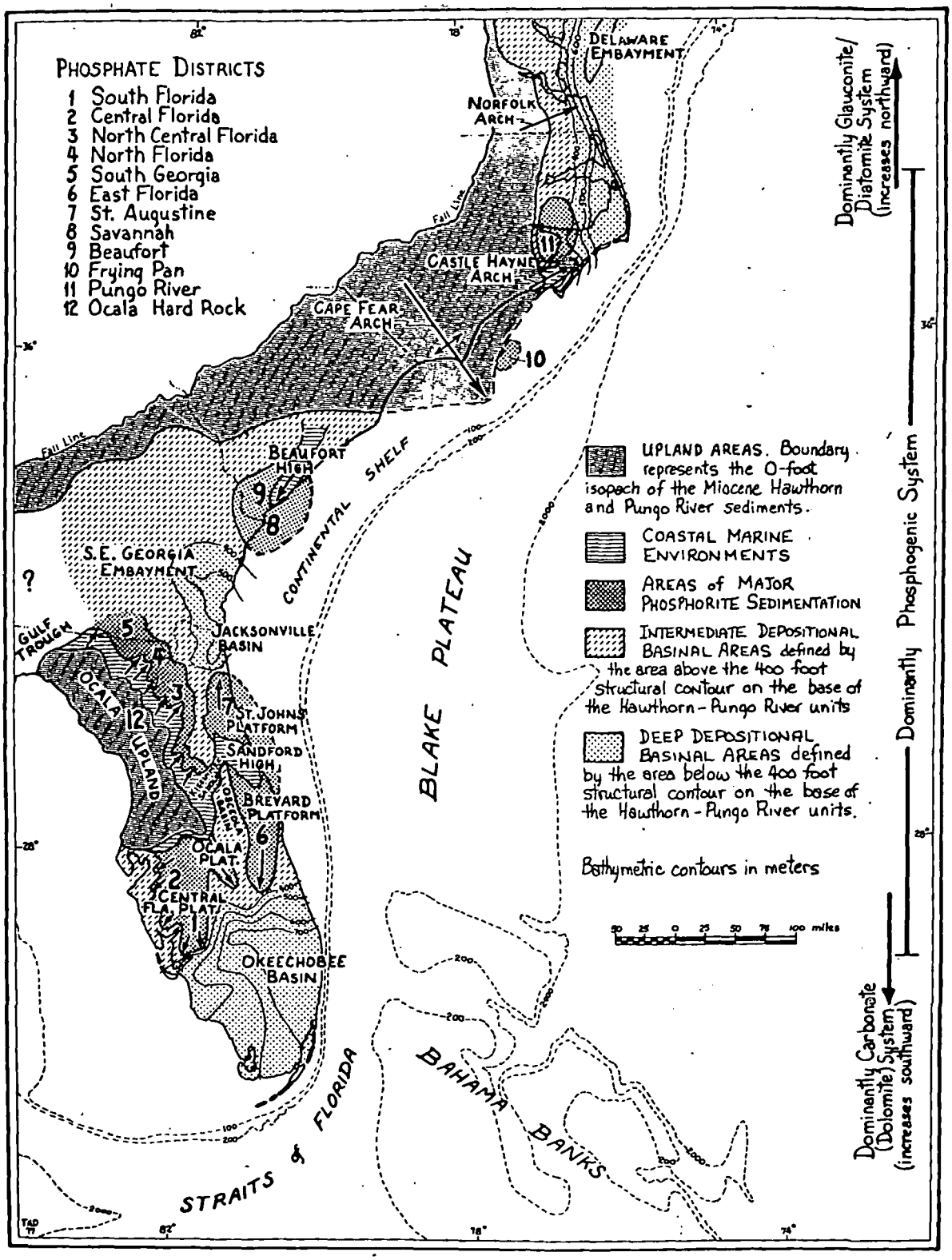

FIG. 1. Map showing the relationship between the major Miocene phosphorite deposits and the structural framework of the southeast Atlantic Coastal Plain-continental shelf system.

and analyze each component mineralogically and chemically. Due to the size of the cryptograined and micrograined constituents, few such systematic studies have been done. Consequently, individual phosphorite grain analyses are usually nothing more than bulk rock analyses. Such analyses are generally

good enough for characterizing the gross chemical and mineralogical compositions but are often not adequate for detailed interpretations of the genesis of phosphorites. The third factor which makes sedimentary phosphorites still more complex is that they are easily and commonly modified by secondary weathering processes. Thus, before the petrography, mineralogy, and chemistry of an original phosphorite grain can be understood and interpreted, the primary constituents must be differentiated from the secondary components. Therefore, the major stumbling blocks to understanding phosphorite genesis have been the fine grain size, complex mixtures, and alteration of the phosphate components.

The understanding and interpretation of any natural system first requires a thorough description. The description necessitates a well-defined terminology and is in essence nothing more than the utilization of many classifications of various parameters or variables that occur within that system. For example, the description of sediments or sedimentary rocks considers the classifications of grain size and shape, sorting, color, mineralogy, sedimentary structures, and so forth. Thus, description leads directly to and constitutes the cornerstone of classification, which is an attempt to organize and order a complex natural system. It is important to remember that any classification scheme can be no better than the level of understanding of the system at the time of consideration. Thus, any given classification should continue to evolve with the development of knowledge of the natural system.

Many sediment and sedimentary rock classifications exist in the geologic literature. However, most existing detailed classifications consider only the sediments which are either of single-mineral systems (such as the carbonate and coal classifications) or of single-source and grain-size systems (such as the terrigenous sandstone and clay classifications). However, the sediments which are deposited and represent those sometimes broad and extensive "mixing" environments between the pure end members are rarely considerd in existing classifications. Many such extensive deposits do exist both in the modern environments and in the geologic column; the world's phosphate deposits are an important example.

Phosphorite and phosphatic sediments are inherently complex since they are generally the product of three or more *different* sedimentary systems, and are, therefore, exceedingly difficult to describe. They are the product of the intermixing of numerous pure end members of sedimentation which generally include the phosphate, carbonate (both dolomite and calcite), and terrigenous systems and commonly include glauconite, organic matter, and siliceous sediments such as chert and diatomite. The Atlantic Coastal Plain deposits, as well as most other sedimentary phosphate deposits around the world, consist of complex mixtures of some or all of these terrigenous-authigenic systems. Another important system is the supergene alteration of many of the primary components which is often superimposed upon the other systems and further complicates the entire assemblage, particularly in the Central and North Florida phosphate districts.

It is my intent to present in the two papers of this symposium volume the basic description of the Tertiary phosphatic and phosphorite sediments and rocks of the Florida peninsula. The first paper will consider the basic phosphate petrology while the subsequent paper will consider the structural and stratigraphic framework, the processes of sedimentation, and the genesis of the phosphorite sediments. These two papers represent only a portion of the extensive studies of the phosphatic sediments of the United States Atlantic Coastal Plain and continental shelf by International Minerals and Chemical Corporation (Fig. 1). The ideas and interpretations in the included papers are not only applicable to the entire southeastern United States Tertiary but have been used and corroborated with field and laboratory investigations by myself and other geologists in many other regions of the world including Central and South America, western and southern Africa, the Mediterranean area, and Australia.

Regional Setting

The Florida peninsula is a portion of a much larger structural platform which extends southward between the Gulf of Mexico Basin and the Atlantic Blake Plateau and Florida Straits (Fig. 1). The peninsula itself has a central highlands which consists of the Ocala Upland surrounded by an extensive sequence of coastal lowlands with extensive marine terraces. Eastward the peninsula is bounded by the Florida-Hatteras shelf with its abundant submarine terraces. The shelf narrows southward, until below West Palm Beach the shelf is only a few miles wide and then drops abruptly into the Florida Straits. To the west, the peninsula is bounded by a very broad, gently sloping shelf cut by numerous terraces.

The dominant subsurface structure, which has defined the Florida peninsula itself, is the Peninsular Arch (Puri and Vernon, 1964). This Paleozoic-Mesozoic structure formed the axis of the peninsula and controlled pre-Tertiary sedimentation. The Cenozoic rocks of the Florida peninsula are characterized by a thick section which is dominated by carbonates. The oldest exposed rocks are the various formations of the Eocene Ocala Group, a series of pure fossiliferous limestones deposited on a shallow shelf separated from the mainland to the north by the negative area called the Gulf Trough (Pat-

terson and Herrick, 1971). The Ocala sediments were deposited on an isolated bank system much like the Bahama Banks today. The Ocala Arch is a slightly irregular uplift and deformation of the Eocene rocks forming an upland area which controlled all subsequent Tertiary sedimentation. The resulting Ocala Upland constitutes the Central Highlands physiographic province with its extensive karst topography and springs. The Oligocene rocks, mainly the Suwannee Limestone, are similar to the Eocene limestones but commonly contain a slight increase in terrigenous content.

The Miocene sediments, the subject of this paper, were a product of a dramatic change in the entire sediment system operating throughout the Atlantic Coastal Plain. In Florida, the Miocene is characterized by authigenic dolomite and phosphorite mixed with a flood of terrigenous sediments which transgressed across the Florida peninsula as the Gulf Trough ceased to exist. The phosphatic portion of the section is defined as the Hawthorn Group. The Hawthorn is subdivided into three lithologic formations, the Miocene Arcadia and Noralyn Formations and the Pliocene Bone Valley Formation. The extensive open-marine Arcadia Formation consists dominantly of dolomite mixed with primary allochemical phosphorite and subordinant amounts of terrigenous sediments. This unit contains the vast phosphate resources of the future. The Noralyn Formation consists of the shallow-water coastal-marine terrigenous sands and clays mixed with primary orthochemical and allochemical phosphorite. This unit constitutes the bulk of the phosphate presently being mined in Florida. The Pliocene Bone Valley Formation is a thin and local unit of fluvial, estuarine, and coastal-marine sediments composed of terrigenous sands and clays, abundant shell material, and reworked lithochemical phosphorite. This unit contains the abundant fossils for which the Central Florida phosphate district is so famous, however, only locally does it constitute a major portion of the mined phosphate. The fluctuations of Pleistocene sea level across the Florida peninsula deposited a sequence of coastal and barrier-island deposits of mixed shell and terrigenous sand and clay with carbonate reefoid sedimentation in the southernmost region. Most of the present topography of peninsular Florida, other than the Central Highlands themselves, is a product of the coastal sedimentation patterns of the Pleistocene-Holocene sea-level fluctuations, which are still in progress.

The Macroscopic Components of Primary Phosphorites

Phosphate is a mineralogical component, which, at best, occurs in minor amounts in most sedimentary rocks of the world. The presence of phosphate in concentrations of greater than 1 percent is anomalous and an important sediment component since its appearance reflects changing and specialized depositional conditions, as well as the potential of an economic concentration. The description of thousands of drill holes throughout the Atlantic Coastal Plain and measurement of hundreds of detailed mine sections have led to the following definitions as major parts of the descriptive sediment or rock name.

Phosphorite: A rock term which applies to all sediments or rocks containing 10 percent or more (volumetrically) individual phosphate grains mixed with any other mineral components and is used to describe either the phosphate component of a given sample (i.e., pelletal phosphorite, orthochemical phosphorite, etc.) or the total rock or sample. In the later case, this term precedes all of the predominant mineralogical and/or textural components of a given sample (i.e., phosphorite quartz sand, phosphorite dolomite, etc.). If the phosphate grains are the predominant mineralogical component, then the term phosphorite follows the subordinant mineralogical components and precedes the dominant textural character (i.e., quartz phosphorite sandstone, dolomitic phosphorite mud, etc.). The 10 percent figure represents a significant natural break between two major sample populations within the sediments of the Hawthorn Group of Florida.

Phosphatic: A rock term which applies to all sediment or rock samples which contain 1 percent or greater but less than 10 percent (volumetrically) individual phosphate grains mixed with any other mineral components. This term modifies the predominant mineralogical and/or textural components of the sample (i.e., phosphatic quartz conglomerate, phosphatic dolomite, etc.).

Phosphate: A general term which applies to a class of chemical compounds, a group of minerals, individual sedimentary grains or particles, or a mineral deposit.

Sedimentary phosphorites are composed of three different basic size categories. The phosphate mineral component, which is the basic crystallite size and consequently not discernable with normal optical systems, is the cryptograined material ($<0.1\mu$). The grains of the second scale, the micrograins (<0.0625 mm $>0.1\ \mu$, silt and finer) are only discernable microscopically. The cryptograins and the micrograins aggregate to produce grains of the third order of magnitude, the macrograins which are larger than silt size (>0.0625 mm). These grains are discernible without the aid of a microscope and con-

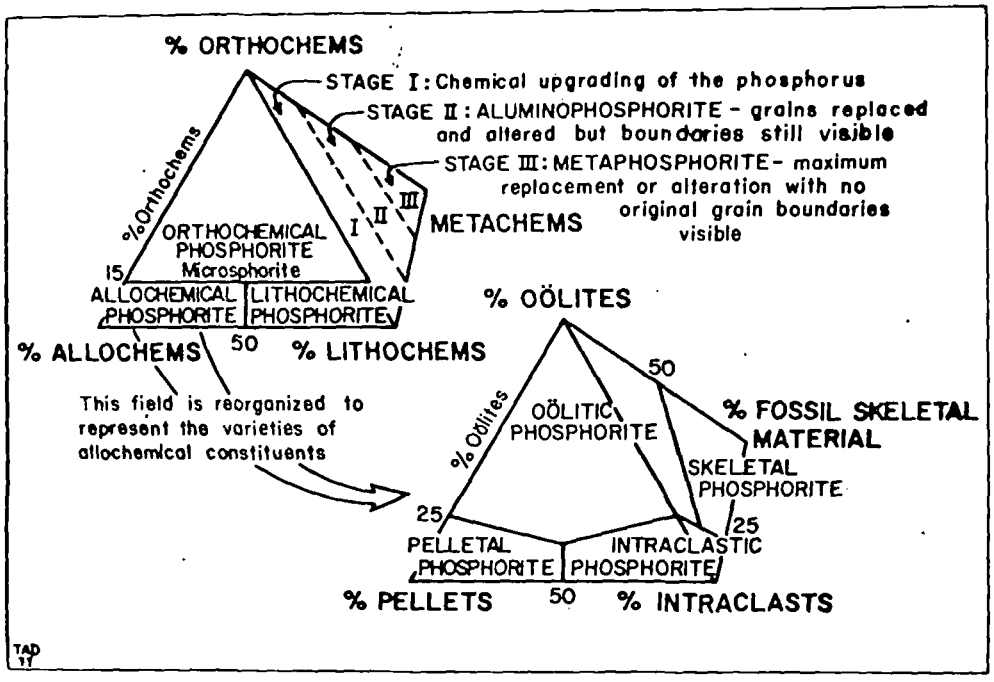

FIG. 2. Classification of the macroscopic components of sedimentary phosphorites.

stitute the macroscopic sedimentary particles which are most familiar.

Sedimentary phosphorites are initially authigenic minerals which form on the sea floor. Consequently, the study of these sediments can be approached in an analogous way to other better known authigenic sediments. Studies of carbonate sediments by Folk (1959, 1962, and 1968) and others have shown that the complexity of carbonate rocks can be greatly simplified by considering two broad classes of sedimentary particles, orthochemical (orthochems) and allochemical (allochems). Orthochemical constituents are nonclastic, clay-sized sediments formed physicochemically or biochemically within the area of deposition and show little or no evidence of transportation or aggregation into more complex entities (Folk, 1968). Allochemical grains are larger than clay-sized, clastic sediments that have formed physicochemically or biochemically within the area of deposition, but which are organized into discrete aggregated bodies and have for the most part suffered some transportation within the area of deposition (Folk, 1962).

The description of phosphorite sediments can be approached similarly since they are also composed of orthochemical and allochemical components. Riggs (1967) recognized that under certain circumstances, the primary phosphorites are modified by secondary processes. Thus, he described two additional broad classes of sedimentary particles which are often important and essential in unraveling the complex phosphate sediment system, lithochemical (lithochems) and metachemical (metachems). The term lithochemical was introduced to describe older clastic rock fragments of similar composition formed physicochemically or biochemically during a prior geologic age and which were initially deposited and lithified beyond their present site of deposition. Thus, any or all of the other classes of phosphorite sediments which have been later eroded, transported, and redeposited as lithified grains in a significantly different and younger sequence of sediments are included in this class of sediments.

The term metachemical was introduced to describe clastic or nonclastic, primary or reworked constituents of physicochemical or biochemical origin which have been mineralogically and chemically modified by supergene alteration and weathering. Thus, any or all of the above classes of phosphorite sediments which are subsequently modified by supergene alteration are included in this class of sediments.

Each class of grains has definite stratigraphic, sedimentological, and petrographic characteristics which must be recognized and separated before the genesis of these complex sediments can be adequately worked out. The influence of organisms, turbulence, and other characteristics of the primary depositional environments can be inferred by describing the sediments using the first two parameters. The subsequent geologic history and secondary modifications of the original phosphorite deposits can be interpreted using the second two parameters. Figure 2 presents the classification of macroscopic phosphorite components.

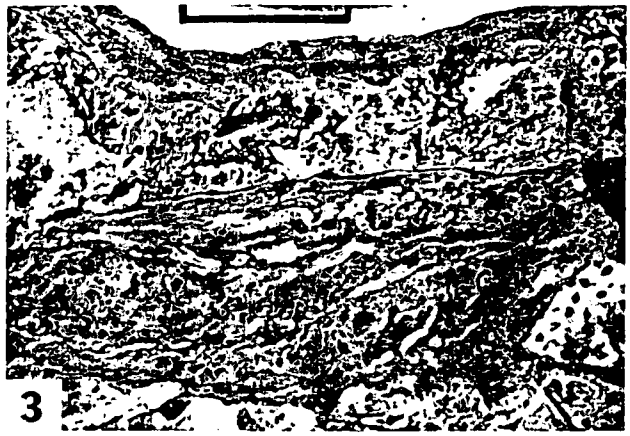
3


4


5

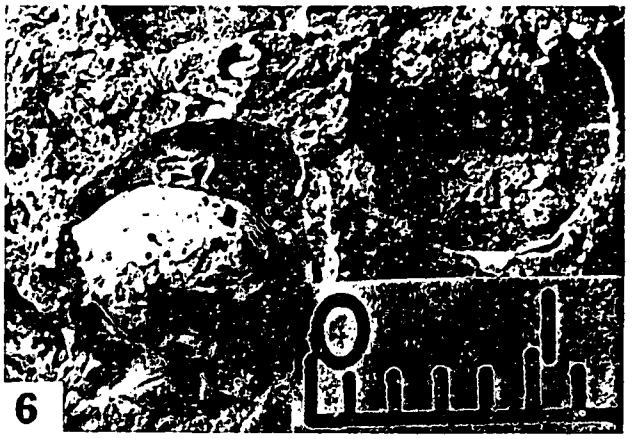
6

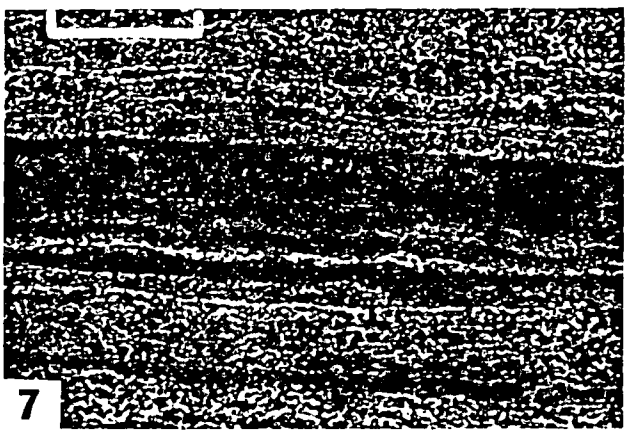
7


8


9


10

Orthochemical phosphorite sedimentation

Orthochemical phosphorites are clay-sized phosphate minerals formed physicochemically or biochemically in situ in the marine environment and show little or no evidence of transportation. Such deposits are composed of cryptograined phosphate constituents, as well as any other micro- and/or macrograined material which is in the environment at the time of deposition. Riggs and Freas (1965) and Riggs (1967) proposed the name "microsphorite" for this primary phosphorite mud; this is a contraction of microcrystalline phosphorite, which is analogous to micrite in the carbonate terminology. Mineralogically and chemically, orthochemical phosphorite may not differ from allochemical phosphorite. Thus, the most critical parameters for its recognition are the stratigraphic occurrence and the textural and structural relationships of the phosphorite material with the associated sediments and rocks. The orthochemical phosphorites occur preserved as distinct beds or laminae within discrete stratigraphic units, disseminated mud binding the clastic diluents, or as organically produced structures such as burrows and fossil molds. Consequently, it is advantageous to start with a detailed stratigraphic framework prior to working with this concept.

Description of orthochemical phosphorite: The microsphorite beds in the Florida Miocene are generally graded. The grading is defined by a general upward increase in phosphorite mud and degree of induration of each microsphorite sequence. The lower portion is a nonindurated to semiindurated phosphorite mud matrix in a mixed terrigenous and allochemical phosphorite sand sediment. This portion often has the superficial appearance of a marl. The mud grades upward into an indurated, predominantly microcrystalline phosphorite mud with minor amounts of included terrigenous grains and allochemical phosphorite. The indurated mud portion most commonly occurs as laminae a centimeter or less thick; however, under specialized conditions, it may be up to one meter thick and may be composed of one or more sets of graded sequences (Fig. 3). The upper indurated surface of each graded sequence is generally slightly undulating and highly polished with truncated inclusions of terrigenous and allochemical phosphorite grains, pelecypod borings, and accretionary fillings and laminations of additional phosphorite mud (Fig. 4). Occasionally, layers of microsphorite will occur on top of and grade down into a fossiliferous mold and cast carbonate horizon. In such instances, carbonate replacement structures are quite apparent in thin section.

Where a single microsphorite bed is more than 15 cm thick, a complex anastomosing burrow network extends down into the middle portion from an upper microsphorite surface. The uniform tube-shaped burrows range from about 1 cm up to 2.5 cm in diameter, extend downward 3 to 30 cm from a microsphorite surface, and then turn and run parallel to the surface bifurcating and connecting with other burrows. The burrow walls are generally coated

FIG. 3. Microsphorite sample slabbed perpendicular to the bedding to show thin microsphorite interlaminae of semiindurated, very pale orange and indurated, moderate brown microsphorite. The figure shows three sediment surfaces and quartz sand inclusions (dark grains). Scale bar is 5 mm long.

FIG. 4. A close-up of a microsphorite surface which shows pelecypod borings, filled pelecypod borings, included and truncated quartz grains (dark colored specks), phosphorite mud accretions, and the high surface polish. Scale in centimeters.

FIG. 5. Microsphorite sample which shows part of a complex anastomosing soft sediment burrow system which is lined with concentric interlaminations of dark indurated and lighter semiindurated microsphorite mud. Scale in centimeters.

FIG. 6. Top view of a microsphorite surface which shows two filled borings with the steinkern of the boring pelecypod in the left mold. Scale bar is 1 cm long.

FIG. 7. Photomicrograph of microsphorite section cut perpendicular to the bedding. The very thin, moderate brown microsphorite laminae in Figures 3 and 5 are characterized by the denser lamellar zones of bacterial-like rods; the lighter microsphorite laminae are characterized by a less dense concentration of rods and an increase in phosphorite matrix. Scale bar is 50 microns long.

FIG. 8. The internal pelecypod mold in a microsphorite bed filled with fecal pellets. The pelecypod shell was partially filled with phosphate mud and fecal pellets prior to induration, then the filling was indurated, and the original shell material leached away. Scale in centimeters.

FIG. 9. Extremely angular phosphorite intraclast granules which show the original microsphorite laminations and zones. These allochemical grains occurred immediately adjacent to a partially disrupted microsphorite bed from which they were derived and deposited with minimal transport or grain modification. Scale bar is 5 mm long.

FIG. 10. Generally very well rounded phosphorite intraclasts which contain recognizable microsphorite textures and structures. These grains occurred in a sediment unit where there was no evidence of adjacent microsphorite beds; thus, the grains were probably transported considerable distances and abraded. Notice that most of the grains have a flat surface, and that with decreasing grain size there is a marked increase in rounding, decrease in grain complexity, a decrease in recognizable microsphorite textures and structures, and an increase in the regular subspherical and oval allochemical pellets. Scale bar is 1 mm long.

with an extensive sequence of thin concentric laminations (Fig. 5). The surface muds were swept into the burrows by currents or carried in by the organisms themselves and packed or molded against the burrow walls.

The burrows are commonly filled with various materials. Some contain clusters of very uniform, regularly shaped phosphate pellets, which are without much question of fecal origin. When phosphorite mud precipitation momentarily ceased, phosphorite sand and clay were deposited as thin, discontinuous lenses and filled the inactive burrows. Subsequent formation of phosphorite muds then filled or cemented over the tops of the old burrows. The microsphorite burrows appear to represent a burrowing crustacean which lived in a shallow neritic to littoral marine environment. The microsphorite was probably a soft, sticky mud when it was burrowed. The burrows are well preserved and very commonly occur as part of allochemical pebbles.

The microsphorite surfaces contain abundant borings that range from 6 to 12 mm in diameter and from slight surface impressions to 4 cm deep (Fig. 4). These structures are considered to be hard-rock pelecypod borings rather than soft-sediment burrows because they are identical in size and shape to the borings on bones and lithoclast pebbles. Also, the internal molds of some of the pelecypods are occasionally preserved within the borings (Fig. 6). Some of the borings pass through the upper indurated microsphorite zone and extend into the softer underlying microsphorite mud. Many of the borings were subsequently filled by sediments producing internal casts of the borings. The casts are occasionally preserved in the microsphorite unit and also as allochemical pebbles. The borings, which are no deeper than surface impressions, were probably formed by animals that bored through the sediment that overlaid the microsphorite and that only penetrated the top of the indurated microsphorite bed.

The microsphorite beds contain abundant included phosphorite allochems and terrigenous sediments (Fig. 4). Many of these sand grains are truncated at the microsphorite surface, others protrude slightly above the microsphorite surface and are rounded to the surface with microsphorite lips, while still other protruding grains are angular and unpolished. Some of the quartz grains in the microsphorite have moderate reddish brown, high-relief coatings of rods and aggregates on one or more faces. The coatings, up to 3 microns thick with irregular upper surfaces, may have formed as growths on the grain surfaces while the grains were at the sediment interface. Surface coatings on clastic grains suggest intermittent periods of low energy prior to burial.

The microsphorite is generally mottled under low magnification; the mottles are mostly areas of higher concentration of various micrograined inclusions in a lighter colored cryptograined matrix. Horizontal laminae are often preserved near the microsphorite surfaces, and concentric laminae around the burrows (Figs. 3 and 5). The laminae are from 5 microns to several millimeters or more thick and are generally fairly regular and sharply defined. Some laminae are zoned into three parts. From bottom to top or from the outside inward the three zones are:

Zone 1. Soft, light-colored microsphorite in which the cryptograined matrix is dominant and rods or rod aggregates, if present, occur as minor constituents. Sometimes this zone is finely granular.

Zone 2. Indurated, light-colored microsphorite in which the rods and rod aggregates increase gradually and irregularly upward until they are as abundant as the matrix and occur either as mottles or completely disseminated. Occasionally the aggregates form columns perpendicular to the laminations. These possibly represent some sort of upward organic growth structure.

Zone 3. Indurated, moderate to dark brown or black microsphorite in which the rods and rod aggregates are dominant. The rods are intertwined and in some laminae lie horizontally. The concentration of rods and rod aggregates are terminated abruptly producing sharp and fairly regular upper surfaces.

All three zones are not developed in every laminae, nor are all zones necessarily of equal thickness or composition. This sequence may be repeated many times in a single burrow or in a set of horizontal laminae. The coloration of the microsphorite is directly dependent upon the concentration of the rods and rod aggregates, the most intense colors occurring where they are the densest (Fig. 7). Supergene alteration appears to remove the coloring matter and produces progressively increased lightness values.

Mottles in the microsphorite range from microscopic to macroscopic and are far more common than the laminar structures. Many of the laminae appear irregular and grade into mottles. The laminar structures, where preserved, reflect either more rapid deposition of the microsphorite, more rapid induration of the mud, or the absence of certain animals. The lack of microscopic bedding and the occurrence of mottling is probably the result of animals churning the sediments before the microsphorite was indurated. Fecal pellets occur as grains included

within the microsphorite. The pellets range in size from about 0.1 to 0.5 mm in diameter, range in shape from spherical to oblong, and occur in small clusters or aggregates, sometimes filling burrows or internal fossil molds (Fig. 8). Most fecal pellets are composed of the same material as the encompassing microsphorite, and therefore, are difficult to identify.

The microsphorite is occasionally fossiliferous, containing a limited macrofaunal assemblage of marine invertebrates. Except for a few siliceous casts, the fossils occur completely as internal and external molds (Figs. 6 and 8). I have rarely found original calcareous shell fragments or phosphate replaced shell fragments in the microsphorites of the Noralyn Formation. The faunal assemblage of the microsphorite occurs primarily in the lower zones, appears to be mostly in place, and probably represents the indigenous population of macroinvertebrates inhabiting the environment prior to the major pulse of phosphate sedimentation. The organisms were killed, buried, and infilled with phosphorite mud prior to the induration of the sediments. If carbonate was actively replaced by phosphate during deposition, one would expect to find some of the unstable, high-magnesium calcite and aragonite shells replaced by phosphate. The lack of phosphate replaced shells and the undeformed fossil molds suggests that the invertebrate shells were leached from the sediment following the induration of the mud, and any phosphate replacement followed the shell dissolution.

Paragenesis: The sedimentary structures of the microsphorite beds suggest the following paragenetic sequence. First, a pulse of soft phosphorite mud was deposited at the sediment interface killing the preexisting invertebrate fauna. The shells were buried and filled with the soft sediment; a subsequent colony of bacteria, fungi, and invertebrate organisms reinhabitated the soft muds; these muds were injested and excreted as fecal pellets and were molded to the burrow walls. Second, the surface mud was indurated during periods of change from mud deposition in environments of low turbulence to nondeposition and total sediment by-pass during brief periods of high turbulence. Third, the indurated surfaces remained exposed long enough to establish a boring molluscan infauna. Also, the abundant clastic sediments that moved across the surface truncated the included quartz and phosphate grains, smoothed and polished the surface, and accreted minor amounts of new phosphorite muds. Fourth, the calcareous shell material was leached some time after the muds were indurated since the molds were not deformed by sediment compaction nor were casts subsequently produced. Finally, when the environmental conditions were right again, deposition of the microsphorite muds resumed, and the above sequence was repeated.

Some of the microsphorite beds were subsequently torn up and removed by an erosional process which is both very common and very important in the formation of the phosphorites throughout the inner perimeter belt around the Ocala Upland. This process was documented in detail by Riggs (1967) in his study of the Noralyn mine where it was excellently preserved. The microsphorite unit was 60 cm thick and the upper 30 cm consisted of three 10-cm indurated microsphorite laminae. The entire unit was abruptly truncated on the south side by erosion and reappeared in stair-step fashion from 3 to 6 m to the north. Sandy gravel, consisting of 15 to 30 cm platy pebbles and cobbles of the microsphorite beds littered the erosional pocket from which the microsphorite had been torn. The pebbles and cobbles were generally flat lying, and some were upside down with the smoth, bored surface downward. The gravel decreased in size and graded to a clayey, gravelly sand both upward and laterally from this area. The broken edges of both the clasts and the microsphorite bed were quite irregular but generally rounded.

The formation of the microsphorite is thought to take place in relatively low energy environments. However, the erosion and fragmentation of the beds is thought to be a response to periodic high-energy storm events. The combination of the organic burrowing and boring activity, with the waves undercutting the indurated microsphroite beds, breaks off gravels of all sizes and shapes. The gravels may then accumulate in adjacent lows or may be transported from the immediate area with continued fragmentation. The subsequent rounding of the gravels may be in part a response to abrasion during transport, but much of it is a product of accretion of mud by blue-green algae and/or bacteria as the normal low-energy conditions return to the system. I have commonly observed such processes in diverse modern depositional systems such as the terrigenous muds in the North Sea tidal flats and the low-energy carbonate mud environments on the northwest side of Andros Island in the Bahamas. On the basis of the textural and structural similarity of the phosphorite gravels of the Noralyn Formation to the microsphorite beds, there is little question that they were a product of a similar process of sedimentation (see the following section for a discussion of the gravels). Beds of phosphorite mud were indurated in the intertidal zone, bored, undercut, and fragmented. The broken irregularities on the gravels and the initial bed were then rounded by the accretion of phosphorite mud by bacteria, blue-green algae, and by subsequent transport.

The development and preservation of microsphorite has very strong environmental controls (see Riggs, 1979). Major developments of microsphorite were limited to the shallow-water coastal system around the Ocala Upland; the areas of optimum development were in the upslope feather edges of the Noralyn Formation. In these areas, however, the Noralyn Formation is only preserved as irregular and scattered remnants. The Hard Rock phosphate district may represent some of these scattered remnants. The northernmost mines in the Central Florida district often contain the thickest and best developed beds of microsphorite within the Noralyn Formation. In many portions of this perimeter zone, the microsphorite was deposited and subsequently torn up. Consequently, it is not everywhere preserved. The implications of this will be discussed later. Down the depositional slope of the Noralyn Formation, the microsphorite development was thinner, but it is more commonly preserved. Most of the mines in the central portion of the Central Florida district contain minor stratigraphic beds of microsphorite. Further down the depositional slope, little or no microsphorite was deposited, and, consequently, it does not occur in the mines in the southern portion of the Central Florida or in the South Florida districts.

Allochemical phosphorite sedimentation

Allochemical phosphorite grains (allochems) are produced by the physicochemical or biochemical formation of phosphate within the area of deposition and are subsequently transported within the depositional basin as clastic constituents. Since the allochems are clastic grains, they may best be described by their textural characteristics—size, shape, rounding, and surface textures. These parameters best reflect the mechanisms of formation, the currents of transportation, the environments of deposition, and the proximity of the source material to the area of deposition. The allochemical particles comprise the bulk of the phosphate components in the deposits of the Atlantic Coastal Plain, as well as many other major sedimentary deposits around the world. Four major varieties of allochemical grains have been recognized and are presented in Figure 2.

Of the four varieties of allochems recognized in the Florida phosphorites, two varieties constitute 80 to 90 percent of the phosphate grains. The intraclastic phosphorite is the overwhelmingly dominant variety in the perimeter zone around the Ocala Upland including the North and Central Florida phosphate districts. In the outer belt, down the depositional slope from the Ocala Upland and including the area of the Sanford High, pelletal phosphorite is the overwhelmingly dominant form. Since both are of equal importance in the Miocene section, the geologically significant relative concentration of the two is set at 50 percent (Fig. 2). The fossil skeletal material can locally be important. Under these conditions, a concentration of 25 percent or greater is geologically significant and takes priority. The fourth variety, oolitic, or nucleated phosphorite, is of very minor importance in Florida and throughout the southeastern Atlantic Coastal Plain system. However, it is feasible and apparently some deposits in the world do contain significant concentrations and thus oolites are included here with a 25 percent level of significance. Each of these allochems has a considerably different mechanism of formation and is totally dependent upon the specific environmental conditions. Thus, an understanding of the origin of the phosphorites must first depend on identifying and understanding the specific types of phosphate particles.

Intraclasts: Intraclasts are fragments of penecontemporaneous phosphorite sediments that have been torn up from adjoining parts of the sea bottom and redeposited by currents to form a new sediment—broken from within the area of deposition and within the same formation (Folk, 1962, 1968). "Intraclasts may be produced by erosion of sedimentary layers almost immediately after they have been laid down, or under more severe conditions, may be produced by erosion of layers that had become buried some feet below the sea floor. Consequently, the sediment layers from which they are derived can show a complete range of degrees of consolidation or lithification. . . . These fragments (which commonly show bedding) are then abraded to rounded or somewhat irregular shapes, and the abraded margin of the intraclast cuts indiscriminately across fossils, earlier intraclasts, oolites, or pellets that were contained inside the intraclast. This indicates abrasion of intraclasts that had become consolidated enough so that these included objects would wear equally with the matrix (Folk, 1962)." As in carbonates, phosphate intraclasts might be formed either by submarine erosion or by wave attack on exposed phosphorite mud flats. This definition specifically excludes, as in carbonates, those fragments that are eroded from older phosphorite beds cropping out on the sea floor or on an emergent land area—these are the lithochems.

The petrographic evidence supports the hypothesis that at least 80 to 90 percent of the phosphorite allochems in the coastal perimeter zone around the Ocala Upland are intraclasts. The evidence supporting this concept can be summarized as follows.

1. Most of the allochemical grains are somewhat irregular to angular, especially in the coarse sand and gravel fractions (Figs. 9, 10, and 11).

2. The included sedimentary structures of the allochemical grains are the same as those of the orthochemical phosphorites: laminae, sediment surfaces, burrows, borings, invertebrate fossil molds, and terrigenous and allochemical inclusions (Figs. 11, 12, 13, 14, and 15).

3. The margins of the allochemical grains cut indiscriminately across the structures which have been subsequently abraded (Figs. 11 and 12).

4. The inclusions protrude from and have been abraded to the allochemical grain surfaces and have affected the resulting shape of the abraded allochem (Fig. 15).

5. The same microscopic components occur in both the orthochemical microsphorite and the bulk of the intraclastic grains; they are present in about the same abundance and have the same structural relationships.

6. Fragments of external fossil molds of invertebrates occur as individual allochemical grains.

As a matter of fact, the intraclastic phosphate pebbles and cobbles commonly can be distinguished from microsphorite only by their stratigraphic occurrence, the rounded surfaces, and the truncated structures.

All of the sedimentary structures described in the section on orthochemical phosphorite are unquestionably recognizable in the intraclast gravels (Figs. 11, 12, and 14). As the grain size of the intraclasts decreases and becomes smaller than the size of the individual structures, only parts of the structures are recognizable, and finally they are completely unrecognizable or absent. All of the sedimentary structures, except the inclusions and fossil molds, are readily recognizable in the intraclasts down to 3.36 mm and commonly to 1.0 mm. Occasionally laminae and their associated zones are recognizable, especially microscopically, in grains smaller than 1 mm but are completely lost below 0.42 mm. The number of intraclasts which consist entirely of whole invertebrate fossil molds are at a maximum above 0.42 mm size (Fig. 14). Below this size most of the fossil molds are only fragments and become increasingly difficult to recognize below 0.149 mm (Fig. 10). The amount of macroscopic terrigenous and allochemical phosphate inclusions (Fig. 15) decreases as fragmentation decreases the size of the intraclasts. Fragmentation breaks grains from between the inclusions, freeing the inclusions and decreasing the percent of total grains containing the inclusions. This continues until the size of the intraclasts approaches the size of the macroscopic inclusions; at this point the grains contain only microscopic inclusions. The macroscopic terrigenous and allochemical phosphate inclusions persist down to 0.0625 mm in size. Consequently, with decrease in grain size, fewer and fewer parameters can be recognized and related back to the coarser parent material.

The shape of phosphate intraclasts is very distinctive. Within each size fraction, the grains of most samples grade from completely angular to highly rounded. (Fig. 16). The grains occur in varying proportions and appear to reflect the process of continual fragmentation of the intraclasts during transport, rather than different origins or grain histories. Most intraclasts are angular with low sphericity. They become rounder and more spherical with decreasing size (Figs. 9 and 10). Only rarely do the finer fractions have a high sphericity. Even the most spherical intraclasts commonly show a slightly flattened surface on one side (Fig. 10), suggesting that probably they also formed as angular fragments torn from microsphorite beds. The shape of many of the smaller grains is directly related to protruding quartz and allochemical phosphate inclusions (Fig. 15). These protruding inclusions have also been modified by subsequent abrasion. Occasionally they are truncated and polished almost flush with the abraded surface of the enclosing grains. In the coarser fraction (+1 mm), some of the individual intraclasts are both partially angular and partially very well rounded. Some of these are highly abraded allochems which were broken or fragmented during transport and just prior to deposition. On many of the grains the rounded surfaces commonly represent portions of fossil molds, particularly in the −1.0 mm fractions (Fig. 16).

In unweathered samples in Central Florida, the dark grains (moderate brown) and some light grains (very pale orange) generally are very well rounded; whereas the majority of the light-colored grains has a high angularity. This relationship of color to rounding reflects the original sources of the grains from the three microsphorite zones previously described. The darker colored (moderate brown), very well rounded intraclasts came from the darker colored, indurated microsphorite surfaces of zone 3. The very well rounded, very pale orange grains originated in the thin light-colored, indurated microsphorite of zone 2, below the moderate brown surface zone. The angular, predominantly light-colored grains originated in the less indurated microsphorite of zone 1. Some of the angular grains have a fine sucrosic texture and are composed of phosphate pseudomorphs after dolomite. These latter grains were formed by the replacement of a preexisting carbonate bed at and just below the sedimentary interface by the interaction with the newly deposited phosphorite mud on the carbonate surface. Because of the sucrosic texture, these grains, as well as those from the less indurated microsphorite, tend to shatter

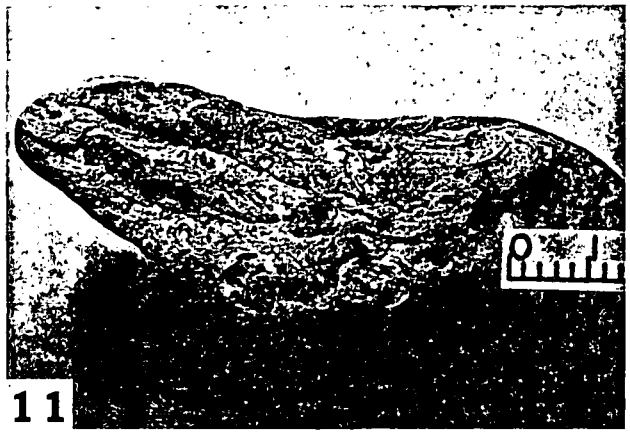
11

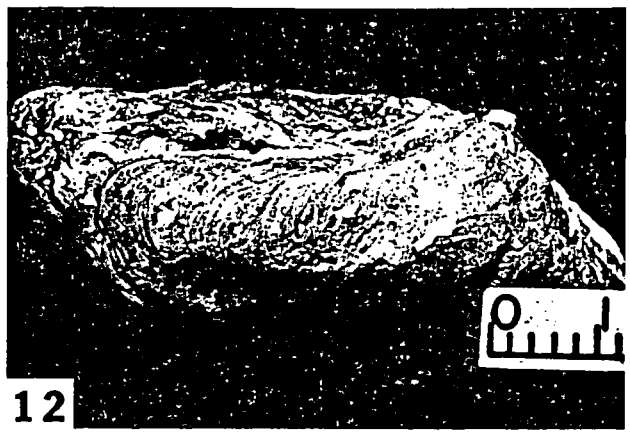
12

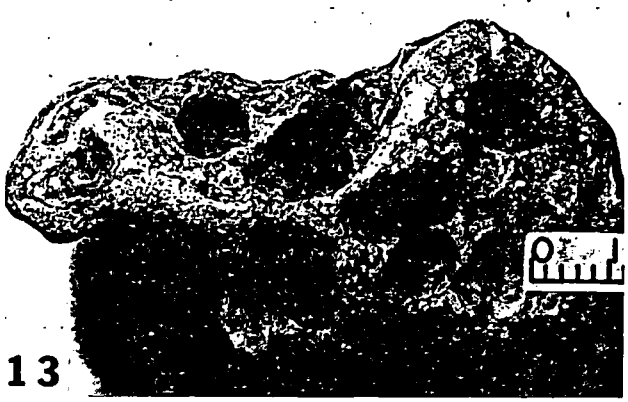
13


14

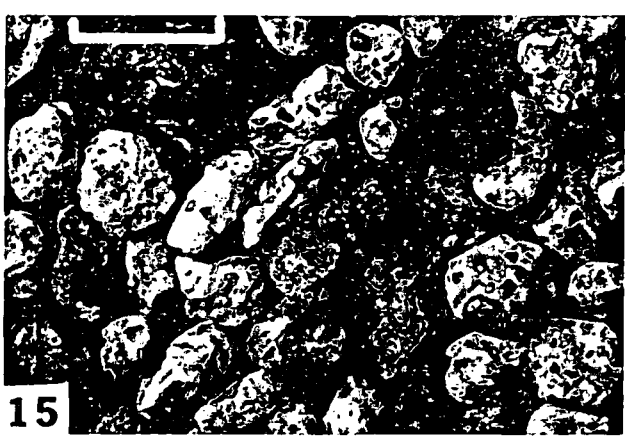
15


16

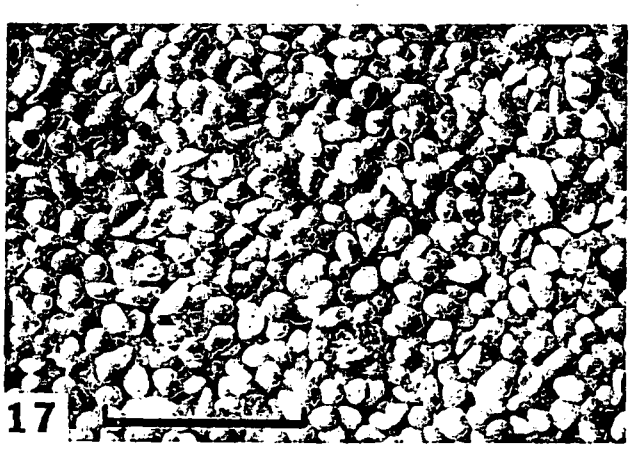
17


18

and fragment rather than round and abrade during transport. Consequently, they tend to occur as relatively fine sand-size grains and are quite angular. This latter variety of intraclast constitutes up to 8 percent of the allochemical phosphorite grains within certain stratigraphic facies in the Central Florida phosphate district. Thus, the ratios of rounded to nonrounded grains, as well as the color differences, reflect the type of transporting system and the distance from the source area and/or the type and degree of microsphorite development.

Pellets: The second important type of allochemical grains are the pelletal phosphorites. The individual pellets occur as the major phosphate grains in the size fraction between 0.177 and 0.062 mm. Some of the pellets get up to 1 mm in size, and some are finer than 0.06 mm; however, their abundance and importance drops off very quickly in both directions. In the inner perimeter around the Ocala Upland (Fig. 1), pelletal phosphorite constitutes an average of 5 to 15 percent of the total phosphate macrograins. In this area the phosphorite is dominantly intraclastic and, consequently, is primarily of medium sand and gravel size. However, the sediments down the depositional slope and into the outer belt, including the St. Augustine, East, and South Florida districts (Fig. 1), are dominated by the very fine pelletal phosphorite sands. In this area the pellets constitute 80 to 90 percent of the phosphate macrograins. The remainder consists of 5 to 10 percent medium to coarse sand intraclasts, 5 to 15 percent fine sand fossil material, and a few percent psuedooolites or nucleated grains. The pelletal phosphorites are extremely well sorted, very fine sand which is very leptokurtic. It is generally finer than any phosphorite which is presently being mined in Florida and represents the vast and extensive phosphate reserves of the future.

Pellets are often difficult to distinguish from highly abraded and fine-grained intraclasts. The main distinguishing characteristic of the pellets is their uniformity in size and the regular geometric shapes (Figs. 8, 17, and 18). Whereas the intraclasts are characterized by their diversity and irregularity of shapes with a high degree of angularity (Fig. 16), even in the finer size fractions, the most common pellets are ovoid, semispherical, and rod shaped depending on the organisms producing them. They are most readily recognized when they occur as clusters or aggregates filling internal fossil molds, infilling burrows, and in clusters on the microsphorite surfaces. The shape of the pellets is only a perfect geometric form when they are clustered without any transport. However, most of the pellets are nonclustered grains and are generally slightly deformed. This suggests that the excreted pellets remained soft during subsequent grain transport and became indurated only prior to burial by subsequent sedimentation.

The pelletal grains consist primarily of cryptograined matrix with varying amounts of microscopic inclusions disseminated through it. The included "garbage" consists of rods and rod aggregates, dolomite rhombs, microfossil hash, and minor terrigenous inclusions. The included material ranges from 0 percent up to 75 percent of an individual grain. The concentrate grade of these grains is often low with

FIG. 11. A well-rounded and highly polished allochemical intraclast pebble shows the following textures and structures of the original microsphorite bed: the horizontal interlaminae of dark and light colored microsphorite, abundant smaller phosphorite allochem inclusions, and abundant inclusions of quartz grains. Scale in centimeters.

FIG. 12. An allochemical intraclast pebble which contains the rounded and polished cast of a burrow partly filled by microsphorite laminae. The burrow was initially formed in a microsphorite bed which was subsequently torn up; the fragments were rounded and polished as clastic particles. Scale in centimeters.

FIG. 13. An allochemical intraclast pebble which contains abundant pelecypod borings. Note that the edges of the borings are rounded. The borings were probably formed on the surface of a microsphorite bed which was subsequently torn up and rounded and polished as a clastic particle. Scale in centimeters.

FIG. 14. Coarse sand to fine granule composite sample of phosphorite intraclasts which consists of internal and external fossil molds of pelecypods, gastropods, and bryozoans in all degrees of preservation and recognition. Notice the very fine quartz sand inclusions which occur in many of the smooth surfaces of the fossil molds. Scale bar is 5 mm long.

FIG. 15. Sample of phosphorite sand intraclasts which show abundant, generally well rounded, and highly polished inclusions of quartz (transparent) and phosphorite allochems (opaque). Many of the inclusions protrude from the surfaces of the parent grains and have influenced the resulting shape during abrasion. Scale bar is 2 mm long.

FIG. 16. An allochemical phosphorite sample consists entirely of intraclasts, many of which occur as fossil molds. Notice the high degree of rounding of the intraclasts which suggests major transport and grain modification prior to deposition. Scale bar is 5 mm long.

FIG. 17. Allochemical phosphorite sample of the −0.149 to +0.105 mm size fraction which consists predominantly of subspherical to oval fecal pellets and a few intraclasts. The clear grains are quartz. Scale bar is 1 mm long.

FIG. 18. Thin section which shows a cluster of oval to spherical phosphate pellets in a phosphate mud matrix with some quartz grains. Notice the very high and similar concentration of included material both within the pellets and within the mud matrix. Scale bar is 0.2 mm long.

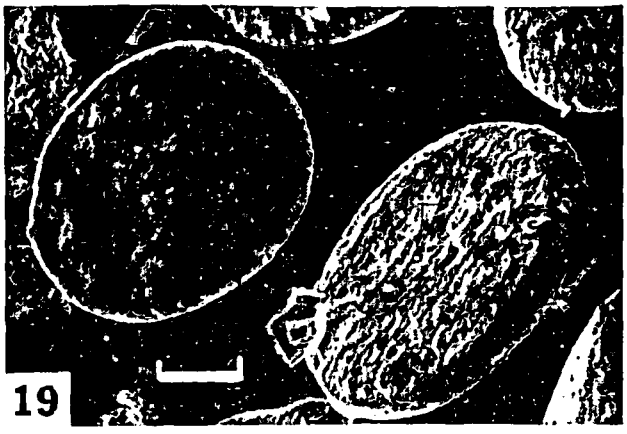
19


20

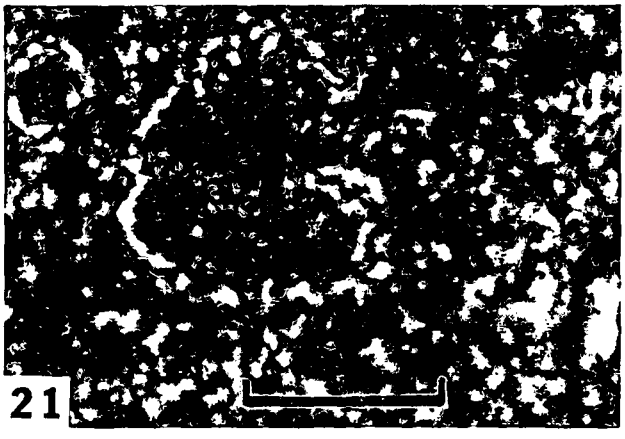
21


22


23

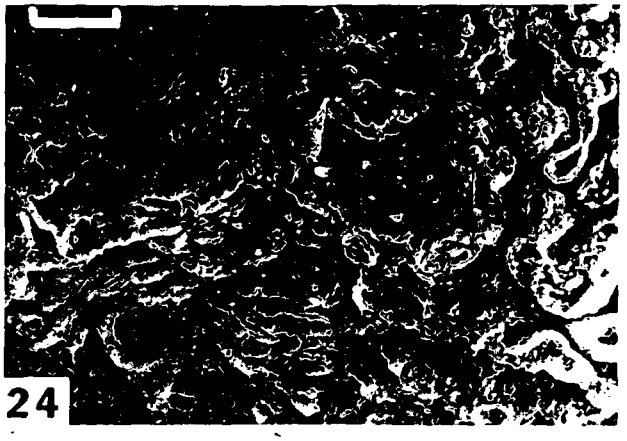
24


25


26

a relatively high magnesium content due to the amount of included dolomite.

None of the pelletal grains studied petrographically have displayed any recognizable concentric layering or microbotroyoidal textures. Doyle et al. (1978) have described both as being characteristic of the biologically precipitated phosphate kidney stones from various types of modern pelecypods. They have proposed that the kidney stones could be the origin of the phosphate deposits of the southeast Atlantic continental margin. At present, this does not seem to be a likely explanation for the majority of the pellets due to the high concentration of included garbage within the grains, the absence of the structures and textures observed within the mollusk kidney stones, and the stratigraphic evidence which suggests there was a paucity of mollusks during phosphorite sedimentation (Riggs, 1979). The paleontologic evidence suggests that the phosphogenic system created a highly stressed chemical environment which was characterized by a very low species diversity with a high population of nonshelled benthic invertebrates such as polychaetes and crustaceans. I presently consider it highly plausible that polychaetes, crustaceans, and possibly several other types of benthic organisms injested the phosphorite mud along with all of the included garbage. The excretory system played a significant role in concentrating the phosphorus, bacteria, and associated trace metals and excreted it as fecal pellets. The compacted pellets were subsequently transported as clastic particles.

A group of discoid shaped grains is another prominent grain type which is tentatively included in this category of allochems (Fig. 19). The discoid grains are very uniform in size, generally ranging between 0.2 and 0.125 mm, and contain a distinctive organic structure as grain nuclei. The organic nucleus is characterized by distinctive layers of teardrop to rod-shaped structures which occur in a specific geometric arrangement on both surfaces and continue around a very prominent flat disc edge (Fig. 20). The disc structure is composed of phosphorite mud which contains abundant included material and appears identical to all of the pelletal or intraclastic phosphate grains. Thus it does not appear to be actual skeletal material nor a replacement of such. Rather, this might suggest an internal filling or mold of an organic structure which was subsequently lost by dissolution. Whichever it is, the nucleus grain subsequently accreted varying amounts and thicknesses of phosphorite mud along with all of the included garbage (i.e., dolomite rhombs, fossil hash, terrigenous grains, etc.) to produce the resulting thin to fat discoid grains (Fig. 19). The accreted muds cannot be differentiated from the material of the organic structure. It is not presently known what the structures are; however, several good possibilities which I am presently investigating include internal molds of diatom valves and frustrules and crustacean statoliths. Crustaceans agglutinate sediments from within the environment to produce their balance structures; these are then shed back to the sediment system with each molt.

The discoid grains are generally associated with the pelletal phosphorites. Thus, they are most abundant in the fine-grained phosphorites of the downdip sections of eastern and southern Florida. The discs generally constitute about 1 to 3 percent of the total phosphate grains; however, within specific grain sizes, up to 50 percent of the phosphate grains may be the discoid variety.

Skeletal material: A much smaller percentage of the allochemical phosphorite consists of individual

FIG. 19. A scanning electron microscope photograph which shows common allochemical discoid phosphate grains. Notice the irregular accretion of phosphate mud and dolomite rhombs to the regular discoid nucleus grain. Scale bar is 100 microns long.

FIG. 20. A scanning electron microscope close-up photograph which shows a broken discoid allochemical phosphate grain as seen in Figure 19. Notice the layered organic rod-like structures which occur within the disc and around the perimeter. Also notice the irregular phosphate mud accretion around the outside of the grain. Scale bar is 40 microns long.

FIG. 21. Photomicrograph of microsphorite which shows a slightly irregular aggregate of bacteria-like rods within the cryptograined phosphate matrix. The individual bacteria-like rods are about 0.5 microns wide by 2 to 3 microns long, slightly irregular, have a high relief, and are accentuated by the darker coloring matter. Scale bar is 10 microns long.

FIG. 22. Photomicrograph of microsphorite which shows a high density of disseminated and loosely aggregated bacteria-like rods in a cryptograined phosphate matrix. Scale bar is 10 microns long.

FIG. 23. Photomicrograph of a fragment of the common microfossil hash which occurs commonly disseminated throughout the cryptograined phosphate matrix in orthochemical and allochemical phosphate grains. Scale bar is 10 microns long.

FIG. 24. A scanning electron microscope photograph of an allochemical phosphorite pellet showing a network of tubular structures which are tentatively interpreted to be some form of burrowing or encrusting protozoan. Scale bar is 10 microns long.

FIG. 25. Photomicrograph which shows phosphate replacement of dolomite including a rhombic dolomite pseudomorph. Scale bar is 10 microns long.

FIG. 26. Photomicrograph of a phosphate intraclast which shows an abundance of macroscopic quartz inclusions floating in a cryptograined phosphate matrix full of micrograined constituents. Scale bar is 1 mm long.

grains of fossil skeletal material. This category includes vertebrate bones and teeth, invertebrate shell material, and miscellaneous unknown material. This category does not include the internal and external fossil invertebrate molds or casts which are so abundant in the Florida phosphate deposits. Such fossils are formed in the orthochemical microsphorite beds and constitute an important part of the allochemical intraclasts. The mold and cast material is actually phosphorite mud and does not represent skeletal material. In the Central Florida district fossil skeletal material generally constitutes about 2 to 3 percent of the phosphorite macrograins. In individual samples, particularly in East Florida, the skeletal material may increase to 10 to 15 percent of the phosphorite.

The fragmented hash of vertebrate bones and teeth which occurs in the sand fractions appears to be mostly fish material of all forms and shapes. Within the primary marine units of the Arcadia Formation, it is mostly concentrated in the very fine sand grain size and shows little evidence of abrasion. A general increase of the bone and tooth material occurs in the gravel fraction in the coastal sediments of the Noralyn Formation around the Ocala Upland. Larger nektonic marine forms are common and include serinian ribs and vertebrae, whale and porpoise vertebrae and teeth, shark teeth, parrot fish beaks, and fish scales; some material is articulated whereas others show evidence of having been abraded and bored.

The skeletal material of the Bone Valley Formation is even more abundant and consists of a much more complex mixture of materials. All of the marine material from the underlying Noralyn and Arcadia Formations occurs reworked into the Bone Valley; where it is highly fragmented, abraded, bored, and often stained black. In addition, there is an abundant assemblage of fresh and often partially articulated terrestrial vertebrate material including rhinocerous, mastodon, camel, wolf, horse, etc.

The phosphorite sand fractions commonly contain up to 1 percent thin, slightly curved amber to dark reddish brown plates of phosphate. Some of these contain the internal structures of bone and teeth and obviously are chips of vertebrate bone material. However, much of this fragmental material contains diagnostic surface ornamentation and has been identified to be a member of the genus *Discinisca*. This is an inarticulate brachiopod with a phosphatic shell which has a small but ubiquitous presence throughout most of Miocene phosphorite section in Florida. Rudwick (1965) states that "almost all living brachiopods are marine, benthonic epifaunal, sessile suspension-feeders. This mode of life probably has been characteristic of the phylum as a whole throughout its history." The inferred life habit and the absence of whole shells suggests an active sediment interface.

A few other varieties of unknown material are both distinct and ubiquitously present as a fraction of a percent of the total phosphate grains. These fine sand-size amber grains include such things as the broad-ribbed grain informally called the "cat's paw" and the doubly crosshatched rod-shaped grain informally called the "unicorn horn."

Oolites: Oolites are also allochems since they are formed and transported as clastic particles within the same environment. Although I have not yet seen any true oolites within the Atlantic Coastal Plain phosphorites or other deposits that I'm familiar with, they are reported in the literature as common in some deposits of the world. Theoretically, given the proper conditions and environments, phosphate oolites should form from the microsphorite mud. Thus, they are included in this classification for completeness. However, I do find some nucleated grains which I call pseudo-oolites, which rarely exceed 5 percent of the phosphate grains. The pseudo-oolites are not very spherical and they generally lack any well-defined concentric laminations. The grains do have a major nucleus of quartz, feldspar, bone fragment, or another phosphate grain and appear to have accreted the phosphorite mud with all of its included garbage around the nucleus grain.

Phosphate Petrology

Microscopically, most of the phosphate macrograins are true aggregates composed of a mixture of various mineralogical and biological components. The primary component is the cryptograined carbonate fluorapatite matrix with various types and amounts of disseminated cryptograined coloring matter. In addition, most nonbiological phosphate grains contain a wide variety of micrograined included material which represents everything that was in the environment at the time of the precipitation of the phosphorite mud. The inclusions consist mainly of bacteria-like rods and rod aggregates, microorganism fossil hash, dolomite rhombs, terrigenous sand and mud, and other clastic phosphate grains. Consequently, most of the phosphate macrograins are complex sedimentary rocks, the chemical composition and physical characteristics of which are totally dependant upon the specific types of inclusions and their abundances.

Cryptograined components of phosphate macrograins

Matrix: The matrix is the fundamental phosphate component and usually the dominant constituent in the phosphate macrograins (Fig. 21). Mineralogically it is carbonate fluorapatite with some dissemi-

nated coloring matter. The color of the matrix generally grades from dark yellow orange where unaltered to clear (in thin section only) where highly altered. According to Lehr et al. (1967), the matrix consists of relatively uniform cryptograined material of highly substituted apatite with crystallite sizes which range from 300 to 1,000 A, based upon phosphate analyses from all over the world. The matrix is present in all phosphate macrograins and constitutes from 10 to 100 percent of any single macrograin or part of a macrograin. In the Central Florida district, the matrix averages 56 percent of the phosphate macrograins.

Because of the extremely fine crystallite size, the matrix appears isotropic at low magnifications but actually has an extremely fine anisotropism with a low order birefringence. A haze of reddish brown to milky gray material is intermixed with the anisotropic material. The hazy material may be either disseminated coloring matter and/or associated with the rods and rod aggregates.

Coloring matter: The coloring matter constitutes a small but conspicious part of the phosphate macrograins. Because the coloring matter is microscopically indistinguishable, it is considered to be cryptogranular. It consists primarily of organic matter and/or various iron oxides or sulfides. Some of the primary coloring matter is intimately intermixed with the matrix crystallites. However, the specific chroma and the lightness-darkness value of many phosphate grains are directly related to the character and abundance of the rods and rod aggregates and the associated coloring matter; this will be discussed in the next section. Regardless of the association of this coloring matter, it appears to have been derived during the genesis of the phosphate grains.

Any single stratigraphic unit, lithofacies, or grab sample generally has a mixture of different colored grains, but grains of one color usually predominate. The general color of any phosphate sample is definitely related to the types and abundance of phosphate particles or grains, the lateral and vertical stratigraphic position, the associated lithology, and the subsequent geologic history at that particular location. The uniformity of the macrograin colors would initially be a function of the regional uniformity of the depositional system. In any given regional system of phosphate formation, it is possible that all or many of the color variations from black to the various shades of brown, tan, and cream colors could be forming simultaneously within different microenvironments. The specific color or hue of any single grain would be dependent upon the processes of formation of that grain, as well as the chemical conditions and the amounts of organic matter and terrigenous sediments within the various microenvironments of the phosphate system. Subsequent transportation and deposition of the clastic grains formed in many different microenvironments produce the wide variety of grain colors characteristic of so many phosphorite sediments. In a regionally more homogenous depositional environment, there would be a much greater uniformity in the hues of the coloring matter and the grain types.

The coloring matter, be it either iron or organic matter, is lost easily and quickly from the phosphate macrograins with weathering or supergene alteration. Supergene alteration generally increases the lightness values, at first around the surface of the grain or along fractures, and then migrates inward through the grain, eliminating the primary coloring matter. Within the Central Florida district, the phosphorite of a given stratigraphic unit generally becomes lighter as the clay content of a stratigraphic unit decreases, as it is followed laterally into the river basins and vertically upward into the weathering profile associated with the aluminum phosphate zone.

Secondary coloring matter of the macrograins is commonly superimposed upon the original coloring matter as surficial brown to black stains. This secondary coloring matter penetrates irregularly into the grains enveloping all of the micrograined and cryptograined constituents. This secondary coloring matter contrasts sharply with the primary black coloring matter. The phosphate grains, as well as bone fragments, chert nodules, and limestone lithoclasts containing the secondary black stain are generally limited to the stratigraphic units composed of reworked phosphorite sands and gravels such as the Bone Valley Formation. It is definitely secondary in origin and is probably produced under reducing conditions below the sediment interface in the fluvial and estuarine environments. Upon weathering, this black stain is also easily destroyed.

Micrograined components of phosphate macrograins

Rods and rod aggregates: The rods and rod aggregates are the second most abundant component of Atlantic Coastal Plain phosphorites. They occur disseminated through the cryptograined matrix and range from 0 percent up to 90 percent of the volume of any single phosphate macrograin, averaging 22 percent in the Central Florida district. The rods are generally straight to slightly twisted micrograins which are about 0.5 microns in diameter by 1 to 3 microns in length and have rounded ends (Fig. 21). The rods are anisotropic with a high birefringence and a fairly intense brown to gray coloration.

A complete spectrum occurs from the individual rods to loose aggregates with poorly defined shapes

(Fig. 22) to clearly defined aggregates with a variety of forms including spheres, ovals, rods, and lamellar layers (Fig. 7). The slightly irregular aggregates are by far the most abundant (Fig. 22); they generally range from 3 to 10 microns in diameter and occasionally reach 50 microns. The lamellar forms are 3 to 5 microns thick, occur in sets, and usually extend through and are truncated by the grain boundaries. Occasionally the lamellar forms occur as irregular surface coatings or encrustations on terrigenous grains and dolomite rhombs. In the Central Florida district, about a third of the rods in the phosphate macrograins occur in distinguishable aggregate forms; however, this varies from sample to sample.

The rods are generally the most intensely colored micrograins. Thus, the presence and abundance of rods and rod aggregates in any given phosphate grain commonly determines the lightness values, the chroma, and the opacity of the macrograin. However, supergene alteration readily destroys the coloring matter, while the rod structures are apparently not initially destroyed. The rod structures are destroyed with continued supergene alteration, which first produces irregular botryoidal micrograins and then destroys them altogether.

On the basis of the physical morphology, size, and the tendency to cluster, I presently consider these structures to be fossil bacteria. Because the identification and classification of microorganisms depends largely on their internal cell structure, pigmentation, and biochemical composition, all of which are either not preserved or not observed with the present available equipment, their identification as bacteria remains tentative.

In 1933 Cayeux (1936) discovered and described bacteria in the phosphate from two different deposits. He subsequently identified bacteria in phosphorites of many different ages from the Precambrian through the Tertiary with the most conclusive specimens coming from Morocco, the Wyoming Rocky Mountains, and Pays de Galles. "The truth is that I have found some bacteria in all the phosphate materials where I have looked for them. In conclusion one can say that *some bacteria exist in some phosphates from one end of the scale to the other in geologic time.*" He describes them as thick-sheathed spherules with dimensions from 0.5 to 2.5 microns in diameter. Most are isolated from each other, but some aggregate into lines or irregular masses. In the Morocco phosphorite, he counted several hundred organisms within a 1,500 square micron field at 800 diameters.

Oppenheimer (1958) examined the phosphates from the early Tertiary deposits at Gafsa, Tunisia. "At magnifications of 1,000 many small uniform rod shaped objects of a diameter of 0.5 to 1 microns were seen which resemble bacteria. The length of the forms varied from 1 to 3 microns, the ends were rounded and chains of two were present."

More recently Kuznetzov et al. (1963) discussed the occurrence of fossil bacteria in the geologic column. The fossil "bacteria may be represented by cells encrusted with iron oxides, silica or other materials. It is naturally difficult to identify the discernable structures reliably as fossil forms of bacteria, but in numerous cases the identification of these structures as fossilized bacteria cannot be doubted."

Vologdin (1947, *in* Kuznetzov et al., 1963) has studied thin sections of the Cambrian phosphorite from the Karatau deposit in Kazakhstan. He recognized three components: "one was a group of yellow-brown ferruginous cells of iron bacteria; another was a group of small bodies of coccus-bacillus form, which were gray in reflected light (the phosphate was concentrated here), and the third was a dense, collomorphic mineral mass apparently made up of carbonates.". Vologdin found similar structures in phosphorite from the Mesozoic Salir deposits. These bacteria were very similar to those he found in limonite, brown ironstone, hematite, bauxite, and kaolinite from various deposits in Russia.

Examination of the phosphorites from many different localities in the world has demonstrated to me also that bacteria-like rods are ubiquitous components of certain types of phosphate grains. These structures were absent in samples from zones of contact-metamorphosed Phosphoria Formation from Montana and samples of altered and recrystallized phosphorite from the Bone Valley Formation in the Central Florida phosphate district. Petrographic work has demonstrated that the rods are readily destroyed by supergene alteration and are probably likewise destroyed by metamorphism.

Thus, at least four different investigators, looking at different materials prepared in different ways and observed with different equipment, have found abundant rods in unaltered primary marine phosphorites from around the world. Therefore, they are probably primary bodies, active during deposition and are locally absent where they have been subsequently destroyed. The almost universal association of bacteria-like rods with sedimentary phosphorites may suggest that the two are genetically related. It is not known which is the cause and which is the effect, if either; however, the possibility that bacteria may play an active role in the formation of the phosphorite must be seriously considered (Riggs, 1979).

The residues from numerous phosphate samples dissolved in dilute HCl consist mostly of the bacteria-like rods with varying amounts of clastic quartz, feldspar, and clay. X-ray diffraction analyses of the

residues showed a high concentration of amorphous materials and minor peaks from crystalline quartz, clays, and some unidentified minerals. X-ray spectroscopic analyses showed a high iron content, moderate titanium and sulfur content, moderate calcium content in some samples, and a negligible phosphorus content. Before a silica spectroscopic analysis can be meaningful, a technique must be developed to separate the abundant clastic terrigenous silicate grains from the rod structures.

Some of the bacteria-like rods in the residues were encased within a clear irregular sheath. I am tentatively identifying this isotropic material as amorphous silica. All of the rods occurring in the undissolved phosphate grains apparently either did not have an equally thick coating sheath or possibly no sheath at all since only some of the estimated total rods survived dissolution. This may be the material that the mining companies report in their chemical analyses as soluble silica which ranges from about 1.0 to 1.6 percent.[1]

The rods are thought to contain much of the fairly high concentrations of amorphous iron which can be seen microscopically as a brown material within the structures. Also, the similarity of the rods to the "yellow-brown ferruginous cells of iron bacteria" found in phosphorites by Vologdin (1947, in Kuznetzov et al., 1963) would further support this conclusion. By no means can the rods be composed entirely of iron oxide since the rods and aggregates form about 22 percent of the phosphorite grains in the Central Florida district and the average iron oxide content of the phosphorite is 1.34 percent [1] ranging from 0.25 to 3.5 percent. Assuming that the rods are fossil bacteria and that the iron is primary, one might expect the iron oxide to occur within the cell walls or as a layer around them. This iron could then account for the very high relief of the rods and also the great numbers of rods, but low percent iron oxide.

Much of the organic matter, which averages from about 0.5 to 1.0 percent [1] may occur as decomposition products of the bacteria within the bacteria-like rods. Because of the geographic proximity to known oil fields and their inferred high organic content, phosphate deposits have often been considered to be a probable source of crude oil (McKelvey, 1959). This may be true; however, in a study of the organic matter in phosphorite sediments from various deposits around the world, Powell et al. (1975) found that the average organic carbon content was only 0.62 percent with all of the samples having less than 2 percent. They concluded that phosphorites are not abnormally rich in organic matter; the average organic carbon value falls between those of shales (0.99%) and carbonate rocks (0.33%). These figures agree with those for the Central Florida district. Thus, the organic carbon content of the phosphate macrograins, as well as the iron and soluble silica, appears to be related to the bacteria-like rods. If this is the case, then there should be a direct correlation between the composition and the abundance of the rods and rod aggregates within any grain or sample or deposit.

Fossil inclusions: This category includes any micrograined fossils or fossil hash, other than the bacteria-like rods and aggregates previously discussed, which occur as inclusions within the phosphate macrograins. The fossils include fragments of vertebrate bones and teeth; an array of microfossils such as diatoms, spicules, discoasters, and protozoans; and filamentous boring and encrusting organisms which resemble boring filamentous blue-green algae and fungi such as those described by Ginsburg (1957).

The vertebrate material consists predominantly of various types of small fragments of fish bones and fish and shark teeth. These grains are often amber or honey colored, consist of extremely high grade phosphate, and are readily distinguishable in thin section by their typical internal porous character, fibrous undulatory extinction, or salt-and-pepper bone structure under crossed nicols. Fungal borings are also common structures in the bone. Vertebrate material generally constitutes less than a few percent of the disseminated included fossil material. However, a bone fragment will occasionally constitute the nucleus grain in a pseudo-oolite.

The microfossil inclusions are varied and abundant, particularly in the pelletal phosphorites. Most of the microfossil material occurs as fragmental hash disseminated through the phosphate matrix giving it the appearance of a virtual vegetable and meat soup. Most of these fossils are very subtle features and are only visible when using oil immersion lenses at 1,000× magnification, with carefully prepared and extra thin sections, and with the proper light transmission through the microscope. The most common forms appear to be various types of diatoms, spicules, and bryozoans (Fig. 23); I have not yet been able to identify any of this material definitely. Most of the hash appears not to be phosphatic; differences in the birefringence suggests that some of it is silica and some could be calcite. Some microfossil material generally occurs in most phosphate macrograins, particularly the pellets, but rarely exceeds 20 to 25 percent of the volume of the grains.

Figure 24 presents another type of fossil material which I have just discovered in the pelletal phosphorites. I am tentatively interpreting these tubes

[1] International Minerals and Chemical Corporation, 1965, Product specifications: unpub. memo.

to be some form of burrowing or encrusting microorganism, possibly a protozoan. They occur as components of some of the phosphate macrograins along with all of the other included garbage. Ongoing research suggests that the relationships of these microorganisms to the phosphate particles may be extremely important with respect to the origin and processes of phosphate sedimentation.

Carbonate inclusions: The included carbonate grains consist of detrital dolomite rhombs and relict carbonate patches in samples partly replaced by phosphate. The detrital dolomite grains occur as euhedral rhombic crystals of varying size, as partly abraded and etched dolomite rhombs, and some occur as transported rock aggregates. The rhombs range from several microns to several hundred microns in diameter and occur floating within the phosphate matrix. In the Central Florida district less than 1 percent of the phosphate grains contain dolomite inclusions; however, within certain stratigraphic horizons the number of grains may reach 90 percent. The latter generally occurs in the contact zone above the Arcadia Formation. In general, the phosphorite of the Noralyn Formation throughout the perimeter zone around the Ocala Upland has very low concentrations of included dolomite and thus low magnesium contents (see Riggs, 1979). On the other hand, the phosphorite in the Noralyn Formation, down the depositional slope and away from the Ocala Upland, and in the Arcadia Formation contains relatively higher concentrations of included dolomite. Thus, the phosphates in the south, east, and northeast sections of Florida all have relatively high magnesium contents. In the latter areas, the included dolomite ranges from 0 percent up to about 75 percent of any single phosphate grain. It is not uncommon to find up to 90 percent of the phosphate grains containing some dolomite inclusions.

The dolomite rhombs are generally floating in the cryptograined phosphate matrix along with all the other included material such as the bacteria-like rods, quartz grains, fossil hash, other phosphate micrograins, etc. This, along with the regional distribution and the evidence that some of the rhombs or rhomb aggregates show possible abrasion and/or corrosion suggests that the phosphate and dolomite were forming simultaneously in adjacent areas. The dolomite was subsequently transported into the area of phosphate formation and included with the phosphorite muds along with all of the other detrital inclusions and vice versa.

Some of the included floating dolomite rhombs have been either partially or totally replaced by phosphate. Occasionally an entire phosphate macrograin will be composed of phosphate pseudomorphs after dolomite. Both of these are discussed in the section on alteration of the crypto- and micrograined components.

Clastic phosphate grain inclusions: Any preexisting phosphate grain which exists as a discrete clastic particle within the environment at the time primary phosphate mud is forming may be included within the phosphate muds (Figs. 4 and 15). The muds are then either lithified and broken into intraclast grains or injested, pelletized, and excreted as pelletal phosphate grains. In the Central Florida district, the individual phosphate macrograins are composed of about 4.9 percent smaller clastic phosphate inclusions; however, the inclusions may range from 0 percent to 90 percent of any single macrograin. The number of macrograins containing inclusions, as well as the percent of inclusions per grain, decreases rapidly with decrease in grain size. These inclusions have the same composition and contain the same basic textures and structures as the larger phosphate macrograins and are described in the section on allochemical phosphorite sedimentation.

Terrigenous inclusions: In sedimentary environments, the purity of any authigenic sediment is entirely dependent upon the rate of terrigenous dilution. Throughout the formation and deposition of the Miocene phosphate, there was a low to moderate supply of terrigenous sediment contributed to the Florida depositional system (see Riggs, 1979). Consequently, some of this terrigenous material was deposited and included within the phosphate muds of the microsphorite beds. Therefore, the microsphorite beds, the individual intraclastic phosphate macrograins derived from the microsphorite beds (Fig. 26), and the pelletal phosphate grains formed from the muds all contain varying amounts of quartz and feldspar sand and silt, and some clay. In Central Florida, the phosphate macrograins contain an average of about 5.3 percent included terrigenous material. This is supported by the chemical analyses of acid insolubles of mine plant concentrates which average 5.1 percent. The average percent of phosphate macrograins containing terrigenous sand and silt inclusions decreases with decreasing size of the phosphate macrograins. As the phosphate intraclasts are broken into small and smaller grains, the more the included quartz and feldspar grains are freed until finally the finest phosphate grains contain only rare inclusions.

Feldspar from random grain counts of Central Florida mine plant tailings (the +150 mesh −16 mesh floatation separations) ranges from 8 to 12 percent of the nonphosphate sand population. Orthoclase predominates over microcline and plagioclase, all of which show no evidence of alteration. The feldspars are the same grain size as the quartz and are generally highly rounded and polished; some of

the grains are broken along cleavage planes. The ratio of feldspar to quartz is the same as inclusions in the phosphate grains as it is in the associated terrigenous sediments.

The clay component of the phosphate macrograins is minor, constituting only a small percentage of the total insoluble residue. The clay mineralogy of the associated sediments is unique; it is dominantly attapulgite and montmorillinite which alters to kaolinite during weathering.

Lastly, heavy minerals are present as inclusions within the phosphate grains but constitute only a very minor component. The phosphorite sediments as a whole average between 0.33 and 0.03 percent heavy minerals in the total sediment and are characterized by unweathered garnet and epidote (Pirkel et al., 1965).

Alteration of the crypto- and micrograined components

This category includes all of the phosphate which has been replaced or altered subsequent to its deposition. Since the chemistry and mineralogy of both the primary and secondary material are not fully known, the alteration varieties are simplistically differentiated by petrographic description. Two main categories of alteration have been recognized. The first category is the chemical reaction between two or more primary constituents, primarily phosphate and carbonate, soon after deposition. The second category is the subaerial supergene weathering of the primary mineral grains by secondarily introduced materials and ground water and takes place after the emergence of the sediments. It is essential to recognize both of these common processes prior to the interpretation of the origin and the geologic history of the phosphorites.

Carbonate replacement: The first category is readily recognized when phosphate replaces carbonate, particularly rhombic dolomite and calcite or aragonite shell material. In the first case, the phosphate occurs as prominent rhombic pseudomorphs after dolomite (Fig. 25). The rhombs range from about 3 to 30 microns in length and are composed of light gray cryptograined carbonate fluorapatite. Replacement of the dolomite rhombs appears to be a progressive process beginning on the rhomb faces with pits that coalesce into an irregular front of phosphate which advances toward the grain centers. All stages of replacement have been observed in the Florida samples. Bacteria-like rods and aggregates occasionally coat the surfaces of the rhombic phosphate pseudomorphs, as they occasionally do on dolomite rhombs, producing slightly irregular and poorly defined rhombs.

Within the small percentage of phosphate macrograins containing the pseudomorph variety of replacement, the abundance of dolomite rhombs, partially replaced dolomite rhombs, or rhombic phosphate pseudomorphs varies from minor disseminated grains up to 100 percent of an individual macrograin. Within any sample of phosphate macrograins, the degree of replacement ranges widely between grains, but within any single macrograin it is uniform. Therefore, the carbonate was probably replaced before the macrograins within any sample were finally brought together and deposited.

When the replaced carbonate was fine grained, the replacement appears as poorly defined, closely packed granular phosphate material which is several microns in diameter. The granules are mostly yellowish gray or pale yellowish orange in transmitted light and form whole macrograins or portions of individual macrograins which grade into unreplaced calcite or dolomite. Since the primary phosphate macrograins normally consist of uniform carbonate fluorapatite crystallites, in the range of hundreds of angstrom units, and contain abundant very fine micrograin structures, it is logical to conclude that this increase in grain size and destruction of fine primary structures represents replacement and recrystallization.

Phosphate does replace calcareous shell material, but it is uncommon to rare in the Florida phosphorites. Replaced invertebrate shells are rare while replaced microfossils such as ostracodes and foraminifera occur locally and in various stages of replacement. The phosphatized microfossils have never been observed as a common component of the phosphorite sediments. Internal and external molds of both the invertebrates and microfossils are common to very abundant sediment components.

The marine conditions of carbonate replacement by phosphate are poorly known. Ames (1959) found that in the laboratory calcite was readily replaced by phosphate when exposed to alkaline phosphate solutions. He believes that this is the probable mode of formation for large marine phosphorite deposits. However, Ames used a chemical system which far from approximates the natural marine system.

The bulk of the Florida phosphate shows no direct evidence of replacement. In fact, the lack of replaced carbonate shells in the phosphorite sediments argues against universal replacement, especially since many shells were probably composed of unstable high-magnesium calcite and aragonite. The rarity of replaced shells and the presence of undeformed fossil molds suggests that the primary phosphorite mud filled in and around the calcite and aragonite shells, the mud was indurated, and the shells leached from the sediment without any phosphate replacement.

Little doubt exists that some phosphate did replace carbonate in the marine environment during the formation of the Florida phosphorites. This replacement can probably be explained by one of several possible sequences of events: (1) the replacement of a preexisting carbonate directly from sea water, (2) the simultaneous formation and deposition of a phosphorite and carbonate sediment followed by replacement, (3) the formation and deposition of a primary phosphorite sediment on a preexisting carbonate which was followed by replacement at the contact, and/or (4) the inclusions of transported clastic carbonate within the primary phosphorite mud which was subsequently replaced. Field relationships and petrographic evidence suggest that the minor amount of replacement which took place, and which is readily recognized, usually took place as the third and fourth possibilities when the two constituents occurred together after deposition, but before subaerial weathering. Phosphorite and carbonate sediments do not appear to have formed simultaneously within the same environment in Florida. Carbonate was either formed in one area and orthochemical phosphorite in another and/or they formed alternately through time and were mixed laterally and vertically (see Riggs, 1979).

Consequently, I believe that phosphate does replace carbonate in the marine environment. However, replacement does not appear to be the primary mechanism or the process of initial formation of the bulk of the Florida phosphorites as proposed by many workers. Rather, replacement is a result of phosphate deposition in association with carbonates, occurs subsequently to its formation and prior to its emergence, and is not essential to the origin or the process of phosphorite formation and deposition.

Phosphate alteration: The second category is represented by the alteration of the phosphate resulting from subaerial supergene weathering some time after the emergence of the phosphorite unit from the marine environment. The alteration grades from the early stages of slight supergene alteration to the latter stages of severe weathering and recrystallization of the aluminum phosphate zone.

In the perimeter areas of the Ocala Upland, where the Noralyn Formation has been at least partially weathered, concentric zoning of the macrograins is common. This zonation begins on the edges or along voids and fractures within the macrograins and occurs as a series of wave fronts moving inward. The alteration begins with a color change and is followed by the alteration of the rods and aggregates to a clear matrix. If weathering continues, the clear matrix alters to a botryoidal granular texture. Occasionally, iron oxide is concentrated in this granular zone producing an area of dark reddish brown to dark yellowish orange color with high relief. This whole sequence may be partly or totally developed in any single grain. The zoning is usually gradational over several microns and commonly parallels the grain boundaries. The zones commonly cross primary structures or are superimposed upon other zones producing a complexly zoned grain, and occasionally they develop only on a single side of a grain. At this point the mineralogy is probably still carbonate fluorapatite. Continued supergene weathering alters the calcium phosphate to calcium aluminum phosphate to aluminum phosphate. In addition to the chemical alteration, the granular phosphate material is recrystallized to fibrous micrograined crystals. The latter is best developed in the severely weathered aluminum phosphate zone at the top of the phosphorite section around the perimeter of the Ocala Upland.

The microscopic zoning in the phosphate macrograins has a great effect on the color of the allochemical phosphorites in hand specimen. The presence of alteration zones, their degree of development, and their thickness increases the lightness values of the grains. When the early stages of the alteration zones are superimposed upon the primary grain colors, a multitude of color variants are produced. However, as weathering proceeds to the stage of mineralogical alteration of the phosphate grains, all of the coloring matter is lost. This results in very uniform grain colors of very high lightness values, ultimately becoming white as the alteration reaches the pure aluminum phosphate stage.

In the perimeter belt around the Ocala Upland, the phosphate becomes increasingly altered upward in the section into the aluminum phosphate zone, above which the phosphate is totally leached. The phosphate is increasingly altered into the major drainage basins. The degree of phosphate alteration is extremely variable, ranging from 0 to 100 percent, depending upon the relationship to regional structures, the position within the stratigraphic section, the associated lithologies, and the postdepositional history. Random counts of phosphate macrograins from the Noralyn mine plant concentrates in Central Florida show that about 12 percent of the macrograins contain minor alteration and only about 1 percent of the macrograins are entirely altered. However, the aluminum phosphate zone is generally stripped off as overburden during the mining operations.

The Secondary Modification of Phosphorites

Lithochemical phosphorite sedimentation

Lithochemical phosphorite grains (lithochems) are fragments that have been eroded from older

phosphorite rocks or sediments either off an emergent land area or submarine outcrops, transported, and redeposited in younger sediments. In the perimeter zone around the Ocala Upland (Fig. 1), the lithochems are restricted to the Bone Valley Formation of Pliocene age. The phosphorite gravels and sands were derived from the subjacent Noralyn Formation by fluvial erosion. The eroded sediments were abraded and modified by the streams and were deposited in the upslope areas as complex fluvial sands and gravels. Down the depositional slope the streams passed into clayey sand estuarine and coastal environments with a prolific invertebrate fauna. The phosphorite sands and gravels were significantly diluted as they were deposited within this system.

Lithochems are mostly reworked allochemical and orthochemical phosphorite sediments. Therefore, petrographically, the lithochems have the same internal features as the allochemical and orthochemical phosphate grains except where they have been modified by erosion and weathering during their subsequent transport and depositional history.

Four general criteria have been established for the identification and differentiation of lithochemical phosphorite from other phosphorite in Florida. The first and main criteria is its stratigraphic association in combination with the associated lithologies and sedimentary structures. Often these sediments occur in complex facies of fluvial and deltaic channel systems. The sediment units are extremely varied, abruptly discontinuous with abundant cut and fill structures and bars with highly cross-bedded sands and gravels. Second, there is an extremely abundant and complex composite of marine, estuarine, and terrestrial vertebrate and invertebrate fossils in varied degrees of disarticulation, fragmentation, and abrasion. The older set of marine vertebrate and invertebrate fossils are highly disarticulated, broken, abraded, bored, and stained. These are mixed with a fairly fresh looking assemblage of terrestrial vertebrate material, completely or partially articulated, in the fluvial and deltaic channel deposits. The estuarine and coastal deposits contain both assemblages plus a very rich and well-preserved population of calcite invertebrate material; such material was limited in the primary phosphorite beds. Third, a black stain penetrates portions of the lithochemical grains and masks but does not alter any of the primary constituents. The black stain also coats occasional bone fragments, quartz pebbles, chert nodules, and rock fragments. However, not all lithochems are stained black; in fact, in some areas the primary marine phosphorites have a black coloration which completely permeates the grains. Thus, the presence or absence of black grains is not conclusive evidence. Fourth, there is a common bimodal population of quartz with a distinctive mode in the coarse sand and fine pebble fraction. In the perimeter area around the Ocala Upland, discoid-shaped quartz pebbles up to 2 to 5 cm in diameter are a common association with the lithochemical phosphorite.

Metachemical phosphorite alteration

The fourth major category of phosphorite is metachemical phosphorite (Fig. 2). This constitutes the orthochemical, allochemical, and lithochemical grains which have been altered by supergene weathering. The primary sedimentary phosphate minerals, along with the associated clays, etc., in many of the world's phosphate deposits are readily altered by subsequent weathering processes. Such modifications are superimposed upon and cross the primary stratigraphy and sedimentary structures, eventually destroying them. Any geologic evaluation of such a modified section, whether it be for reasons of economics or genesis, must first recognize and then unravel the secondary processes and components from the primary. I consider this an essential facet of any consideration and classification of the Florida phosphorites and, consequently, include a brief summary in this paper. I believe that much of the disagreement and confusion that exists between workers in the Central Florida district is due to the difficulties in "seeing through" the often severely weathered and modified sediments. This is a critical step in relating the weathered portion of the system around the Ocala Upland to the downdip unweathered stratigraphic equivalents.

The detailed mineralogical changes due to supergene weathering have been studied in considerable detail in the Central Florida phosphate district by numerous workers, the most noteworthy being Altschuler and Young (1960), Altschuler et al. (1952, 1956, 1958, 1963, and 1964), and Owens et al. (1960). In Central Florida, the unaltered calcium phosphate occurs as a carbonate fluorapatite which grades upward to calcium-aluminium phosphate, occurring as crandallite and millisite. These change upward to the pure aluminum phosphate, wavellite. Some of the petrographic changes of the phosphate minerals were discussed in a previous section. The clay minerals have a similar gradational sequence. The clay minerals at the base consist of a montmorillonite-attapulgite assemblage which grades upward to a montmorillonite assemblage overlain by a montmorillonite-kaolinite assemblage and finally to a kaolinite assemblage. These same general alteration sequences are applicable to most of the inner perimeter zone around the Ocala Upland where the updip portion of the phosphorites has been exposed and subjected to subaerial weathering.

In the Central Florida phosphate district, min-

eralogical alteration due to weathering migrates downward as a series of "alteration fronts" dividing the section into zones and producing the textural sequence described below. These zones can best be described by examining a section progressively upward from an unaltered base (zone 1). This approximates what happens to a sediment section during weathering.

Zone 7. Complete leaching and translocation of all the clay constituents produces a clean quartz sand.

Zone 6. Continued leaching and translocation of the clay matrix produces a predominately clean quartz sand which contains isolated remnants of the vesicular rock. The boundaries between the quartz sand and remnants of the vesicular rock are gradational.

Zone 5. Progressive leaching of the tightly bound clay-sized constituents of the matrix, the kaolin and wavellite, produces a rubble composed of pebbles, cobbles, and boulders of vesicular rock.

Zone 4. The soft sand- and pebble-sized calcium-aluminum phosphate grains, bound in a porous but hard matrix, begin to leach away. This leaching produces a vesicular rock; the size and texture of the vesicules depends upon the size and texture of the original phosphate sand and gravel.

Zone 3. The sand-sized calcium phosphate grains alter to calcium-aluminum phosphate, beginning with the finer grains. This is the point at which the hard, polished phosphate grains change their texture to soft, dull-surfaced grains. The clay-sized phosphate grains, intimately intermixed with the kaolin clay minerals, alter from calcium-aluminum phosphate to aluminum phosphate (wavellite). This stage of the alteration produces an indurated matrix enclosing the coarser grained constituents. In the mining districts, the sediments from this zone up are discarded as overburden.

Zone 2. The clay-sized phosphate particles alter to calcium-aluminum phosphate (crandallite and/or millisite), the attapulgite is gone, and the montmorillonite alters to kaolinite.

Zone 1. In the unaltered zone the gravel, sand, and clay phosphate are calcium phosphate (carbonate fluorapatite) and the clay minerals are either montmorillonite or montmorillonite-attapulgite.

Each of the seven major zones crosses the primary stratigraphic units and grades one to another as alteration migrates down the section as waves. However, in any single section, all seven zones may not be developed. Frequently several zones form common fronts and coincide. The advance of the alteration zone is commonly directly effected by the clay content of the original sediments. This same sequence of alteration advances inward from fracture zones, around sinks or collapse structures and, to a much lesser degree, advances laterally along stratigraphic units.

The primary stratigraphic units can commonly be recognized (at least to formation and often to facies) through zone 4. Occasionally the primary units can be recognized through zone 5 and rarely into zone 6.

Discussion

The importance of understanding the petrology of the phosphate grains can best be appreciated when considered in terms which are of direct economic importance—phosphate grade or percent P_2O_5. In this respect there are two levels of consideration: the P_2O_5 content of an individual phosphate grain or a bulk sample of concentrated phosphate grains (concentrate grade) and the P_2O_5 content of the total sediment or rock as it occurs within the stratigraphic section (feed grade). The actual concentrate grade is directly dependent upon three variables. First, the P_2O_5 content of a specific macrograin is dependent upon the type of macrograin (i.e., allochemical intraclast, skeletal material, etc.). The grade of any given sample or bed or deposit is then dependent upon the relative proportions of these grain types. Second, the grade of a specific phosphate macrograin is dependent upon the proportion of phosphate components to nonphosphate inclusions within the grains. These inclusions of microscopic garbage consist of quartz grains, dolomite rhombs, siliceous fossil hash, iron-coated bacteria-like grains, clay minerals, etc. Variations in the type and abundance of these inclusions also determine the color of a given grain and dictate the differences in general chemical composition between any two phosphate grains, or the phosphorite in different stratigraphic units or phosphate deposits. Third, the P_2O_5 content of a specific grain or a deposit is determined by the subsequent geologic history; that is whether it has been subjected to erosion, reworking, and weathering (i.e., lithochemical or metachemical phosphorite). In addition to each of the three variables stated above, the percent P_2O_5 content of the total sediment or rock sample (feed grade) is dependent upon the relative proportion of phosphate grains to the nonphosphate grains (i.e., terrigenous sand and clay and authigenic carbonate, etc.) in the stratigraphic section or phosphate deposit.

Thus, the phosphate petrology is tremendously important not only because it directly affects the economics of any deposit but also because it supplies the basic information upon which the model for the origin and deposition of the Florida phosphorites has been built. This sumary paper is based upon the results of extensive descriptive stratigraphic, sedimentologic, and petrographic studies on the phosphorite section throughout the state of Florida and the southeast Atlantic Coastal Plain. The present paper, along with comparative studies in other parts of the world, represents the foundation for my subsequent paper in this issue of *Economic Geology*. The other paper is the synthesis of phosphorite sedimentation, a working and evolving model which is not without problems or questions, but does seem to come closer to fitting the real world system of phosphorite sedimentation than existing models. Thus, the subsequent paper represents the summary and conclusions for the present paper.

Acknowledgments

This paper is the product of the work of many individuals and a long-term program extending over the past 17 years under the leadership of Dr. Donald L. Everhart, former Vice-President of Research and Development for International Minerals and Chemical Corporation. Numerous people have supplied basic input for this work: a few individuals should be recognized for major contributions. The initial work on the Florida phosphorites was done by Donald H. Freas and myself, parts of which have been presented in the following publications: Riggs and Freas (1965), Riggs (1967), Freas and Riggs (1964, 1968), and Freas (1968). As chief geologist, Peter O. Sandvik both supported our work and contributed to our present understanding. More recently, Henry S. Johnson and John Maddry have contributed extensively to the regional understanding of the Florida phosphate system. I wish to specifically thank Dr. Don Winston, University of Montana, for instilling in me a fundamental appreciation of the total natural system; Dr. Everhart, who has persistently encouraged and supported the application of new geological knowledge and techniques to exploration; and the International Minerals and Chemical Corporation for permission to publish this paper.

GEOLOGY DEPARTMENT
EAST CAROLINA UNIVERSITY
GREENVILLE, NORTH CAROLINA 27834
September 29, 1978

REFERENCES

Altschuler, Z. S., and Young, E. J., 1960, Residual origin of the "Pleistocene" sand mantle in Central Florida Uplands and its bearing on marine terraces and Cenozoic uplift: U. S. Geol. Survey Prof. Paper 400-B, p. B202–B207.

Altschuler, Z. S., Cisney, E. A., and Barlow, I. H., 1952, X-ray evidence of the nature of carbonate-apatite [abs.]: Geol. Soc. America Bull., v. 63, p. 1230–1231.

Altschuler, Z. S., Jaffe, E. B., and Cuttitta, Frank, 1956, The aluminum phosphate zone of the Bone Valley Formation, Florida, and its uranium deposits (Florida), *in* Page, L. R., Stocking, H. E., and Smith, H. B., compilers, Contributions to the geology of uranium and thorium by the United States Geological Survey and Atomic Energy Commission for the United Nations International Conference on Peaceful Uses of Atomic Energy, Geneva, Switzerland, 1955: U. S. Geol. Survey Prof. Paper 300, p. 459–504.

Altschuler, Z. S., Clarke, R. S., and Young, E. J., 1958, Geochemistry of uranium in apatite and phosphorite: U. S. Geol. Survey Prof. Paper 314-D, p. 45–90.

Altschuler, Z. S., Dwornik, E. J., and Kramer, Henry, 1963, The transformation of montmorillonite to kaolinite during weathering: Science, v. 141, p. 148–152.

Altschuler, Z. S., Cathcart, J. B., and Young, E. J., 1964, The geology and geochemistry of the Bone Valley Formation and its phosphate deposits, west Central Florida: Geol. Soc. America Ann. Mtg., Guidebook, Field Trip 6, 68 p.

Ames, L. L., 1959, The genesis of carbonate apatites: ECON. GEOL., v. 54, p. 829–841.

Cayeux, M. L., 1936, Existence de nombreuses bactéries dans les phosphates sédimentaries de tout age. Conséquences: Acad. Sci. [Paris] Comptes rendus, v. 203, p. 1198–1200.

Doyle, L. J., Blake, N. J., Woo, C. C., and Yevich, P., 1978, Recent biogenic phosphorite: Concretions in mollusk kidneys: Science, v. 199, p. 1431–1433.

Folk, R. L., 1959, Practical petrographic classification of limestones: Am. Assoc. Petroleum Geologists Bull., v. 43, p. 1–38.

—— 1962, Spectral subdivision of limestone types, *in* Ham, W. E., ed., Classification of carbonate rocks, A Symposium: Am. Assoc. Petroleum Geologists Mem. 1, p. 62–84.

—— 1968, Petrology of sedimentary rocks: Austin, Univ. of Texas, Hemphill Pub. Co., 170 p.

Freas, D. H., 1968, Exploration for Florida phosphate deposits, *in* Proceedings of the seminar on sources of mineral raw materials for the fertilizer industry in Asia and the Far East: New York, United Nations, Economic Commission for Asia and the Far East, Bangkok, Thailand, Mineral Resources Devel. Ser. 32, p. 187–200.

Freas, D. H., and Riggs, S. R., 1964, Stratigraphy and sedimentation of phosphorite in the Central Florida Phosphate District [abs.]: ECON. GEOL., v. 59, p. 1619.

—— 1968, Environments of phosphorite deposition in the Central Florida Phosphate District, *in* Brown, L. F., ed., Fourth forum on geology of industrial minerals: Austin, Univ. Texas, Bureau Econ. Geol., p. 117–128.

Ginsburg, R. N., 1957, Early diagenesis and lithification of shallow-water carbonate sediments in South Florida, *in* LeBlanc, R. J., and Breeding, J. G., eds., Regional aspects of carbonate deposition—a symposium: Soc. Econ. Paleontologists Mineralogists Spec. Pub. 5, p. 80–100.

Kuznetsov, S. I., Ivanov, M. V., and Lyalikova, N. N., 1963, Introduction to geological microbiology, Oppenheimer, C. H., English Ed.: New York, McGraw-Hill Book Co., 252 p.

Lehr, J. R., McClellan, G. H., Smith, J. P., and Frazier, A. W., 1967, Characterization of apatites in commercial phosphate rocks: Internat. Colloquium Solid Inorganic Phosphates, Toulouse, France, 1967, Proc., p. 29–44.

McKelvey, V. E., 1959, Relation of upwelling marine waters to phosphorite and oil [abs.]: Geol. Soc. America Bull., v. 70, p. 1783–1784.

Oppenheimer, C. H., 1958, Evidence of fossil bacteria in phosphate rocks: Inst. Marine Sci. Pub., v. 5, p. 156–159.

Owens, J. P., Altschuler, Z. S., and Berman, R. M., 1960, Millisite in phosphorite from Homeland, Florida: Am. Mineralogist, v. 45, p. 547–561.

Patterson, S. H., and Herrick, S. M., 1971, Chattahoochee Anticline, Apalachicola Embayment, Gulf Trough and related structural features, southwestern Georgia, fact or fiction: Georgia Geol. Survey Inf. Circ. 41, 16 p.

Pirkel, E. C., Yoho, W. H., and Allen, A. T., 1965, Hawthorne, Bone Valley, and Citronelle sediments of Florida: Florida Acad. Sci. Quart. Jour., v. 28, p. 7–58.

Powell, T. G., Cook, P. J., and McKirdy, D. M., 1975, Organic geochemistry of phosphorites: relevance to petroleum genesis: Am. Assoc. Petroleum Geologists Bull., v. 59, p. 618–632.

Puri, H. S., and Vernon, R. O., 1964, Summary of the geology of Florida and a guidebook to the classic exposures: Florida Geol. Survey Spec. Pub. 5, 312 p.

Riggs, S. R., 1967, Phosphorite stratigraphy, sedimentation, and petrology of the Noralyn Mine, Central Florida Phosphate District: Ph.D. dissert., Univ. Montana, Missoula, 268 p., Univ. Microfilm no. 67-13, 473, Ann Arbor, Mich.

—— 1979, Phosphorite sedimentation in Florida—A model phosphogenic system: Econ. Geol., v. 74, p. 285–314.

Riggs, S. R., and Freas, D. H., 1965, Stratigraphy and sedimentation of phosphorite in the Central Florida Phosphate District: AIME Preprint 65-H-84, 13 p.

Rudwick, M. J. S., 1965, Ecology and paleoecology, *in* Moore, R. C., ed., Treatise on invertebrate paleontology, Part H, Brachiopoda, v. 1: Geol. Soc. of America and Univ. of Kansas Press, Lawrence, p. H199–H214.

Stowasser, W. F., 1975, Phosphate rock, *in* Minerals yearbook 1973, v. I, Metals, minerals, and fuels: U. S. Bureau of Mines, p. 1019–1035.

Vologdin, A. G., 1947, The geologic activity of microorganisms: Izv. Akademiia Nauk SSSR, Ser. Geologicheskaya, no. 3, *in* Kuznetsov, S. I., et al., 1963, Introduction to geological microbiology, Oppenheimer, C. H., English Ed.: New York, McGraw-Hill Book Co., 252 p.

THE POSSIBLE USES OF NEW OXIDATION-REDUCTION PROCESSES IN HYDROMETALLURGY

UDC 621.785.5:546.74

V. M. Gershov and N. T. Vanaga

The transition from energy dehydration to coordination dehydration in strong electrolyte leads to the appearance of new physical and chemical properties in the solutions and to reactions which are impossible under normal conditions. This phenomenon is due to the fact that beyond the limit of complete hydration there is a change in the nature of the energy effects which are reflected in the thermodynamic values, for example, in the integral heat of solution. In this case the endothermic term which takes account of disturbances in the structure of water drops out completely and effects become apparent which are connected with the inevitable redistribution of molecules of H_2O among the electrolyte constituents favoring the more hydrophilic ion; this leads to changes in the composition and structure of the complexes in the solution.

Thus there is an appreciable bathochromic shift in the absorption peaks in the absorption spectra of nickel and copper solutions containing an alkali or alkali earth metal chloride if the salt concentration reaches values at which coordination dehydration begins to occur [1].

In these circumstances the d-electron activation energy decreases more in a copper complex than in a nickel complex ($\Delta E_{Cu} - \Delta E_{Ni} > 0$). Since $\Delta E_{Cu} - \Delta E_{Ni} = f(\phi^0_{Cu} - \phi^0_{Ni})$ (ϕ^0_{Cu} and ϕ^0_{Ni} are the standard potentials of copper and nickel in these systems), conditions may be achieved as a result of artificially increasing the value $u = \Delta E_{Cu} - \Delta E_{Ni}$ by increasing the chlorine ion concentrations and the temperature (> 100° C) in which ϕ_{Ni} will become more positive than ϕ_{Cu}, because of changes in the standard potentials of the interacting metals and in the activities of the ions in the solution. Thus it becomes possible to implement these reactions [1,2]:

$$Cu + Ni^{2+} \rightarrow Ni + Cu^{2+}. \quad (1)$$

For example, cementation of nickel by copper proceeds actively in a calcium chloride medium at $CaCl_2$ molar concentrations of 0.9-1.35 M/kg in the 130-145° C range [2]. The thickness of the nickel coating on the copper does not exceed 0.5μ. The process is complete in 10-30 min, its duration depending mainly upon the activity of the copper powder. The pH of the working solution must not be less than 3 because of the increased speed of corrosion of the metal surface layer. At pH ≈ 6 the solution begins to grow cloudy because of precipitation of nickel hydroxide compounds.

The reaction is highly selective: of all the impurities normally associated with nickel, only the platinum group metals can be cemented out under these conditions. The selectivity of the reaction is practically independent of the relationship between the electrolyte constituents, which makes it possible to isolate pure nickel from heavily concaminated solutions. The optimum concentration of nickel salt (in the form of $NiCl_2 \cdot 6H_2O$) in the electrolyte is 20-60 g/liter.

Reaction (1) may be used to produce pure nickel powder on the basis of the carbonyl method.

The following reaction is of great interest in hydrometallurgy:

$$Co + Ni^{2+} \rightarrow Ni + Co^{2+}. \quad (2)$$

It procees to the end in the conditions under examination [3,4]. Thus the complete removal of nickel from cobalt solutions becomes possible, using a purely electrochemical method, a difficult process under normal conditions.

The following heterogeneous reaction has great potential in technology:

$$2Co(OH)_2 + N_2H_4 \rightarrow 2Co + N_2 + 4H_2O. \quad (3)$$

It proceeds with great speed at > 100° C (atmospheric pressure) and with a free hydroxyl ion concentration of 2-3 g-ion/liter [5]. Reaction (3) is remarkably selective. Of cobalt impurities, only nickel, copper, and platinoids are reduced to metal; iron, cadmium, zinc, manganese and p-metals do not pass into the elementary state under these conditions.

Having regard to the large scale of hydrometallurgical production, the direct use of hydrazine compounds to produce cobalt is unprofitable (the relatively high cost of hydrazine is largely due to the difficulties in its concentration and fractional distillation). However, Raschig synthesis can be used for reaction (3):

$$NaCl + 2NH_3 \rightarrow N_2H_4 + NaCl + H_2O. \quad (4)$$

which yields a ready-to-use hydrazine-bearing solution on the basis of constituents widely used in metallurgy.

Hydrazine is formed by mixing solutions of ammonia (conc.) with addition of commercial gelatin and sodium hypochlorite (active chlorine concentration ~ 60 g/liter) cooled to 0-10° C in the ratio of 2.5 : 1 by volume. Under these conditions the maximum N_2H_4 concentration (20-30 g/liter) is reached after holding the solution for one or two days at 18-20° C with a gelatin content of ~ 0.030 g/liter.

Reactions (2) and (3) can be used to produce pure cobalt with preliminary separation of copper be cementation with cobalt powder.

REFERENCES

1. V. M. Gershov and P. I. Dzyubenko, Izv. Akad. Nauk. Latv. SSR, Seriya Khimicheskaya, 1973, No. 2, 139-141.

2. V. M. Gershov and P. I. Dzyubenko, USSR Inventors' Cert. No. 417534, Otkrytiya, Izobreteniya, Promyshl. Obraztsy, Tov. Znaki, 1974, No. 8, 88.

3. V. M. Gershov and N. T. Vanaga, in: Hydrometallurgy 1974, Moscow, Izd-vo Akad. Nauk SSSR, 1974, 54-56.

4. V. M. Gershov and N. T. Vanaga, Inventors' Cert. No. 449956, Otkrytiya, Izobreteniya, Promyshl. Obraztsy, Tov. Znaki, 1974, No. 42, 57.

J. Rock Mech. Min. Sci. & Geomech. Abstr. Vol. 16, pp. 225 to 234
Pergamon Press Ltd 1979. Printed in Great Britain

0020-7624/79/0801-0225$02.00/0

The Permeability of Whole and Jointed Barre Granite

R.L. KRANZ*†
A.D. FRANKEL*†
T. ENGELDER*
C.H. SCHOLZ*†

The permeability of whole and jointed Barre granite was measured at pressures up to 2 kbars. Jointed samples were actually split cylinders joined by surfaces with controlled surface roughness. Samples with induced tension fractures were also measured. The permeability of the whole rock ranged from about 10^{-6} to 10^{-7} darcies. The permeability of the jointed rock ranged from about 8×10^{-5} darcies at low pressure down to that of the whole rock at high pressures. Permeability was not a simple function of the difference between external confining pressure (P_c) and internal fluid pressure (P_f). Changes in permeability were found to be proportional to ($b\,dP_f - a\,dP_c$) where $b/a < 1$ for the jointed rock and $b/a \approx 1$ for whole rock. The order of application of P_c and P_f was also important. Permeability hysteresis and an ultimate decrease in permeability in both *whole and jointed rock resulted when internal fluid pressure was cycled. This effect seems to diminish with increasing confining pressure. At a particular P_c, the volume flow rate, q, is proportional to $(P_c - P_f)^{-n}$. Increasing the surface roughness of the joints decreased the value of* n, *which was smallest for the tension fracture and the whole rock. Within the uncertainty of joint aperture measurements, a flat plate model of the joint seem inadequate.*

INTRODUCTION

part of a larger study designed to investigate the ects of joint roughness, geometry and filling on fluid w at geologic pressures and temperatures, we report re initial results on Barre granite. Specifically, we sured the permeability of whole and jointed Barre nite at room temperature and pressures up to bars. Jointed samples were of two kinds: split linders joined by surfaces with controlled surface ughness and cylinders with artificially induced ten- n fractures. Some of our results corroborate previous vestigations, but we have also determined that the ss history and joint surface roughness have a large ect on the hydraulic properties of rock and, as this s rarely been specifically taken into account, is, we el, of major importance.

Data on the permeability of low porosity, crystalline k are scarce. Westerly granite is the only rock that as been extensively investigated. Brace *et al.* [1] reported on the permeability of Westerly granite as a function of effective stress (commonly taken as the difference between the external confining pressure and internal fluid pressure). Zoback & Byerlee [2] investigated the effect of deviatoric stress on the permeability of Westerly granite, and Summers *et al.* [3] described permeability changes in Westerly granite at temperatures between 100° and 400°C. With one exception, [3], all measurements were on whole, unjointed rock. The permeability of jointed granite has been measured *in situ* by Pratt *et al.* [4] and in a large granite core by Witherspoon *et al.* [5]. Both studies were restricted by sample size to stresses below 300 bars‡.

Brace [6] has concisely summarized the results from the literature dealing with the permeability of geologic materials. The following points are worth repeating: (1) stress produces large changes in permeability, both increases and decreases, in all porous material but joints are extemely sensitive to stress changes relative to the surrounding whole rock; (2) the permeability of jointed rock is several orders of magnitude greater than that of intact rock (at least over the stress range measured); (3) the simple effective stress law of confining pressure minus pore pressure may be adequate for unjointed granite, is not adequate for sandstones and

* Lamont-Doherty Geological Observatory of Columbia Univer- . Palisades, NY 10964, U.S.A.
† Also, at the Dept. of Geological Sciences, Columbia University.
‡ 1 bar = 10^5 N/m^2 = 0.1 MPa.

there are not yet enough data to even test it for jointed rock.

SAMPLE PREPARATION

Whole samples

All cores, approximately 3.5 cm in diameter and 9 cm in length were taken in the same direction from a single block of Barre granite. Their ends were surface ground parallel to within 0.001 cm from side to side.

Split samples

Another block of Barre granite was saw-cut into large prismatic sections with ground sides. Two sections with parallel sides were clamped together and cores, also approximately 3.5 cm in diameter, were taken centered on the joint between the sections. These split, cylindrical samples were then reclamped and saw-cut to be approximately 9 cm in length. The ends were ground parallel like the whole samples. The split samples were then unclamped and the interior, opposing surfaces were ground with number 120 grit. Some samples were subsequently ground with number 600 grit and others further polished with Linde 0.3 μ alumina polishing compound. All surfaces were prepared, stored and protected *in pairs*.

For our *tension fracture* samples, two grooves, approximately 1 mm in depth, were made 180° apart down the length of several of the whole samples. They were then placed between two V-shaped anvils and split from groove to groove as in a Brazilian strength test.

PROCEDURE

Experiments were conducted in a triaxial, servo-controlled, hydraulic press equipped with a 5.08 cm bore pressure vessel. Kerosene was used as the pressure medium as well as the fluid pumped through the rock. It is chemically inert with respect to the rock so we are looking at mechanical effects of pressure only. The confining pressure system was independently controlled and separate from the internal fluid system.

All whole samples were covered with a thin copper jacket. Steel end caps with center holes and radial grooves were affixed to the whole samples. To permit fluid access to the entire end surface of the sample, a thin layer of grit from a pulverized grinding wheel was placed between the sample and each end cap. A steel piston was affixed to one side of this assembly and the pressure vessel closure to the other. Fluid could be admitted or withdrawn through central ports in the piston and top closure.

Strain gauges were cemented to the copper jacket in an array which permitted strain to be measured at a number of points along the length of the sample.

Split cylinder assemblies were made in the same way except the layer of grit was omitted and the samples were jacketed with polyolethane.

To measure joint aperture changes, a four-armed cantilever device was used (Fig. 1). It consisted of four thin, rectangular beryllium-copper beams connected in a radially symmetric pattern to an aluminum ring which was slipped over the sample. A certain amount of tension kept pads at the end of each arm firmly pressed against the sample. Each arm had an electric resistance strain gauge on it. It was arranged on the sample so that two of the arms measured the sum of joint closure and rock compression, and the other two measured rock compression only. The output of one pair was subtracted electrically from the output of the other pair so that the result was proportional to the joint closure. The dilatometer was calibrated against a micrometer. The effect of pressure on the dilatometer was also measured and taken into account.

Both confining pressure and internal fluid pressure were measured outside the pressure vessel in two ways. For recording, we used the output from two high pressure BLH, Inc. pressure transducers. In addition, we visually monitored confining pressure with a Heise gauge and internal fluid pressure with two Heise gauges connected within the system above and below the sample column. A differential pressure transducer capable of detecting differences of 0.1 bars under ambient pressures as high as 3 kbars was also connected between the top and bottom of the sample column. Schematically, our pore pressure system is similar to that shown in [2].

Permeability measurements were made with a procedure which closely follows that of Brace *et al.* [1]. A similar procedure has been used by Zoback & Byerlee [2]. Briefly, a pressure step (about 5–10 bars) much smaller than the ambient pore pressure was introduced to either the top or bottom of the sample column assembly and the decay in the pressure head was monitored with the differential pressure transducer. The pulse decays in time according to the equation

$$P = P_0 e^{-\alpha t} \tag{1}$$

with

$$\alpha = \frac{kA(V_2 + V_1)}{\beta\mu L V_2 V_1} \tag{2}$$

where k is the permeability, A is the cross section through which fluid flows, β is the isothermal compressibility of the fluid, μ is the dynamic viscosity, L is the sample length and V_1 and V_2 are the volumes of pore fluid reservoirs at the top and bottom of the sample, respectively. For our system, $V_1 = 20\,\text{cm}^3$, $V_2 = 15\,\text{cm}^3$, $L = 9$ cm, $A = 9.6\,\text{cm}^2$ for the whole rock samples. Isothermal compressibility and dynamic viscosity of kerosene as a function of pressure can be found in [7] and [8], respectively. Once α is evaluated from the pulse decay curve, equation (2) can be used to calculate the permeability for the whole rock.

This method assumes that Darcy's law holds. That is

$$q = \frac{kA}{\mu}\frac{dP}{dL} \tag{3}$$

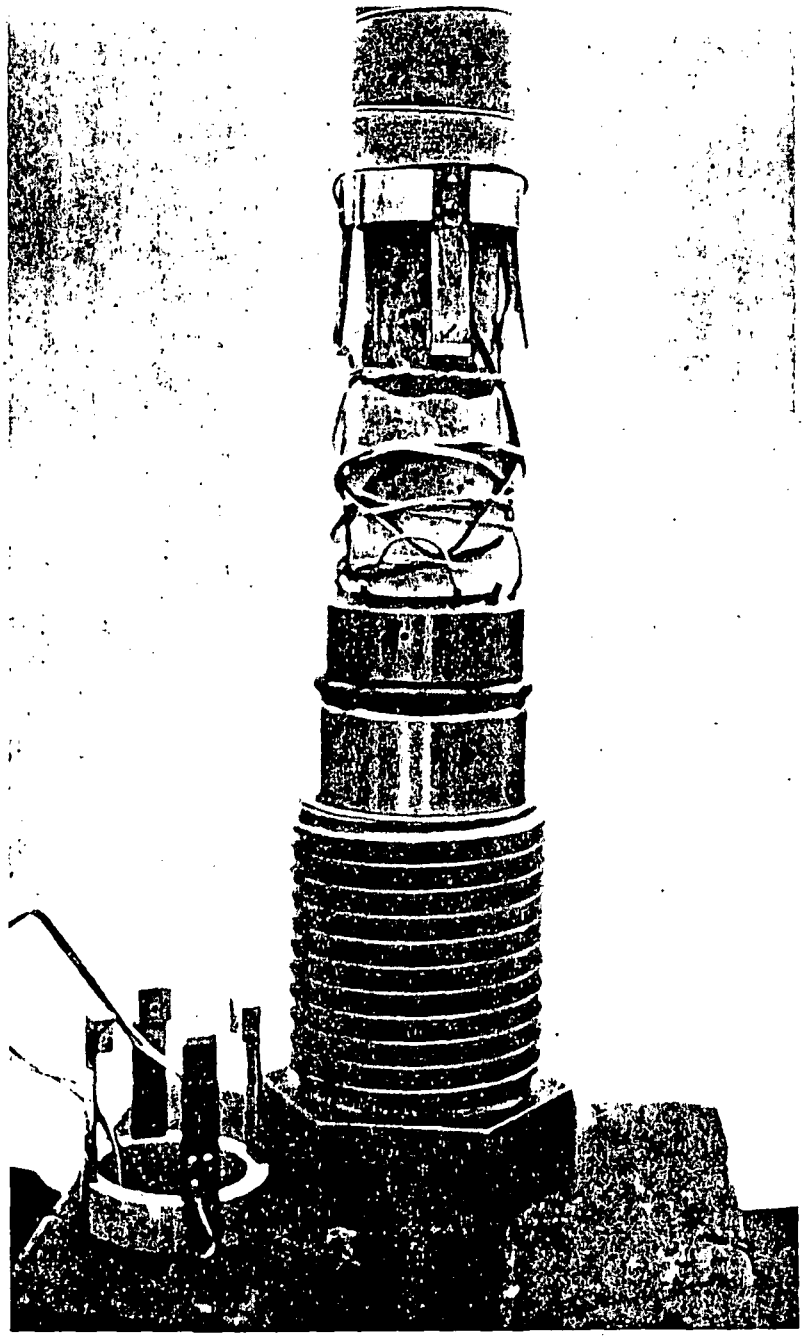

Fig. 1. Sample column assembly showing four-armed dilatometer around sample. A second dilatometer can be seen at the base of the column.

where q is the volume flow rate. It also assumes that a linear pressure gradient exists along the length of the sample.

The same procedure was used for all split cylinder samples. This allows a direct comparison between whole rock and rock with a joint, but will not give an absolute value of permeability for the joint itself because the assumptions made in deriving (2) do not necessarily apply to joints.

Joints are often approximated as a parallel plate opening, for which [5,9,10] the volume flow rate per plate width is

$$q = \frac{d^3}{12\mu}\frac{dP}{dL} \tag{4}$$

where d is the plate opening. Comparing (3) and (4), a single joint permeability may be defined as

$$k_j = d^2/12 \tag{5}$$

One can modify (2) by taking A, the cross section exposed to the fluid, to be simply the joint opening d times the cylinder diameter (3.5 cm). Permeability calculated in this fashion for the joint alone can be compared to permeability calculated using (5) if the absolute value of d is known. Differences in the two calculations will be, in a sense, a measure of the deviation of the actual joint from the flat plate model. Implicit in this modification is an assumption that essentially all flow occurs through the joint. This may not be the case for rock with higher porosities than that

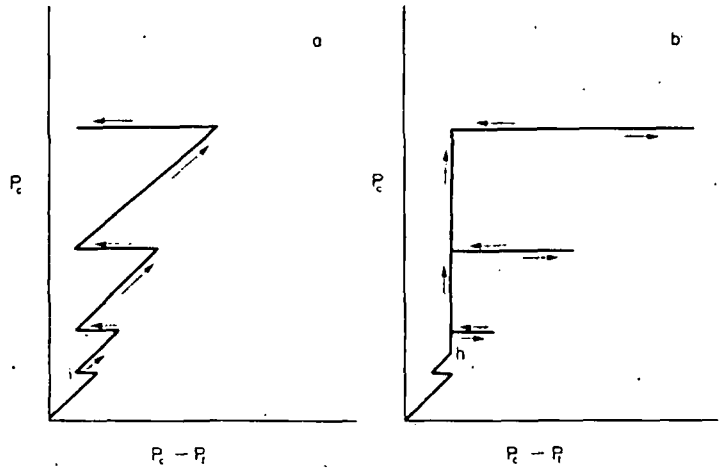

Fig. 2. Schematic representation of changes in P_c and P_f for two different experimental procedures. See text for explanation.

considered here, or where whole rock permeability is of the same order of magnitude as joint permeability.

The cumulative uncertainty in the constants in equation (2) is less than 25%. Uncertainty in α may be as high as 10%. Absolute values of the whole rock and jointed rock permeability as reported may thus be considered accurate to within 35%. It is not known how great the permeability anisotropy is. Absolute values of the permeability of the joint alone are not as accurate, uncertainty in the joint aperture being the main reason.

Measurements made with the dilatometer do not give an absolute value for the joint aperture, but rather a change in aperture. To get an absolute value, the joint must be closed down to the point where no further changes in aperture are discernable, and that point taken as $d = 0$. We did not reach such a point in any of our experiments. From the asymptotic approach to complete closure we can, with some uncertainty, get absolute values of d as a function of $P_c - P_f$. At low pressures the estimated uncertainty in the aperture may be as high as 200% but it decreases rapidly with pressure, so that above 500 bars the estimated uncertainty in the permeability of the joint may be considered as $\pm 25\%$. The absolute values are not as important as are the *relative changes* in permeability which we report.

It became apparent after several experiments that the order in which confining pressure (P_c) and internal fluid pressure (P_f) were changed from measurement to measurement was important. Figure 2 shows schematically how P_c and P_f were changed. Our initial procedure was as in Fig. 2a. A certain amount of confining pressure was applied, then a lesser amount of internal fluid pressure was introduced. Some time for equilibration was allowed, then measurements began at point i. Subsequent measurements were made following further changes in P_c and allowance for equilibrium. Then P_f was raised again, more measurements were made, then the procedure was repeated. As near as we can tell from the literature, this is exactly or very close to the same procedure used by most investigators.

If we tried to repeat a set of measurements or if we had a leak and had to begin again we found a certain amount of non-repeatability. This was more apparent with jointed samples. Because pressure cycling is known to cause irreversible damage in whole rock [11] and cumulative irrecoverable closure of joints (Fig. 7 in [4]) we decided to change our procedure to test for hysteresis effects, as in Fig. 2b.

From tests on solid samples we determined that a minimum $P_c - P_f$ value of 50 bars was required to inhibit surface flow between the jacket and the sample. Thus a confining pressure in excess of 50 bars must always be applied first. We started as in Fig. 1a but at point h we raised P_c and P_f *simultaneously*, maintaining a constant difference of 200 bars plus or minus the small P_f pulses needed to make a measurement. At a particular value of confining pressure we lowered the internal fluid pressure, then raised it back to the point where $P_c - P_f$ was again 200 bars, making measurements along the way. Both P_c and P_f were raised simultaneously again to new values and the procedure was repeated as shown in Fig. 2b.

OBSERVATIONS

Figures 3, 4, and 5 give the permeability as a function of $P_c - P_f$ for jointed samples with surfaces prepared with 0.3 μ alumina polish, number 600 grit and number 120 grit, respectively. Measurements were made following the procedure of Fig. 2a. Isobars connect points where the confining pressure was the same but internal fluid pressure changed. Permeability was calculated without any assumptions about the real or effective cross-sectional area for fluid flow. That is, in equation (2), A was taken to be the entire sample end surface of 9.6 cm^2. Note that the permeability for the whole rock with joint ranges from tens of microdarcies* at low pressure for the 120 grit surface to less than one microdarcy at high pressures.

* 1 microdarcy = 10^{-14} cm^2.

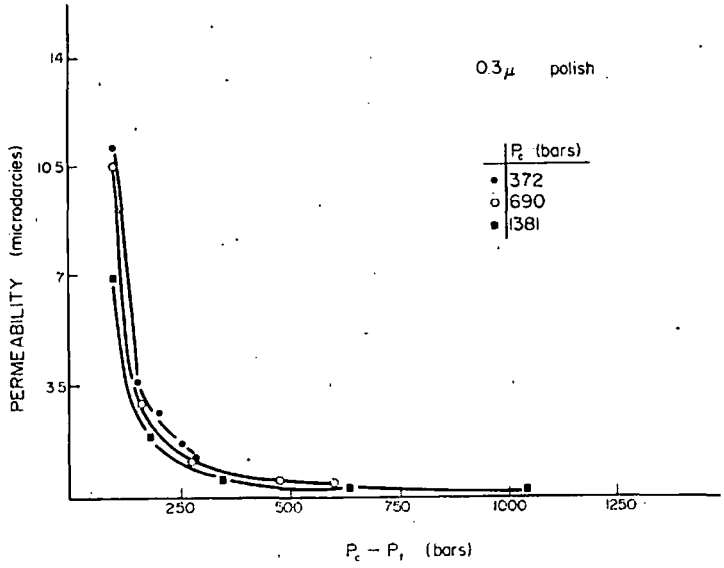

Fig. 3. Permeability at various pressures of jointed Barre granite with joint surfaces prepared with 0.3 μ alumina polish.

The following details should be noted. At a particular value of $P_c - P_f$, the higher the P_c value the lower the permeability. This is particularly striking for the 120 grit surface and becomes less marked as the surface becomes smoother. The rate of change of permeability with changing $P_c - P_f$ is greatest at low pressure and decreases almost to zero at high pressure. The rougher the joint surface, the slower the decline of permeability with increasing $P_c - P_f$.

The data in Fig. 6, which are for a tension fracture, were collected following the procedure of Fig. 2b. The hysteresis is quite apparent for this rough joint surface. At any particular confining pressure, lowering the internal fluid pressure (raising $P_c - P_f$) resulted in a decrease in permeability which was not entirely recovered when the internal fluid pressure was raised to its initial value. Note that the hysteresis *decreases* as the confining pressure is increased. Part of this decrease is undoubtedly due to cycling alone. At 2 kbars of confining pressure there was almost no hysteresis and the permeability was almost constant above the 500 bar value of $P_c - P_f$.

The permeability of the whole rock as a function of $P_c - P_f$ is shown in Fig. 7. Note that the permeability is on the order of a microdarcy or less at high pressures. Measurements were made following the procedure of Fig. 2a in most cases. The results of 3 hysteresis tests following the procedure of Fig. 2b are also given. The open symbols represent initial permeabilities before pore pressure was dropped. The closed symbol directly beneath each open symbol represents the permeability after pore pressure was raised to its initial value. As in the tension fracture, the difference between the two seems to decrease with increasing confining pressure.

From equation (3) we note that the volume flow rate q is proportional to kA, which may be calculated using (2) once α is measured. A direct comparison between the whole rock and each jointed rock sample can be

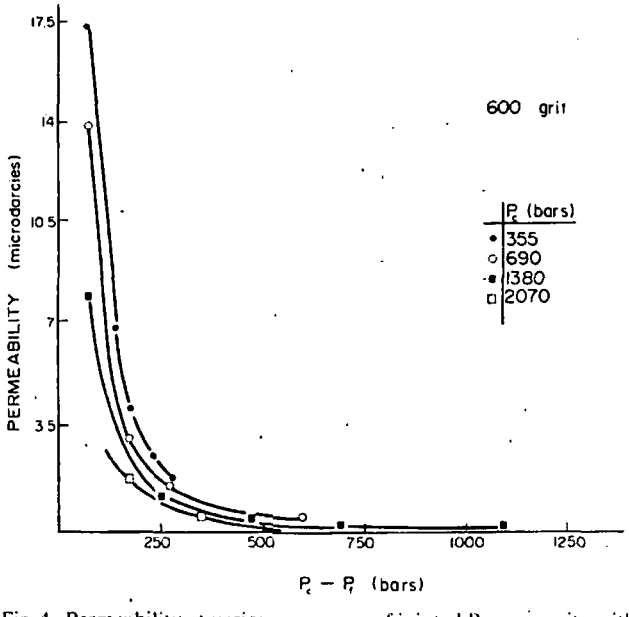

Fig. 4. Permeability at various pressures of jointed Barre granite with joint surfaces ground with number 600 grit.

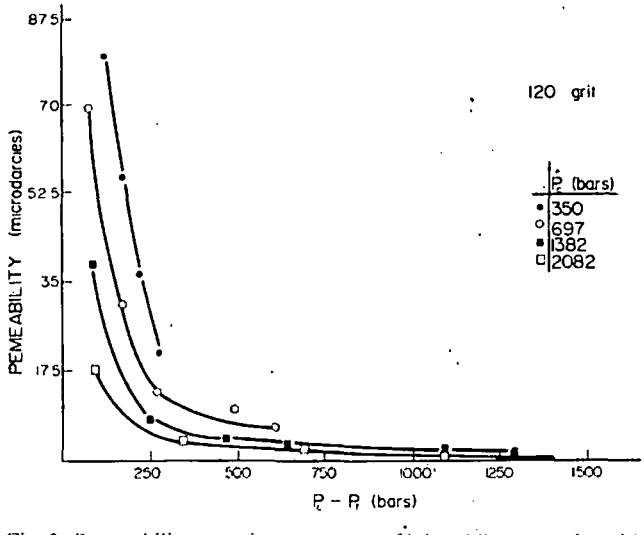

Fig. 5. Permeability at various pressures of jointed Barre granite with joint surfaces ground with number 120 grit.

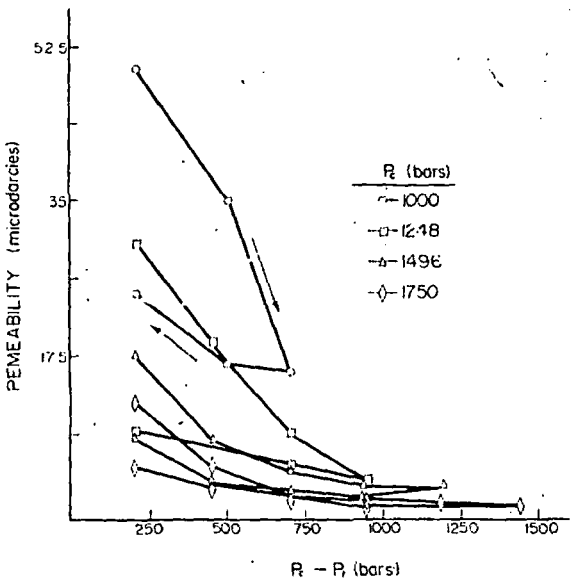

Fig. 6. Permeability at various pressures of Barre granite with a tension fracture, measured using the procedure of Fig. 2b.

made using kA rather than k. This eliminates any questions about what value one should take for A for the jointed sample. Because of the stress history effect, comparisons should be limited to measurements at the same P_c or P_f. We fit kA to an equation of the form

$$kA = [kA]_0([P_c - P_f]^{-n}) \tag{6}$$

By plotting log $[kA]$ vs log $[P_c - P_f]$ we find n. Figure 8 gives an example for the jointed rock samples at $P_c = 690$ bars. Table 1 lists the values of n at various pressures for all available data. Two things become immediately apparent. First, as confining pressure is raised, all samples show a decreasing dependency on $P_c - P_f$. Also, as mentioned previously, the rougher the surface the smaller the pressure effect *at all pressures*. It should also be noticed that since the n values for the jointed rock samples are greater than for the whole rock, the curves will intersect at some $P_c - P_f$ value. That is, at some pressure there will be no apparent difference in the flow rate between a rock with a joint and an unjointed rock. For the sample with the smoothest joint surface this projected pressure is between 2 and 3 kbars. For the roughest joint surface it is between 10 and 15 kbars. Obviously, such a projection ignores the effects of temperature and other natural variables.

As mentioned previously, using the dilatometer to measure the joint aperture at the same time that permeability is being measured offers the opportunity to evaluate the flat plate model of a joint. If one assumes that the joint aperture alone is the effective cross sectional area to which fluid is exposed, then in equation (2), A equals 3.5 cm times the joint opening (d). We found, for example, that the joint with surfaces prepared with 120 grit could be squeezed down about 36 μm. From the change of aperture with pressure we estimated the maximum joint closure possible to be about 40 μm. Using this value for d at zero pressure, we calculated the permeability of the joint alone. In Fig. 9 we compare this with the flat plate model (equation 5). Data collected are given in Table 2. Uncertainty in d is about 1 μm.

Data points 1 through 6 in Table 2 indicate how rapidly the joint closes down as confining pressure is raised. Data points 7 through 13 show that with the introduction of internal fluid pressure the joint recovers most, but not all, of the aperture closure produced by an equivalent value of $P_c - P_f$ (compare data points 5 and 8, for example). Permeability measurements were made starting at the conditions of data point 14. Confining pressure was raised and, after data point 21, internal fluid pressure was raised until near the value of P_c. After data point 26, P_f was lowered and a second cycle begun.

It is apparent from Fig. 9 that, within the uncertainty of the aperture measurements, a flat plate does not adequately model this joint. The flat plate model predicts permeabilities and orders of magnitude higher than determined. The model also does not consider the stress history. The joint apparently suffers enough damage during the first cycle of measurements (data points 1 through 26 in Table 2) that it no longer responds in the predicted way. During the second cycle (after data point 27 in Table 2), permeability is significantly lower than during the first cycle, even though the measured apertures are about the same. Once the joint has been squeezed down, the two sides tend to remain close together until the internal fluid pressure is raised to a substantial percentage of the external confining pressure, after which the aperture opens rapidly (compare data points 7–13 and 21–26). The phenomenon of the joint being wedged open by high internal fluid pressure requires more clarification and is under current investigation.

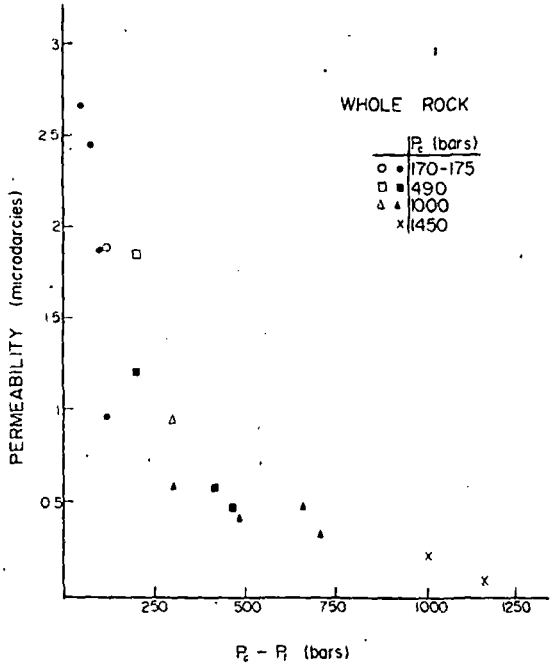

Fig. 7. Permeability of whole, unjointed Barre granite at various pressures. Open symbols and closed symbols directly beneath them are beginning and end points of cyclic experiments following the procedure of Fig. 2b.

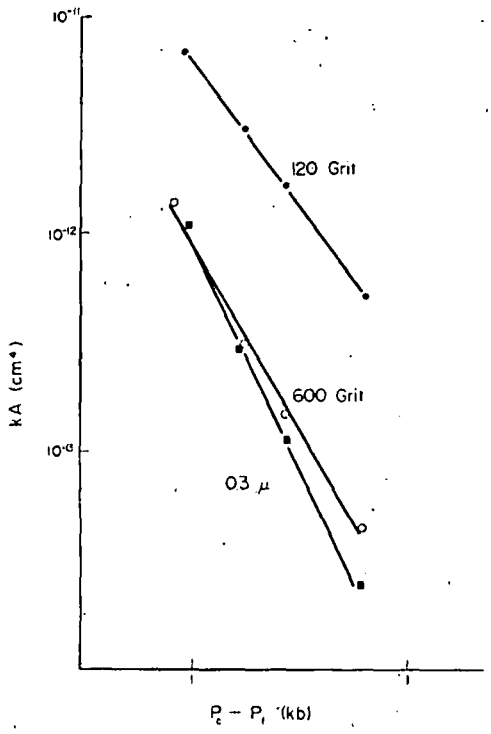

Fig. 8. Permeability times cross-sectional area (kA) as a function of $P_c - P_f$ (with P_c held constant at 690 bars) for different jointed samples.

DISCUSSION

Effective stress

Permeability k is a function of many variables, the most important of which are evidently confining pressure, internal fluid pressure, temperature, and in the case of joints, surface roughness. Unfortunately, k does not appear to be simply proportional to $P_c - P_f$. When one of these pressures is held constant and the other is changed two things become apparent. First, the relative effects on the change of permeability are not always equal for equal changes in P_c and P_f and second, the order in which the two pressures are varied also has an effect on the permeability. That is, k is stress history-dependent.

Suppose k to be a function only of P_c and P_f. Then we may write

$$dk = \left[\frac{\partial k}{\partial(P_c - P_f)}\right]_{P_f} d(P_c - P_f) + \left[\frac{\partial k}{\partial(P_c - P_f)}\right]_{P_c} d(P_c - P_f)$$

$$= \left[\frac{\partial k}{\partial(P_c - P_f)}\right]_{P_f} dP_c - \left[\frac{\partial k}{\partial(P_c - P_f)}\right]_{P_c} dP_f$$

$$= -a\,dP_c + b\,dP_f. \qquad (7)$$

From this we see that the coefficients a and b give the relative effects of confining and internal fluid pressure changes. They are the slopes of equal P_f and equal P_c lines on a permeability vs $P_c - P_f$ graph. When P_c and P_f are changed by equal amounts, the value of $b - a$ is proportional to the change in k. For example, if both P_c and P_f are increased by δ, then $dk = (b - a)\delta$. If dk is positive (permeability increases) then b is greater than a and internal fluid pressure is evidently of greater importance than confining pressure. This, as we have shown, is decidedly not the case for jointed Barre granite. Permeability was *less* at higher confining pressures when compared at the same $P_c - P_f$ value (e.g. $b/a < 1$). Zoback [12] found $2.2 < b/a < 4$ for several unjointed sandstone. That is, P_f had a greater effect than P_c. Brace *et al.* [1] implied that a simple effective stress law of $(P_c - P_f)$ held for Westerly granite. This is equivalent to having $b/a = 1$. For whole Barre granite b/a is also close to one but we hesitate to try and assign a value because it is apparent that b/a is stress history dependent. In addition, for joints b/a is apparently also a function of surface roughness and the ambient pressure.

Taking all of this into account, we conclude that there is no *simple* effective stress law for the permeability of jointed rock. We have purposely avoided using the term 'effective stress' for this reason and because no effective stress law has yet to be developed which accounts for stress history dependence.

Surface roughness

The more highly polished a surface is the smaller the mean asperity height. In this sense, grinding has the same effect as normal pressure. For any particular initial statistical roughness, the greater the pressure, the greater the real area of contact with the opposing surface. Similarly, at any particular normal pressure, we would expect more real area of contact the less rough or more highly ground the two opposing surfaces are.

Asperities in contact affect permeability in two direct ways. They change the path length or tortuosity of flow path and they inhibit joint closure. Joint permeability defined by equation (5) does not take this into account. The effect of surface roughness can easily be seen by comparing Figs 3, 4, and 5. The highly polished surface (Fig. 3) most closely resembles a flat plate. Asperities are small so the joint closes rapidly at low pressures until enough of these asperities make contact with the

Table 1. Dependence of kA on $P_c - P_f$

$$\mu q\left[\frac{dP}{dL}\right]^{-1} = kA = [kA]_0([P_c - P_f]^{-n})$$

P_c (bars)	Joint surface	kA_0^*	$n \pm 0.2$
350	120 grit	12.3	1.6
355	600 grit	1.2	1.9
372	0.3 μ polish	1.2	2.4
697	120 grit	7	1.3
690	600 grit	0.9	1.7
690	0.3 μ polish	0.9	2.1
1382	120 grit	3.3	1.2
1380	600 grit	0.5	1.5
1381	0.3 μ polish	0.7	2.1
2082	120 grit	1.1	0.8
2070	600 grit	0.4	1.5?
1000	tension fracture	60	1.3
1248	tension fracture	25	1.1
1496	tension fracture	10	1.0
1750	tension fracture	?	?
170–175	whole rock	1	0.9
1000	whole rock	0.65	0.8

* $\times 10^{-12}$ cm⁴; $[kA]_0 = kA$ at $P_c - P_f = 100$ bars.

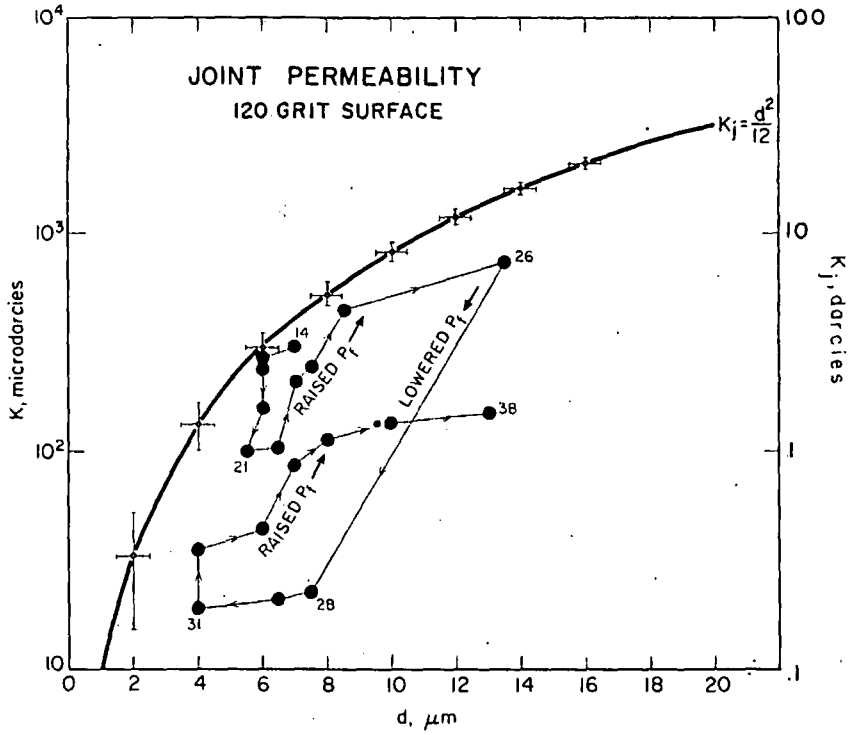

Fig. 9. Permeability of the joint alone as a function of joint aperture. K_j is the theoretical value assuming a flat plate model. Data points taken from Table 2.

opposing surface to increase the flow tortuosity and decrease the closure rate. Contrast this with Fig. 5 where the asperities are larger and tend to prop the joint open, thereby diminishing the rate of permeability decline as pressure is raised. Figure 4 shows intermediate behavior.

Iwai [13] has investigated the effects of contact area and asperity geometry on permeability. He found that at low pressure (2.6 bars) the real area of contact of a granite was less than 0.1% of the apparent total area and increased to 10–20% at 200 bars. He found a relation of the form

$$\gamma \frac{k}{k_0} + 1 = \frac{\psi}{\gamma A_r/A + 1} \tag{8}$$

where γ and ψ are empirical constants, k_0 is the zero pressure permeability, A_r is the real area of contact and A is the apparent joint surface area.

Though we have no data for the relationship between $P_c - P_f$ and A_r/A, Iwai [13] claims that the contact area increases linearly with normal load. This is consistent with the results of Bowden & Tabor [14] who show that, neglecting time effects,

$$A_r = N/h \tag{9}$$

where N is the average normal load on an asperity and h is the indentation hardness for the asperity material.

Consider the model of a part of a joint sketched in Fig. 10. Confining pressure acts on the entire joint surface area A. Equilibrium demands that

$$P_c A = N + P_f (A - A_r) \tag{10}$$

Table 2. Joint aperture and permeability changes for sample with 120 grit surface

Data Pt.	P_c (bars)	P_f	d (μm)	K (microdarcies) (×1)	$K_j = d^2/12$ (×10⁴)
	0	0	40		
1	10	0	19		
2	20	0	16		
3	40	0	12		
4	75	0	9		
5	150	0	7		
6	300	0	4		
7	300	55	4.5		
8	300	150	5.5		
9	300	205	7		
10	300	255	9.5		
11	300	265	10.5		
12	300	275	11.5		
13	300	285	13.5		
14	300	205	7	~300	408
15	500	205	6	~275	300
16	700	205	6	~260	300
17	1000	205	6	248	300
18	1200	205	6	243	300
19	1400	205	6		
20	1400	100	6	159	300
21	1400	50	5.5	98	252
22	1400	350	6.5	105	352
23	1400	600	7	210	408
24	1400	850	7.5	239	468
25	1400	1100	8.5	455	602
26	1400	1350	13.5	~750	1518
27	1400	200	7.5		
28	1700	230	7.5	22	468
29	2165	230	7.0	23	408
30	2700	230	6.5	21	352
31	3435	230	4	19	133
32	2735	230	4	21	133
33	2100	230	4	35	133
34	1425	230	6	44	300
35	1425	430	7	88	408
36	1455	985	8	103	533
37	1455	1275	10	135	833
38	1455	1395	13	149	1400

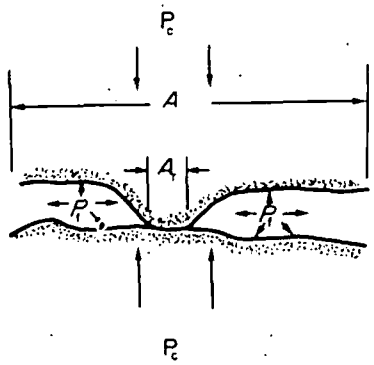

Fig. 10. An idealized joint section with an asperity subjected to external, P_c, and internal, P_f, pressures.

Substituting for N from (9) we get

$$\frac{A_r}{A} = \frac{P_c - P_f}{h - P_f}. \tag{11}$$

To determine whether P_c or P_f has a greater effect on A_r we compare

$$\frac{1}{A}\left[\frac{\partial A_r}{\partial P_c}\right]_{P_f} = \frac{1}{h - P_f}$$

and

$$\frac{1}{A}\left[\frac{\partial A_r}{\partial P_f}\right]_{P_c} = \frac{P_c - h}{[h - P_f]^2}.$$

We see that

$$\left|\left[\frac{\partial A_r}{\partial P_c}\right]_{P_f}\right| > \left|\left[\frac{\partial A_r}{\partial P_f}\right]_{P_c}\right|$$

whenever $P_c + P_p < 2h$.

This condition is certainly met for all of our experiments so we conclude that the confining pressure will have a greater effect on the real area of contact than the internal fluid pressure. This simple model is therefore compatible with our experimental results. It is clear from Table 1, however, that changes in joint surface topography with normal stress are much more complicated than we have supposed. We have initiated a program to measure these changes in order to better understand the physics of joint deformation.

Whole rock

The absolute values of permeability for Barre granite are about a factor of 3 higher than those reported by Brace *et al.* [1] for Westerly granite over the pressure range measured here. The average grain size of Barre granite is about a factor of 2 greater than that for Westerly granite. In addition, Barre granite has a strong fabric because of a preferred crack orientation [15]. Our whole rock cores were oriented so that flow was forced along the rift-grain plane. These two factors probably account for the differences in permeability.

Stress history

Unrecovered permeability changes for jointed crystalline rock have been observed in the laboratory [5, 13, 17] and joint closure hysteresis has been observed [4] in the field. These were a result of cycling the external normal stress. Since overburden pressures generally remain constant while internal fluid pressures change in natural rock systems, our method of demonstrating permeability hysteresis by cycling the internal pressure is preferable.

Witherspoon *et al.* [5] observed that flow rates showed a considerable difference between injection and withdrawal of fluid, but that the difference decreased with increasing normal stress. No significant permeability losses were observed by Zoback [12] when pore pressure was raised, then lowered in sandstone. We observed permeability hysteresis in jointed samples *and* whole rock when the internal fluid pressure was first lowered, then raised to its initial value (Figs 6 and 7). This hysteresis also seemed to decrease with increasing confining pressure.

Since hysteresis occurs in joint closure with a considerable non-recoverable part, some asperities must be deforming plastically or else are crushed when P_c is increased. Either plastic deformation or asperity crushing will increase the contact area and thus decrease the amount of surface area available for P_f to work against, in addition to increasing the flow tortuosity. Thus lowering the P_f value apparently permits non-recoverable surface damage. The permeability can be recovered only if the joint or crack aperture is increased.

Permeability hysteresis within whole rock is probably a result of irrecoverable damage done to bridging material between grains and crack walls. Sprunt & Brace [11] have shown that pressure produces such damage in granite. Feves & Simmons [18] have shown that pressure cycling decreases the crack porosity substantially. If pore pressure is decreased and cracks close down, raising the pore pressure to its initial value may not be sufficient to wedge the cracks open again. If the test is performed in reverse by first raising the pore pressure, the cracks will stay open and no damage is expected. Zoback's results [12] are not incompatible with ours in this respect.

One of the observations which we cannot so easily explain is found in Fig. 6. After completing a cycle of lowering and raising P_f, both were raised *simultaneously* (as in Fig. 2b). This had the apparently incongruous result of *raising* the permeability slightly, though it was still lower than the beginning of the previous cycle. We suggest that this may have been a result of not letting sufficient time elapse for P_f within the joint to come into equilibrium with the reservoir pressure. Thus $P_c - P_f$ may have been less within the joint than we measured outside of the sample column. Alternatively, it may be that when a joint is subjected to internal pressures not previously experienced, even when the $P_c - P_f$ value is constant, the contact area between asperities decreases.

CONCLUSIONS

Because the permeability of jointed rock is greater than unjointed, low porosity rock, fluid flow will be

confined essentially to joints and fractures in the rock. Large differences in permeability persist at least up to 2 kbars of pressure though the decrease in permeability with pressure is greater for joints than for whole rock. In addition, since joint surface roughness has an effect on the decline of permeability with pressure, some joints will probably be effective fluid conductors at even higher pressures. Eventually, however, a pressure is reached where jointed and unjointed rock become indistinguishable.

Changes in external (overburden) and internal (fluid) pressures have significant effects on the hydraulic properties of unjointed and jointed rock. It appears that these effects are similar but of different magnitude in whole as compared with jointed rock. Jointed rock is much more sensitive to pressure than whole rock. In a porous rock, flow is through interconnected pores and cracks. The mean cross sectional area along the flow path is much smaller than for a joint. In addition, the flow path length is much greater in whole rock. These two differences alone can account for the magnitude difference in permeability, but not for the fact that the permeability decreases more rapidly with pressure for jointed than for unjointed rock. Rather, it is apparently because the compressibility of jointed rock is much greater than for whole rock [4, 6, 19]. That is, the joint aperture closes more readily under pressure than cracks within the whole rock.

We find that external confining pressures produce greater changes than internal fluid pressures for jointed rock. In whole Barre granite, the relative changes are about equal. This may not be true of other rock types. One should be cautious when applying the term *effective stress* to jointed media. At least for the hydraulic properties of jointed rock it is *not* simply the difference between external confining and internal fluid pressures.

For flow through joints, a flat plate model of the joint seems inadequate and the stress history must be considered. Deviations from the flat model may occur under high stress or for very rough surfaces.

The stress history of both whole and jointed rock affects its hydraulic character. Increasing the mean normal stress to values higher than previously experienced will certainly lower the permeability. That is, raising the confining pressure *or* lowering the internal fluid pressure will result in lower permeabilities even when the original conditions are restored. This fact has obvious implications for oil field production and geothermal energy extraction schemes. If the internal fluid pumping pressures are allowed to drop, some subsequent decrease in hydraulic efficiency will ensue.

Finally, as there seems to be a substantial difference in the response of low porosity rock like granite and high porosity rock like sandstone to changes in fluid pressure, more work needs to be done to clarify the reasons for this difference. More jointed sandstones, granites, and other rock types need to be tested. Joint surface topography changes need to be examined also, and as mentioned, we have begun such an investigation. *In situ* experiments, perhaps in mines, are also needed to help characterize further the differences in hydraulic response to changes in external and internal pressure.

Acknowledgements—The data in this report were collected as part of an on-going project supported by the Department of Energy under contract EY-S-02-4054 and the National Science Foundation under contract EAR-77-13000. T. Koczynski provided technical support. The manuscript was reviewed by D. Holcomb and K. Jacob. H. Murphy provided useful comments on an earlier version. Lamont-Doherty Contribution No. 2830.

Received 5 September 1978.

REFERENCES

1. Brace W. F., Walsh J. B. & Frangos W. T. Permeability of granite under high pressure. *J. geophys. Res.* **73**, 2225–2236 (1968).
2. Zoback M. D. & Byerlee J. D. The effect of microcrack dilatancy on the permeability of Westerly granite. *J. geophys. Res.* **80**, 752–755 (1975).
3. Summers R., Winkler K. & Byerlee J. Permeability changes during the flow of water through Westerly granite at temperatures of 100°–400 C. *J. geophys. Res.* **83**, 339–344 (1978).
4. Pratt H. R., Swolfs H. S., Brace W. F., Black A. D. & Handin J. W. Elastic and transport properties of an *in situ* jointed granite. *Int. J. Rock Mech. Min. Sci. & Geomech. Abstr.* **14**, 35–45 (1977).
5. Witherspoon P. A., Amick C. H. & Gale J. E. Stress-flow behavior of a fault zone with fluid injection and withdrawal, Report No. 77–1, Dept. of Materials Science and Mineral Engineering, University of California– Berkeley (1977).
6. Brace W. F. A note on permeability changes in geologic material due to stress. *Proc. of Conference II: Experimental Studies of Rock Friction with Application to Earthquake Prediction.* U.S.G.S., Menlo Park, CA (1977).
7. *International Critical Tables.* (Edited by Washburn E. W.), Vol. II, p. 146. McGraw-Hill, New York (1927).
8. Bridgeman P. W. The effect of pressure on the viscosity of 43 pure liquids. *Proc. Am. Acad. Arts Sci.* **61**, 57–99 (1926).
9. Snow D. T. A parallel plate model of fractured permeable media. Ph.D. Thesis, University of California—Berkeley (1965).
10. Norton D. & Knapp R. Transport phenomena in hydrothermal systems: the nature of porosity. *Am. J. Sci.* **277**, 913–936 (1977).
11. Sprunt E. & Brace W. F. Some permanent structural changes in rock due to pressure and temperature. *Proc. 3rd Cong. ISRM* Vol. IIA, 524–529, Denver, CO (1974).
12. Zoback M. D. High pressure deformation and fluid flow in sandstone, granite and granular materials. Ph.D. Thesis, Stanford University (1975).
13. Iwai K. Fundamental studies of fluid flow through a single fracture. Ph.D. Thesis, University of California—Berkeley (1976).
14. Bowden F. P. & Tabor D. *The Friction and Lubrication of Solids* Vol. I, Clarendon Press, Oxford (1950).
15. Douglas P. M. & Voight B. Anisotropy of granites: A reflection of microscopic fabric. *Geotechnique* **19**, 376–398 (1969).
16. Mordecai M. & Morris L. H. An investigation into the changes of permeability occurring in a sandstone when failed under triaxial stress conditions. *12th Symp. Rock Mech., Rolla, MO.* (Edited by Clark G. B.), Chap. 11, Port City Press, Baltimore, MD (1971).
17. Nelson R. A. & Handin J. Experimental study of fracture permeability in porous rock. *Am. Ass. Pet. Giol. Bull.* **61**, 227–236 (1977).
18. Feves M. & Simmons G. Effects of stress on cracks in Westerly granite. *Bull. Seism. Soc. Am.* **66**, 1755–1765 (1976).
19. Daw G. P., Howell F. T. & Woodhead F. A. The effect of applied stress upon the permeability of some Permian and Triassic sandstones of northern England. *Proc. 3rd Congr. ISRM* Vol. IIA, 537–542, Denver, CO (1974).